

University of Nevada, Reno

**The Impact of Meteorology on Ozone Levels in the Lake Tahoe Basin**

A dissertation submitted in partial fulfillment of the requirements for the degree of Doctor of Philosophy  
in Atmospheric Sciences

by

Sandra Theiss

Dr. Alan Gertler / Dissertation Advisor

December, 2015



THE GRADUATE SCHOOL

We recommend that the dissertation  
prepared under our supervision by

**SANDRA THEISS**

Entitled

**The Impact Of Meteorology On Ozone Levels In The Lake Tahoe Basin**

be accepted in partial fulfillment of the  
requirements for the degree of

DOCTOR OF PHILOSOPHY

Alan W. Gertler, Advisor

Vera Samburova, Committee Member

John Mejia, Committee Member

Pat Arnott, Committee Member

Heather Holmes, Graduate School Representative

David W. Zeh, Ph. D., Dean, Graduate School

December, 2015

## ABSTRACT

The Lake Tahoe Basin is located on the California-Nevada border and occasionally experiences elevated levels of ozone exceeding the 70 ppb California Air Resources Board (CARB) ambient air quality standard (8-hour average). Previous studies indicate that both the local generation of ozone in the Basin and long-range transport from out-of-Basin sources are important in contributing to ozone exceedances, but little is known about the impact of meteorology on the distribution of ozone source regions. In order to develop a better understanding of the factors affecting ozone levels and sources in the Lake Tahoe Basin, this study combines observational data from a 2010 and 2012 summer field campaigns, HYSPLIT back trajectories, and WRF model output to examine the meteorological influences of ozone transport in the topographically complex Lake Tahoe Basin. Findings from the field work portions of this study include enhanced background ozone levels at higher elevations, the local circulation pattern of lake breezes occurring at Lake level sites, and an indication that ozone precursors are coming off the Lake. Our analysis also showed that if transport of ozone does occur, it is more likely to come from the San Joaquin Valley to the south rather than originate in the large cities to the west, such as Sacramento and San Francisco. Analysis of modeled PBL schemes as compared with observational data showed that the ACM2 PBL scheme best represented the geographical domain. The ACM2 PBL scheme was then used to show wind circulation patterns in the Lake Tahoe Basin and concluded that there is decent vertical mixing over the Basin and no indication of ozone transport from the west however some indication of transport from the east. Overall this study concludes that transport from the west is less significant than transport from the south and east, and that transport only influences ozone values at higher elevations. Within the Basin itself (at lower elevations), local factors including mixing depth, rising or sinking air, and lake/land breeze circulations are more significant in influencing ozone values.

## **ACKNOWLEDGEMENTS**

Firstly, I would like to express my sincere gratitude to my advisor Professor Alan W. Gertler for the continuous support of my Ph.D study and related research, for his patience, motivation, and immense knowledge. I thank him for everything he has done for me, especially allowing me the opportunity to work with and learn from him. I could not have imagined having a better advisor and mentor for my Ph.D study.

I would like to thank the rest of my committee members: Dr. Vera Samburova, Dr. John Mejia, Dr. Pat Arnott and Dr. Heather Holmes for their insightful comments and encouragement. I would also like to acknowledge Dr. Michael Kaplan who inspired me to get my Ph.D and continued to aid in my research and teaching experience and the Desert Research Institute for the research facilities and continued financial support.

I would also like to thank my fellow graduate students, in particular K.C. King, for the stimulating discussions, computer programming guidance, coffee breaks and all the fun we have had for the past several years.

Finally, my sincerest gratitude goes out to my family: my love Nyssa Perryman Rayne, my sons Marshall and Luke, my parents Ellen and Paul and my brothers Sal, Paul and John, for always supporting me with this dissertation and my life in general, and bearing the time being away from me, this Ph.D would not have been possible without you.

## TABLE OF CONTENTS

ABSTRACT.....	i
ACKNOWLEDGEMENTS.....	ii
TABLE OF CONTENTS.....	iii
LIST OF TABLES.....	vi
LIST OF FIGURES.....	vii
<b>Chapter 1: Introduction</b> .....	<b>1</b>
1.1 Overview and Objectives.....	1
1.2 Sources and Formation of O <sub>3</sub> .....	4
1.3 O <sub>3</sub> Transport.....	11
1.4 O <sub>3</sub> Impacts.....	19
1.5 Meteorology of Lake Tahoe.....	25
1.6 Washoe Zephyr.....	27
1.7 Weather Research and Forecast (WRF) Model.....	29
1.8 Overall Goal and Specific Objectives.....	31
References.....	32
<b>Chapter 2: Surface Ozone in the Lake Tahoe Basin: Impact of Regional Meteorology</b> ....	<b>50</b>
Abstract.....	51
2.1 Introduction.....	52
2.2 Methodology.....	55
2.3 Results.....	56
2.4 Discussion.....	58
2.5 Summary and Conclusions.....	61
Acknowledgments.....	62

References.....	64
Figures and Tables.....	68
<b>Chapter 3: Impact of Regional Meteorology on Ozone Levels in the Lake Tahoe Basin .</b>	<b>83</b>
Abstract.....	84
3.1 Introduction.....	85
3.2 Methodology.....	87
3.3 Results and Discussion.....	90
3.4 Summary and Conclusions.....	94
Acknowledgments.....	95
References.....	97
Tables.....	101
List of Figures.....	102
Figures.....	103
<b>Chapter 4: Improving Air Quality Modeling for the Lake Tahoe Basin: Investigating Planetary Boundary Layer Schemes in the WRF Model.....</b>	<b>115</b>
Abstract.....	116
4.1 Introduction.....	117
4.2 Methodology.....	118
4.2.a Model Configuration.....	119
4.2.b Description of PBL Schemes.....	120
4.2.c Meteorological Evaluation Data.....	122
4.2.d Field Experiment and Ozone Data.....	123
4.2.e Cross Sections.....	123

4.3 Results .....	124
4.4 Discussion.....	130
4.5 Summary and Conclusions .....	132
Acknowledgments.....	133
References.....	134
Tables.....	139
List of Figures.....	141
Figures.....	144
<b>Chapter 5: Summary and Conclusions</b> .....	164
APPENDIX 1: Surface Ozone in the Lake Tahoe Basin .....	168

**LIST OF TABLES**

2-1 Elevation and distance from road of each site.....	81
2-2 Correlation matrix between sites .....	82
3-1 Elevation and description of O <sub>3</sub> measurement sites .....	101
4-1 Daily statistics of three PBL schemes with 77 observational sites in domain 3 (4-km resolution) .....	139
4-2 0000 UTC Hour statistics of three PBL schemes with 77 observational sites in d03 .....	140

## LIST OF FIGURES

1-1	Typical O <sub>3</sub> isopleths. Source: Adapted from Finlayson-Pitts and Pitts, 2000 .....	10
1-2	The diurnal evolution of the planetary boundary layer while high pressure prevails over land. Three major layers exist (not including the surface layer): a turbulent mixed layer; a less turbulent residual layer which contains air formerly in the mixed layer; and a nocturnal, stable boundary layer which is characterized by periods of sporadic turbulence. Source: Adapted from Stull (1988) .....	15
1-3	Schematic diagram showing the diurnal behavior of O <sub>3</sub> and the development of secondary O <sub>3</sub> maxima resulting from downward transport from the residual layer when a low-level jet is present. Source: Adapted from Reitbuch et al. (2000); Corsmeier et al. (1997); and Salmond and McKendry (2002).....	17
1-4	Image of Lake Tahoe and surrounding areas. Source: Google earth 2012.....	26
2-1	Location of Lake Tahoe.....	68
2-2	Location of measurement sites around the lake, the red sites are the WRCC observation sites: North Tahoe High School (NTHS) and South Lake Tahoe (KTVL) .....	69
2-3	Max 1-hr daily ozone concentrations (ppb) for each site from July 1 2010 – September 23 2010.....	70
2-4	Max 8-hr averaged ozone (ppb) for each site from July 1 2010 – September 23 2010 .....	71
2-5	Averaged hourly ozone (ppb) from July 1 2010 – September 23 2010, time is in Pacific Daylight Time .....	72
2-6	Daytime wind roses including the hours of 8am, 11am, 2pm and 5pm for each site during the summer of 2010 .....	73
2-7	Nighttime wind roses including the hours of 2am, 5am, 8pm and 11pm for each site during the summer of 2010 .....	74
2-8	Hysplit trajectories of Angora High Day.....	75
2-9	Hysplit trajectories of Angora Low Day. ....	76
2-10	Daytime wind rose from WRCC observation site North Tahoe High School (NTHS) .....	77

2-11	Nighttime wind rose from WRCC observation site North Tahoe High School (NTHS) ...	78
2-12	Daytime wind rose from WRCC observation site South Lake Tahoe (KTVL) .....	79
2-13	Nighttime wind rose from WRCC observation site South Lake Tahoe (KTVL).....	80
3-1	Location of Lake Tahoe and the ten measurement sites.....	103
3-2	Maximum 8 hr O <sub>3</sub> averaged over all ten sites. Top red line indicates one standard deviation above and bottom red line indicates one standard deviation below.....	104
3-3	Washoe Zephyr Index (difference between Sacramento mean sea level pressure and Reno mean sea level pressure) Positive value indicates Washoe Zephyr day, negative value indicates no Washoe Zephyr day .....	105
3-4	HYSPLIT example of a high O <sub>3</sub> day .....	106
3-5	HYSPLIT example of a low O <sub>3</sub> day .....	107
3-6	Scatter plot of Washoe Zephyr Index and Max 8 hr O <sub>3</sub> for the summer of 2010.....	108
3-7	Scatter plot of Washoe Zephyr Index and Max 8 hr O <sub>3</sub> for the high O <sub>3</sub> days .....	109
3-8	Scatter plot of Washoe Zephyr Index and Max 8 hr O <sub>3</sub> for the medium O <sub>3</sub> days .....	110
3-9	Scatter plot of Washoe Zephyr Index and Max 8 hr O <sub>3</sub> for the low O <sub>3</sub> days .....	111
3-10	Sounding composite for the high O <sub>3</sub> days .....	112
3-11	Sounding composite for the medium O <sub>3</sub> days .....	113
3-12	Sounding composite for low O <sub>3</sub> days .....	114
4-1	Location of Lake Tahoe and site locations of 2012 field study.....	144
4-2	Model domains. The mother domain (d01) is the black box, first nested domain (d02) is the white box and second nested domain (d03) is the red box .....	145
4-3	Hourly ozone values for the 2012 sites: LH is Lower Homewood, UH is Upper Homewood, HE is Heavenly Ski Resort, and HQ is Tahoe Regional Planning Agency .....	146
4-4	Averaged hourly ozone values for the 2012 sites: UH is Upper Homewood, HV is Heavenly Ski Resort, LH is Lower Homewood and TRPA is Tahoe Regional Planning Agency .....	147
4-5	Temperature comparison between observations and the three WRF PBL model schemes. Data is hourly, observations taken at NWS surface observational site Reno, NV .....	148
4-6	Temperature comparison between observations and the three WRF PBL model schemes. Data is hourly, observations taken at NWS surface observational site Elko, NV .....	149
4-7	Dew point temperature comparison between observations and the three WRF PBL model schemes. Data is hourly, observations taken at NWS surface observational site Reno, NV ...	150

4-8	Dew point temperature comparison between observations and the three WRF PBL model schemes. Data is hourly, observations taken at NWS surface observational site Elko, NV....	151
4-9	PBL comparison between observations calculated two different ways and the three WRF PBL model schemes. Observations taken at NWS sounding site Reno, NV. Only 0000 UTC data was used.....	152
4-10	PBL comparison between observations calculated two different ways and the three WRF PBL model schemes. Observations taken at NWS sounding site Elko, NV. Only 0000 UTC data was used.....	153
4-11	PBL height calculated using the +1.5 theta method comparison between observations and the three WRF PBL model schemes. Observations taken at NWS sounding site Reno, NV. Only 0000 UTC data was used.....	154
4-12	PBL height calculated using the +1.5 theta method comparison between observations and the three WRF PBL model schemes. Observations taken at NWS sounding site Elko, NV. Only 0000 UTC data was used.....	155
4-13	PBL height calculated using the critical bulk Richardson number of 0.25 method comparison between observations and the three WRF PBL model schemes. Observations taken at NWS sounding site Reno, NV. Only 0000 UTC data was used.....	156
4-14	PBL height calculated using the critical bulk Richardson number of 0.25 method comparison between observations and the three WRF PBL model schemes. Observations taken at NWS sounding site Elko, NV. Only 0000 UTC data was used.....	157
4-15	Washoe Zephyr Index calculated using the pressure difference between Sacramento and Reno comparison between observations and the three WRF PBL model schemes. Hourly observations taken at NWS sounding sites Sacramento, CA and Reno, NV.....	158
4-16	Region of cross sections. Black line indicates line of cross section.....	159
4-17	Cross section 25 July 1900 UTC. Top graph indicates u (east-west) component of winds, positive is red (coming from west). Middle graph indicates v (north-south) component of winds, positive is red (coming from south). Bottom graph indicates w (up-down) component of winds, positive is red (rising air). Black lines indicate potential temperature. Left point of graph is Sacramento, CA, right point is Fallon, NV.....	160
4-18	Cross section 24 July 1900 UTC. Top graph indicates u (east-west) component of winds, positive is red (coming from west). Middle graph indicates v (north-south) component of winds,	

- positive is red (coming from south). Bottom graph indicates  $w$  (up-down) component of winds, positive is red (rising air). Black lines indicate potential temperature. Left point of graph is Sacramento, CA, right point is Fallon, NV..... 161
- 4-19 Cross section 24 July 1000 UTC. Top graph indicates  $u$  (east-west) component of winds, positive is red (coming from west). Middle graph indicates  $v$  (north-south) component of winds, positive is red (coming from south). Bottom graph indicates  $w$  (up-down) component of winds, positive is red (rising air). Black lines indicate potential temperature. Left point of graph is Sacramento, CA, right point is Fallon, NV..... 162
- 4-20 Cross section 25 July 1900 UTC. Top graph indicates  $u$  (east-west) component of winds, positive is red (coming from west). Middle graph indicates  $v$  (north-south) component of winds, positive is red (coming from south). Bottom graph indicates  $w$  (up-down) component of winds, positive is red (rising air). Black lines indicate potential temperature. Left point of graph is Sacramento, CA, right point is Fallon, NV..... 163

## Chapter 1:

### Introduction

#### 1.1 Overview and Objectives

Vacation destinations and resort areas are sought after as places of refuge from ozone and particulate pollution and are valued for their pristine water, and air quality. Lake Tahoe is a prime example of this. It is nestled in between the two states of Nevada and California, with the San Joaquin Valley to the west. Historically, the complex terrain of the Sierra Nevada mountains kept Lake Tahoe isolated with few vehicles and limited human activities. With the construction of casinos at the state line on the north and south ends of Lake Tahoe and the development of a summer boating and winter ski industry, Tahoe gradually attained the status of a resort destination while at the same time increasing the pollution from human activities.

Air pollution concentrations are the result of interactions among local weather patterns, atmospheric circulation features, wind, topography, human activities (i.e., transport and coal-fired electricity generation), human responses to weather changes (i.e., the onset of cold or warm spells may increase heating and cooling needs and therefore energy needs), and other factors. Some locations, because of their general climate and topographic setting, are predisposed to poor air quality because of the climate is conducive to chemical reactions leading to the transformation of emissions, and the topography restricts the dispersion of pollutants including Ozone ( $O_3$ ) (Ebi and McGregor 2008; Kossmann and Sturman 2004; Rappengluck et al. 1999). These episodes of poor air quality have a negative impact on human health and the environment.

$O_3$  impacts our lives in various ways depending on where it is located in the Earth's atmosphere. In the stratosphere,  $O_3$  attenuates harmful ultraviolet radiation and protects the Earth's biosphere (WMO, 1998). However, the Clean Air Act (U.S. Environmental Protection

Agency (EPA) 1970) identified tropospheric O<sub>3</sub> as one of six “criteria pollutants”- pervasive pollutants considered harmful to human health. Ambient levels of tropospheric O<sub>3</sub> today has also been shown to have negative effects on vegetation and lower the yield of several crop species (Fuhrer 2002) which is why it is important to understand the sources and formation of tropospheric O<sub>3</sub>.

Tropospheric O<sub>3</sub> forms as a result of atmospheric reactions of nitrogen oxides (NO<sub>x</sub>) and volatile organic compounds (VOCs) in the presence of sunlight (Hubbell et. al. 2005). The lifetime of O<sub>3</sub> in the free troposphere is sufficiently long (several weeks) that anthropogenic O<sub>3</sub> pollution can circumnavigate the globe and enhance O<sub>3</sub> over the entire northern midlatitudes belt (Logan 1985). Therefore, O<sub>3</sub> can easily transport many miles downwind of the source via wind circulations and weather patterns. The San Joaquin Valley of California is consistently among those regions with the highest experienced ozone (O<sub>3</sub>) levels in the US (Lagarias and Sylte, 1991; Ranzieri and Thuillier, 1994; Dabdub et. al. 1999). The prevailing west winds make the San Joaquin Valley prone to long range transport of O<sub>3</sub> and potentially into the Lake Tahoe Basin.

Tahoe is so popular in the summer that it is not unusual to record a million vehicle miles around the lake in a single day (Goldman, 2006). O<sub>3</sub> concentrations at Lake Tahoe are highest during the summer, when sunlight drives the chemical processes that create O<sub>3</sub>. The California Air Resources Board provides an emissions inventory for the Lake Tahoe Air Basin every few years, using the EMFAC (Motor Vehicle Emission Inventory Model) model (California Air Resources Board (CARB), 2013). O<sub>3</sub> concentrations in the Lake Tahoe Basin were stable during the 1980s, hovering at or slightly above California standards. However, two factors puzzled scientists. First, the Lake Tahoe Basin’s highest O<sub>3</sub> concentrations were observed in the late

afternoon and early evening, not closer to solar noon as predicted. Second, despite a decrease in emissions of oxides of nitrogen in the Basin (a result of the cleaner vehicles), O<sub>3</sub> concentrations did not decrease. These two factors led air pollution experts to suggest that O<sub>3</sub> was, in fact being transported into the Basin from upwind areas (Elliott-Fisk et al., 1996). However, since Lake Tahoe is surrounded by the Sierra Nevada mountains, the complex meteorology arising from the topography can trap air pollutants in the basin. It is still unclear to what extent episodes of poor air quality are a result of local (cars, human activity) vs transported emissions (San Joaquin or Bay Area ozone) around Lake Tahoe.

Assessing the contributions of distant sources on local pollution levels remains a challenging problem and reducing the uncertainty in estimates requires a better understanding of transport patterns that bring together long-range transported air masses and local pollutants (NAS, 2010). The goal of this research is to investigate the nature of O<sub>3</sub> formation in the Lake Tahoe basin. In particular, to address the source of O<sub>3</sub>, whether it is due to local formation or long-range transport. In order to achieve that goal, we must first understand how O<sub>3</sub> is formed and O<sub>3</sub> sources and precursors.

Chapter 1 continues on to cover the sources and formation of O<sub>3</sub>, O<sub>3</sub> transport, and O<sub>3</sub> impacts on health and environment. Chapter 1 also includes three sections relating to the meteorology and meteorological modeling of the Lake Tahoe Basin. Chapter 2 focuses on the impact of local meteorology in the Lake Tahoe Basin on O<sub>3</sub> and O<sub>3</sub> precursors. Chapter 3 describes a regional impact of meteorology, including the Washoe Zephyr, and its effect on O<sub>3</sub> and O<sub>3</sub> precursors in the Lake Tahoe Basin. Chapter 4 describes the meteorological modeling approach as well as analyzing how local wind circulations in the basin influence O<sub>3</sub>. Chapter 5 summarizes the various findings and conclusions of this study.

## 1.2 Sources and Formation of O<sub>3</sub>

O<sub>3</sub> pollution is now widespread in urban areas in the United States and many other countries. Its rise reflects primarily increased numbers of motor vehicles and miles traveled; vehicle emissions are a major source of precursor hydrocarbons and nitrogen oxides (NO<sub>x</sub>) (Bell et al. 2004). In the United States, more than a hundred areas are not in compliance with the 8-hour NAAQS for O<sub>3</sub>, with the most extreme violations in California (US EPA, 2004).

Transport from the stratosphere was long thought to be the dominant source of O<sub>3</sub> in the troposphere (Junge 1962; Danielsen 1964). Stratospheric O<sub>3</sub> is formed first by the dissociation of O<sub>2</sub> at wavelengths below 242 nm. This produces the ground-state oxygen atoms, O (3P) and the electronically excited oxygen atoms O (1D) and O (1S). These atoms then react with O<sub>2</sub> in the presence of M, which is any third molecule that stabilizes the excited intermediate before it dissociates back into reactants, to form stratospheric O<sub>3</sub> (Finlayson-Pitts and Pitts, 2000).

Brewer (1949) described the basic overturning of the stratosphere more than sixty years ago, with low O<sub>3</sub> tropospheric air entering the stratosphere in the tropics and high O<sub>3</sub> air returning to the troposphere in the mid and high latitudes (Hsu et al. 2005). This global circulation is related to the dissipation of extratropical planetary and gravity waves in the stratosphere (Haynes et al. 1991). On a more local scale, stratosphere to troposphere exchange in tropopause folds (Danielsen, 1968; Vaughan, 1988; Ebel et al., 1991; Vaughan et al., 1994; Beekmann et al. 1997), cut-off lows (Vaughan, 1988; Ebel et al., 1991; Ancellet et al, 1994) in mesoscale convective complexes (Poulida et al., 1996) and thunderstorms (Tremblay and Servranckx, 1993) and due to breaking gravity waves (Lamarque et al., 1996) have received attention (Stohl et al., 2000). The stratosphere-troposphere exchange (STE) flux of O<sub>3</sub> is an important component of the tropospheric O<sub>3</sub> budget: it is approximately matched by deposition

to the surface, it influences the abundance of O<sub>3</sub> from the surface to the tropopause, and it is believed to drive some of the observed seasonal variations (Logan, 1999; Logan et al., 1999; Monks, 2000).

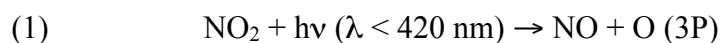
A literary review by Hsu et al. (2005) shows that there is a mounting convergence on the net annual STE flux of O<sub>3</sub> being in the range of 400-600 Tg-O<sub>3</sub>/year (Murphy and Fahey, 1994; McLinden et al., 2000; Olsen et al., 2001) despite no agreement as to when and where stratospheric O<sub>3</sub> enters the troposphere. A few studies show that the cross-tropopause air mass flux has a late spring/early summer maximum in the Northern Hemisphere (Appenzeller and Holton, 1996; Gettelman and Sobel, 2000; Seo and Bowman, 2002; Schoeberl, 2004). James et al. (2003), however, argue that deep intrusion events, which are effective in transporting stratospheric air into the lower troposphere, have a clear winter maximum. In general most studies find that the maximum distributions of STE are associated with midlatitude baroclinic activities, which usually occur during the winter, such as cut-off cyclones and tropopause folds within the storm tracks. The relative STE locations within the storm tracks are quite different for the different studies (Gettelman and Sobel, 2000; Seo and Bowman, 2002; Stohl et al. 2003; Sprenger and Wernli, 2003). On the other hand, studies focusing on isentropic mass flux across the subtropical jet find the summer/fall maximum in the subtropics, associated with summer monsoon and large-scale wave breaking over the Pacific and Atlantic oceans (Chen, 1995; Postel and Hitchman, 1999; Jing et al., 2004). Deep tropical intrusions of O<sub>3</sub> occur in equatorial westerly ducts (regions of westerly winds in the tropics bounded by the zero-wind lines), preferentially in the winter (Waugh and Polvani, 2000; Waugh and Funatsu, 2003). On the smaller scale however, lightning during thunderstorms provides an important O<sub>3</sub> precursor, NO<sub>x</sub>.

Lightning is an important source of  $\text{NO}_x$ , particularly for the upper troposphere (Ridley et al., 1996; DeCaria et al., 2000). Though lightning accounts for only roughly 15% of the  $\text{NO}_x$  input to the troposphere (Bradshaw et al., 2000), lightning  $\text{NO}_x$  is primarily found in the upper troposphere (Pickering et al., 1998) where its lifetime is longer and its  $\text{O}_3$  producing potential greater (Liu et al., 1987; Pickering et al., 1990) than in the boundary layer, where the majority of  $\text{NO}_x$  is added to the atmosphere (DeCaria et al., 2005). Zhang et al. (2003) have shown that summertime lightning plays a dominant role in controlling middle and upper tropospheric  $\text{NO}_x$  and  $\text{O}_3$  over the United States with a global source strength of  $7 \text{ TgN yr}^{-1}$ . However, the uncertainty in global lightning  $\text{NO}$  production stems from two primary sources: the global flash rate and the production of  $\text{NO}$  per flash (DeCaria et al., 2005). Although lightning can bring  $\text{NO}_x$  down from the upper troposphere it is more widely believed that tropospheric  $\text{O}_3$  is formed within the lower troposphere itself.

In the early 1970s, Crutzen (1973) and Chameides and Walker (1973) suggested instead that the troposphere  $\text{O}_3$  originates mainly from production within the troposphere by photochemical oxidation of  $\text{CO}$  and hydrocarbons catalyzed by  $\text{NO}_x$  and  $\text{HO}_x$  ( $\text{OH} + \text{HO}_2$ ). The term “photochemical” air pollution reflects the essential role of solar radiation in driving the chemistry. At the Earth’s surface, radiation of wavelengths 290 nm and greater –the so-called actinic region – is available for inducing photochemical reactions (Finlayson-Pitts and Pitts, 1997). By the mid1980s, global budget analyses indicated that chemical production of  $\text{O}_3$  within the troposphere was at least as large as transport from the stratosphere, although with large uncertainties due in part to limited observations of  $\text{NO}_x$  concentrations (e.g. Fishman 1985). Liu et al. (1987) calculated the in situ production of tropospheric  $\text{O}_3$  in the northern hemisphere by scaling hemispheric estimates of  $\text{NO}_x$  emissions with the  $\text{O}_3$  production efficiency ( $\text{O}_3$  molecules

produced per NO<sub>x</sub> molecule oxidized); they concluded that this in situ source of O<sub>3</sub> was much larger than transport from the stratosphere (Wang et. al 1998).

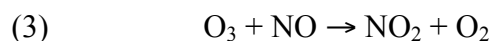
The sole known anthropogenic source of tropospheric O<sub>3</sub> is the photolysis of NO<sub>2</sub>. This produces the ground-state oxygen atoms, O (3P) which then react with O<sub>2</sub> in the presence of M to create O<sub>3</sub> as summarized in Finlayson-Pitts and Pitts, 2000.



followed by



The photolysis of NO<sub>2</sub> to produce O<sub>3</sub> is then reversed by the reaction of O<sub>3</sub> with NO thus completing the “nitrogen cycle”.

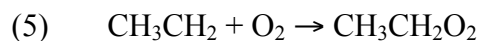


Reactions 2 and 3 are comparatively fast. Therefore, the slower photolysis reaction (1) is usually the rate-limiting reaction for the nitrogen cycle and the reason why O<sub>3</sub> is not formed in abundance at night. It is also the reason why O<sub>3</sub> concentrations are higher during the summer months, when temperatures are high and the solar radiation influx is at a max. The nitrogen cycle operates fast enough to derive a photostationary-state equation:

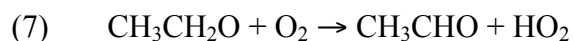
$$[\text{O}_3] = (k_1/k_3) \times [\text{NO}_2]/[\text{NO}]$$

The net effect of the nitrogen cycle however, neither generates nor destroys O<sub>3</sub>. Since NO<sub>2</sub> is important, there needs to be a way to convert NO to NO<sub>2</sub> without destroying O<sub>3</sub>. Most NO<sub>2</sub> is formed by the oxidation of NO (the major nitrogenous byproduct of combustion) after dilution in air, some NO<sub>2</sub> is emitted directly into the atmosphere by combustion processes. This conversion of NO to NO<sub>2</sub> occurs as part of the oxidation of hydrocarbons (RH) and VOCs,

initiated by reactive species such as the OH (Hydroxyl) radical. A simple example using ethane is provided below.



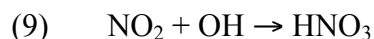
Reaction (5) produces the alkyl peroxy radical,  $\text{RO}_2$  (where  $\text{CH}_3\text{CH}_2 = \text{R}$ ) which oxidizes NO to  $\text{NO}_2$  as shown below.



Reaction (7) produces the hydroperoxy radical,  $\text{HO}_2$  which also oxidizes NO to  $\text{NO}_2$  as shown below.

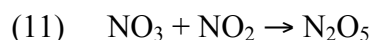
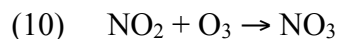


Once NO is converted to  $\text{NO}_2$ , a variety of potential reaction paths are available. These include the photolysis to form ground-state oxygen atoms O (3P) which generate  $\text{O}_3$  as mentioned in reactions (1) and (2) as well as the reaction with OH to form nitric acid in reaction (9).



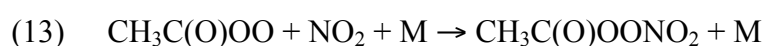
Reaction (9) is one way  $\text{NO}_2$  is removed from the atmosphere, reducing  $\text{O}_3$  levels. Nitric acid ( $\text{HNO}_3$ ) is usually removed by surface deposition or rain.

When there are sufficient concentrations of both  $\text{NO}_2$  and  $\text{O}_3$ , the nitrate radical ( $\text{NO}_3$ ) and dinitrogen pentoxide ( $\text{N}_2\text{O}_5$ ) are formed. This pathway is ineffective in the daytime however, because  $\text{NO}_3$  photolyzes back to  $\text{NO}_2$  on a time scale of the order of 10 s (Jacob, 2000).



Like OH, NO<sub>3</sub> reacts with organics to initiate their oxidation. NO<sub>3</sub> has been detected in both polluted and remote regions and is believed to be the driving force in the chemistry at night when the photolytic production of OH shuts down (Finlayson Pitts and Pitts, 1997).

Formation of CH<sub>3</sub>C(O)OONO<sub>2</sub> (peroxyacetylnitrate, abbreviated as PAN) is another sink for NO<sub>x</sub> in hydrocarbon-rich environments. It takes place for example by oxidation of acetaldehyde.



The main sink for PAN in most of the troposphere is thermolysis, regenerating NO<sub>x</sub> (Jacob, 2000).



The lifetime of PAN against thermolysis is about 1 h at 295 K but several months at 240 K. PAN is an important contributor to total NO<sub>y</sub> (sum of NO<sub>x</sub> and its oxidation products) in polluted regions such as the eastern United States (Parrish et al., 1993). Long-range transport of PAN at high altitude (low temperature) is a major source of NO<sub>x</sub> in the remote troposphere (Moxim et al., 1996).

Although VOCs are necessary to generate high concentrations of O<sub>3</sub>, NO<sub>x</sub> emissions can be the determining factor in the peak O<sub>3</sub> concentrations observed in many locations (Chameides, 1992). VOCs are emitted from both natural and anthropogenic sources. Statewide, natural VOC sources dominate, primarily from vegetation. However, in urban and suburban areas, anthropogenic VOC emissions dominate and, in conjunction with anthropogenic NO<sub>x</sub> emissions, lead to the peak concentrations of O<sub>3</sub> observed in urban areas and areas downwind of major urban areas (California, EPA).

The relative balance of VOCs and NO<sub>x</sub> at a particular location helps to determine whether the NO<sub>x</sub> behaves as a net O<sub>3</sub> generator or a net O<sub>3</sub> inhibitor. When the VOC/NO<sub>x</sub> ratio in the ambient air is low (NO<sub>x</sub> is plentiful relative to VOC), NO<sub>x</sub> tends to inhibit O<sub>3</sub> formation. In such cases, the amount of VOCs tends to limit the amount of O<sub>3</sub> formed, and the O<sub>3</sub> formation is called “VOC-limited”. When the VOC/NO<sub>x</sub> ratio is high (VOC is plentiful relative to NO<sub>x</sub>), NO<sub>x</sub> tends to generate O<sub>3</sub>. In such cases, the amount of NO<sub>x</sub> tends to limit the amount of O<sub>3</sub> formed, and O<sub>3</sub> formation is called “NO<sub>x</sub>-limited”.

One of the approaches to explain NO<sub>x</sub> and VOCs interactions in O<sub>3</sub> formation is the isopleths curve (Figure 1). The x-axis in this graph displays increasing concentrations of VOCs from left to right, while the y-axis displays increasing concentrations of NO<sub>x</sub> from bottom to top. The isopleths –these are the c-shaped curves in the body of the graph that represent increasing concentrations of O<sub>3</sub> from the bottom left corner to the top right corner; the concentration of O<sub>3</sub> remains constant along each isopleth but changes when going from one isopleth to another.

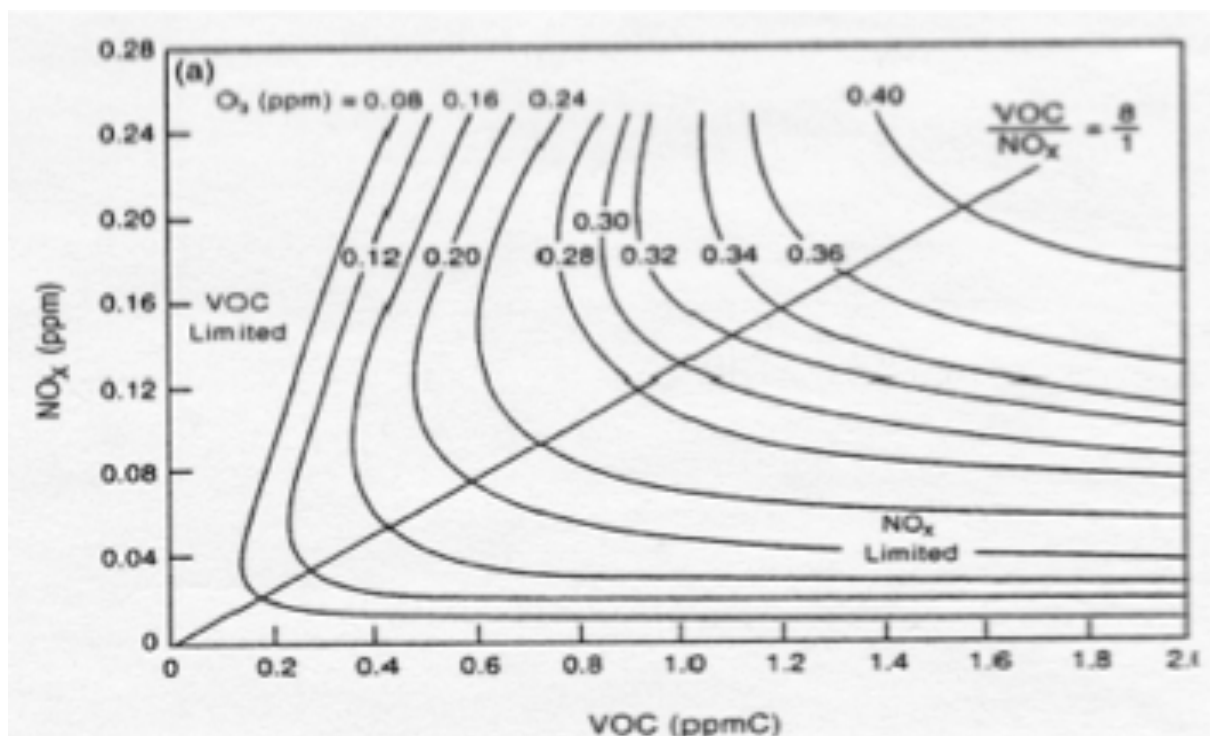


Figure 1.1 Typical O<sub>3</sub> isopleths. Source: Adapted from Finlayson-Pitts and Pitts, 2000

The isopleths are used for determining O<sub>3</sub> levels at specific combinations of NO<sub>x</sub> and VOCs in the atmosphere and to determine whether a region is NO<sub>x</sub> or VOCs limited. If a region is satiated in the bottom right corner of the graph, it is NO<sub>x</sub> limited since the amount of NO<sub>x</sub> determines the amount of O<sub>3</sub> created. This is because an increase in NO<sub>x</sub> moves the point to another isopleth with higher O<sub>3</sub> concentrations whereas an increase in VOCs only moves the point in question along the same isopleth, not increasing the O<sub>3</sub> concentration. If a region is situated in the upper left corner of the graph, it is VOCs limited since the amount of VOCs determines the amount of O<sub>3</sub> created. This is because an increase in VOCs moves the point to another isopleth with higher O<sub>3</sub> concentrations while an increase in NO<sub>x</sub> may actually move the point in question towards a decreasing O<sub>3</sub> concentration. The VOC/NO<sub>x</sub> ratio can differ substantially by location and time of day within a geographic area. Furthermore, the VOC/NO<sub>x</sub> ratio measured near the ground might not represent the ratio that prevails in the air above the ground where most of the tropospheric O<sub>3</sub> is generated (California, EPA), leading to an investigation of the transport of O<sub>3</sub>.

### 1.3 O<sub>3</sub> Transport

Even though the lifetime of the major oxidant precursors, NO<sub>x</sub> and reactive hydrocarbons may only be 1-2 days in the lower troposphere, the O<sub>3</sub> they form has a lifetime of days to months (Wild and Akimoto, 2001). In fact, Liu et al. (1987) calculated the photochemical lifetime of O<sub>3</sub> in the winter in the mid latitudes to be approximately 200 days, and about a week during the summer. Typical transport times between continents are 5-10 days, and there is significant potential for one continental region to affect another, suggesting that regional pollution should be considered in a global context (Wild and Akimoto, 2001). The lifetime of tropospheric O<sub>3</sub> in a

sufficiently aged photochemical air mass is dependent on proximity to the earth's surface (where deposition or chemical destruction by fresh injections of NO can occur), and on the distribution of water vapor and the amount of solar radiation available (Fishman et al., 1990). Therefore, the abundance and distribution of O<sub>3</sub> in the atmosphere is determined by complex interactions between meteorology and chemistry.

There are an increasing number of studies which attempt to assess impacts of pollution in the industrialized regions such as the United States, Europe, and Asia on the regional and hemispheric levels of oxidants including O<sub>3</sub> (Holloway et al., 2003). These studies generally pay a particular attention to the major long-range transport pathways in the Northern Hemisphere such as the typical transport pathway from Asia to North America across the Pacific (the trans-Pacific). Stohl et al. (2002) examined pathways and timescales for intercontinental transport of passive CO tracers using a Lagrangian model (Sudo and Akimoto, 2007).

Jaffe et al. (1999) showed that a number of primary and secondary industrial pollutants (e.g. carbon monoxide (CO), peroxyacetyl nitrate (PAN), aerosols, non-methane hydrocarbons (NMHCs)) were transported across the Pacific to Washington State during an episode in March 1997. Springtime is when trans-Pacific transport is thought to be the most efficient due to prefrontal flow lofting pollutants from the surface followed by southeastward moving cold fronts which transport the pollutants above the boundary layer (Liu et al., 2003).

Berntsen et al. (1999) and Jacob et al. (1999,2003) studied transport of O<sub>3</sub> and related species over the trans-Pacific pathway and evaluated influences of Asian emissions on air quality in the United States. Li et al., (2002) and Auvray and Bey (2005) similarly investigated impacts of long-range transport from Asia and North America on surface O<sub>3</sub> levels in Europe. In addition, Wild et al. (2004) examined the characteristics of the trans-Eurasian transport and

assessed impacts of European and North American anthropogenic emissions on surface O<sub>3</sub> and CO in eastern Asia (Sudo and Akimoto, 2007).

Major episodes of O<sub>3</sub> concentrations in the eastern United States and in Europe are associated with slow moving high pressure systems. High pressure systems during the warmer seasons are associated with the sinking of air, resulting in warm, generally cloudless conditions, with light winds. The sinking of air results in the development of stable conditions near the surface which inhibit or reduce the vertical mixing of O<sub>3</sub> precursors. The combination of inhibited vertical mixing and light winds minimizes the dispersal of pollutants emitted in urban areas, allowing their concentrations to build up. Photochemical activity involving these precursors is enhanced because of higher temperatures and the availability of sunlight. In the eastern United States, high O<sub>3</sub> concentrations during a large scale episode can extend over a hundred thousand square kilometers for several days (EPA 2006).

After the O<sub>3</sub> concentration builds up, it can be transported in various ways such as through airstreams which are associated with synoptic weather systems. For instance, the pseudo-Lagrangian conveyor belt model (Carlson, 1980; Browning, 1990; Browning and Roberts, 1994, 1996) describes three characteristic streams in a coordinate system moving with a synoptic system: the warm conveyor belt (WCB), the cold conveyor belt (CCB), and the dry intrusion. The WCB is an ascending airstream at the leading edge of a trough (Browning, 1990), the CCB is an airflow ahead of a surface warm front, and the dry intrusion is a descending airstream related to tropopause folding (Browning, 1997). Wernli and Davies (1997) and Wernli (1997) explored the Lagrangian characteristics of these airstreams and found that especially the WCB and the dry intrusion are associated with coherent ensembles of trajectories (CETs) exhibiting strong vertical motions. Bethan et al. (1998) demonstrated the capacity of the

airstreams for causing strong gradients in trace gas concentrations near fronts. Evidence suggests that a coherent long-range transport of O<sub>3</sub> is within a WCB (Stohl and Trickl, 1999).

Another form of transport for O<sub>3</sub> are Low-Level Jets (LLJ). LLJ can transport pollutants hundreds of kilometers from their source. Nocturnal low-level jets are coincident with synoptic weather patterns involved with high O<sub>3</sub> episodes implying that they may play an important role in the formation of severe O<sub>3</sub> events (Rao and Zurbenko, 1994). Nocturnal LLJs form at night in the residual boundary layer (see figure). During calm conditions, the planetary boundary layer is stably stratified and as a result vertical mixing is inhibited at night. On cloud-free evenings the LLJ begins to form shortly after sunset. The wedge of cool air in the stable nocturnal boundary layer decouples the surface layer from the residual layer and acts like a smooth surface allowing the air just above it (in the residual layer) to flow rapidly past the inversion mostly unencumbered by surface friction (Stull, 1988). The width of the jet can vary from location to location and from one weather pattern to another, but it is typically less than several hundred km and not greater than 1000 km long. In extreme cases, winds in a LLJ can exceed 60 ms<sup>-1</sup> but average speeds are typically in the range of 10 to 20 ms<sup>-1</sup>. As the sun rises, its energy returns to heat the land and the lower atmosphere begins to mix as the warm air rises. The jet diminishes as the nocturnal temperature inversion erodes and surface friction slows wind speeds. If stable synoptic conditions persist, the same conditions the next night could allow the low-level jet to reform with equal strength and similar consequences. LLJ formation results in vertical wind shear that induces mixing between the otherwise stratified layers (EPA 2006).

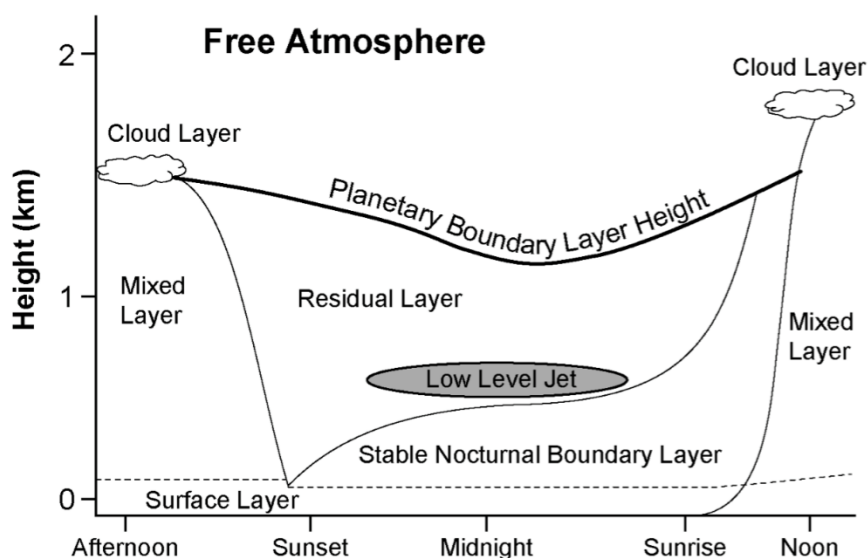


Figure 1.2. The diurnal evolution of the planetary boundary layer while high pressure prevails over land. Three major layers exist (not including the surface layer): a turbulent mixed layer; a less turbulent residual layer which contains air formerly in the mixed layer; and a nocturnal, stable boundary layer which is characterized by periods of sporadic turbulence. Source: Adapted from Stull (1988)

LLJs are often associated with mountain ranges. Mountains and pressure gradients on either side of a developing LLJ help concentrate the flow of air into a corridor or horizontal stream (Hobbes et al., 1996). LLJs commonly form east of the Rocky Mountains and east of the Appalachian Mountains (Bonner, 1968). However, Bao et al., 2008 shows evidence of a LLJ forming in the San Joaquin Valley. Once the marine air enters the Central Valley, it splits into northward and southward flows because of the blocking effect of the Sierra Nevada. There is a diurnal change in the intensity of the incoming marine flow, leading to the diurnal variation of both the northward and southward flows. During the night, the southward flow experiences a nocturnal acceleration, which leads to the formation of the nocturnal low-level jet in the San Joaquin Valley (Bao et al., 2008).

Nocturnal LLJs are not unique to the United States; they have been detected in many other parts of the world (Corsmeier, 1997, Reitebuck, et al., 2000). Corsmeier et al. (1997)

observed secondary maxima in the surface O<sub>3</sub> at nighttime at a rural site in Germany (see figure), supporting the notion that downward transport from the residual layer was occurring. The secondary maxima were, on average, 10% of the next day's O<sub>3</sub> maximum but at times could be as much as 80% of the maximum (Corsmeier et al., 1997). The secondary O<sub>3</sub> maxima were well correlated with an increase in the wind speed and wind shear. The increased vertical shear over the very thin layer results in mechanical mixing that leads a downward flux of O<sub>3</sub> from the residual to the near surface layer. Analysis of wind profiles from aerological stations in northeastern Germany revealed the spatial extent of that particular LLJ was up to 600 km in length and 200 km in width. The study concluded the importance of O<sub>3</sub> transport by LLJs was twofold: O<sub>3</sub> and other pollutants could be transported hundreds of kilometers at the jet core level during the night and then mixed to the ground far from their source region. Salmond and McKendry (2002) also observed secondary O<sub>3</sub> maxima (in the Lower Fraser Valley, British Columbia) associated with LLJs that occasionally exceeded half the previous day's maximum O<sub>3</sub> concentration. The largest increases in surface O<sub>3</sub> concentration occurred when boundary layer turbulence coincided with O<sub>3</sub> levels greater than 80 ppb were observed aloft. In addition, the study suggests horizontal transport efficiency during a LLJ event could be as much as six times greater than transport with light winds without an LLJ. Reitebuch et al. (2000) observed secondary O<sub>3</sub> maxima associated with LLJ evolution in an urban area in Germany (EPA 2006).

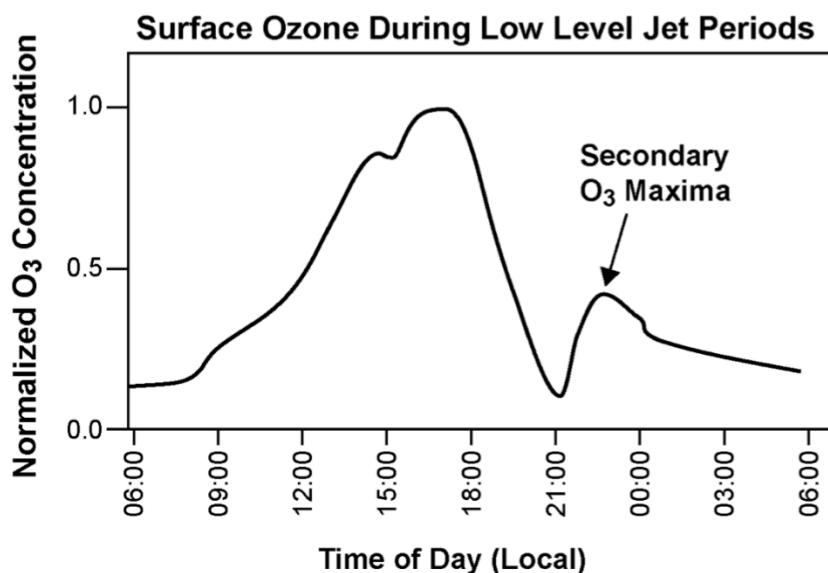


Figure 1.3. Schematic diagram showing the diurnal behavior of O<sub>3</sub> and the development of secondary O<sub>3</sub> maxima resulting from downward transport from the residual layer when a low-level jet is present. Source: Adapted from Reitbuch et al. (2000); Corsmeier et al. (1997); and Salmond and McKendry (2002).

Transport of pollutants within mesoscale weather systems has been observed to occur as well. These systems include sea-land breezes, upslope-downslope winds and circulations driven by the urban heat island. The circulations associated with these phenomena typically occur on spatial scales of tens of kilometers. The sea-land breeze affects many urban areas such as Washington, Baltimore, Philadelphia, New York, Chicago (as a lake breeze), Houston and Los Angeles. All of these locations have experienced high O<sub>3</sub> concentrations as a result of the sea-land breeze.

During the day, heating of the land surface results in upward motion that is compensated by air flowing in from the adjacent water body, i.e., the sea breeze or the lake breeze. Winds gradually rotate with height to produce a return flow aloft. This circulation generally reaches maximum strength in the late afternoon. Afterwards, the sense of the circulation is reversed and a land breeze develops, which reaches maximum strength shortly after the land-sea temperature

contrast is largest. This also implies that winds are rotating at the surface as the sense of the circulation changes. The circulation can interact with the larger synoptic scale flow pattern to either attenuate surface winds or to increase them.

Because of these effects, sea-land breezes can exert significant effects on concentration of pollutants emitted in coastal areas. If there is onshore flow (sea breeze) when there is opposing large scale flow, a transition zone (known as a sea breeze front) in which convergence of the opposing flows forms. In this zone, horizontal winds are weak. Furthermore, air pollutants are concentrated and are transported upwards. This situation was found during O<sub>3</sub> episodes occurring in Houston in August 2000, in which a “wall of pollution” formed (Banta et al., 2005). If the sea breeze is dominant, it can transport pollutants well inland, even to central-eastern Texas. During the land breeze phase, pollutants at the surface tend to be transported out over the adjacent water body, resulting in dilution and dispersion of pollutants (EPA 2006).

Like the sea-land breeze, in areas of complex terrain thermally driven slope winds can set up. Slope winds blow parallel to the incline of the valley sidewalls and are driven by buoyancy forces produced by temperature differences between the air adjacent to the slope and the ambient air at the same altitude. Heating during the day and radiative cooling at night near the surface contribute to this temperature differential. The daytime flow is typically upslope (anabatic flow) whereas the nighttime flow is downslope (katabatic flow). As a result of the cooler air draining into the basin at night and the stably stratified air, an inversion develops which inhibits vertical mixing allowing for pollutants to build up. When the sun comes up, the upslope flow breaks up the inversion allowing the polluted air to get mixed and transported out of the basin. Slope currents are characterized by sustained wind speeds, typically 1 to 5 ms<sup>-1</sup>, and the transition between slope flows in the early morning and in the late afternoon is characterized by periods of

very low winds  $< 0.5 \text{ ms}^{-1}$ . Associated with such low winds are the reduced dispersion and transport that contribute to serious air pollution problems which are known to plague many complex-terrain airsheds (Whiteman, 1990) which lead to negative impacts of  $\text{O}_3$  on health and the environment in these regions.

#### 1.4 $\text{O}_3$ Impacts

High concentrations of near-surface  $\text{O}_3$  are known to have negative impacts on human health, vegetation, materials, climate, and atmosphere composition (WHO, 2000). Associations between air pollution and multiple health effects are now well established (Pope 2007; Pope and Dockery 2006; Pope et al. 2002). For key pollutants such as particulate matter (PM) and  $\text{O}_3$  (Green et al. 1999), there are no established thresholds of exposure below which population health impacts are absent. Given that everyone is exposed to some level of air pollution, the attributable health burden can be high, particularly for vulnerable subpopulations. Recent evidence that air pollution leads to inflammatory processes that mediate a variety of diseases suggests an expanding range of health impacts related to air pollution exposure (Giles et al. 2011).

According to McClellan et al. (2009)  $\text{O}_3$  affects the human respiratory system in several ways.  $\text{O}_3$  is a highly reactive gas that is deposited throughout the entire respiratory tract from the airways to the alveoli. Its solubility in water is greater than that of oxygen and its oxidant nature renders it able to react with almost any biomolecule along the respiratory tract. The solubility and reactivity likely account for the reported approximately 40% uptake of inspired  $\text{O}_3$  by the human nasopharynx (in contrast to  $\text{SO}_2$ , which is  $>98\%$ ). Dosimetry models predict that the tissue dose of inhaled  $\text{O}_3$  is greatest at the bronchoalveolar junction, which is the pulmonary region experimentally most sensitive to  $\text{O}_3$ . Recent  $\text{O}_3$  bolus studies in humans have confirmed

that inspired O<sub>3</sub> reaches the distal airways and alveoli of sedentary volunteers, and during exercise O<sub>3</sub> penetrates deeper and in greater amounts to the distal lung regions. Thus, O<sub>3</sub> can affect the entire respiratory tract but maneuvers such as exercise or oral breathing alter regional deposition of the gas. In addition to effects on pulmonary mechanics, exposure to O<sub>3</sub> at levels near the current National Ambient Air Quality Standard (NAAQS) causes cellular and biochemical changes in the upper and lower respiratory tracts characteristic of an acute inflammatory response. Respiratory tract inflammation and increased cellular permeability are two of the best-studied biological markers of O<sub>3</sub>-induced mechanisms of lung injury in animals, including humans.

The US EPA (2006) states that the responses observed in young healthy nonsmoking human adults exposed to ambient O<sub>3</sub> concentrations include decreased inspiratory capacity; mild bronchoconstriction; rapid, shallow breathing pattern during exercise; and symptoms of cough and pain on deep inspiration. Specifically, that young healthy adult subjects exposed in clinical studies to O<sub>3</sub> concentrations  $\geq 0.08$  ppm for 6 to 8h during moderate exercise exhibit symptoms of cough and pain on deep inspiration. An increase in the incidence of cough has been found in clinical studies as low as 0.12 ppm in healthy adults during 1 to 3 h with very heavy exercise and other respiratory symptoms, such as pain on deep inspiration and shortness of breath, have been observed at 0.16 ppm to 0.18 ppm with heavy and very heavy exercise. These O<sub>3</sub> induced respiratory symptoms gradually decrease in adults with increasing age.

In addition the US EPA (2006) says that O<sub>3</sub> has been shown to result in airway hyperresponsiveness as demonstrated by an increased physiological response to a nonspecific bronchoconstrictor, as well as airway injury and inflammation assessed via bronchoalveolar lavage and biopsy. Reflex inhibition of inspiration and consequent decrease in inspiratory

capacity results in a decrease in forced vital capacity (FVC) and total lung capacity (TLC) and, in combination with mild bronchoconstriction, contributes to a decrease in the forced expiratory volume in 1 second (FEV<sub>1</sub>).

Human studies consistently report that inhalation of O<sub>3</sub> alters the breathing pattern without significantly affecting minute ventilation. A progressive decrease in tidal volume and a “compensatory” increase in frequency of breathing to maintain steady minute ventilation during exposure suggests a direct modulation of ventilatory control. These changes parallel a response of many animal species exposed to O<sub>3</sub> and other lower airway irritants (Tepper et al., 1990). Although alteration of a breathing pattern could be to some degree voluntary, the presence of the response in animals and the absence of perception of the pattern change by subjects, even before appearance of the first subjective symptoms of irritation, suggests an involuntary reflex mechanism (US EPA 2006).

The US EPA synthesis of ambient O<sub>3</sub> health effects concludes that children with asthma suffer acute adverse health consequences at current ambient levels of O<sub>3</sub> (US EPA 2006). A study done by Moore et al. (2008) focusing on southern California has conducted exhaustive analyses to address many of the outstanding issues related to reported associations between O<sub>3</sub> and the use of hospital services for children with asthma. They have concluded that ambient O<sub>3</sub> (highly oxidant, ambient, warm-season environments) causes increases in hospital admissions in children with asthma. Moreover, the linearity of the relation observed indicates that these excess asthma hospital discharges can be expected to continue at levels of air quality experienced in southern California.

Most O<sub>3</sub> exposure studies in humans with existing respiratory disease have focused on lung diseases like COPD and asthma. However, chronic inflammatory disorders of the nasal

airway, especially allergic rhinitis, are very common in the population. People with allergic rhinitis have genetic risk factors for the development of atopy that predispose them to increased upper airway responsiveness to specific allergens as well as nonspecific air pollutants like O<sub>3</sub>. O<sub>3</sub> exposure of subjects with allergic rhinitis has been shown to induce nasal inflammation and increase airway responsiveness to nonspecific bronchoconstrictors, although to a lesser degree than experienced by asthmatics (US EPA 2006).

O<sub>3</sub> has also been shown to have cardiovascular impacts. US EPA (2006) says that direct O<sub>3</sub> effects such as O<sub>3</sub> induced release from lung epithelial cells of platelet activation factor (PAF) that may contribute to blood clot formation that would increase the risk of serious cardiovascular outcomes (e.g., heart attack, stroke, mortality). Also, interactions of O<sub>3</sub> with surfactant components in epithelial lining fluid of the lung results in production of oxysterols and reactive oxygen species that may exhibit PAD-like activity contributing to clotting and/or exert cytotoxic effects on lung and heart cells.

A recent study done by Jarrett et al. (2009) investigated the effect of tropospheric O<sub>3</sub> on the risk of death from any cause and cause-specific death in a large cohort, using data from 96 metropolitan statistical areas across the United States and controlling for the effect of particulate air pollutants. Even though they were unable to detect a significant effect of exposure to O<sub>3</sub> on the risk of death from cardiovascular causes when particulates were taken into account, they did demonstrate a significant effect of exposure to O<sub>3</sub> on the risk of death from respiratory causes. They found for every 10-ppb increase in exposure to O<sub>3</sub>, there was an increase in the risk of death from respiratory causes. They have determined that the risk of dying from a respiratory cause is more than three times as great in the metropolitan areas with the highest O<sub>3</sub> concentrations as in those with the lowest O<sub>3</sub> concentrations.

When plants are grown in an atmosphere enriched with O<sub>3</sub>, visible signs of injury may appear within a few hours or days, or in the absence of these signs of acute injury, leaf discoloration as a sign of long-term effects may develop in the course of the growing season. The occurrence of leaf injury symptoms in areas with substantial photochemical air pollution was first observed in the mid-1940s in the Los Angeles basin and later in New England, and the cause was identified during the 1950s. Since then, symptoms were also recorded in other parts of the U.S., in Mexico, and large parts of Europe and Asia. Because of concerns over significant negative effects of O<sub>3</sub> on crop yields, large-scale experiments were initiated in the US and Europe (Fuhrer 2001).

The U.S. Forest Service in cooperation with other federal and state agencies developed a network of O<sub>3</sub> bioindicators to detect the presence of O<sub>3</sub> in forested systems throughout the United States (Smith et al., 2003). This ongoing program was initiated in 1994; and 33 states currently participate. In a coordinated effort, a systematic grid system is used as the basis of plot selection and field crews were trained to evaluate O<sub>3</sub> symptoms on sensitive plant species within the plots (Coulston et al., 2003; Smith et al., 2003). The network has provided evidence of O<sub>3</sub> concentrations high enough to induce visible symptoms on sensitive vegetation. From repeated observations and measurements made over a number of years, specific patterns of areas experiencing visible O<sub>3</sub> injury symptoms can be identified (US EPA 2006).

O<sub>3</sub> affects vegetation by direct cellular damage once it enters the leaf through the stomates, so that O<sub>3</sub> uptake is a function of both ambient O<sub>3</sub> levels and stomatal conductance (Mauzerall and Wang, 2001). The cellular damage is probably the result of changes in membrane permeabilities and may or may not result in visible injury or reduced growth or yield (Krupa and Manning, 1988). A secondary response to O<sub>3</sub> is a reduction in stomatal conductance,

as the stomates close in response to increased internal CO<sub>2</sub> (Reich, 1987). Stomates generally open in response to light and warmth and close in response to aridity, water stress, and high CO<sub>2</sub> (Mauzerall and Wang, 2001). It has been suggested that the decrease in stomatal conductance caused by O<sub>3</sub> is similar in magnitude to that caused by CO<sub>2</sub> increases since preindustrial conditions (Taylor and Jonson, 1994). Tjoekler et al. (1995) found a decoupling of photosynthesis from stomatal conductance as a result of long-term O<sub>3</sub> exposure. Such a decoupling implies that O<sub>3</sub>-induced reductions in photosynthesis would also be accompanied by decreased water use efficiency, resulting in even larger productivity reductions, particularly at arid sites (Ollinger et al., 1997).

There is, of course, an economic cost associated with this reduced productivity. Some national studies have found that a 25% reduction in ambient O<sub>3</sub> would provide benefits of at least 1-2 billion dollars annually in the United States (Adams and Crocker 1989). Further, Mauzerall and Wang (2001) cite several recent studies estimating benefits of 2-3.3 billion dollars in the U.S. by eliminating O<sub>3</sub> precursors from motor vehicle emissions (Murphy et al. 1999), and 310 million € in the Netherlands (Kuik et al. 2000), and 2 billion dollars in China (Mauzerall and Wang 2001) by reducing O<sub>3</sub> to background levels. Also, due to the non-linear shape of many crop-O<sub>3</sub> dose-response curves, we might expect a disproportionately larger effect for each unit increase in global average O<sub>3</sub> concentrations (Fiscus et al. 2005).

O<sub>3</sub> and other photochemical oxidants react with many economically important man-made materials, decreasing their useful life and aesthetic appearance. Much of what is known about O<sub>3</sub> effects on man-made materials however, is derived from research conducted in the 1970's, 1980's and early 1990's, with very little new research on the subject having been conducted since then (US EPA 2006). Some materials known to be damaged by O<sub>3</sub> include elastomers

(Lake and Mente 1992), fibers (Bogaty et al. 1952), dyes (Grosjean et al. 1989), and paints (Spence et al. 1975).

Because ozone is generated by photochemical processes, its levels can rise substantially on hot sunny days, particularly when these are associated with slow-moving anticyclonic weather systems and stagnant air that traps emissions in the boundary layer. Hence, the direct health impacts of high temperatures can potentially be exacerbated due to high ozone levels (Doherty et al. 2009). Thus it is important to understand the meteorology of the region.

### 1.5 Meteorology of Lake Tahoe

Lake Tahoe is a high altitude lake at 1900 m (6200 ft), and is separated from the Sacramento Valley by the Sierra Nevada divide, ranging from 2200 m (7200 ft) at the passes to 3050 m (10000 ft) at the summit of the Crystal Range. With the lower ridges of the Carson Range to the east which separate it from the Great Basin, this terrain forms a bowl-shaped basin that develops very strong, shallow subsidence and radiation inversions at all times throughout the year (Elliott-Fisk et al., 1996). The volume of the lake is  $156 \text{ km}^3$ , and its surface area is  $501 \text{ km}^2$ , 38% of the total basin area of  $1313 \text{ km}^2$  (Coats & Goldman, 2001). The eutrophication of the lake has been studied intensively since the early 1960s (Goldman, 1981) and has attracted considerable political attention. In spite of increased land-use controls and export of treated sewage effluent from the basin, primary productivity of the lake is increasing by more than 5% annually, and its clarity is decreasing at an average rate of  $0.25 \text{ m yr}^{-1}$  (Reuter et al., 2000).

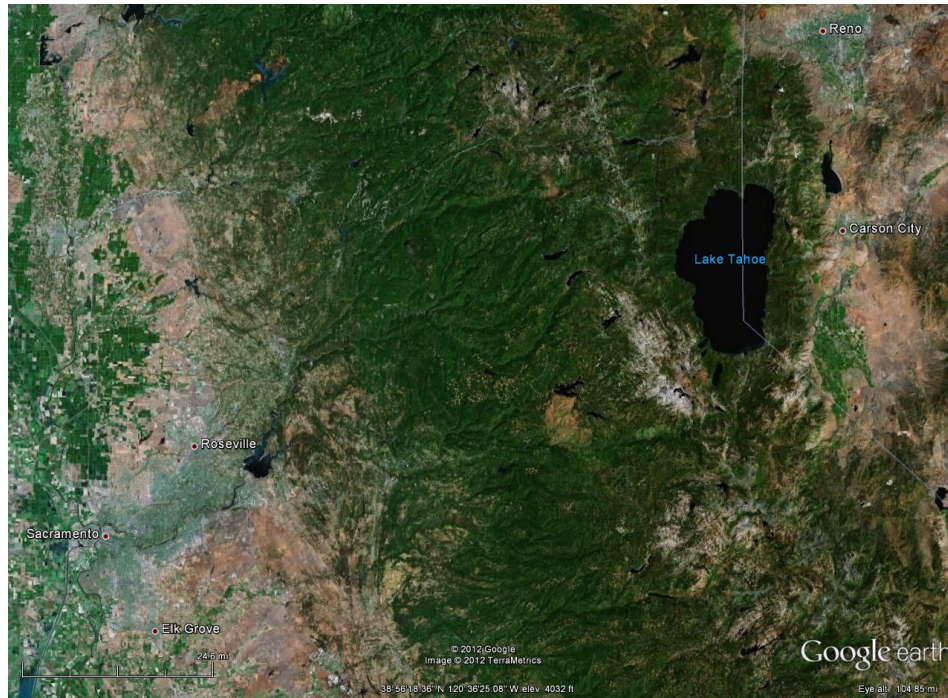


Figure 1.4. Image of Lake Tahoe and surrounding areas. Source: Google earth 2012

The Basin's climate is one of long cool-to-moderate winters and short moderate-to-warm summers and is a function of the latitude, proximity to the Pacific Ocean, and the elevation of the Basin. Interannual climatic variability on the west coast is known to be related to the indices of El Nino-Southern Oscillation, or ENSO (Wolter and Timlin, 1998) and the Pacific Decadal Oscillation, or PDO (Mantua et al., 1997). Positive values of the PDO are associated with warmer winters and springs in the eastern North Pacific and western North America. El Nino/Southern Oscillation (ENSO) is a high frequency (i.e. 2-5 years) coupled ocean-atmosphere process in the eastern and central equatorial Pacific Ocean and, through teleconnections with mid-latitude climate systems, is the primary driver of North American interannual climatic variability (Diaz & Markgraf, 2000). During El Nino conditions (warm phase ENSO), the SW is

typically wet, and dry conditions prevail during La Nina (cool phase ENSO) events (Kahya & Dracup, 1995).

Precipitation occurs primarily between October and May, with winter precipitation predominately in the form of snow. Thunderstorms occur sporadically throughout the summer, but do not produce significant amounts of precipitation. There are many local climates within the Basin, due to topographic influences, as well as a pronounced rainshadow effect and decreasing precipitation from west to east across the Basin, with the Carson Range more arid than the main Sierra Nevada crest to the west (Elliott-Fisk et al., 1996). A unique local meteorological impact for the Basin is the thermally-driven wind system known as the Washoe Zephyr.

#### 1.6 Washoe Zephyr

Thermally-driven wind systems are a common phenomenon found in mountainous regions throughout the world. These wind systems, along with the structure of the atmospheric boundary layer, are important for understanding the distribution and transport of atmospheric pollutants in mountainous areas, forest fire control, thunderstorm and precipitation, and wind energy potential (Furger et al. 2000; Zhong et al. 2008). Typically, under quiescent synoptic conditions, thermally-driven circulations in mountainous terrain blow up slope and up valley during the day and down slope and down valley at night. This is due to a horizontal temperature gradient between the air adjacent to the heated (daytime) or cooled (nighttime) slope surface and the ambient air at the same altitude (Atkinson 1981; Whiteman 1990; Zhong et al. 2008). Over the eastern slopes of the Sierra Nevada however, a daytime downslope flow occurs regularly during the summer season which goes against this local thermal forcing. This daytime downslope flow is known historically as Washoe Zephyr following author Samuel Clemens. The

flow is usually originated at the mountain crest and is generally strong in magnitude with peak speeds occurring in the afternoon or early evening. Strong winds associated with this downslope flow have been linked to dust storms in Carson City, NV (Twain, 1871; Zhong et al. 2008) as well as some of the convective activities occurring to the east of the Sierra crest (Hill 1980; Zhong et al. 2008). More recently, observations were made (Clements 1999) to investigate valley flows in an eastern Sierra valley. This study, which took place in Lee Vining Canyon during both summer and winter seasons, concluded that daytime down-slope winds were a regular feature of this canyon and had a distinct vertical structure. Furthermore, Kingsmill (2000) used a doppler sodar to investigate the vertical structure of this flow phenomena over a two-month period in Reno, Nevada (Clements and Zhong 2005). He found that the onset time of several Washoe Zephyr events sampled over the 2-month period varied significantly, ranging from 1200 to 1800 LST, as did their duration, which varied from 3 to 9 h. The sodar data also revealed the kinematic evolution of the downslope wind, which usually consisted of a downward shift of stronger westerly momentum at onset and an upward shift at decay, and a strong downward motion immediately before onset and strong upward motion just after decay.

According to Zhong et al. (2008) there are two hypotheses to explain the Washoe Zephyr wind system that appears to behave differently from the typical mountain slope circulations. The first hypothesis is that the flow is a result of the pressure difference between a mesoscale thermal low over the elevated desert topography in the interior of Nevada and higher pressure west of the Sierra Nevada (Hill 1980). The pressure difference, which usually peaks in the afternoon, draws air from west of the sierra crest down to the eastern slope, bringing more polluted air from the coastal region or from the Central Valley to areas in the Great Basin. Similar flows driven by the regional-scale pressure gradient associated with thermal lows have been found in the coast range

of California (Schroeder and Countryman 1960), in the Columbia basin of eastern Washington on the lee side of the Cascade Mountains (Doran and Zhong 1994), in the Mexico City basin (Bossert 1997), and at the Bolivian Altiplano (Egger et al. 2005; Zangl and Egger 2005; Zhong et al. 2008).

The Second hypothesis is that the strong surface downslope wind is caused by downward mixing of higher momentum aloft as the convective boundary layer over the eastern slopes of the Sierra Nevada grows above ridge-top levels where westerly winds usually prevail. Downward momentum transfer is considered a regular source for strong surface winds over areas of complex terrain. An example of strong surface winds as a result of downward momentum transfer is the afternoon wind system found in areas of the Rocky Mountains in Colorado (Banta 1984; King 1997; Zhong et al. 2008). Since the westerly wind aloft would be sheltered from surface pollutant emissions by the subsidence inversion usually present over California, the daytime downslope flows would bring air with only low background O<sub>3</sub> concentration to the surface. On the other hand, higher O<sub>3</sub> concentration from west of the Sierra Nevada would be brought into the Great Basin by the flow if the first hypothesis is correct (Zhong et al. 2008). One way to thoroughly examine these hypothesis and their impacts is through the use of meteorological and chemical modeling. However since the meteorological modeling data is fed into the chemical models, we must first assess the meteorological model and determine the most accurate output.

### 1.7 Weather Research and Forecast (WRF) Model

The importance of meteorological inputs on regional air quality modeling has been clearly stated (Pielke and Uliasz, 1998; Seaman, 2000) and consequently, the need to have a better insight on the sensitivity and performance of meteorological models. The planetary

boundary layer (PBL) scheme is an important meteorological parameterization used in these models. As surface-layer variables such as temperature, humidity and wind speed are simulated within the PBL scheme, they are fed back into the land-surface model (LSM) scheme which simulates outgoing radiation and soil moisture. These two processes interplay closely (Misensis and Zhang, 2010) therefore accurately simulating the meteorological processes within the PBL is critical for correctly simulating pollution events. Different PBL schemes adopt different assumptions regarding the transport of mass, moisture and energy, which may lead to differences in the boundary layer itself and subsequently the whole model domain (Hu et al. 2010). Two frequently used PBL schemes are the Yonsei University (YSU) scheme and the Mellor-Yamada-Janjic (MYJ) scheme. However the asymmetric convective model version 2 (ACM2) scheme is the default PBL scheme used by the Community Multiscale Air Quality (CMAQ) model (Hu et al. 2010). Hu et al. (2010) gives a detailed description of these three PBL schemes. The YSU PBL scheme (Hong et al. 2006) is a first order nonlocal scheme, with a countergradient term in the eddy-diffusion equation.

The YSU scheme is modified in WRF version 3 from the Hong et al. (2006) formulation by increasing the critical bulk Richardson number from zero to 0.25 over land, thereby enhancing mixing in the stable boundary layer (Hong and Kim 2008). The MYJ PBL scheme uses the 1.5-order turbulence closure model of Mellor and Yamada (1982) to represent turbulence above the surface layer (Janjic 1990, 1994, 2001). The MYJ scheme determines eddy diffusion coefficients from prognostically calculated turbulent kinetic energy. Mellor and Yamada (1982) argue that the scheme is appropriate for all stable and slightly unstable flows, but that errors are more likely as the flow approaches the free-convection limit. The ACM2 PBL scheme (Pleim 2007) includes a first-order eddy-diffusion component in addition to the explicit

nonlocal transport of the original ACM1 scheme (Pleim and Chang 1992). This modification is designed to improve the shape of vertical profiles near the surface. For stable or neutral conditions, the ACM2 scheme shuts off nonlocal transport and uses local closure. An evaluation of these three PBL schemes is crucial for accurate meteorological and chemical modeling of the Lake Tahoe Basin especially since this has not yet been done for this region.

### 1.8 Overall Goal and Specific Objectives

The purpose of this research is to investigate the ozone environment in the Lake Tahoe Basin in order to better understand the sources of ozone in the Basin. The methodology adopted was to first analyze the spatial and temporal patterns of ozone around the Basin, then to look at the synoptic-scale weather patterns associated with periods of higher ozone concentrations and finally to evaluate different PBL schemes within the WRF model in order to recommend the best meteorological modeling set-up to feed into chemical models. The ultimate goal of these studies is to aid agencies in developing recommendations and strategies that reduce pollution emissions and hence reduce the impacts on the lake environment and public health for the Lake Tahoe Basin. In order to achieve this goal, the dissertation is laid out in the following sections: chapter 2 – Surface Ozone in the Lake Tahoe Basin: Impact of Regional Meteorology, chapter 3 – Impact of Synoptic Scale Meteorology on Ozone Levels in the Lake Tahoe Basin, chapter 4 – Improving Air Quality Modeling for the Lake Tahoe Basin: Investigating Planetary Boundary Layer Schemes in the WRF Model, chapter 5 – Summary and Conclusions, and an Appendix which includes a paper submitted to Atmospheric Environment entitled “Surface Ozone in the Lake Tahoe Basin” and additional figures.

## References

- Adams, R. M. and Crocker, T. D. (1989). The agricultural economics of environmental change: some lessons from air pollution. *Journal of Environmental Management* 28, 295-307.
- Ancellet, G., Beekman, M., Papayannis, A., 1994. Impact of a cutoff low development on downward transport of ozone in the troposphere. *Journal of Geophysical Research* 99, 3451-3468.
- Appenzeller, C., and J. R. Holton (1996), Seasonal variation of mass transport across the tropopause, *J. Geophys. Res.*, 101, 15,071– 15,078.
- Atkinson, B. W., 1981: *Meso-Scale Atmospheric Circulations*. Academic Press, 495 pp.
- Auvray, M., and I. Bey (2005), Long-range transport to Europe: Seasonal variations and implications for the European ozone budget, *J. Geophys. Res.*, 110, D11303, doi:10.1029/2004JD005503.
- Banta, R. M., 1984: Daytime boundary-layer evolution over mountainous terrain. Part I: Observations of the dry circulations. *Mon. Wea. Rev.*, 112, 340–356.
- Banta, R. M.; Senff, C. J.; Nielsen-Gammon, J.; Darby, L. S.; Ryerson, T. B.; Alvarez, R. J.; Sandberg, S. P.; Williams, E. J.; Trainer, M. (2005) A bad air day in Houston. *Bull. Am. Meteorol. Soc.* 86: 657-669.
- Bao, J-W., S. A. Michelson, P. O. G. Persson, I. V. Djalalova, J. M. Wilczak, 2008: Observed and WRF-Simulated Low-Level Winds in a High-Ozone Episode during the Central California Ozone Study. *J. Appl. Meteor. Climatol.*, 47, 2372–2394. doi: 10.1175/2008JAMC1822.1

- Beekmann, M., Ancellet, G., Blonsky, S., De Muer, D., Ebel, A., Elbern, H., Hendricks, J., Kowol, J., Mancier, C., Sladkovic, R., Smit, H.G.J., Speth, P., Trickl, T., Van Haver, Ph., 1997. Regional and global tropopause fold occurrence and related ozone flux across the tropopause. *Journal of Atmospheric Chemistry* 28, 29-44.
- Bell, M. L., A. McDermott, S.L. Zeger, J.M. Samet, F. Dominici. 2004. Ozone and Short-term Mortality in 95 US Urban Communities, 1987-2000. *JAMA*, 292, 19:2372-2378.
- Berntsen, T. K., S. Karlsdóttir, and D. Jaffe (1999), Influence of Asian emissions on the composition of air reaching the North Western United States, *Geophys. Res. Lett.*, 26, 2171– 2174.
- Bethan, S., G. Vaughan, C. Gerbig, A. Volz-Thomas, H. Richer, and D. A. Tiddeman, Chemical air mass differences near fronts, *J. Geophys. Res.*, 103, 13,413–13,434, 1998.
- Bogaty, H.; Campbell, K. S.; Appel, W. D. (1952) The oxidation of cellulose by ozone in small concentrations. *Text. Res. J.* 22: 81-83.
- Bonner, W. D. (1968) Climatology of the low level jet. *Mon. Weather Rev.* 96: 833-850.
- Corsmeier, U.; Kalthoff, N.; Kollé, O.; Motzian, M.; Fiedler, F. (1997) Ozone concentration jump in the stable nocturnal boundary layer during a LLJ-event. *Atmos. Environ.* 31: 1977-1989.
- Bossert, J. E., 1997: An investigation of flow regimes affecting the Mexico City region. *J. Appl. Meteor.*, 36, 119–140.
- Bradshaw, J., D. Davis, G. Grodzinsky, S. Smyth, R. Newell, S. Sandholm, and S. Liu (2000), Observed distributions of nitrogen oxides in the remote free troposphere from the NASA Global Tropospheric Experiment programs, *Rev. Geophys.*, 38, 61–116.
- Brewer, A. M. (1949), Evidence for a world circulation provided by the measurements of helium

- and water vapor distribution in the stratosphere, *Q. J. R. Meteorol. Soc.*, 75, 351–363.
- Browning, K. A., Organization of clouds and precipitation in extratropical cyclones, in *Extratropical Cyclones: The Erik H. Palmén Memorial Volume*, edited by C. Newton and E. Holopainen, pp. 129–153, Am. Meteorol. Soc., Boston, Mass., 1990.
- Browning, K. A., and N. M. Roberts, Structure of a frontal cyclone, *Q. J. R. Meteorol. Soc.*, 120, 1535–1557, 1994.
- Browning, K. A., and N. M. Roberts, Variation of frontal and precipitation structure along a cold front, *Q. J. R. Meteorol. Soc.*, 122, 1845–1872, 1996.
- Browning, K. A., The dry intrusion perspective of extra-tropical cyclone development, *Meteorol. Appl.*, 4, 317–324, 1997.
- California Air Resources Board, 2013, Almanac Emission Projection Data. Available at:  
[[http://www.arb.ca.gov/app/emsmv/2013/emseic1\\_query.php?F\\_DIV=-4&F\\_YR=2012&F\\_SEASON=A&SP=2013&F\\_AREA=AB&F\\_AB=LT&F\\_DD=Y](http://www.arb.ca.gov/app/emsmv/2013/emseic1_query.php?F_DIV=-4&F_YR=2012&F_SEASON=A&SP=2013&F_AREA=AB&F_AB=LT&F_DD=Y)]
- Carlson, T. N., Airflow through midlatitude cyclones and the comma cloud pattern, *Mon. Weather Rev.*, 108, 1498–1509, 1980.
- Chameides, W. L., and J. C. G. Walker, A photochemical theory for tropospheric ozone, *J. Geophys. Res.*, 78, 8751–8760, 1973. Crutzen, P. J., A discussion of the chemistry of some minor constituents in the stratosphere and troposphere, *Pure Appl. Geophys.*, 106–108, 1385–1399, 1973.
- Chameides WL, Fehsenfeld F, Rodgers MO, Cardelino C, Martinez J, Parrish D, Lonneman W, Lawson DR, Rasmussen RA, Zimmerman P, Greenberg J, Middleton P, Wang T. 1992. Ozone Precursor Relationships in the Ambient Atmosphere. *Journal of Geophysical Research* 97:6037-55.

- Chen, P. (1995), Isentropic cross tropopause mass exchange in the extratropics, *J. Geophys. Res.*, 100, 16,661–16,673.
- Clements, C. B., 1999: Mountain and Valley Winds of Lee Vining Canyon, Sierra Nevada, California, U.S.A. *Arctic, Antarctic and Alpine Research*, Vol. 31(3), pp.293-302.
- Clements, C., and S. Zhong, 2005: Daytime downcanyon flows in the eastern Sierra Nevada, California. *Proceedings. ICAM/MAP 2005, Zadar, Croatia*, <http://www.map.meteoswiss.ch/mapdoc/icam2005/pdf/sesion-01/S1-04.pdf>
- Coats, R.N. and C.R. Goldman. 2001. Patterns of nitrogen transport in streams of the Lake Tahoe basin, California-Nevada. *Water Resources Research*, 37, 2: 405-415.
- Dabdub, D., L.L. DeHaan, J.H. Seinfeld., 1999. Analysis of ozone in the San Joaquin Valley of California. *Atmospheric Environment* 33: 2501-2514.
- Diaz, H.F. & Markgraf, V. (eds) (2000) *El Niño and Southern Oscillation: multiscale variability and global and regional impacts*. Cambridge University Press, New York. Kahya, E. & Dracup, J.A. (1995) The influence of type 1 El Niño and La Niña events on streamflow in the Pacific Southwest of the United States. *Journal of Climate*, 7, 965–976.
- Danielsen, E. F., Stratosphere-troposphere exchange based on radioactivity, ozone, and potential vorticity, *J. Atmos. Sci.*, 25, 502-518, 1968.
- DeCaria, A. J., K. E. Pickering, G. L. Stenchikov, J. R. Scala, J. L. Stith, J. E. Dye, B. A. Ridley, and P. Laroche (2000), A cloud-scale model study of lightning-generated NO<sub>x</sub> in an individual thunderstorm during STERAO-A, *J. Geophys. Res.*, 105, 11,601– 11,616.
- DeCaria, A. J., K. E. Pickering, G. L. Stenchikov, and L. E. Ott (2005), Lightning-generated NO<sub>x</sub> and its impact on tropospheric ozone production: A three-dimensional modeling study of a Stratosphere-Troposphere Experiment: Radiation, Aerosols and Ozone

- (STERAO-A) thunderstorm, *J. Geophys. Res.*, 110, D14303,  
doi:10.1029/2004JD005556.
- Doherty R.M., M.R. Heal, P. Wilkinson, S. Pattenden, M. Vieno, B. Armstrong, R. Atkinson, Z. Chalabi, S. Kovats, A. Milojevic and D.S. Stevenson. 2009. Current and future climate- and air pollution- mediated impacts on human health. *Environmental Health* 8: 1-8.
- Doran, J. C., and S. Zhong, 1994: Regional drainage flows in the Pacific Northwest. *Mon. Wea. Rev.*, 122, 1158–1167.
- Ebel, A., Hass, H., Jakobs, H.J., Laube, M., Memmesheimer, M., Oberreuter, A., Geiss, H., Kuo, Y.-H., 1991. Simulation of ozone intrusion caused by a tropopause fold and cut-off low. *Atmospheric Environment* 25A, 2131}2144.
- Ebi K, McGregor G. 2008. Climate change, Tropospheric Ozone and Particulate Matter and Health Impacts. *Environ Health Perspectives* 116: 1449-1455.
- Egger, J., and Coauthors, 2005: Diurnal circulation of the Bolivian Altiplano. Part I: Observations. *Mon. Wea. Rev.*, 133, 911–924.
- Elliot-Fisk DL, Rowntree RA, Cahill TA, Goldman CR, Gruell G, Harris R, Leisz D, S. Lindstroöm, Kattelmann R, Machida D, Lacey R, Rucks P, Sharkey DA, Ziegler DS (1996) Lake Tahoe Case study. In: Status of the Sierra Nevada. Sierra Nevada ecosystem project. Final report to Congress. Wildland Resources Center Report number 38. University of California, Davis, California.
- EPA factsheet: Science in Action Innovative Research for a Sustainable Future. Community Multi-Scale Air Quality Model offers tools for controlling air pollution; studying climate change. Available online at [http://epa.gov/nerl/download\\_files/documents/CMAQFactSheet.pdf](http://epa.gov/nerl/download_files/documents/CMAQFactSheet.pdf), 2011.

- Finlayson-Pitts, B. J., Pitts, J. N., 1997: Tropospheric Air Pollution: O<sub>3</sub>, Airborne Toxics, Polycyclic Aromatics Hydrocarbons, and Particles. *Science* 276: 1045–1052.
- Finlayson-Pitts, B., Pitts, J., 2000: *Chemistry of the Upper and Lower Atmosphere: Theory, Experiments, and Applications*. Academic Press, San Diego, CA.
- Fiscus, E. L., F. L. Booker and K. O. Burkely. (2005). Crop responses to ozone: uptake, modes of action, carbon assimilation and partitioning. *Plant, Cell and Environment*, 28, 997–1011.
- Fishman, J., Ozone in the troposphere, in *Ozone in the Free Atmosphere*, edited by R. C. Whitten and S. S. Prasad, pp. 161-194, Van Nostrand Reinhold, New York, 1985.
- Fishman, J., Watson, C. E., Larsen, J. C. and Logan, J. A. 1990: Distribution of tropospheric O<sub>3</sub> determined from satellite data. *Journal of Geophysical Research* 95: 3599–617.
- Fuhrer, J. 2001. Ozone Impacts on Vegetation. *Ozone Science and Engineering*, 24:60-74.
- Furger, M. J. Dommen, W.K. Graber, L. Poggio, A.S.H. Pervot S. Emeis, G. Grell, T. Trickl, B. Gomiscek, B. Neiningen, G. Wotawa, 2000: The VOTALP Mesocline Valley Campaign 1996. Concept, background and some highlights. *Atmos. Env.*, 34, 1395-1412.
- Gettelman, A., and A. H. Sobel (2000), Direct diagnoses of stratosphere troposphere exchange, *J. Atmos. Sci.*, 57, 3 – 16.
- Giles, L.V., P. Barn, N. Kunzli, I. Romieu, M.A. Mittleman, S. vanEeden, R. Allen, C. Carlsten, D. Stieb, C. Noonan, A. Smargiassi, J.D. Kaufman, S. Hajat, T. Kosatsky and M. Brauer. 2011. From Good Intentions to Proven Interventions; Effectiveness of Actions to Reduce the Health Impacts of Air Pollution. *Environ Health Perspectives*, 119: 29-36.
- Goldman, C. R., Lake Tahoe: Two decades of change in a nitrogen deficient oligotrophic lake, *Verh. Internat. Verein. Limnol.*, 21, 45–70, 1981.

- Goldman, C.R., 2006. Science a decisive factor in restoring Tahoe clarity. *California Agriculture* 60,2: 45-46.
- Green R, Simpson A, Custovic A, Faragher B, Chapman M, Woodcock A. 1999. The effect of air filtration on airborne dog allergen. *Allergy* 54(5):484–488.
- Grosjean, D.; Whitmore, P. M.; Cass, G. R.; Druzik, J. R. (1989) Ozone fading of triphenylmethane colorants: reaction products and mechanisms. *Environ. Sci. Technol.* 23:1164-1167.
- Haynes, P. H., M. E. McIntyre, T. G. Shepherd, C. J. Marks, and K. P. Shine, 1991: On the “downward control” of extratropical diabatic circulations by eddy-induced mean zonal forces. *J. Atmos. Sci.*, 48, 651–678.
- Hill, C. D., 1980: The effects of terrain distribution on summer thunderstorm activity at Reno, Nevada. NOAA Technical Memorandum, NWS WR-156.
- Hobbs, P. V.; Locatelli, J. D.; Martin, J. E. (1996) A new conceptual model for cyclones generated in the lee of the Rocky Mountains. *Bull. Am. Meteorol. Soc.* 77: 1169-1178.
- Holloway, T., A. Fiore, and M. G. Hastings (2003), Intercontinental transport of air pollution: Will emerging science lead to a new hemispheric treaty?, *Environ. Sci. Technol.*, 37(20), 4535– 4542, doi:10.1021/es034031g.
- Hong, S., Y. Noh, and J. Dudhia, 2006: A new vertical diffusion package with explicit treatment of entrainment processes. *Mon. Wea. Rev.*, 134, 2318–2341.
- , and S.-W. Kim, 2008: Stable boundary layer mixing in a vertical diffusion scheme. Proc. Ninth Annual WRF User’s Workshop, Boulder, CO, National Center for Atmospheric Research, 3.3. [Available online at <http://www.mmm.ucar.edu/wrf/users/workshops/WS2008/abstracts/3-03.pdf>.]

- Hsu, J., M. J. Prather, and O. Wild (2005), Diagnosing the stratosphere-to-troposphere flux of ozone in a chemistry transport model, *J. Geophys. Res.*, 110, D19305, doi:10.1029/2005JD006045.
- Hu, X. M., Nielsen-Gammon, J. W., & Zhang, F. (2010). Evaluation of three planetary boundary layer schemes in the WRF model. *Journal of Applied Meteorology and Climatology*, 49(9), 1831-1844.
- Hubbell BJ, Hallberg A, McCubbin DR, Post E. 2005. Health-Related Benefits of Attaining the 8-Hr Ozone Standard. *Environ Health Perspectives* 113: 73-82.
- Jacob, D. J., J. A. Logan, and P. P. Murti (1999), Effect of rising Asian emissions on surface ozone in the United States, *Geophys. Res. Lett.*, 26, 2175– 2178.
- Jacob, D. J. (2000) Heterogeneous chemistry and tropospheric ozone. *Atmos. Environ.* 34: 2131-2159.
- Jacob, D. J., et al. (2003), Transport and Chemical Evolution over the Pacific (TRACE-P) aircraft mission: Design, execution, and first results, *J. Geophys. Res.*, 108(D20), 9000, doi:10.1029/2002JD003276.
- James, P., A. Stohl, C. Forster, S. Eckhardt, P. Seibert, and A. Frank (2003), A 15-year climatology of stratosphere-troposphere exchange with a Lagrangian particle dispersion model: 2. Mean climate and seasonal variability, *J. Geophys. Res.*, 108(D12), 8522, doi:10.1029/2002JD002639.
- Janjic, Z. I., 1990: The step-mountain coordinate: Physical package. *Mon. Wea. Rev.*, 118, 1429–1443.
- , 1994: The step-mountain Eta coordinate model: Further developments of the convection,

- viscous layer, and turbulence closure schemes. *Mon. Wea. Rev.*, 122, 927–945.
- , 2001: Nonsingular implementation of the Mellor-Yamada level 2.5 scheme in the NCEP Meso model. NOAA/NWS/ NCEP Office Note 437, 61 pp.
- Jerrett, M., R.T. Burnett, C.A. Pope III, K. Ito, G. Thurston, D. Krewski, Y. Shi, E. Calle and M. Thun. 2009. Long-Term Ozone Exposure and Mortality. *N Engl J Med* 2009;360:1085-95.
- Jing, P., D. M. Cunnold, H. J. Wang, and E.-S. Yang (2004), Isentropic cross-tropopause ozone transport in the Northern Hemisphere, *J. Atmos. Sci.*, 61, 1068– 1078.
- Junge, C. E., Global ozone budget and exchange between stratosphere and troposphere, *Tellus*, 14, 363–377, 1962.
- King, C. W., 1997: A climatology of thermally forced circulation in oppositely oriented airsheds along the Continental Divide in Colorado. NOAA Tech. Memo. ERL ETL-283, 152 pp.
- Kingsmill, D. 2000: Diurnally driven summertime winds in the lee of the Sierra: The Washoe Zephyr. Preprints, Ninth Conference on Mountain Meteorology, Aspen CO, Amer. Meteor. Soc. Aug. 7-11, 2000
- Kossmann M, Sturman A. 2004. The surface wind field during winter smog nights in Christchurch and coastal Canterbury, New Zealand. *Int J Climatol* 24:93–108.
- Krupa, S.V. and Manning, W.J. 1988. Atmospheric ozone: formation and effects on vegetation. *Environ. Pollut.* 50(101-137).
- Kuik O.J., Helming J.F.M., Dorland C. & Spaninks F.A. (2000) The economic benefits to agriculture of a reduction of low level ozone pollution in the Netherlands. *European Review of Agricultural Economics* 27, 75–90.
- Lagarias, J.S., Sylte, W.W., 1991. Designing and managing the San Joaquin Valley, air quality

- study. *Journal of Air and Waste Management Association* 41, 1176-1179.
- Lake, G. J.; Mente, P. G. (1992) Ozone cracking and protection of elastomers at high and low temperatures. *J. Nat. Rubber Res.* 7: 1-13.
- Lamarque, J.-F., Langford, A.O., Probst, M.H., 1996. Cross-tropopause mixing of ozone through gravity wave breaking: observation and modeling. *Journal of Geophysical Research* 101, 22969-22976.
- Li, Q., D. J. Jacob, T. Fairlie, H. Liu, R. Martin, and R. Yantosca (2002), Stratospheric versus pollution influences on ozone at Bermuda: Reconciling past analyses, *J. Geophys. Res.*, 107(D22), 4611, doi:10.1029/2002JD002138.
- Liu, S. C., M. Trainer, F. C. Fehsenfeld, D. D. Parrish, E. J. Williams, D. W. Fahey, G. Hübler, and P. C. Murphy (1987), Ozone Production in the Rural Troposphere and the Implications for Regional and Global Ozone Distributions, *J. Geophys. Res.*, 92(D4), 4191-4207.
- Liu, H., D. J. Jacob, I. Bey, R. M. Yantosca, B. N. Duncan, and G. W. Sachse (2003), Transport pathways for Asian pollution outflow over the Pacific: Interannual and seasonal variations, *J. Geophys. Res.*, 108(D20), 8786.
- Logan, J. A., Tropospheric ozone: seasonal behavior, trends and anthropogenic influence, *J. Geophys. Res.*, 90, 10,463-10,482, 1985.
- Logan, J. A. (1999), An analysis of ozonesonde data for the troposphere: Recommendations for testing 3-D models and development of a gridded climatology for tropospheric ozone, *J. Geophys. Res.*, 104(D13), 16,115-16,150.
- Logan, J. A., et al. (1999), Trends in the vertical distribution of ozone: A comparison of two analyses of ozonesonde data, *J. Geophys. Res.*, 104(D21), 26,373-26,400.

- Mantua, N. J., Hare, S. R. Zhang, Y., Wallace, J. M., and Francis, R. C.: 1997, 'A Pacific interdecadal climate oscillation with impacts on salmon production', *Bull. Am. Meteorological Soc.* 78, 1069–1079.
- Mauzerall, D.L. and Wang, X. 2001. Protecting agricultural crops from the effects of tropospheric ozone exposure: reconciling science and standard setting in the United States, Europe, and Asia. *Annu. Rev. Energy Environ.* 26, 237-268.
- McClellan R.O., M.W. Frampton, P. Koutrakis, W.F. McDonnell, S. Moolgavkar, D.W. North, A.E. Smith, R.L. Smith and M.J. Utell. 2009. Critical considerations in evaluating scientific evidence of health effects of ambient ozone; a conference report. *Inhalation Toxicology*, 21(S2): 1-36.
- McLinden, C. A., S. C. Olsen, B. J. Hannegan, O. Wild, and M. J. Prather (2000), Stratosphere ozone in 3-D models: A simple chemistry and the cross-tropopause flux, *J. Geophys. Res.*, 105(D11), 14,653– 14,666.
- Mellor, G. L., and T. Yamada, 1982: Development of a turbulence closure model for geophysical fluid problems. *Rev. Geophys.*, 20, 851–875.
- Misenis, C., & Zhang, Y. (2010). An examination of sensitivity of WRF/Chem predictions to physical parameterizations, horizontal grid spacing, and nesting options. *Atmospheric Research*, 97(3), 315-334.
- Monks, P. S. (2000), A review of the observations and origins of the spring ozone maximum, *Atmos. Environ.*, 3545– 3561.
- Moore, K., R. Neugebauer, F. Lurmann, J. Hall, V. Brajer, S. Alcorn and I. Tager. 2008.

- Ambient Ozone Concentrations Cause Increased Hospitalizations for Asthma in Children: An 18-Year Study in Southern California. *Environmental Health Perspectives*, 116, 8: 1063-1070.
- Moxim, W.J., Levy II, H., Kasibhatla, P.S., 1996. Simulated global tropospheric PAN: its transport and impact on NO<sub>x</sub>. *Journal of Geophysical Research* 101, 12621-12638.
- Murphy, D. M., and D. W. Fahey (1994), An estimate of the flux of stratospheric reactive nitrogen and ozone into the troposphere, *J. Geophys. Res.*, 99(D3), 5325– 5332.
- Murphy J.J., Delucchi M.A., McCubbin D.R. & Kim H.J. (1999) The cost of crop damage caused by ozone air pollution from motor vehicles. *Journal of Environmental Management* 55, 365–376.
- NAS report: global sources of local pollution-An Assessment of Long-Range Transport of Key Air Pollutants to and from the United States, 35–66, available online at: <http://books.nap.edu/openbook.php?recordid=12743&page=35>, 2010.
- Ollinger, S.V., Aber, J.D. and Reich, P.B. 1997. Simulating ozone effects on forest productivity: interactions among leaf-, canopy-, and stand-level processes. *Ecol. Appl.* 7(4), 1237-1251.
- Olsen, S. C., C. A. McLinden, and M. J. Prather (2001), Stratospheric N<sub>2</sub>O-NO<sub>y</sub> system: Testing uncertainties in a three-dimensional framework, *J. Geophys. Res.*, 106, 28,771–28,784.
- Parrish, D.D., et al., 1993. The total reactive oxidized nitrogen levels and the partitioning between the individual species at six rural sites in eastern North America. *Journal of Geophysical Research* 98, 2927-2939.
- Pickering, K. E., A. M. Thompson, R. R. Dickerson, W. T. Luke, D. P. McNamara, J. Greenberg,

- and P. R. Zimmerman (1990), Model calculations of tropospheric ozone production potential following observed convective events, *J. Geophys. Res.*, 95, 14,049– 14,062.
- Pickering, K. E., Y. Wang, W.-K. Tao, C. Price, and J.-F. Müller (1998), Vertical distributions of lightning NO<sub>x</sub> for use in regional and global chemical transport models, *J. Geophys. Res.*, 103, 31,203– 31,216.
- Pielke, R.A., Uliasz, M., 1998. Use of meteorological models as input to regional and mesoscale air quality models - limitations and strengths. *Atmospheric Environment* 32, 1455-1466.
- Pleim, J. E., 2007: A combined local and nonlocal closure model for the atmospheric boundary layer. Part I: Model description and testing. *J. Appl. Meteor. Climatol.*, 46, 1383–1395.
- , and J. S. Chang, 1992: A non-local closure model for vertical mixing in the convective boundary layer. *Atmos. Environ.*, 26A, 965–981.
- Pope CA III, Dockery DW. 2006. Health effects of fine particulate air pollution: lines that connect. *J Air Waste Manag Assoc* 56(6):709–742.
- Pope CA III. 2007. Mortality effects of longer term exposures to fine particulate air pollution: review of recent epidemiological evidence. *Inhal Toxicol* 19(suppl 1):33–38.
- Pope CA III, Burnett RT, Thun MJ, Calle EE, Krewski D, Ito K, et al. 2002. Lung cancer, cardiopulmonary mortality, and long-term exposure to fine particulate air pollution. *JAMA* 287(9):1132–1141.
- Postel, G. A., and M. Hitchman (1999), A climatology of Rossby wave breaking along the subtropical tropopause, *J. Atmos. Sci.*, 56(3), 359–373.
- Poulida, O., Dickerson, R.R., Heymsfield, A., 1996. Stratosphere troposphere exchange in a midlatitude mesoscale convective complex. *Journal of Geophysical Research* 101, 6823-6836.

- Ranzieri, A.J., Thuillier, R.H., 1994. SJVAQS and AUSPEX: a Collaborative Air Quality Field Measurement and Modeling Program. Solomon, P.A. (Ed.), Planning and Managing Regional Air Quality, Lewis Publishers, Florida, in conjunction with Pacific Gas and Electric Company.
- Rao, S. T.; Zurbenko, I. G. (1994) Detecting and tracking changes in ozone air quality. *J. Air Waste Manage. Assoc.* 44: 1089-1092.
- Rappengluck B, Oyola P, Olaeta I, Fabian P. 1999. The evolution of photochemical smog in the metropolitan area of Santiago de Chile. *J Appl Meteorol* 39:275–290.
- Reich, P.B. 1987. Quantifying plant response to ozone: a unifying theory. *Tree Physiol.* 3, 63-91.
- Reitebuch, O.; Strassburger, A.; Emeis, S.; Kuttler, W. (2000) Nocturnal secondary ozone concentration maxima analysed by sodar observation and surface measurements. *Atmos. Environ.* 34: 4315-4329.
- Reuter, J. E., C. R. Goldman, T. A. Cahill, S. S. Cliff, A. C. Heyvaert, A. D. Jassby, S. Lindstrom, and D. M. Rizzo, An integrated watershed approach to studying ecosystem health at Lake Tahoe, CA-NV, USA, paper presented at International Congress on Ecosystem Health, Univ. of Calif., Davis and Int. Soc. for Ecosyst. Health, Sacramento, Calif., 1999.
- Ridley, B. A., J. E. Dye, J. G. Walega, J. Zheng, F. E. Grahek, and W. Rison (1996), On the production of active nitrogen by thunderstorms over New Mexico, *J. Geophys. Res.*, 101, 20,985– 21,005.
- Salmond, J. A.; McKendry, I. G. (2002) Secondary ozone maxima in a very stable nocturnal boundary layer: observations from the Lower Fraser Valley, BC. *Atmos. Environ.* 36: 5771-5782.

- Schoeberl, M. R. (2004), Extratropical stratosphere-troposphere mass exchange, *J. Geophys. Res.*, 109, D13303, doi:10.1029/2004JD004525.
- Schroeder, M. J., and C. M. Countryman, 1960: Exploratory fireclimate surveys on prescribed burns. *Mon. Wea. Rev.*, 88, 123–129.
- Seaman, N.L., 2000. Meteorological modeling for air-quality assessments. *Atmospheric Environment* 34, 2231-2259.
- Seo, K.-H., and K. P. Bowman (2002), Lagrangian estimate of global stratosphere- troposphere mass exchange, *J. Geophys. Res.*, 107(D21), 4555, doi:10.1029/2002JD002441.
- Spence, J. W.; Haynie, F.; Upham, J. B. (1975) Effects of gaseous pollutants on paints: a chamber study. *J. Paint Technol.* 47: 57-63.
- Sprenger, M., and H. Wernli (2003), A Northern Hemispheric climatology of cross-tropopause exchange for the ERA15 time period (1979–1993), *J. Geophys. Res.*, 108(D12), 8521, doi:10.1029/2002JD002636.
- Stohl, A., T. Trickl. A textbook example of long-range transport: Simultaneous observation of ozone maxima of stratospheric and North American origin in the free troposphere over Europe. *J. of Geo Res.*, 104, D23, 30445-30462. 1999.
- Stohl, A., N. Spichtinger-Rakowsky, P. Bonasoni, H. Feldmann, M. Memmesheimer, H.E. Scheel, T. Trickl, S. Hubener, W. Ringer and M. Mandl. 2000. The influence of stratospheric intrusions on alpine ozone concentrations. *Atmospheric Environment*, 34: 1323-1354.
- Stohl, A., S. Eckhardt, C. Forster, P. James, and N. Spichtinger (2002), On the pathways and timescales of intercontinental air pollution transport, *J. Geophys. Res.*, 107(D23), 4684, doi:10.1029/2001JD001396.

- Stohl, A., et al. (2003), Stratosphere-troposphere exchange: A review and what we have learned from STACCATO, *J. Geophys. Res.*, 108(D12), 8516, doi:10.1029/2002JD002490.
- Stull, R. B. (1988) An introduction to boundary layer meteorology. Dordrecht, The Netherlands: Kluwer Academic Publishers, pp. 9-16; 499-506. (Atmospheric Sciences Library, v. 13).
- Sudo, K., and H. Akimoto (2007), Global source attribution of tropospheric ozone: Long-range transport from various source regions. *J. Geophys Res.*, 112, D12302, doi:10.1029/2006JD007992.
- Taylor, J., G.E. and Johnson, D.W. 1994. Air pollution and forest ecosystems: a regional to global perspective. *Ecol. Appl.* 4(4), 662-689.
- Tepper, J. S.; Wiester, M. J.; Weber, M. F.; Ménache, M. G. (1990) Measurements of cardiopulmonary response in awake rats during acute exposure to near-ambient concentrations of ozone. *Fundam. Appl. Toxicol.* 10: 7-15.
- Tjoekler, M.G., Volin, J.C., Oleksyn, J. and Reich, P.B. 1995. Interaction of ozone pollution and light effects on photosynthesis in a forest canopy experiment. *Plant Cell Environ.* 18, 895-905.
- Tremblay, J., Servranckx, R., 1993. Beryllium-7 as a tracer of stratospheric ozone: a case study. *Journal of Radioanalytical and Nuclear Chemistry* 172, 49-56.
- Twain, M., 1871: *Roughing It*. New York: Harper and Brothers. 330 pp.
- U.S. EPA. 1970. Clean Air Act. 40CFR50.
- U.S. EPA. Air Quality Criteria for Ozone and Related Photochemical Oxidants (2006 Final). U.S. Environmental Protection Agency, Washington, DC, EPA/600/R-05/004aF-cF, 2006. US Environmental Protection Agency. Green book nonattainment areas for criteria pollutants. Available at: <http://www.epa.gov/oar/oaqps/greenbk/>.

- Vaughan, G., 1988. Stratosphere troposphere exchange of ozone. In: Isaksen, I.S.A. (Ed.), Tropospheric Ozone. D. Reidel Publishing Company, Dordrecht, The Netherlands, pp. 125-135.
- Vaughan, G., Price, J.D., Howells, A., 1994. Transport into the troposphere in a tropopause fold. Quarterly Journal of the Royal Meteorological Society 120, 1085-1103.
- Wang, Y., D.J. Jacob, and J.A. Logan, Global simulation of tropospheric O<sub>3</sub>-NO<sub>x</sub>-hydrocarbon chemistry; Origen of tropospheric ozone and effects of nonmethane hydrocarbons, American Geophysical Union, 98JD00156, 0148-0227, 1998.
- Waugh, D.W., and L. M. Polvani (2000), Climatology of intrusions into the tropical upper troposphere, Geophys. Res. Lett., 27, 3857– 3860.
- Waugh, D. W., and B. M. Funatsu (2003), Intrusions into the tropical upper troposphere: Three-dimensional structure and accompanying ozone and OLR distributions, J. Atmos. Sci., 60, 637– 653.
- Wernli, H., and H. C. Davies, A Lagrangian-based analysis of extratropical cyclones, I, The method and some applications, Q. J. R. Meteorol. Soc., 123, 467–489, 1997.
- Wernli, H., A Lagrangian-based analysis of extratropical cyclones, II, A detailed case study, Q. J. R. Meteorol. Soc., 123, 1677–1706, 1997.
- Whiteman, C. D., 1990: Observations of thermally developed wind systems in mountainous terrain. Atmospheric Processes over Complex Terrain, Meteor. Monogr., No. 45, Amer. Meteor. Soc., 5–42.
- WHO(World Health Organization). 2000. Air Quality Guidelines,World Health Organization Regional Office, Copenhagen, Denmark
- Wild, O., and H. Akimoto, Intercontinental transport of ozone and its precursors in a three-

- dimensional global CTM, *J. Geophys. Res.*, 106, 27,729– 27,744, 2001.
- Wild, O., P. Pochanart, and H. Akimoto (2004), Trans-Eurasian transport of ozone and its precursors, *J. Geophys. Res.*, 109, D11302, doi:10.1029/ 2003JD004501.
- Wolter, K. and Timlin, M. S.: 1998, ‘Measuring the strength of ENSO—how does 1997/98 rank?’, *Weather* 53, 315–324.
- World Meteorological Organization. Scientific Assessment of Ozone Depletion 1998. Global Ozone Research Monitoring Project Report 44 (WMO, Geneva, 1999).
- Zängl, G., and J. Egger, 2005: Diurnal circulation of the Bolivian Altiplano. Part II: Theoretical and model investigations. *Mon. Wea. Rev.*, 133, 3624–3643.
- Zhang, R., X. Tie, and D. W. Bond 2003, Impacts of anthropogenic and natural NO<sub>x</sub> sources over the U. S. on tropospheric chemistry, *Proc. Natl. Acad. Sci. U. S. A.*, 100, 1505–1509.
- Zhong, Shiyuan, Ju Li, Craig B. Clements, Stephan F. J. De Wekker, Xindi Bian, 2008: Forcing Mechanisms for Washoe Zephyr—A Daytime Downslope Wind System in the Lee of the Sierra Nevada. *Journal of Applied Meteorological Climatology*, 47, 339–350.

## **Chapter 2: Surface Ozone in the Lake Tahoe Basin: Impact of Regional Meteorology**

Sandra Theiss <sup>a,\*</sup>, Alan Gertler <sup>a</sup>, Barbara Zielinska <sup>a</sup>, Joel Burley <sup>b</sup>, and Andrzej Bytnerowicz <sup>c</sup>

<sup>a</sup>*Desert Research Institute, 2215 Raggio Parkway,  
Reno, NV 89512, USA*

<sup>b</sup>*Department of Chemistry, Saint Mary's College of California,  
Moraga, CA 94575-4527, USA*

<sup>c</sup>*USDA Forest Service, Pacific Southwest Research Station,  
4955 Canyon Crest Drive, Riverside, CA 92507, USA*

**Abstract**

The Lake Tahoe Basin occasionally experiences elevated levels of ozone that exceed the 70 ppb ambient air quality standard (8-hour average) from the California Air Resources Board (CARB). Previous studies have indicated that local generation of ozone in the Basin is likely to be more important than the long-range transport from out-of-basin sources due to the Sierra Nevada crest posing as a barrier to prevent polluted air masses from entering the Basin. Until recently, however, very little was known about the impact of regional meteorology on the distribution of ozone within the Tahoe Basin. In order to develop a better understanding of the factors affecting ozone levels within the Basin, a comprehensive field study was performed in the summer of 2010. Analysis of the regional meteorology and data from the Hybrid Single Particle Lagrangian Integrated Trajectory (HYSPLIT) model indicates that background ozone levels are enhanced via transport at the Angora and Genoa 9000 sites. Wind roses indicate local circulation patterns i.e. lake breezes, occurring at the lower elevation sites. Thunderbird has high ozone values due to the dominant wind flow and lake breeze coming from the west, an indication that ozone precursors are coming from the Lake.

*Keywords:* wind roses

local meteorology

transport

## 2.1. Introduction

The Lake Tahoe Basin is located on the border of California and Nevada northeast of San Francisco, Sacramento and the San Joaquin Valley (Figure 1). Lake Tahoe is a high altitude lake at 1900 masl (6200 fasl), and is separated from the Sacramento Valley by the Sierra Nevada divide, ranging from 2200 masl (7200 ft) at the passes to 3050 m (10000 ft) at the crest of the Crystal Range. The development of a summer boating and winter ski industry and the construction of casinos at the state line on the north and south ends of the Lake has caused Tahoe to evolve into a year-round resort destination. The Lake is so popular in the summer that it is not unusual to record a million vehicle miles around the Lake in a single day (Goldman, 2006). Lake Tahoe possesses many characteristics that result in unusual water clarity, however, with this increased activity the water clarity has been decreasing. The Basin forms a natural sink, as local air pollutants are frequently trapped by inversions, and wind and water carry very fine inorganic and organic particles into the huge lake, where they can remain suspended for years (Swift et al. 2006). The ratio of watershed to lake area is only 1.6; the Lake has a maximum depth of 505 m, rendering it the eighth deepest freshwater body in the world; the major rock type in the Basin is granite (Hyne et al. 1972). Since Secchi disk measurements (a way to measure water clarity) at Lake Tahoe began, Secchi depths have decreased from over 40 m to under 30 m. This decline is a matter of great concern to the residents of the Tahoe Basin, as well as to the millions of visitors who are attracted to the Lake because of its physical beauty (Jassby et al 1999). In addition to the water clarity issue, there has been an increasing awareness of the impacts of other pollutants in the Lake Tahoe Basin including surface-level ozone.

The Tahoe Basin had been in compliance with ambient air quality standards for ozone until 2005, when the Air Resources Board of the State of California (CARB) adopted a more stringent 8-hour ozone standard (not to exceed 70 ppb). Now some areas within the Basin violate this standard a few times each summer. Efforts to understand ozone concentrations in the Basin had been limited with the primary concern being for the impact of ozone on the health of the extensive pine forests in the Tahoe Basin due to the historical compliance (Dolislager 2012b). Ambient ozone has pronounced adverse effects on forest health in California's mountain regions (Arbaugh et al. 1998). According to large-scale distribution maps of the Sierra Nevada bioregion, the Lake Tahoe Basin's summer-season, 24-hour ozone levels are 50 parts per billion (ppb) to 60 ppb (Fraczek et al. 2003). Such ozone levels may be toxic to vegetation (Krupa et al. 1998) and can adversely affect tree health (Arbaugh et al. 1998). Ozone causes foliar injury (an indicator of health) to ponderosa (*Pinus ponderosa*) and Jeffrey (*Pinus jeffreyi*) pines in the central Sierra Nevada (Miller et al. 1996), including in the Lake Tahoe Basin (Pedersen 1989).

With the lower ridges of the Carson Range to the east acting as a barrier from the Great Basin, the terrain around Lake Tahoe forms a bowl-shaped Basin that develops very strong, shallow subsidence and radiation inversions at all times throughout the year (Elliott-Fisk et al., 1996). For many areas within the Basin ozone concentrations are highest during the summer, when sunlight drives the chemical processes that create ozone from airborne hydrocarbons and oxides of nitrogen. Meteorological factors that affect ozone concentrations include temperature, humidity, turbulence, mixing height and boundary layer depth. In addition, the Lake Tahoe Basin has many local-scale meteorological influences including a thermally direct circulation known as the lake breeze. The physical concept of a lake breeze may be stated as a heat transfer problem. During periods of insolation the land surface is heated and its temperature increases,

whereas the water surface remains at a relatively constant temperature due to its thermal characteristics. The surface temperature influences the overlying air and as a result there is warmer and less dense air over land while over the water the overlying air is cooler and denser. Near the shore line between the two surfaces, a pressure gradient is established due to the buoyant effects created by the temperature differences. Thus, if the prevailing synoptic conditions are such that the gradient wind is light, the buoyant force is the dominant force and a lake breeze is established (Biggs and Graves, 1962). Lyons and Olsson (1973) showed that the lake breeze favors the occurrence of high air pollution in shoreline areas. This is due to three factors: 1) formation of low-level temperature inversions as cool lake air moves inland, 2) continuous fumigation of elevated plumes from shoreline pollution sources, and 3) recirculation of pollutants within the lake breeze circulation pattern. All of these factors are a consequence of the unique features of the lake breeze temperature and wind structure.

Recent studies have focused on the transport of ozone and ozone precursors from upwind source regions. Carroll and Dixon (2002) used aircraft measurements of a Sacramento pollution plume and found the maximum ozone concentrations were frequently observed in the afternoon, 40-80 km downwind of the city, but these decreased to about one-half those values at distances 120 km downwind. Zhang et al (2002) used aircraft measurements to study nitrogen and phosphorus in and around the Lake Tahoe Basin. Bytnerowicz et al. (2004) studied the spatial and temporal patterns of ozone distribution as 2-week integrated averages characterized with passive samplers during the 2002 summer season for the entire Lake Tahoe Basin and for upwind areas on the western slopes of the Sierra Nevada. They concluded that the Sierra Nevada crest west of the Lake Tahoe Basin acts as a barrier that prevents polluted air masses and high ozone concentrations from the Sacramento Valley and Sierra Nevada foothills from entering the

Basin. Dolislager et al. (2012a) assessed the impacts of transport and local generation by making continuous measurements at various locations along the axis of predominant airflow (i.e., roughly southwest to northeast). They established two transport assessment sites at Big Hill and Echo Summit, a few routine monitoring sites at various altitudes primarily on the western slope of the Sierra Nevada and four in-Basin monitoring sites. Also incorporating aircraft data, they concluded that the pollutants from the upwind regions act to raise regional background concentrations entering the Tahoe Basin to the extent that local contributions do not need to be large to cause exceedances of air quality standards. VanCuren et al. (2012) used measurements taken while cruising the Lake to show that aerosol concentrations in near-shore areas are primarily controlled by a combination of diurnal cycling of land and lake breezes and particle emissions driven by cycles of human activity near the shore.

In order to better understand the sources of ozone in the Lake Tahoe Basin, this study focused on an analysis of regional meteorology concentrations around the Lake during the months of July, August and September. Wind analyses were performed to incorporate micro- to meso-scale local phenomena that can influence temporal and spatial variations in ozone. Back trajectories using the Hybrid Single-Particle Lagrangian Integrated Trajectory (HYSPPLIT) model were used to analyze the sources of long range transport emissions. This paper is a companion paper to Burley et al. (2014) which looks at the spatial and temporal distribution of the ozone and the ozone precursors collected. The objective was to improve our understanding of ozone within the Tahoe Basin and assist in the development of pollution control strategies.

## **2.2. Methodology**

The methodology of the field study is discussed at length in the report by Bytnerowicz et al. (2013) and the Burley et al. (2014) paper. To investigate the ozone environment in the Lake

Tahoe Basin, an ozone monitoring network was set up in the summer of 2010. Hourly ozone concentrations were measured at 10 sites around the Lake (Figure 2, Table 1). Real-time ozone concentrations were measured with active UV-absorption 2B Technologies (Bognar and Birks, 1996) instruments powered by 12 V batteries and solar panels.

Meteorological data were obtained through the National Weather Service's National Centers for Environmental Prediction (NCEP), which runs a series of computer analyses and forecasts. NOAA's Air Resources Laboratory (ARL) routinely uses NCEP model data for use in air quality transport and dispersion modeling calculations. In 1989 ARL began to archive some of these datasets for future research studies (Air Resources Laboratory, 2014). Archived 10 m wind data for the summer were collected from the North American Mesoscale (NAM) 12 km meteorological model from the ARL. The NAM 12 km model was used because it provided the smallest resolution and was verified against the National Climatic Data Center (NCDC) observational cooperative data site, Tahoe Valley. The NAM model outputs data at 3 hour intervals starting with 0Z. For the present analysis, the data are restricted to July 1<sup>st</sup> through September 23<sup>rd</sup>, 2010, which coincides with the collection of ozone data at the ten sampling sites. The daily data times are every 3 hours starting with 2 am PDT giving eight collection times within a 24-hour period. Wind roses were also created using the Western Regional Climate Center (WRCC) at the sites: North Tahoe High School (NTHS) and South Lake Tahoe (KTVL) (Figure 2).

### **2.3. Results**

The maximum 1-hour daily ozone levels (Figure 3) show a low period of ozone (33 ppb – 62 ppb) from July 10 - July 20 whereas August 1 - August 28 stays high with ozone values between 50 ppb and 89 ppb. September had large variability between high and low ozone days

but begins a more downward trend of ozone for all sites. The high elevation Angora and Genoa 9000 sites stand out as being higher than the rest. The maximum 8-hour averaged ozone levels (Figure 4) show the general trends of the maximum 1-hour daily ozone levels. Angora and Genoa 9000 violate the CARB standard several times (11 and 16 times, respectively), while Incline (2 times) and Watson Creek (once) have fewer violations.

The average hourly ozone (Figure 5) shows three distinct groups of diurnal patterns. Angora and Genoa 9000 have a similar pattern, which tends to be inverted compared to the other sites with a small increase in average ozone values during the nighttime hours. Incline and Thunderbird have a similar pattern that has a smaller increase in afternoon ozone than the rest of the sites. During the daytime hours all sites converge on ozone values around 52 ppb, but during the nighttime hours the ozone values range from 11 ppb to 59 ppb.

The daytime wind roses for the summer (Figure 6) show a dominant southwesterly flow. Blackwood and Sugar Pine Point on the west side of the Lake have a stronger easterly component than the other sites. The WRCC site NTHS does not show this easterly component as strong, however, shows a stronger southerly component (Figure 10). The Genoa sites on the east side of the Lake have more of a westerly component than southwesterly and show a small northwesterly component that increases with elevation. The southern sites of Angora and Valhalla also have a small northwesterly component but the WRCC site KTVL has a strong northeasterly component (Figure 12). The nighttime wind roses for the summer (Figure 7) show a dominant westerly component except for the southern sites of Angora and Valhalla, which show a more southwesterly component. The WRCC site NTHS is the only one that shows a strong northerly component (Figure 11) and the WRCC site KTVL shows a strong southerly component. Angora, Valhalla and Watson Creek also show a southeasterly component as well.

The nighttime wind roses for the three Genoa sites are very similar to the analogous daytime wind roses.

A correlation matrix was performed (Table 2) to determine which sites were closely correlated with one another. Ozone levels at Angora and Genoa 9000 are closely correlated with a value of 0.83. Despite elevation differences Incline and Thunderbird are closely correlated with a value of 0.83. The sites on the west side of the lake, Watson Creek, Blackwood, Sugar Pine Point and Valhalla, are closely correlated with values ranging from 0.86 - 0.94, and Genoa 7000 is correlated to Genoa 8000 with a value of 0.88. The ozone patterns reflect these correlations as well.

#### **2.4. Discussion**

The sites that are strongly correlated display similar maximum 1-hour and 8-hour ozone maxima. Angora and Genoa 9000 are typically higher than the other sites and are closely correlated to each other. The correlated sites Genoa 7000 and Genoa 8000 have some of the lowest values on certain days, such as July 17, 26, 29, August 12 and September 2. The correlated sites of Incline and Thunderbird display very similar diurnal patterns, despite elevation differences. The closely correlated western sites of Watson Creek, Blackwood, Sugar Pine Point and Valhalla also show similar diurnal patterns.

The diurnal patterns of ozone show an increase in ozone variability with decreasing elevation except for Thunderbird. The Genoa 9000 site shows an ozone pattern with very little diurnal variation. Genoa 9000 also has the highest ozone values at night and dips slightly to have lower ozone values during the day-time hours. This is possibly due to the high elevation and transport of background ozone from the Central Valley. The Angora site shows a dip in ozone around 9:00 PDT but remains high during late evening. The highest values occur during

early night-time hours, just after sunset also suggesting transport from downwind areas. Genoa 7000 and Genoa 8000 greatly differ from Genoa 9000 and show similar diurnal curves to each other with higher values during the day-time and lower values at night. Thunderbird has a similar curve to Incline despite elevation and lake proximity differences, but with a stronger dip in ozone around 7:00 PDT. Sugar Pine Point shows a slight peak around 18:00 PDT and Blackwood shows a slight peak around 17:00 PDT, also suggesting the influence of a lake breeze. Possible causes of the observed diurnal patterns include the topography, elevation and any possible NO titration as discussed in Burley et al. (2014) as well as the influences of the lake/land breeze wind circulations.

The daytime wind roses (Figure 6) show a lake breeze feature at Blackwood and Sugar Pine Point with an easterly component of wind coming off the lake. This is also shown with the WRCC site NTHS due to the southerly component of the wind, coming off the lake (Figure 10). This is not as clear in the wind rose at the Thunderbird site due to the lake breeze coming from the west, the same as the dominant wind direction. The nighttime wind roses (Figure 7) show a southeasterly component at Valhalla and a strong northerly component at the WRCC site NTHS (Figure 11) which could also indicate a nighttime land breeze setting up. Blackwood and Sugar Pine Point could indicate a nighttime land breeze, however it gets washed out since the dominant wind flow is from the west. This land breeze contributes to the lower ozone concentrations at these sites during the nighttime hours. Thunderbird does not show the land breeze feature since there is steep topography to the east. Since the dominant wind flow is from the Lake for Thunderbird the unusually high ozone concentration indicates high ozone and ozone precursors on the Lake. The dominant wind direction is from the west southwest, this would put the all of the sites downwind of the Central Valley. Therefore, while transport is possible from this

direction the air parcels in question must make it over the Sierra Nevada Mountains and then mix down to Lake level unless a site is high enough to be influenced by the general wind flow.

Previous studies (e.g., Duckworth and Crowe, 1979), routine monitoring (e.g., Echo Summit), and supplemental Lake Tahoe Atmospheric Deposition Study (LTADS) measurements of ozone in the Sierra Nevada west of Lake Tahoe indicate very infrequent one-day transport of high concentrations to the crest of the Sierra Nevada, west of the Tahoe Basin. Air masses following higher altitude paths may move to the east in a given day but there must also subsequently be a mechanism for that air once it traverses the Sierra Nevada to mix downward to impact ozone air quality at ground level (Dolislager et al. 2012b). Another way to evaluate whether or not transport can play a role is to assess the effects of the synoptic-scale atmospheric transport patterns on observations and try to locate the sources of long range transport emissions. To do this, 30-hr air-mass back trajectories at Angora were obtained using the HYSPLIT model available from the United States National Oceanic and Atmospheric Administration (NOAA) website (<http://www.noa.gov>); (Draxler and Rolph, 2010).

August 21 was chosen as a high day (Figure 8) and August 29 was chosen as a low day (Figure 9) in order to show the different back trajectories. Angora was chosen as the arrival point because it had the highest ozone value for the high day. The 10-meter height trajectory and a 1500-meter height trajectory were chosen in order to give the big picture of the whole layer however it should be noted that the 10-meter height is close to the ground and has many interactions with the surface. The 10-meter height trajectory (red line) represents the bottom of the boundary layer. The 10-meter trajectory follows along the ground and for the high day and the trajectory remains constant as it travels across the San Francisco metro area to Angora. This allows the air to steadily pick up ozone precursors and transport them to Angora. For the low

day, the trajectory follows just to the north of San Francisco and through Sacramento at a fast pace, then slows down as it makes it to the forested area to the west of Lake Tahoe. If any ozone precursors were picked up, they had time to be deposited in the forested area. The 1500-meter height trajectory (blue line) represents the top of the boundary layer. For the high day, the trajectory comes from the southwest through the San Joaquin valley whereas for the low day the trajectory has a northerly component through Lassen National Forest. The differences in these two trajectories suggest that the transport of ozone precursors aided in elevating ozone levels during the high day since the high day trajectories come steadily from the southwest through the major cities and the low day trajectories slow down through the forested area to the north and west of the Lake Tahoe Basin.

## **2.5. Summary and Conclusions**

As part of a study designed to investigate the spatial and temporal patterns of ozone around the Lake Tahoe Basin during the summer months of 2010, the regional impact of meteorology on ozone distribution was analyzed. The highest ozone values were observed during the month of August. There was a period of low ozone values (33 – 62 ppb) during the middle of July. The highest site, Genoa 9000 and the southernmost site, Angora, experienced the highest ozone values and violations of the new 8-hour CARB standard for ozone. While all sites had similar ozone concentrations during the day (55 -60 ppb), the low elevation sites had much lower ozone concentrations during the night (10 – 30 ppb). This is due to a combination of factors including lack of long-range transport of ozone and ozone precursors from downwind areas, topography and landscape surfaces, ozone titration of NO emitted from local traffic and local campground wood fires as well as local wind circulation patterns.

Based on the diurnal patterns of ozone showing high ozone values with little diurnal variability, the higher values of the maximum daily 1-hour ozone and the maximum averaged 8-hour ozone as well as the variability in the HYSPLIT trajectories, we find the transport of ozone precursors from Sacramento and the San Francisco Bay area can contribute to the increased background levels of ozone at Genoa 9000 and Angora. This study could not identify a mechanism for mixing free troposphere ozone down to the lower sites however, with the indication of the lake breeze by the wind roses the other sites are affected by local wind flow patterns and local emissions. Even at a low elevation, Thunderbird has high ozone values due to the dominant wind flow and lake breeze coming from the west. This is an indication that high values of ozone and source pollutants occur on the Lake as shown by Burley et al. (2014). Thus based on this work, we observed that ozone levels in the Basin are affected by transport from the west at higher elevations. However more research is needed, including the use of chemical modeling in order to identify if there is a mechanism for downward transport of ozone.

### **Acknowledgements**

This study was supported by the grant from the U.S. Department of Agriculture Forest Service through the Tahoe Science Program funded by the Southern Nevada Public Lands Management Act (SNPLMA). The authors would also like to thank: Joey Keely, Chris Engelhardt, Paul McCulloch and Shana Gross of the USDA Forest Service Lake Tahoe Basin Management Unit for logistical help and data collection; Andrew Strain and Casey Blann of the Heavenly Mountain Skiing Operations, Dennis Malone of the Thunderbird Lodge, and Jack Coughlin of the Diamond Peak Skiing Operations for providing support for monitoring and selection of sites; Brant C. Allen of UC Davis Environmental Research Center and Chris Ross of the USDA Forest Service PSW Research Station for help with installation and collection of data;

Jonathan Long and Tiffany Van Huysen of the USDA Forest Service PSW Research Station for administrative support for the study. A special thanks to the collaborators: Suraj Ahuja, Ricardo Cisneros, Glen Shaw, Don Schweizer, and Trent Procter of the US Forest Service Region 5; Susan Schilling of the US Forest Service Pacific Southwest Research Station; Leora Nanus of San Francisco State University; Mark McDaniel of Desert Research Institute; James Sickman and Michael Bell of University of California; Miriam Rorig of USDA Forest Service PNW Research Station. Thanks to Nyssa Perryman for your help and support.

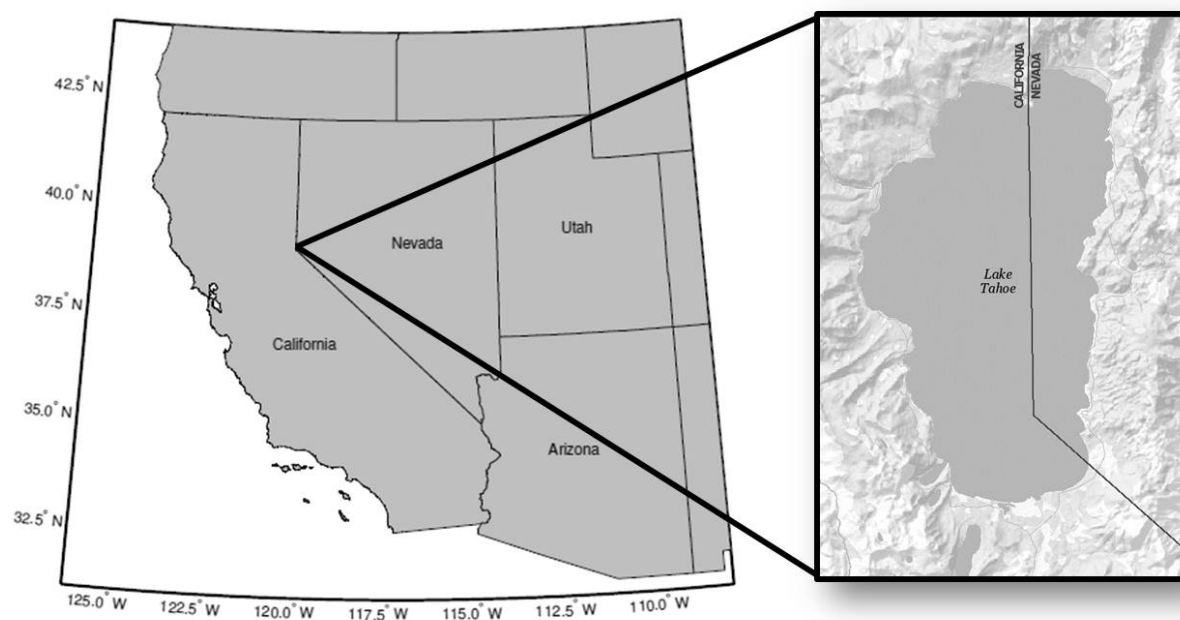
## References

- Air Resources Laboratory. 2014. Ready Archived Meteorology.  
Online, <<http://www.arl.noaa.gov/>>
- Arbaugh MJ, Miller PR, Carroll J, et al. 1998. Relationship of ambient ozone with injury to pines in the Sierra Nevada and San Bernardino mountains of California, USA. *Environ Pollution.*, 101:301. DOI: 10.1016/S0269-7491(98)00027-X
- Biggs, W. Gale, Maurice E. Graves, 1962: A Lake Breeze Index. *J. Appl. Meteor.*, 1, 474–480.
- Bognar, J. A., Birks, J. W. 1996. Miniaturized ultraviolet ozonesonde for atmospheric measurements, *Analytical Chemistry*, 68, 3059-3062
- Burley, J., Bytnerowicz, A., and Zielinska, B. 2014. Surface Ozone in the Lake Tahoe Basin: Spatial and Temporal Distributions. *Atmos Environ.* In submission.
- Bytnerowicz, A., Arbaugh, M, and Padgett, P. 2004. Evaluation of ozone and HNO<sub>3</sub> vapor distribution and ozone effects on conifer forests in the Lake Tahoe Basin and eastern Sierra Nevada. Final Report to California Air Resources Board, Contract No. 01-334, USDA Forest Service, Pacific Southwest Research Station.
- Bytnerowicz, A., Fenn, M., Gertler, A., Preisler, H., Zielinska, B., Ahuja, S., Cisneros, R., Shaw, G., Schweizer, D., Procter, T., Burley, J., Schilling, S., Nanus, L., McDaniel, M., Theiss, S., Sickman, J., Bell, M., Rorig, M., 2013. Distribution of ozone, ozone precursors and gaseous components of atmospheric nitrogen deposition in the Lake Tahoe Basin. Final Technical Report for SNPLMA Contract P063, USDA Forest Service, PSW Research Station, 86 pp.
- Carroll JJ, Dixon AJ, 2002. Regional scale transport over complex terrain, a case study: Tracing the Sacramento plume in the Sierra Nevada of California. *Atmos Environ.* 36, 23-58.

- Dolislager, L. J., VanCuren, R., Pederson, J. R., Lashgari, A., and McCauley, E. 2012a. An assessment of ozone concentrations within and near the Lake Tahoe Air Basin. *Atmos Environ*, 46, 645-654.
- Dolislager, L. J., VanCuren, R., Pederson, J. R., Lashgari, A., & McCauley, E. 2012b. A summary of the Lake Tahoe atmospheric deposition study (LTADS). *Atmos Environ*. 46, 618-630.
- Draxler, R.R., Rolph, G.D., 2010. HYSPLIT (Hybrid Single-Particle Lagrangian Integrated Trajectory) Model Access via NOAA ARL READY Website. NOAA Air Resources Laboratory, Silver Spring, Maryland, U.S.A..  
<http://www.ready.arl.noaa.gov/HYSPLIT.php>
- Duckworth, S. and D. Crowe 1979, "Ozone Patterns on the Western Sierra Slope – Downwind of Sacramento during the Summer of 1978," library call no. TD 885.5 O98 O96 1979, Technical report prepared by the Aerometric Analysis Branch, Technical Services Division, California Air Resources Board, March
- Elliot-Fisk, D.L., T.C. Cahill., O.K. Davis, L.Duan., C.R. Goldman, G.E. Gruell, R. Harris, R. Kattelman, R. Lacey, D. Leisz, S. Lindstrom, D. Machida, R.A. Rowntree, P. Rucks, D.A. Sharkey, S.L. Stephens and D.S. Ziegler, 1996. Lake Tahoe Case Study Sierra Nevada Ecosystem Project: Final report to Congress, Addendum. Davis: University of California, Centers for Water and Wildland Resources.
- Fraczek W, Bytnerowicz A, Arbaugh MJ. Bytnerowicz A, Arbaugh MJ, Alonso R, 2003. Use of geostatistics to estimate surface ozone patterns. *Ozone Air Pollution in the Sierra Nevada: Distribution and Effects on Forests, Developments in Environmental Science 2*. Amsterdam: Elsevier. 215p. 47.

- Goldman, C.R., 2006. Science a decisive factor in restoring Tahoe clarity. *California Agriculture.*, **60**, No. 2, 45-46.
- Krupa SV, Tonneijck AEG, Manning WJ, Flagler RB, 1998. Ozone. Recognition of Air Pollution injury to Vegetation. *Air and Waste Management Assoc.* (2)1p. 28.
- Lyons, W. A., and L. E. Olsson, 1973: Detailed mesometeorological studies of air pollution dispersion in the Chicago lake breeze. *Mon. Wea. Rev.*, 101, 387-403.
- Miller PR, Guthrey R, Schilling S, Carroll J, Bytnerowicz A, Arbaugh MJ, Schilling S. Ozone injury responses of ponderosa and Jeffrey pine in the Sierra Nevada and San Bernardino mountains in California. *Proc Int Symp Air Pollution and Climate Change Effects on Forest Ecosystems* (Feb. 5–9, 1996, Riverside, CA) 1996. USDA Forest Service, Gen Tech Rep No. PSW-GTR-166.
- Pedersen BS, Olson RK, Lefohn AS, 1989. Ozone injury to Jeffrey and ponderosa pines surrounding Lake Tahoe, California and Nevada. *Effects of Air Pollution on Western Forests*. 1989. *Air Waste Management Assoc, Transactions Ser No 16*, p 279–92.
- Swift, T. J., J. Perez-Losada, S. G. Schladow, J. E. Reuter, A. D. Jassby, and C. R. Goldman. 2006. Water clarity modeling in Lake Tahoe: linking suspended matter characteristics to Secchi depth. *Aquatic Sciences.*, 68,1–15.
- VanCuren, R., Pederson, J., Lashgari, A., Dolislager, L., & McCauley, E., 2012. Aerosol generation and circulation in the shore zone of a Large Alpine lake–2–Aerosol distributions over Lake Tahoe, CA. *Atmos Environ.*, 46, 631-644.
- Zhang, Q., J.J. Carroll, A.J. Dixon, and C. Anastasio, 2002, Aircraft Measurements of Nitrogen and Phosphorus in and around the Lake Tahoe Basin: Implications for Possible Sources of Atmospheric Pollutants to Lake Tahoe, *Environmental Science &*

Technology, 36, 4981-4989.

**Figures and Tables****Fig. 2.1** Location of Lake Tahoe

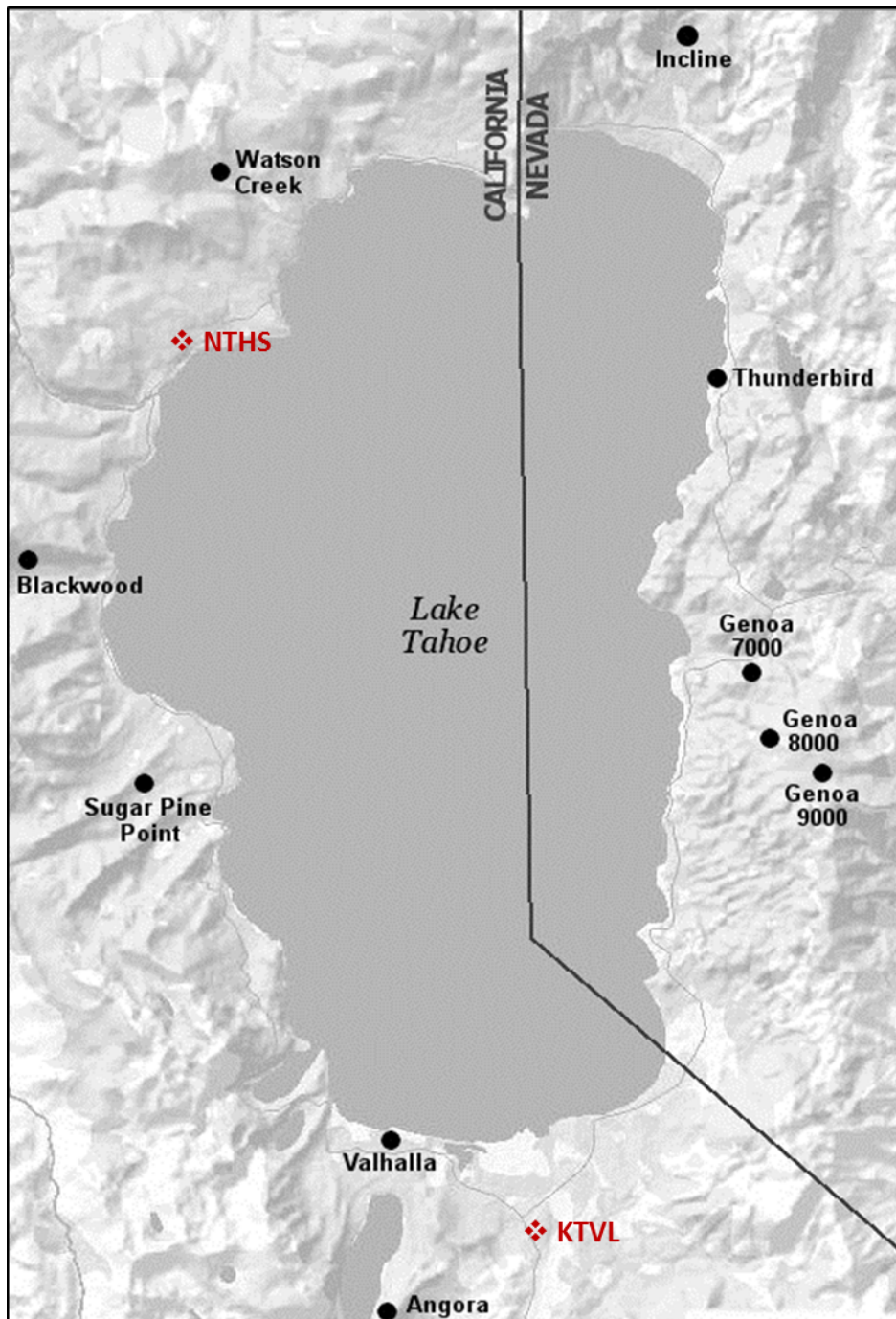


**Fig. 2.2.** Location of measurement sites around the lake, the red sites are the WRCC observation sites: North Tahoe High School (NTHS) and South Lake Tahoe (KTVL)

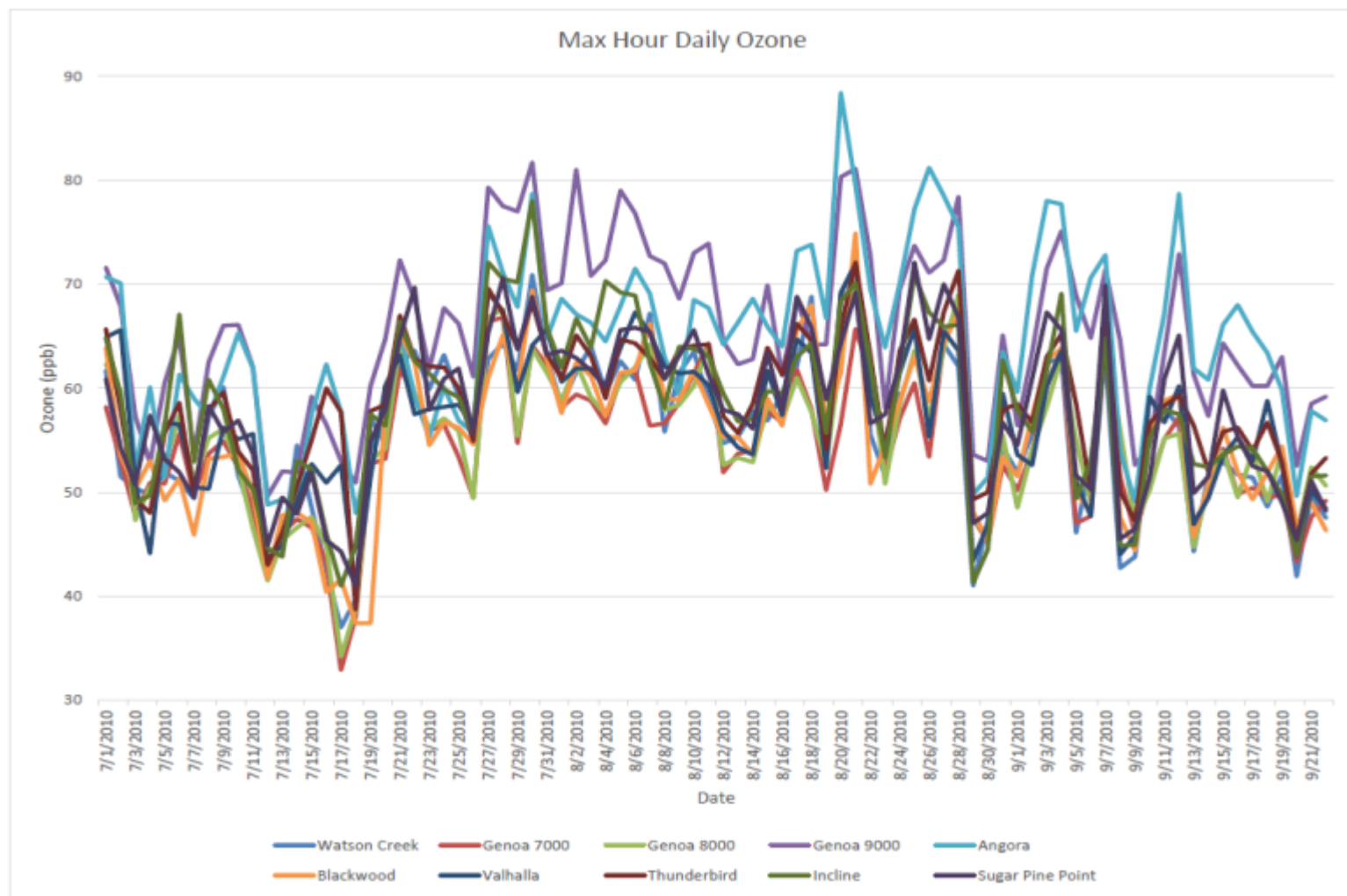


**Fig. 2.3.** Max 1-hr daily ozone concentrations (ppb) for each site from July 1 2010 – September 23 2010

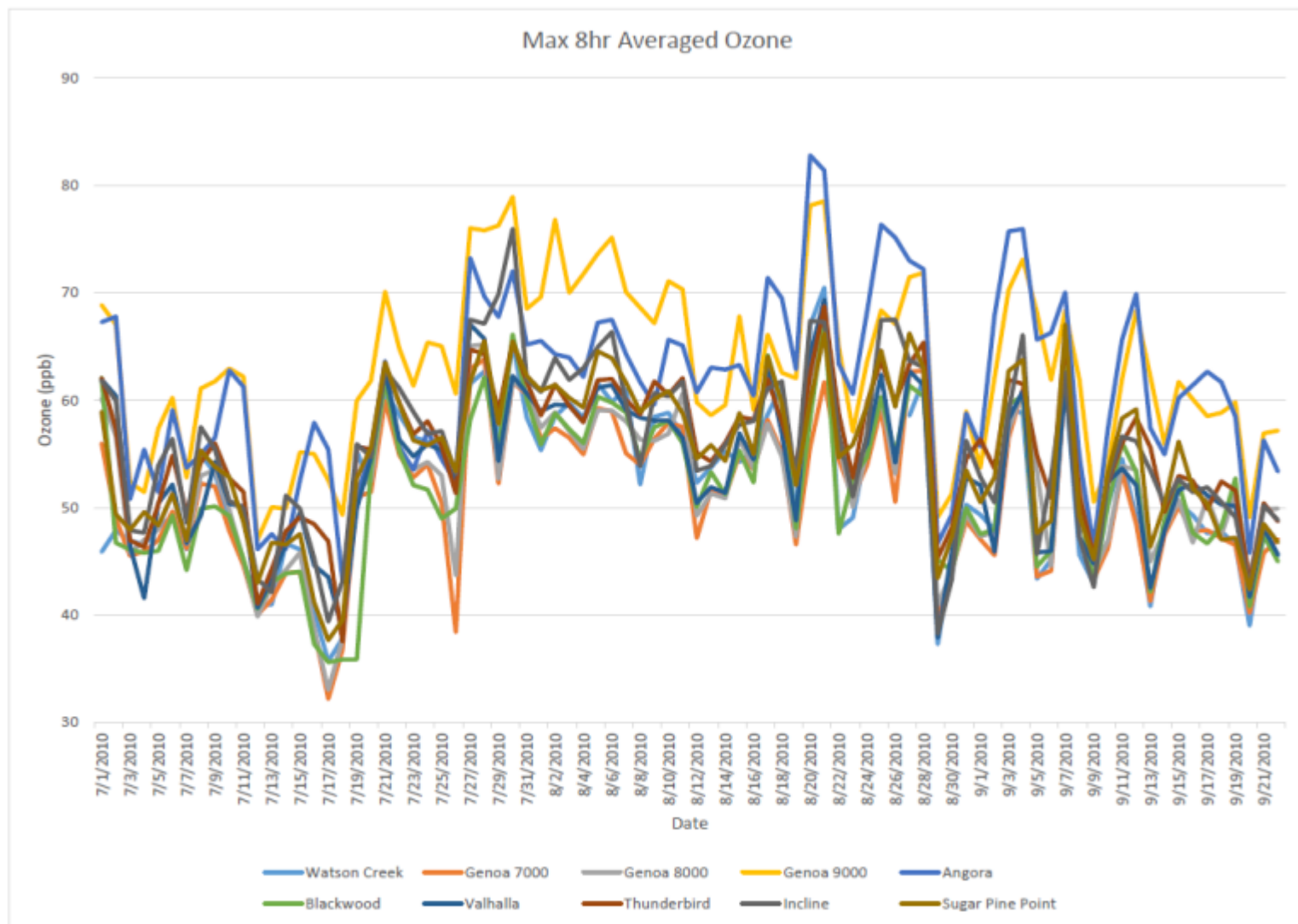


**Fig. 2.4.** Max 8-hr averaged ozone (ppb) for each site from July 1 2010 – September 23 2010

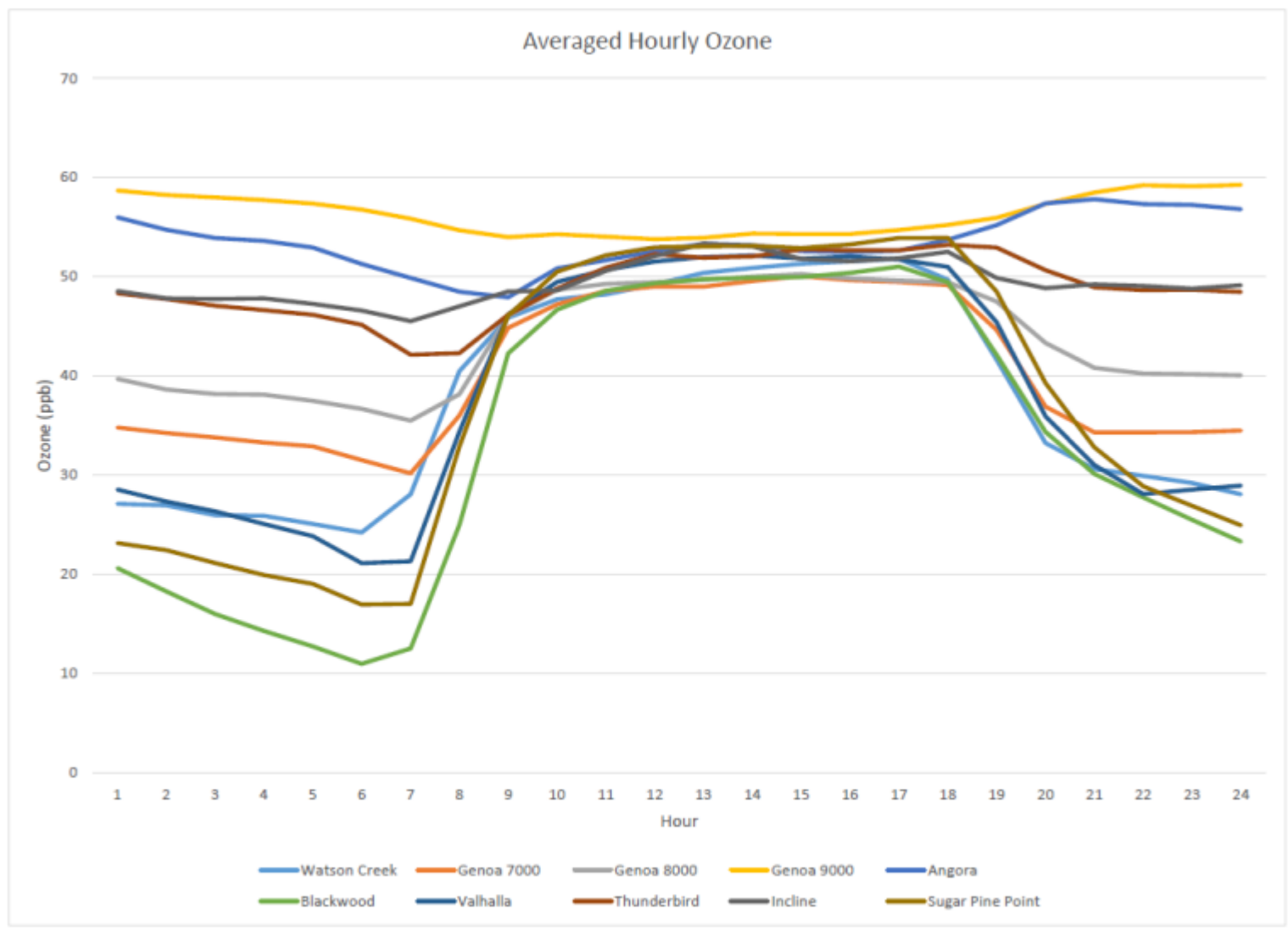


**Fig. 2.5.** Averaged hourly ozone (ppb) from July 1 2010 – September 23 2010, time is in Pacific Daylight Time

### Daytime Wind Roses by Site

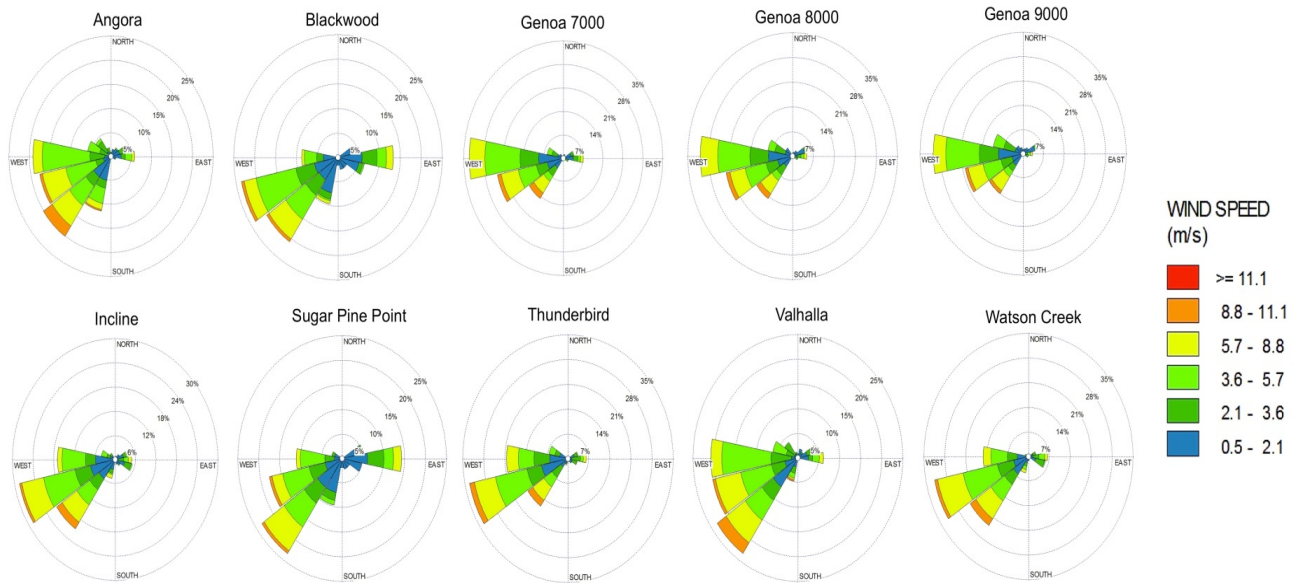


**Fig. 2.6.** Daytime wind roses including the hours of 8am, 11am, 2pm and 5pm for each site during the summer of 2010

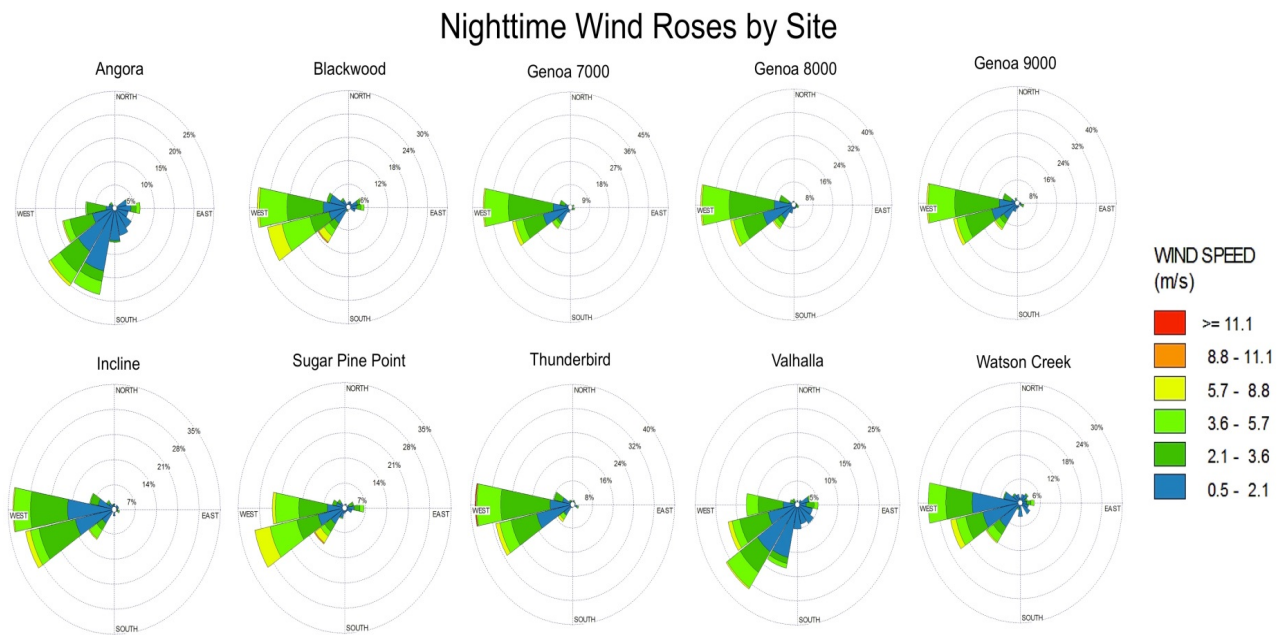


**Fig. 2.7.** Nighttime wind roses including the hours of 2am, 5am, 8pm and 11pm for each site during the summer of 2010

NOAA HYSPLIT MODEL  
 Backward trajectories ending at 0000 UTC 22 Aug 10  
 EDAS Meteorological Data

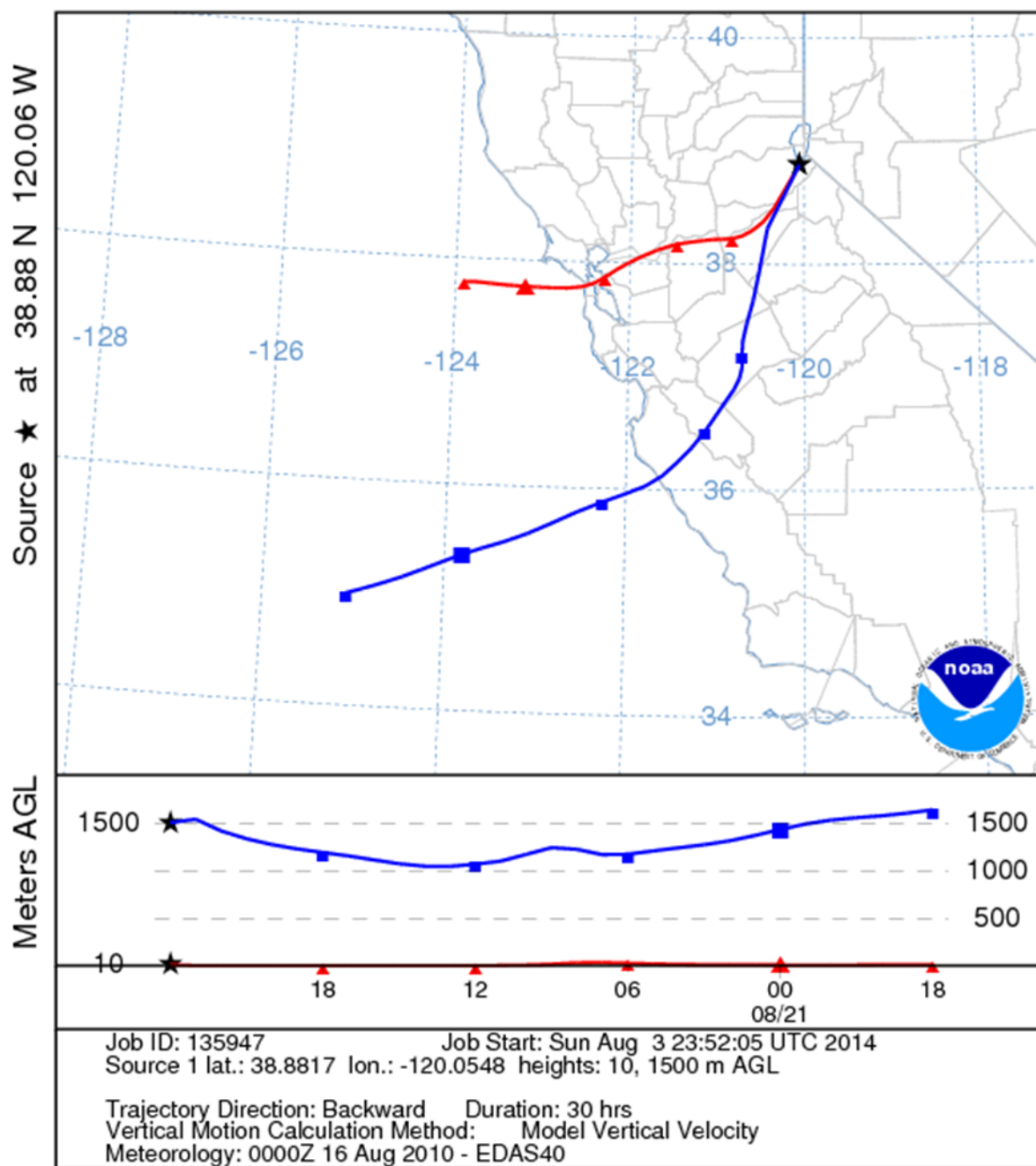


Fig. 2.8. Hysplit trajectories of Angora High Day

NOAA HYSPLIT MODEL  
 Backward trajectories ending at 0000 UTC 30 Aug 10  
 EDAS Meteorological Data

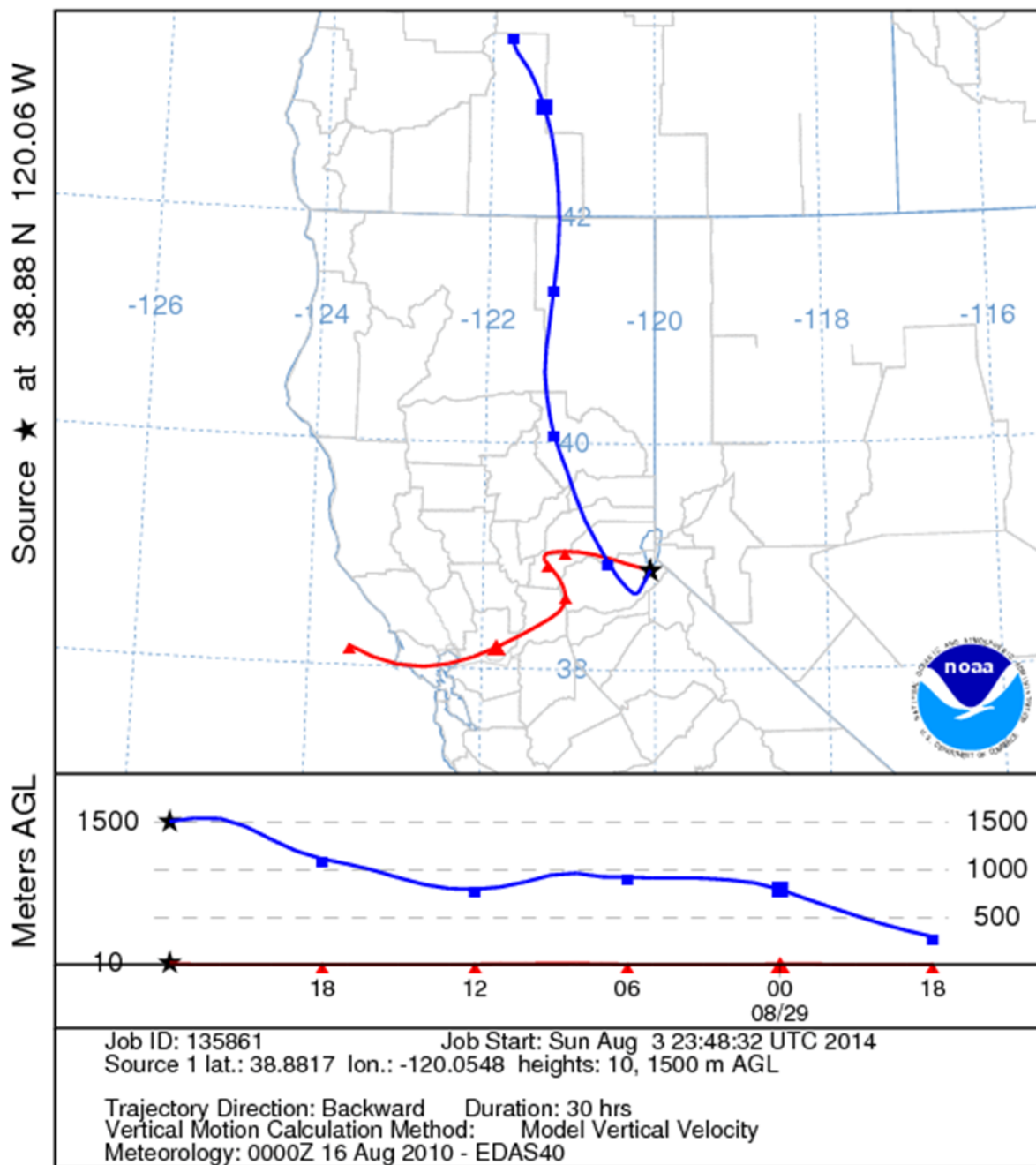
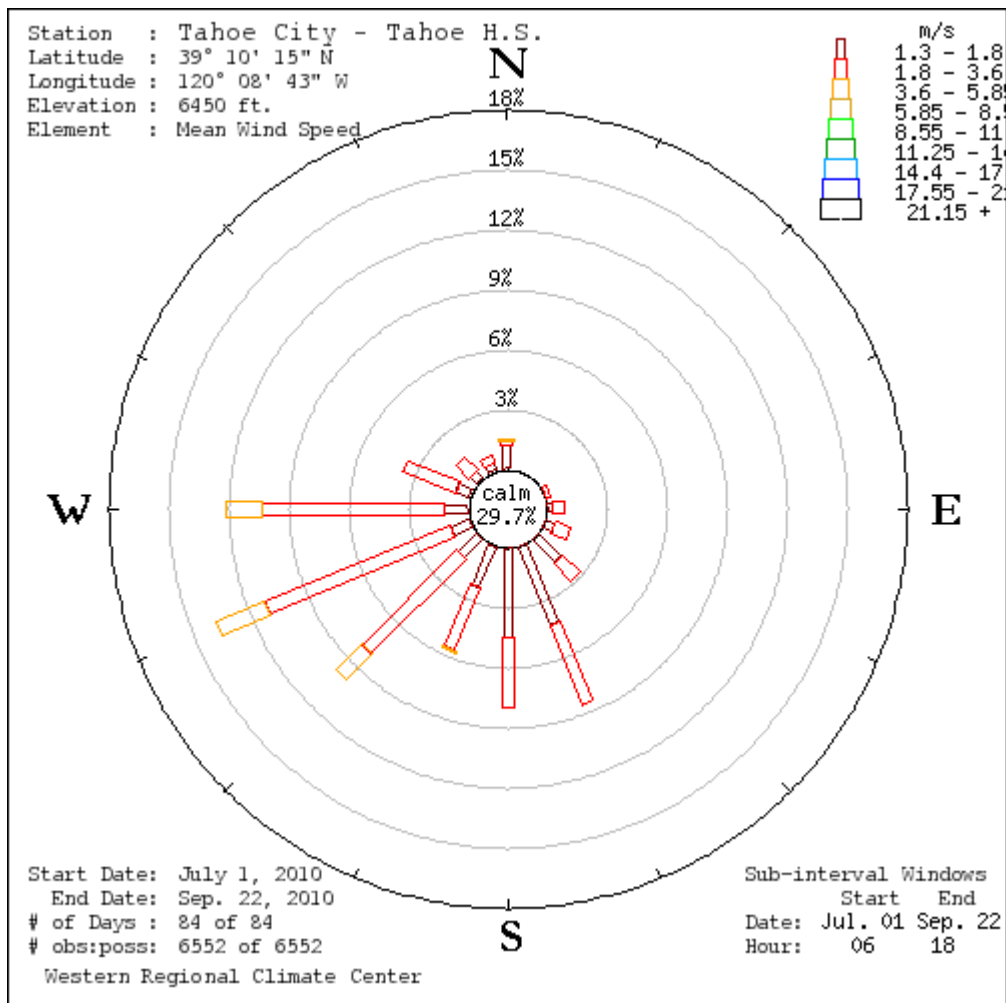
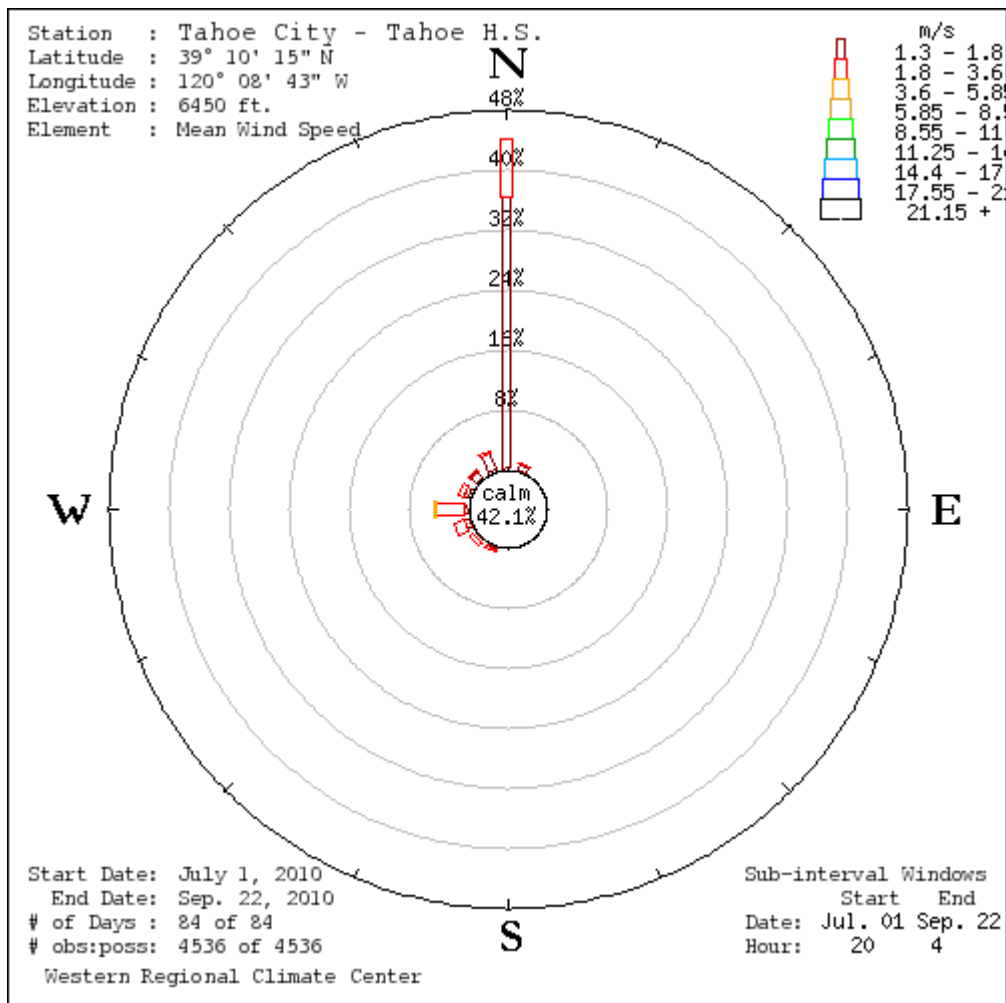


Fig. 2.9. Hysplit trajectories of Angora Low Day



**Fig. 2.10.** Daytime wind rose from WRCC observation site North Tahoe High School (NTHS)



**Fig. 2.11.** Nighttime wind rose from WRCC observation site North Tahoe High School (NTHS)

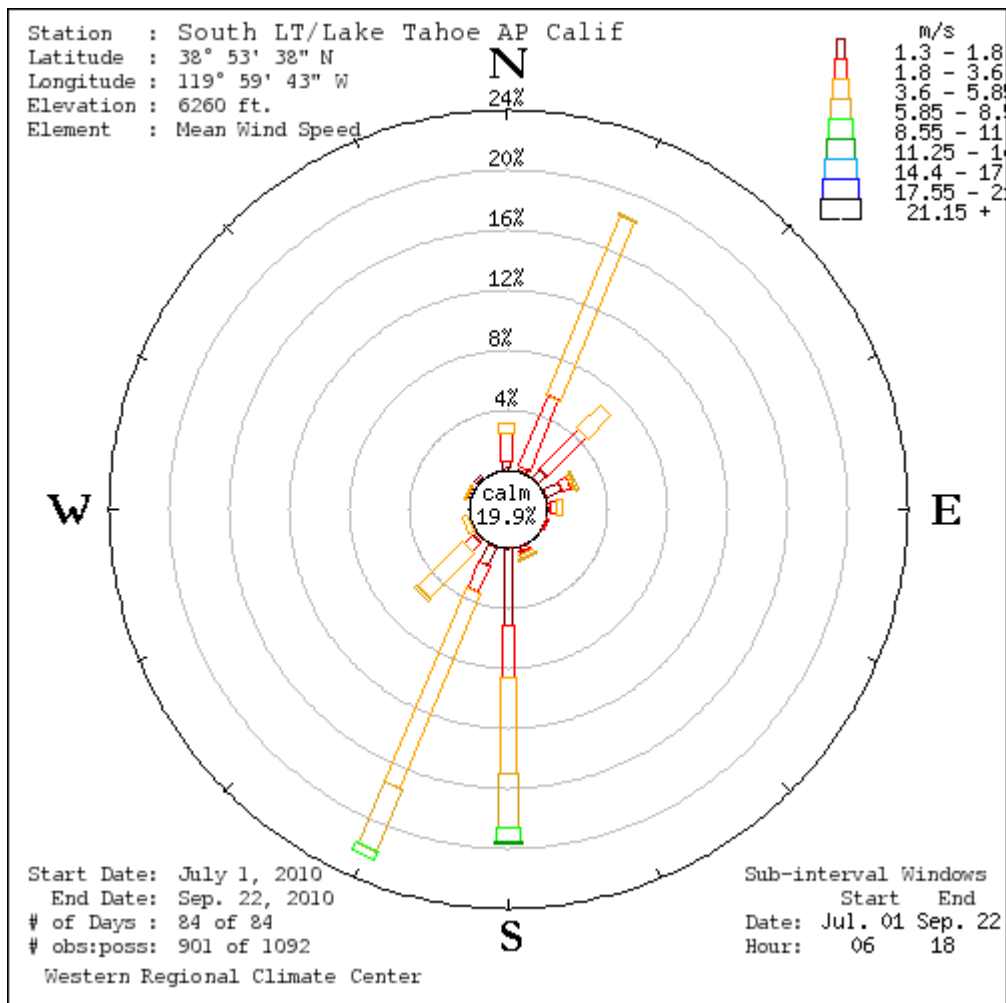
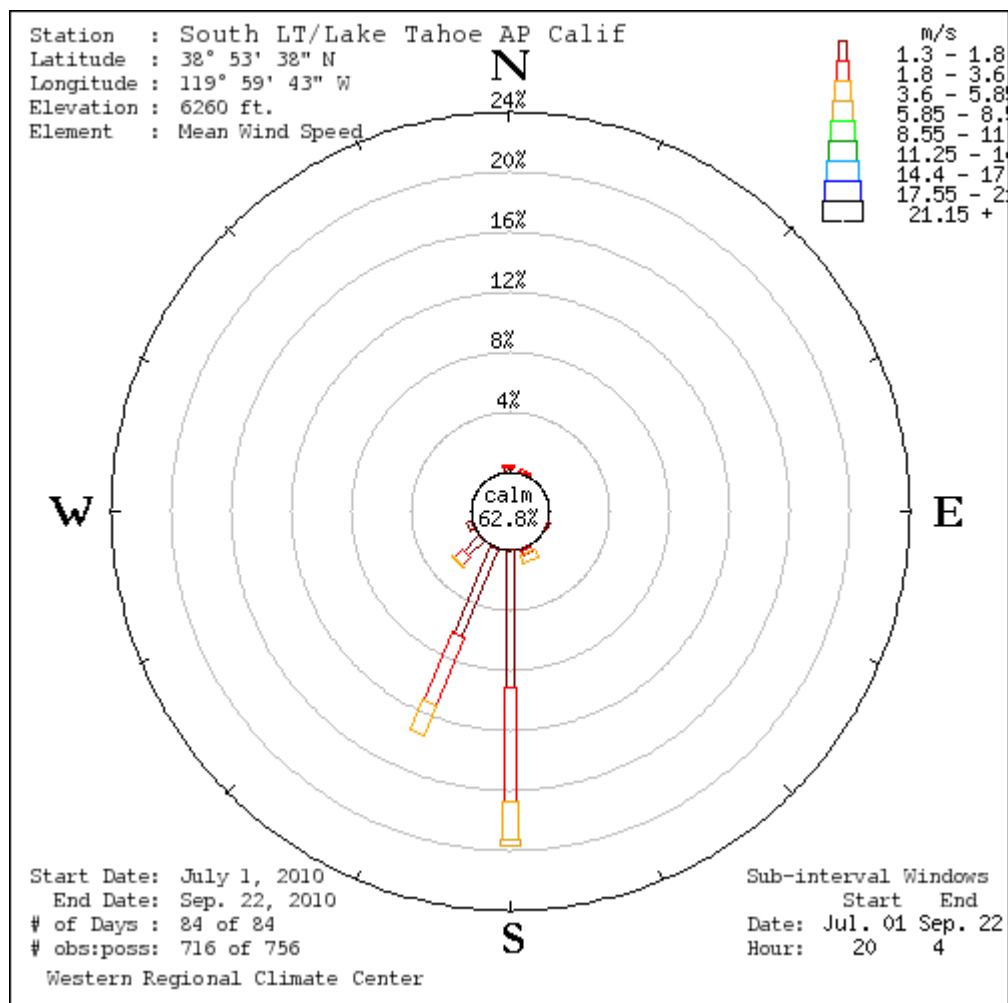


Fig. 2.12. Daytime wind rose from WRCC observation site South Lake Tahoe (KTVL)



**Fig. 2.13.** Nighttime wind rose from WRCC observation site South Lake Tahoe (KTVL)

**Table 2.1.** Elevation and distance from road of each site

Site	Elevation (masl)	Distance from Road (km)
Valhalla	1906	0.18
Thunderbird	1915	0.71
Blackwood	1948	2.5
Sugar Pine Point	1951	1.8
Angora	2218	4.4
Genoa 7000	2232	0.99
Watson Creek	2293	5.3
Genoa 8000	2449	3.2
Incline	2523	4.4
Genoa 9000	2734	5.5

<b>Correlation Matrix</b>	<b>Watson Creek</b>	<b>Genoa7</b>	<b>Genoa8</b>	<b>Genoa9</b>	<b>Angora</b>	<b>Blackwood</b>	<b>Valhalla</b>	<b>Thunderbird</b>	<b>Incline</b>	<b>Sugar Pine Point</b>
<b>Watson Creek</b>	1	0.79773	0.81326	0.31645	0.40462	0.86446	0.89034	0.65876	0.64071	0.89478
<b>Genoa7</b>	0.79773	1	0.87745	0.33171	0.41497	0.7917	0.84511	0.71622	0.56026	0.81142
<b>Genoa8</b>	0.81326	0.87745	1	0.54052	0.59318	0.76183	0.84684	0.7991	0.70781	0.80735
<b>Genoa9</b>	0.31645	0.33171	0.54052	1	0.82725	0.15858	0.25051	0.71676	0.78945	0.2321
<b>Angora</b>	0.40462	0.41497	0.59318	0.82725	1	0.29921	0.37648	0.75088	0.72628	0.36083
<b>Blackwood</b>	0.86446	0.7917	0.76183	0.15858	0.29921	1	0.88794	0.58817	0.46458	0.94114
<b>Valhalla</b>	0.89034	0.84511	0.84684	0.25051	0.37648	0.88794	1	0.65486	0.54952	0.92422
<b>Thunderbird</b>	0.65876	0.71622	0.7991	0.71676	0.75088	0.58817	0.65486	1	0.82828	0.64533
<b>Incline</b>	0.64071	0.56026	0.70781	0.78945	0.72628	0.46458	0.54952	0.82828	1	0.5397
<b>Sugar Pine Point</b>	0.89478	0.81142	0.80735	0.2321	0.36083	0.94114	0.92422	0.64533	0.5397	1

**Table 2.2.** Correlation matrix between sites

### **Chapter 3:**

## **Impact of Regional Meteorology on Ozone Levels in the Lake Tahoe Basin**

Sandra Theiss<sup>a</sup>, Alan Gertler<sup>a\*</sup>, Barbara Zielinska<sup>a</sup>, Andrzej Bytnerowicz<sup>b</sup>, Joel Burley<sup>c</sup>, and Michael Kaplan<sup>a</sup>

<sup>a</sup> *Desert Research Institute, 2215 Raggio Parkway,  
Reno, NV 89512, USA*

<sup>b</sup> *USDA Forest Service, Pacific Southwest Research Station,  
4955 Canyon Crest Drive, Riverside, CA 92507, USA*

<sup>c</sup> *Department of Chemistry, Saint Mary's College of California,  
Moraga, CA 94575-4527, USA*

\* *Corresponding Author: (757)674-7061, Alan.Gertler@dri.edu*

## **Abstract**

The Lake Tahoe Basin is located on the California-Nevada border and occasionally experiences elevated levels of ozone ( $O_3$ ) exceeding the 70 ppb California Air Resources Board (CARB) ambient air quality standard (8-hour average). Previous studies indicate that both the local generation of  $O_3$  in the Basin and long-range transport from out-of-Basin sources are important in contributing to  $O_3$  exceedances, but little is known about the impact of regional meteorology on the distribution of  $O_3$  source regions. In order to develop a better understanding of the factors affecting  $O_3$  levels and sources in the Lake Tahoe Basin, we performed a comprehensive field study in the summer of 2010. Included in this effort was a meteorological analysis addressing potential regional meteorological influences leading to periods of elevated levels of  $O_3$ . Three approaches were used to conduct the analysis: (1) regional atmospheric pressure difference (i.e. the Washoe Zephyr) to assess potential transport, (2) back trajectory modeling using the Hybrid Single-Particle Lagrangian Integrated Trajectory (HYSPLIT) model to determine where the air masses originated and, (3) composite soundings to evaluate in-Basin atmospheric influences. These analyses indicate the Washoe Zephyr did not strongly impact  $O_3$  levels in the Lake Tahoe Basin; however, higher  $O_3$  levels were found to correspond with both a more southerly wind component and a dip in dew point temperature around 400 hPa. The results also indicate that if transport of  $O_3$  does occur, it is more likely to come from the San Joaquin Valley and move to the southern Basin, rather than originating in the large cities to the west of Lake Tahoe (i.e. Sacramento and San Francisco).

### 3.1. Introduction

Lake Tahoe lies along the Nevada-California border at an elevation 1897 m above sea level (ASL), with the San Joaquin Valley to the southwest (Fig. 1) in California. The San Joaquin Valley is consistently among those regions with the highest ozone ( $O_3$ ) levels in the U.S., with over 55 unhealthy  $O_3$  days recorded over a three year period 2010 – 2012 (Lagarias and Sylte, 1991; Ranzieri and Thuillier, 1994; Dabdub et. al., 1999; Held et al., 2004; Cox et al., 2009; American Lung Association, 2014). Prevailing westerly winds in this region make the upwind metropolitan areas of Sacramento and San Francisco potential source regions for long-range transport of  $O_3$  into the Lake Tahoe Basin. Assessing the contributions of distant sources on local pollution levels remains a challenging problem, and requires an understanding of transport patterns that combine both long-range transported air masses as well as local pollutants (NAS, 2010). In addition, any study of  $O_3$  within the Lake Tahoe Basin must take into account the region's unusually complex meteorology, caused by both orographic effects of the Sierra Nevada mountains and the Great Basin, as well as by the Lake itself. One such meteorological factor in this region is the Washoe Zephyr, a thermally-forced regional wind circulation.

Regional thermally driven wind circulation patterns are a common phenomenon found in mountainous regions throughout the world (Whiteman, 1990, 2000; Zhong et al., 2008). These wind circulation patterns and the structure of the atmospheric boundary layer are important for understanding the transport of atmospheric pollutants and their precursors (Furger et al., 2000; Zhong et al. 2008). During summer months, when synoptic conditions are usually benign, thermally driven wind circulation patterns in mountainous terrain move up slope (anabatic wind) and up valley during the day, and down slope (katabatic wind) and down valley at night, due to the evolving slope temperature gradient between the land and neighboring air (Atkinson, 1981;

Whiteman, 1990; Zhong et al., 2008). In the Lake Tahoe region, however, a common thermally driven wind circulation, known as the Washoe Zephyr, occurs during summer afternoons and works on a spatial scale larger than the typical katabatic flow. This wind pattern results from the pressure gradient formed between a thermal low over the Great Basin, which develops during the afternoon hours, and higher pressure off the California coast (Zhong et al., 2008), causing air to flow from west to east and increasing the potential of transporting pollutants from cities to the west (i.e. San Francisco and Sacramento) into the Lake Tahoe Basin.

As discussed in Burley et al. (2015), several studies have investigated the transport of ozone and ozone precursors in the Lake Tahoe Basin from upwind source regions using aircraft (Carroll and Dixon, 2002; Zhang et al., 2002), and spatial and temporal ozone distributions (Bytnerowicz et al., 2004). These efforts have concluded that the Sierra Nevada mountains act as a barrier to prevent pollutants from entering the Lake Tahoe Basin. However, the mixing layer height plays a critical role in determining whether transported air masses either mix down into the basin or pass over the region without entrainment. As the Sierra Nevada Mountains orographically lift air, the presence of a higher mixing layer height allows the transported O<sub>3</sub>-enriched air to be mixed into the basin's atmospheric boundary layer, resulting in higher O<sub>3</sub> levels. If the mixing layer height is too low, then the O<sub>3</sub> enriched air cannot be mixed down into the basin, and lower O<sub>3</sub> concentrations should be observed. There have been several studies in Houston TX that have examined the mixing layer height and its influence on ground-level O<sub>3</sub> (Berman et al., 1999; Rappenglueck et al., 2008; Banta et al., 2011; and Haman et al., 2014) which conclude that the relationship between O<sub>3</sub> levels and the mixed layer height is complex. However, these studies do suggest the possibility that if a high level of O<sub>3</sub> concentrations is

found aloft, a higher mixed layer height would aid to entrain O<sub>3</sub> downward and increase ground-level concentrations.

Recent air quality studies in the Lake Tahoe basin (Gertler et al., 2006; Dolislager et al., 2012; Bytnerowicz et al., 2013; Burley et al., 2015) have shown that local generation of O<sub>3</sub> and long-range transport of O<sub>3</sub> and O<sub>3</sub> precursors are both important when it comes to elevated O<sub>3</sub> and other pollutant levels within the basin. As part of the larger research project to investigate O<sub>3</sub> forming precursors for the Lake Tahoe Basin (Bytnerowicz et al. 2013), Burley et al. (2015) show in-depth local influences, such as meteorological, terrain induced and photochemical including diurnal variability of surface ozone in the Lake Tahoe Basin.

Although Burley et al. (2015) assess smaller-scale meteorological conditions, such as the lake/land breeze, they do not discuss the larger scale, orographically-driven wind circulation patterns, which this paper expands upon. The focus of this effort utilizes O<sub>3</sub> data measured in 2010, along with sea level pressure data from Sacramento and Reno, to show how O<sub>3</sub> concentrations depend on regional weather phenomena (e.g. the Washoe Zephyr). In addition to understanding the effects of the Washoe Zephyr, an analysis of upper air data and back trajectories were used to assess the meteorological trends associated with episodes of high O<sub>3</sub> and low O<sub>3</sub>. To this end, we investigate meteorological influences associated with periods of elevated O<sub>3</sub> concentrations during the summer of 2010.

### **3.2. Methodology**

Burley et al. (2015) and Bytnerowicz et al. (2013) describe in detail, the O<sub>3</sub> measurements used. To investigate surface O<sub>3</sub> concentrations in the Lake Tahoe Basin, an O<sub>3</sub> monitoring network was deployed during a measurement period of July 1, 2010 through September 22, 2010 (Fig. 1). Hourly O<sub>3</sub> concentrations were measured at 10 sites around the

lake using Model 202 active UV-absorption monitors from 2B Technologies, which employ UV absorption at a wavelength of 254 nm (Bognar and Birks, 1996). These sites span the complete circumference of the lake, with lower elevation sites positioned within a few hundred meters of the shoreline and higher elevation sites located within a few kilometers of the shoreline. Most of these sites were located in remote locations except Valhalla (VAL) which was adjacent to a busy highway. The three sites varying in elevation, Genoa 7000 (GP7), Genoa 8000 (GP8) and Genoa 9000 (GP9) were located on Genoa Peak on the east side of the lake. Thunderbird (THB) was also on the east side of the lake, but situated at lake level. Valhalla (VAL) and Angora (AGL) were located on the south side of the lake while Watson Creek (WC) and Incline (ICN) were on the north side. Blackwood (LBC) and Sugar Pine Point (SPP) were at lake level positioned on the west side of the lake. Site descriptions are provided in Table 1. The maximum 8 hr O<sub>3</sub> was averaged over all ten sites, in order to obtain a value for the basin (Fig. 2). This study concluded that the basin is well mixed during the daytime hours and that due to the exposure to nocturnal ozone from the free troposphere, the higher elevation sites with steeply sloped topography experience elevated ozone concentrations, while lake-level sites with flat topography experience lower ozone concentrations.

To assess transport, the following three methods were used: evaluation of the Washoe Zephyr, an upper air analysis, and back trajectories. In order to determine the impact of the Washoe Zephyr, methods were used similar to those found in Zhong et al. (2008), who developed the Washoe Zephyr Index (WZI) based on the finding that Washoe Zephyr days occurred when the mean sea level pressure difference between Sacramento CA and Reno NV was positive. Conversely, when the pressure difference was negative the Washoe Zephyr did not form. This approach by Zhong et al. (2008) can be used to determine if a relationship exists

between O<sub>3</sub> levels and the Washoe Zephyr within the Tahoe Basin. Using mean sea level pressures from Sacramento CA and Reno NV during the summer of 2010, we calculated the WZI in order to determine the likely existence of Washoe Zephyr days (Fig. 3) and compared the WZI to the measured O<sub>3</sub> (Fig. 2).

Back trajectory calculations were also used to assess the influence of synoptic-scale atmospheric transport patterns and identify potential emission source regions. We obtained 24-hr air mass back trajectories using the HYSPLIT model available from the United States National Oceanic and Atmospheric Administration (NOAA) (<http://www.arl.noaa.gov>); (Draxler and Rolph, 2010). Each of the 84 days of the field study was analyzed at 0000 UTC. Three heights were chosen: 100 m which represents near surface trajectories (red line), 1500 m which represents within the boundary layer (blue line) and 3000 m which represents the free atmosphere (green line) (Figs. 4, 5). Although trajectories for each site were similar, the Watson Creek site was used as a generalized example to show the trajectories over the Lake. Using the maximum 8 hr ozone data averaged over all ten sites, these days were separated into the following three categories, based upon the standard deviation of the max 8 hr ozone values: high O<sub>3</sub> days (above one standard deviation from the average), low O<sub>3</sub> days (below one standard deviation from the average), and medium O<sub>3</sub> days (within one standard deviation). There were 22 high O<sub>3</sub> days, 44 medium O<sub>3</sub> days, and 22 low O<sub>3</sub> days. Sounding data were also analyzed for each of these days, and composite soundings were calculated for each category.

In order to perform an analysis of the upper levels in the atmosphere, sounding data – including temperature, dew point temperature, wind speed, and wind direction at mandatory pressure levels, as well as mixing layer height – were obtained through NOAA's Air Resources Laboratory (ARL). The ARL routinely uses National Centers for Environment Prediction

(NCEP) model data for use in air quality transport and dispersion modeling calculations (Air Resources Laboratory, 2014). Archived sounding data and mixed layer heights for the summer were obtained from the North American Regional Reanalysis (NARR) via the ARL. The NARR uses the very high resolution NCEP Eta Model (32km/45 layer) together with the Regional Data Assimilation System (RDAS) which assimilates precipitation along with other variables (Air Resources Laboratory, 2014). Improvements in the model/assimilation system have resulted in a data set with substantial increases in the accuracy of temperature, winds, and precipitation over coarser resolution analyses (Air Resources Laboratory, 2014).

### **3.3. Results and Discussion**

To obtain an overall O<sub>3</sub> value for the entire basin, the maximum 8 hr O<sub>3</sub> across all ten sites was averaged and plotted for the entire measurement period (Fig. 2). The average value of the plotted max 8 hr ozone is 54.97 ppb. One standard deviation above is 61.71 ppb and one standard deviation below is 48.23 ppb as indicated by the red lines on Figure 2. The highest day occurred on August 21<sup>st</sup> at 69.79 ppb and the lowest day occurred on July 18<sup>th</sup> at 39.95 ppb. The trend shows that a low period of ozone occurred from July 1<sup>st</sup> to July 26<sup>th</sup>, followed by a high period of ozone between July 27<sup>th</sup> and August 27<sup>th</sup>, which then steadily declined throughout September.

The WZI remained mostly negative most days in July (Fig. 3). However, days having a positive WZI corresponded to both low O<sub>3</sub> values (July 12) and increasing O<sub>3</sub> values (July 26) (Fig. 2). Also of note, the WZI stayed near zero during the days of August 5<sup>th</sup> to August 10<sup>th</sup>, and corresponded with higher O<sub>3</sub> values during this period. Additionally, when a sharp increase in WZI occurred, there was not always a similar increase in ozone, as seen on August 27<sup>th</sup>. While a positive WZI was found for the highest ozone day (August 21<sup>st</sup>), both values decreased shortly

after this peak. Finally, although the  $O_3$  values trended steadily downward in the month of September, the WZI increased around September 17<sup>th</sup>. The scatter plot for the entire summer (Fig. 6) does not show a strong correlation, with an  $R^2$  value of 0.04 despite a positive sloping linear regression line.

The HYSPLIT analysis showed that the high  $O_3$  days coincided strongly with rising air over the Basin. This suggests that when the transported  $O_3$  enriched air is pushed over the mountains, the rising motion created more turbulent mixing within the Basin, resulting in higher  $O_3$  concentrations at the surface. Also, this process started at lower elevations, first tapping into the polluted boundary layer and then bringing the air up and over the mountains into the Basin. Conversely, the low  $O_3$  days coincided more strongly with sinking air over the Basin, indicating that the parcels started at a higher elevation (above the polluted boundary layer) and lacked turbulent vertical mixing needed to bring polluted air from aloft into the basin. Thus, the sinking air acted as a capping mechanism for the Basin. Additionally, the HYSPLIT analysis showed air masses originating to the south on high  $O_3$  days, and to the west on low  $O_3$  days.

High  $O_3$  days were primarily characterized by a negative WZI and rising air parcels. The averaged WZI for the high  $O_3$  days was -1.08. The air parcels were rising over the Basin on 16 of the high days and sinking on only five days. The remaining day had neither rising nor sinking air over the Basin. The scatter plot for the high  $O_3$  days (Fig. 7) does not show a strong correlation with the WZI, having an  $R^2$  value of 0.08, despite also having a positive sloping linear regression line.

Medium  $O_3$  days were characterized by a slightly less negative WZI, and an equal number of days with rising and sinking air parcels. The averaged WZI for the medium  $O_3$  days was -0.79. Air parcels were rising over the Basin on 14 of the medium  $O_3$  days, and sinking over

the Basin on 14 days. The remaining 16 days had neither rising nor sinking air over the Basin. The scatter plot for the medium O<sub>3</sub> days (Fig. 8) does not show a strong correlation with the WZI, having an R<sup>2</sup> value of 0.01 and a negatively sloping regression line.

Finally, low O<sub>3</sub> days were characterized by an even less negative WZI and primarily sinking air parcels. The averaged WZI for the low O<sub>3</sub> days was -0.19. The air parcels were rising over the Basin on only one of the low O<sub>3</sub> days, while sinking air over the Basin occurred on 12 low O<sub>3</sub> days. The remaining 9 days had neither rising nor sinking air over the Basin. The scatter plot for the low O<sub>3</sub> days (Fig. 9) also does not show a strong correlation with the WZI, having both an R<sup>2</sup> value of 0.01 and a negative sloping linear regression line.

In order to differentiate the major differences in atmospheric temperature and dew point among high, medium and low O<sub>3</sub> days, composite atmospheric soundings were generated from daily NARR sounding data. The composite sounding for high O<sub>3</sub> days (Fig. 10) showed a strong dip in dew point temperature around 400 hPa, but no abnormal or abrupt shifts in temperature throughout the atmospheric column. Around 700 hPa, the winds shifted from a westerly direction to a more southwesterly direction. The averaged mixing layer height for high O<sub>3</sub> days was 2565 m. The composite sounding for the medium O<sub>3</sub> days (Fig. 11) showed no abnormal or abrupt shifts in dew point temperature, temperature, or winds throughout the atmospheric column, with winds primarily from the southwesterly direction. The averaged mixing layer height for medium O<sub>3</sub> days was 2361 m. The composite sounding for the low O<sub>3</sub> days (Fig. 12) shows a slight dip in dew point temperature around 400 hPa and a slight increase in dew point temperature around 725 hPa, but showed no abnormal or abrupt shifts in temperature throughout the atmospheric column. Despite the slight southerly direction of the winds around 625 hPa, the low O<sub>3</sub> composite sounding had the greatest westerly component to the wind throughout the entire column, as

compared to the high O<sub>3</sub> and medium O<sub>3</sub> composite soundings. The averaged mixing layer height for low O<sub>3</sub> days was 2087 m.

One of the main differences among the three composite soundings is a strong dry slot found around 400 hPa in the high O<sub>3</sub> composite. This suggests that drier air from the south is coming into the Basin. The composite sounding for the high O<sub>3</sub> days was generally drier throughout the entire atmospheric column as well. However, the low O<sub>3</sub> days had more moisture at the lower levels and showed a much weaker dry slot at 400 hPa, suggesting more humid air is present on low O<sub>3</sub> days.

Another difference among these soundings is that the composite wind direction for the high O<sub>3</sub> days had a more southerly component near 700 hPa than the other two soundings, suggesting that transported air, enriched with O<sub>3</sub>, comes more from the south than from the west. The composite wind direction for the low O<sub>3</sub> days, however, had a more westerly component throughout the majority of the column. This implies that either the air masses being transported from the west are not as O<sub>3</sub> enriched as those being transported from the south, or that the transported air masses from the west are not being as effectively mixed down into the basin as those coming from the south.

In summary, although the Washoe Zephyr has the potential to bring pollutant enriched air from the west, the statistical scatter plot analysis shows that a positive WZI alone cannot explain the observed O<sub>3</sub> values. The comparison analysis of O<sub>3</sub> levels with the WZI also shows that the higher WZI values occurred on days with lower O<sub>3</sub>, while the lower WZI values occurred on days with higher O<sub>3</sub>. This implies that the Washoe Zephyr led to lower O<sub>3</sub> levels in the Basin, but other factors must also be considered. This fact is validated in the HYSPLIT (Figs. 4, 5) and composite sounding analyses (Figs. 10, 11, 12), which both suggest that variables such as rising /

sinking air, the air parcel's starting elevation, mixing layer height, wind direction at 700 hPa, and dew point temperature, are more important than the WZI in determining high versus low O<sub>3</sub> days.

### **3.4. Summary and Conclusions**

Since routine air quality monitoring is not conducted in most of the northern Sierra Nevada, it is difficult to understand trends in pollutants affecting the Lake Tahoe Basin (Carroll et al., 2003). However, this study, along with Burley et al. (2015), provides a better understanding of the factors affecting O<sub>3</sub> levels and O<sub>3</sub>-forming precursors within the Lake Tahoe Basin. In order to investigate meteorological influences associated with periods of elevated O<sub>3</sub> concentrations, an intensive field study was conducted during summer 2010. A meteorological analysis was then performed to ascertain potential regional-scale influences, such as the Washoe Zephyr, on observed O<sub>3</sub> concentrations. The meteorological assessment of O<sub>3</sub> levels shows that the 700 hPa wind flow increases background concentrations of O<sub>3</sub> when coming from a more southerly direction. This indicates that transport from southern out-of-basin sources (such as the San Joaquin Valley) rather than from western sources (such as Sacramento and San Francisco) has a greater contribution to elevated O<sub>3</sub> levels in the basin. It also indicates that factors other than the Washoe Zephyr (such as mixing layer height, sinking or rising air, and dew point temperature) have a more significant impact on development of high or low O<sub>3</sub> days within the Lake Tahoe Basin or are associated with the southerly airflow from the San Joaquin Valley.

Atmospheric sounding and HYSPLIT analysis of O<sub>3</sub> distribution data indicate that O<sub>3</sub> and O<sub>3</sub>-forming precursors may be transported into the Basin at higher levels in the atmosphere, but also need a high mixing layer height and rising air parcels to be mixed downward into the Basin.

This study thus suggests a need for further research into mixed layer heights and the relationship to ground-level O<sub>3</sub> for the Lake Tahoe Basin. Additionally, this study indicates a need for further modeling and routine measurement studies in order to (i) better quantify the contributions from in-basin and out-of-basin sources (ii) determine the downward mixing mechanisms that operate within the basin and (iii) assess the future trends associated with elevated O<sub>3</sub> levels. Such efforts could contribute to the development and implementation of more effective O<sub>3</sub> control strategies and fewer exceedances of the ambient air quality standards.

### **Acknowledgements**

This study was supported by a grant from the U.S. Department of Agriculture Forest Service through the Tahoe Science Program funded by the Southern Nevada Public Lands Management Act (SNPLMA). The authors also would like to thank Joey Keely, Chris Engelhardt, Paul McCulloch, and Shana Gross of the U.S. Department of Agriculture (USDA) Forest Service Lake Tahoe Basin Management Unit for logistical help and data collection; Andrew Strain and Casey Blann of the Heavenly Mountain Skiing Operations, Dennis Malone of the Thunderbird Lodge, and Jack Coughlin of Diamond Peak Skiing Operations for providing support for monitoring and selection of sites; Brant C. Allen of UC Davis Environmental Research Center and Chris Ross of the USDA Forest Service PSW Research Station for help with installation and collection of data; Jonathan Long and Tiffany Van Huysen of the USDA Forest Service PSW Research Station for administrative support for the study. A special thanks to the collaborators: Suraj Ahuja, Ricardo Cisneros, Glen Shaw, Don Schweizer, and Trent Procter of U.S. Forest Service Region 5; Susan Schilling of the U.S. Forest Service Pacific Southwest Research Station; Leora Nanus of San Francisco State University; Mark McDaniel of

the Desert Research Institute; James Sickman and Michael Bell of the University of California; Miriam Rorig of USDA Forest Service PNW Research Station. Thanks also to Nyssa Perryman for help and support.

## References

- Air Resources Laboratory., 2014. Ready Archived Meteorology. Online,  
<<http://www.arl.noaa.gov/>>
- American Lung Association, State of the air: 2014 report: <http://www.stateoftheair.org>.
- Atkinson, B. W., 1981: Meso-Scale Atmospheric Circulations. Academic Press, 495 pp.
- Banta, R. M., et al. 2011. Dependence of daily peak O<sub>3</sub> concentrations near Houston, Texas on environmental factors: Wind speed, temperature, and boundary-layer depth, *Atmospheric Environment*, **45**, 162–173.
- Berman, S., J. Y. Ku, and S. T. Rao, 1999. Spatial and temporal variation in the mixing depth over the Northeastern United States during the summer of 1995, *Journal of Applied Meteorology*, **38**, 1661–1673.
- Bognar, J. A., Birks, J. W., 1996. Miniaturized ultraviolet ozonesonde for atmospheric measurements, *Analytical Chemistry*, **68**, 3059-3062.
- Burley, J. D., Theiss, S., Bytnerowicz, A., Gertler, A., Schilling, S., and Zielinska, B., 2015. Surface ozone in the Lake Tahoe Basin. *Atmospheric Environment*, **109**, 351-369.
- Bytnerowicz, A., Arbaugh, M, and Padgett, P., 2004. Evaluation of ozone and HNO<sub>3</sub> vapor distribution and ozone effects on conifer forests in the Lake Tahoe Basin and eastern Sierra Nevada. Final Report to California Air Resources Board, Contract No. 01-334, USDA Forest Service, Pacific Southwest Research Station.  
<http://arbis.arb.ca.gov/research/apr/past/01-334.pdf>
- Bytnerowicz, A., Fenn, M., Gertler, A., Preisler, H., and Zielinska, B., 2013. Distribution of

- ozone, ozone precursors and gaseous components of atmospheric nitrogen deposition in the Lake Tahoe Basin. Final Report to California Air Resources Board, Contract No. P063, USDA Forest Service, Pacific Southwest Research Station.
- Carroll, J. J., Miller, P. R., and Pronos, J., 2003. Historical perspectives on ambient ozone and its effects on the Sierra Nevada. *Developments in Environmental Science*, **2**, 33-54.
- Cox, P., Delao, A., Komorniczak, A., and Weller, R., 2009. The California almanac of emissions and air quality, California Air Resources Board, Sacramento, CA. Online, <<http://www.arb.ca.gov/aqd/almanac/almanac09/almanac09.htm>>
- Dabdub, D., DeHaan, L.L. and Seinfeld, J.H., 1999. Analysis of ozone in the San Joaquin Valley of California. *Atmospheric Environment*, **33**, 2501-2514.
- Dolislager, L. J., VanCuren, R., Pederson, J. R., Lashgari, A., and McCauley, E., 2012. An assessment of ozone concentrations within and near the Lake Tahoe Air Basin. *Atmospheric Environment*, **46**, 645-654.
- Draxler, R.R., Rolph, G.D., 2010. HYSPLIT (Hybrid Single-Particle Lagrangian Integrated Trajectory) Model Access via NOAA ARL READY Website. NOAA Air Resources Laboratory, Silver Spring, Maryland, U.S.A.. <http://www.ready.arl.noaa.gov/HYSPLIT.php>
- Furger, M. J. Dommen, W.K. Graber, L. Poggio, A.S.H. Prévôt S. Emeis, G. Grell, T. Trickl, B. Gomiscek, B. Neining, G. Wotawa., 2000: The VOTALP Mesolcina Valley Campaign 1996 Concept, background and some highlights. *Atmospheric Environment*, **34**, 1395-1412.
- Gertler, A.W., A. Bytnerowicz, T.A. Cahill, M. Arbaugh, S. Cliff, J.K. Koračin, L. Tarnay, R.

- Alonso, and W. Frączek., 2006. Local Pollutants Threaten Lake Tahoe's Clarity, *California Agriculture*, **60**, 53-58.
- Haman, C. L., E. Couzo, J. H. Flynn, W. Vizuite, B. Heffron, and B. L. Lefer, 2014. Relationship between boundary layer heights and growth rates with ground-level ozone in Houston, Texas, *Journal of Geophysical Research: Atmospheres*, **119**, 6230–6245, doi:10.1002/2013JD020473.
- Held, T., Ying, Q., Kaduwela, A., and Kleeman, M., 2004. Modeling particulate matter in the San Joaquin Valley with a source-oriented externally mixed three-dimensional photochemical grid model. *Atmospheric Environment*, **38**(22), 3689-3711.
- Kalnay, E., Kanamitsu, M., Kistler, R., Collins, W., Deaven, D., Gandin, L, and Joseph, D. 1996: The NCEP/NCAR Reanalysis 40-year Project. *Bulletin of the American Meteorological Society*, **77**, 437-471.
- Lagarias, J.S., and Sylte, W.W., 1991. Designing and managing the San Joaquin Valley air quality study. *Journal of Air and Waste Management Association*, **41**, 1176-1179.
- NAS report, 2010: global sources of local pollution-An Assessment of Long-Range Transport of Key Air Pollutants to and from the United States, 35–66, Online, <<http://books.nap.edu/openbook.php?recordid=12743&page=35>>
- Ranzieri, A. J., and Thuillier, R. H., 1994. SJVAQS and AUSPEX: a Collaborative Air Quality Field Measurement and Modeling Program; Planning and Managing Regional Air Quality; Ed. *Solomon, PA*.
- Rappenglueck, B., R. Perna, S. Zhong, and G. A. Morris, 2008. An analysis of the vertical

structure of the atmosphere and the upper-level meteorology and their impact on surface ozone levels in Houston, Tex., *Journal of Geophysical Research*, **113**, D17315, doi:10.1029/2007JD009745.

Twain, M., 1871: *Roughing It*. New York: Harper and Brothers. 330 pp.

Whiteman, C. D., 1990: Observations of thermally developed wind systems in mountainous terrain. *Atmospheric Processes over Complex Terrain, Meteorological Monographs*, No. 45, American Meteorological Society, 5–42.

Whiteman, C.D., 2000: *Mountain Meteorology: Fundamentals and Applications*. Oxford University Press, 355 pp.

Zhong, Shiyuan, Ju Li, Craig B. Clements, Stephan F. J. De Wekker, Xindi Bian., 2008: Forcing Mechanisms for Washoe Zephyr—A Daytime Downslope Wind System in the Lee of the Sierra Nevada. *Journal of Applied Meteorological Climatology*, **47**, 339–350.

## Tables

Site	Elevation (masl)	Site Description
Thunderbird (THB)	1915	On the roof of a shed at the base of a steep incline
Valhalla (VAL)	1906	Flat sandy terrain with low scrub; near CA Hwy. 89
Blackwood (LBC)	1948	Flat open meadow with wet grass
Sugar Pine Point (SPP)	1951	Flat open meadow; a few nearby trees
Genoa 7000 (GP7)	2232	Small clearing on mild slope; thick grass
Angora (AGL)	2218	Steep hillside near top of ridge; extensive fire damage
Watson Creek (WC)	2293	Flat open meadow with leafy green plants
Genoa 8000 (GP8)	2449	Open clearing on moderate slope; heavy fire damage
Incline (ICN)	2523	Wide, open, steep slope with lots of green plants
Genoa 9000 (GP9)	2734	Rocky outcropping near summit; excellent exposure

**Table 3.1.** Elevation and description of O<sub>3</sub> measurement sites.

## List of Figures

Fig. 1: Location of Lake Tahoe and the ten measurement sites.

Fig. 2: Maximum 8 hr O<sub>3</sub> averaged over all ten sites. Top red line indicates one standard deviation above and bottom red line indicates one standard deviation below.

Fig. 3: Washoe Zephyr Index (difference between Sacramento mean sea level pressure and Reno mean sea level pressure) Positive value indicates Washoe Zephyr day, negative value indicates no Washoe Zephyr day.

Fig. 4: HYSPLIT example of a high O<sub>3</sub> day.

Fig. 5: HYSPLIT example of a low O<sub>3</sub> day.

Fig. 6: Scatter plot of Washoe Zephyr Index and Max 8 hr O<sub>3</sub> for the summer of 2010.

Fig. 7: Scatter plot of Washoe Zephyr Index and Max 8 hr O<sub>3</sub> for the high O<sub>3</sub> days.

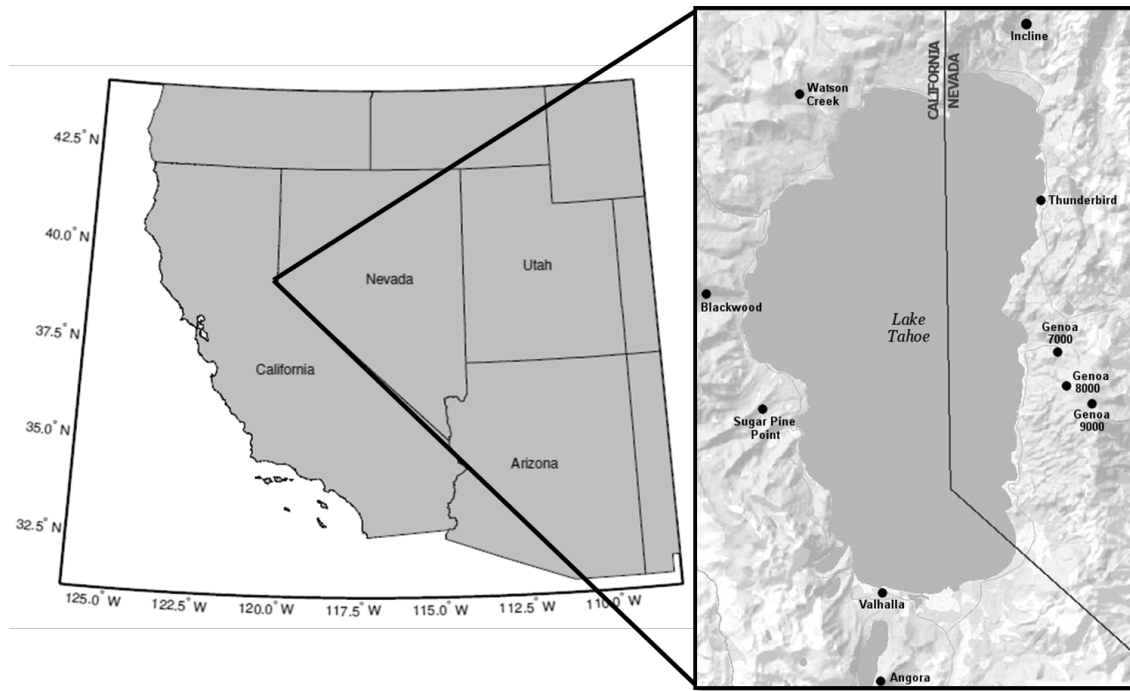
Fig. 8: Scatter plot of Washoe Zephyr Index and Max 8 hr O<sub>3</sub> for the medium O<sub>3</sub> days.

Fig. 9: Scatter plot of Washoe Zephyr Index and Max 8 hr O<sub>3</sub> for the low O<sub>3</sub> days.

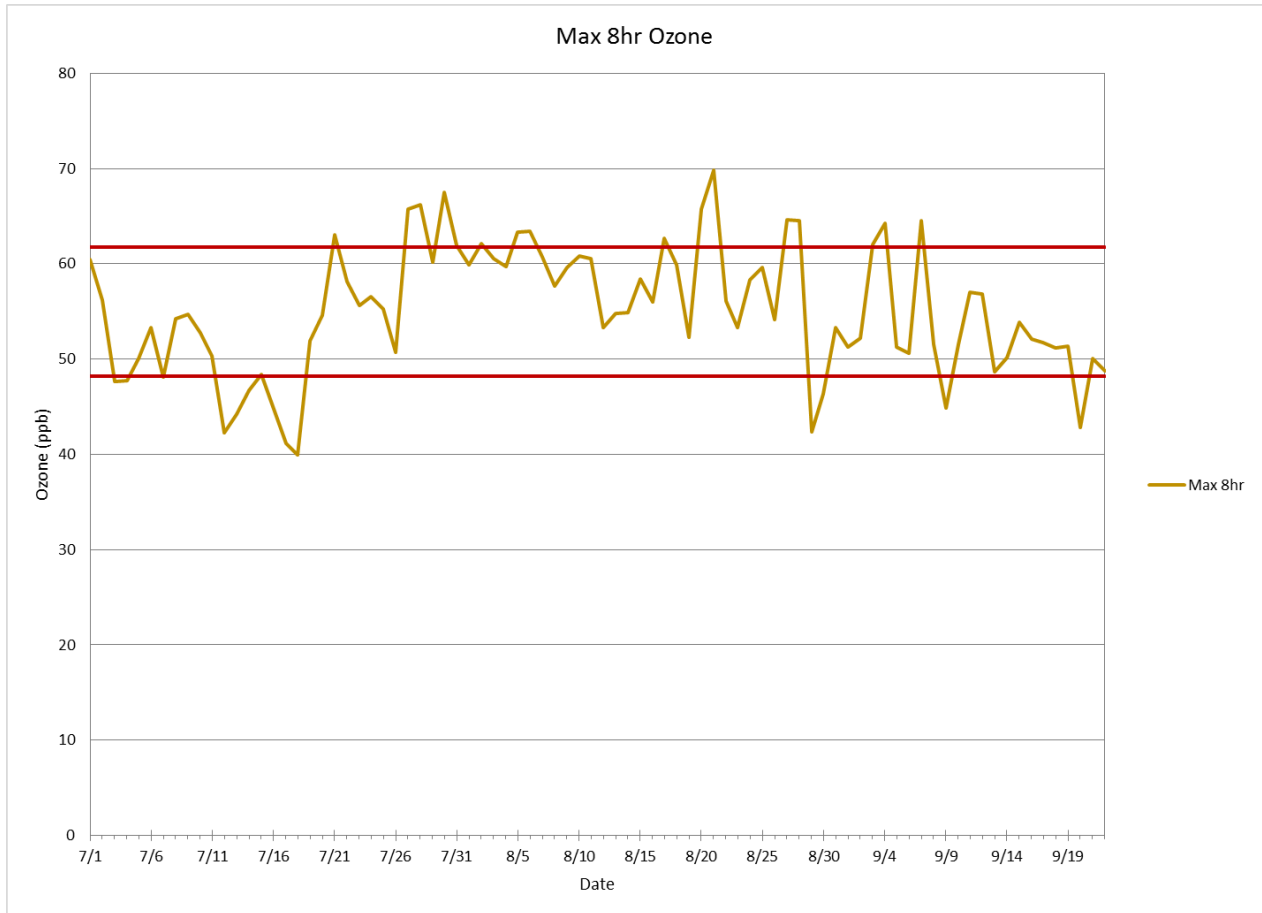
Fig. 10: Sounding composite for the high O<sub>3</sub> days.

Fig. 11: Sounding composite for the medium O<sub>3</sub> days.

Fig. 12: Sounding composite for low O<sub>3</sub> days.

**Figures**

**Figure 3.1.** Location of Lake Tahoe and the ten measurement sites.



**Figure 3.2.** Maximum 8 hr  $O_3$  averaged over all ten sites. Top red line indicates one standard deviation above and bottom red line indicates one standard deviation below.

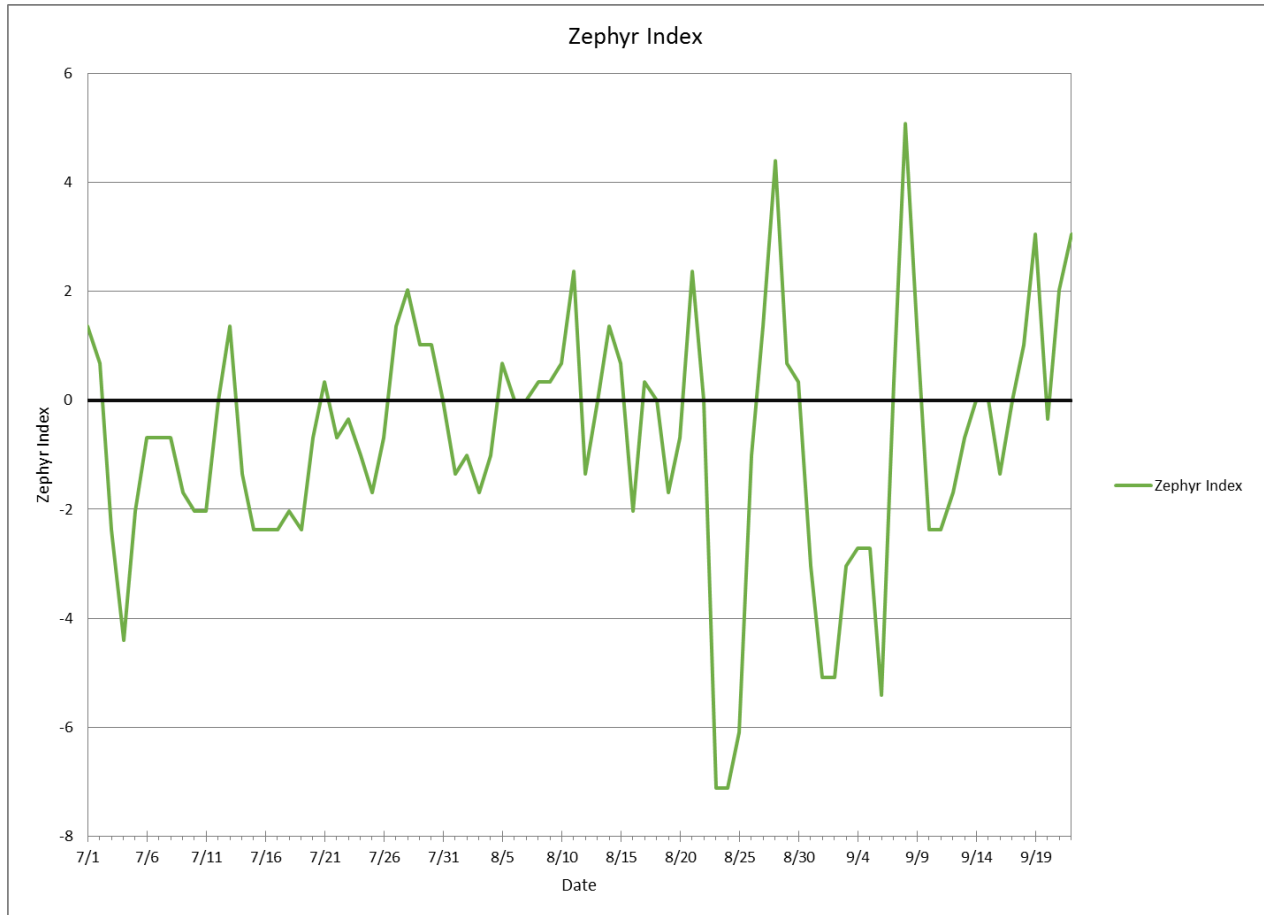


**Figure 3.3.** Washoe Zephyr Index (difference between Sacramento mean sea level pressure and Reno mean sea level pressure) Positive value indicates Washoe Zephyr day, negative value indicates no Washoe Zephyr day.

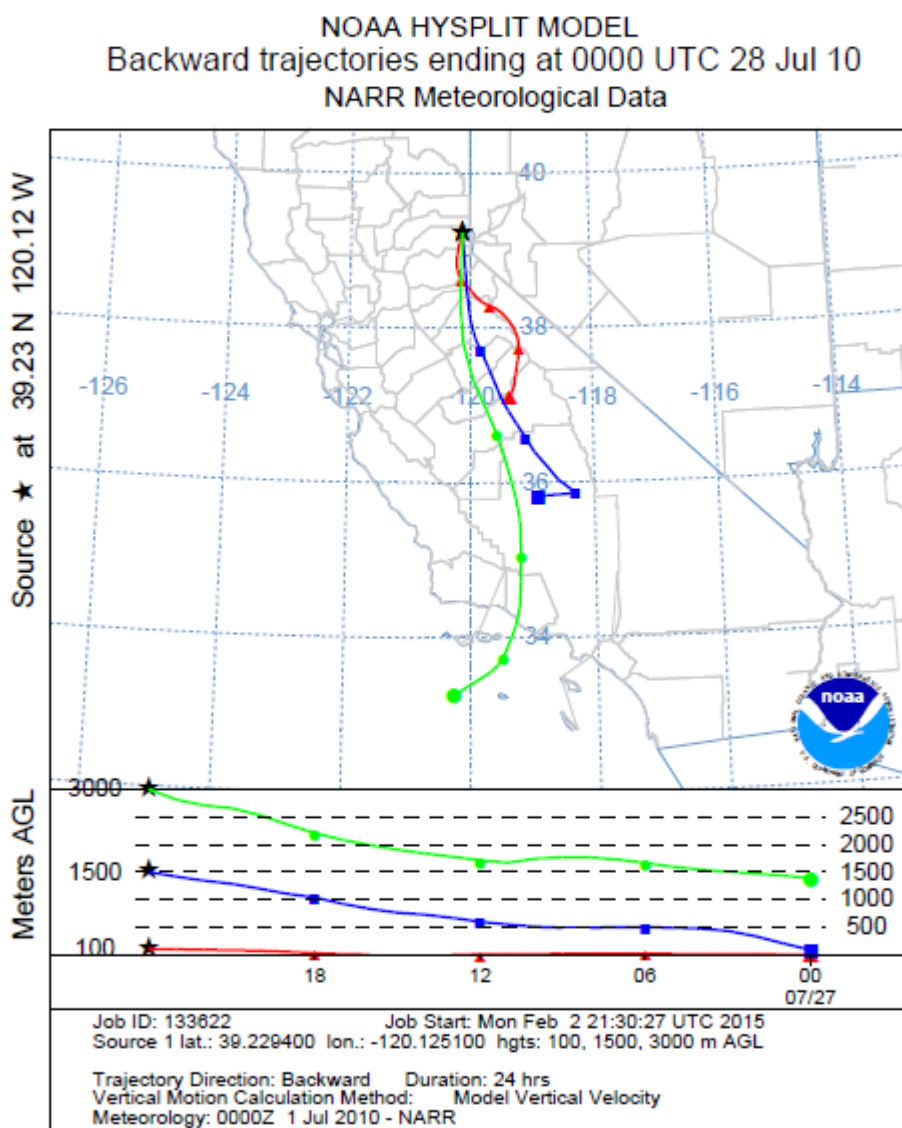
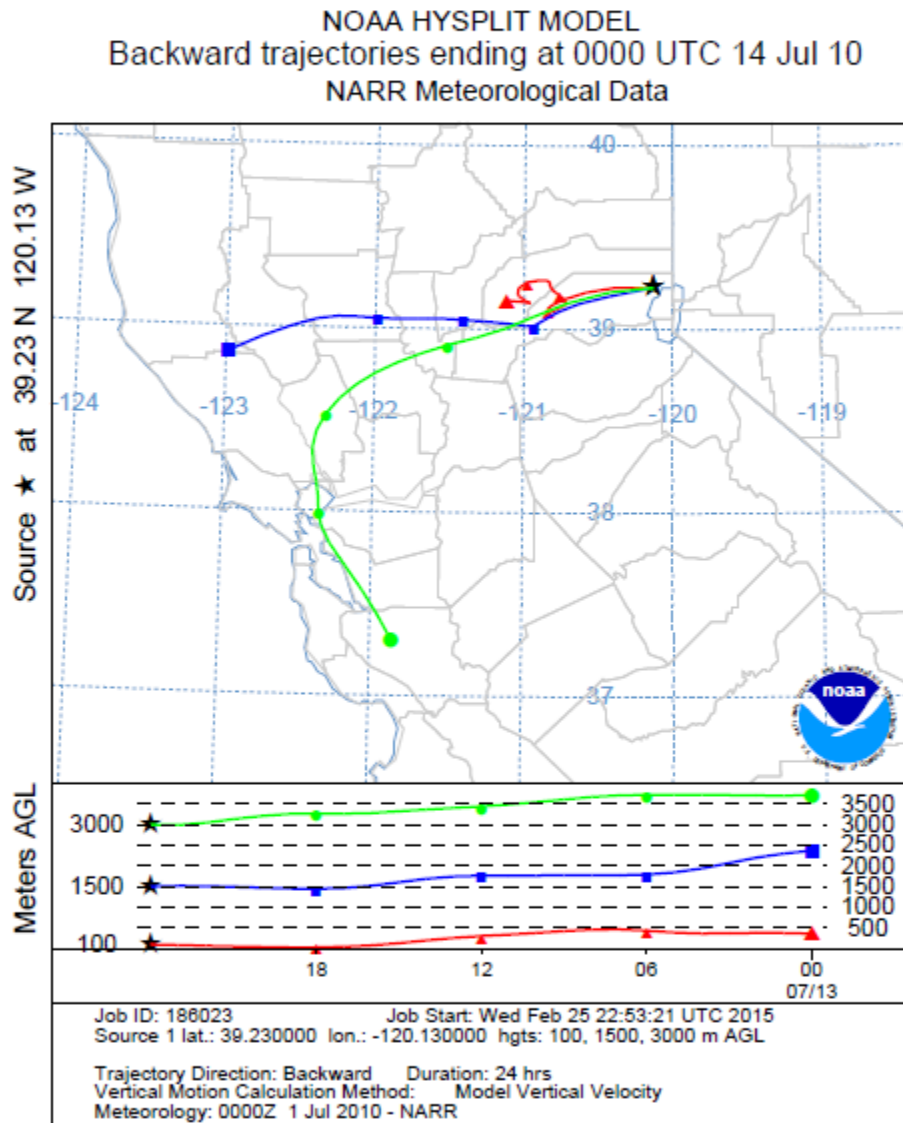
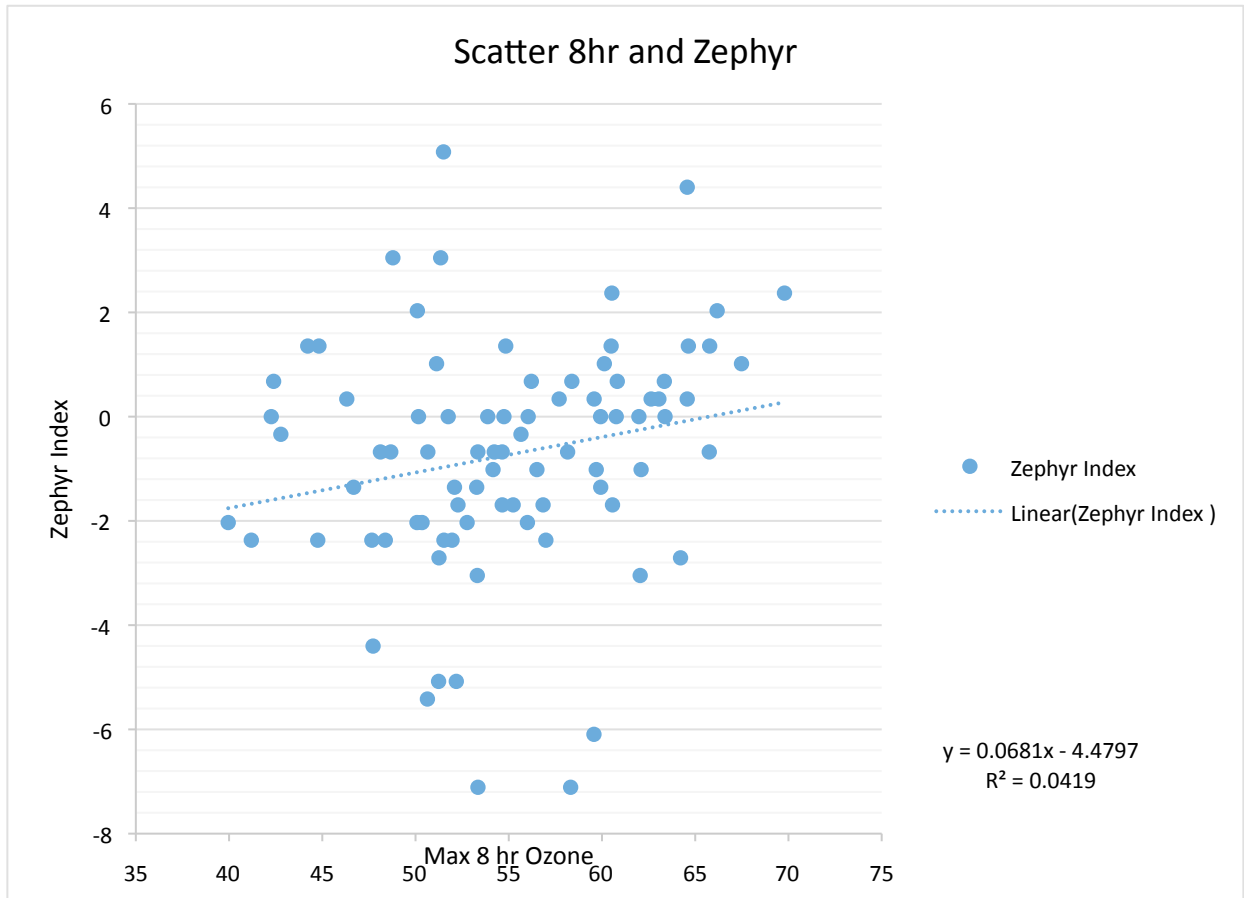


Figure 3.4. HYSPLIT example of a high O<sub>3</sub> day.



**Figure 3.5.** HYSPLIT example of a low O<sub>3</sub> day.



**Figure 3.6.** Scatter plot of Washoe Zephyr Index and Max 8 hr O<sub>3</sub> for the summer of 2010.

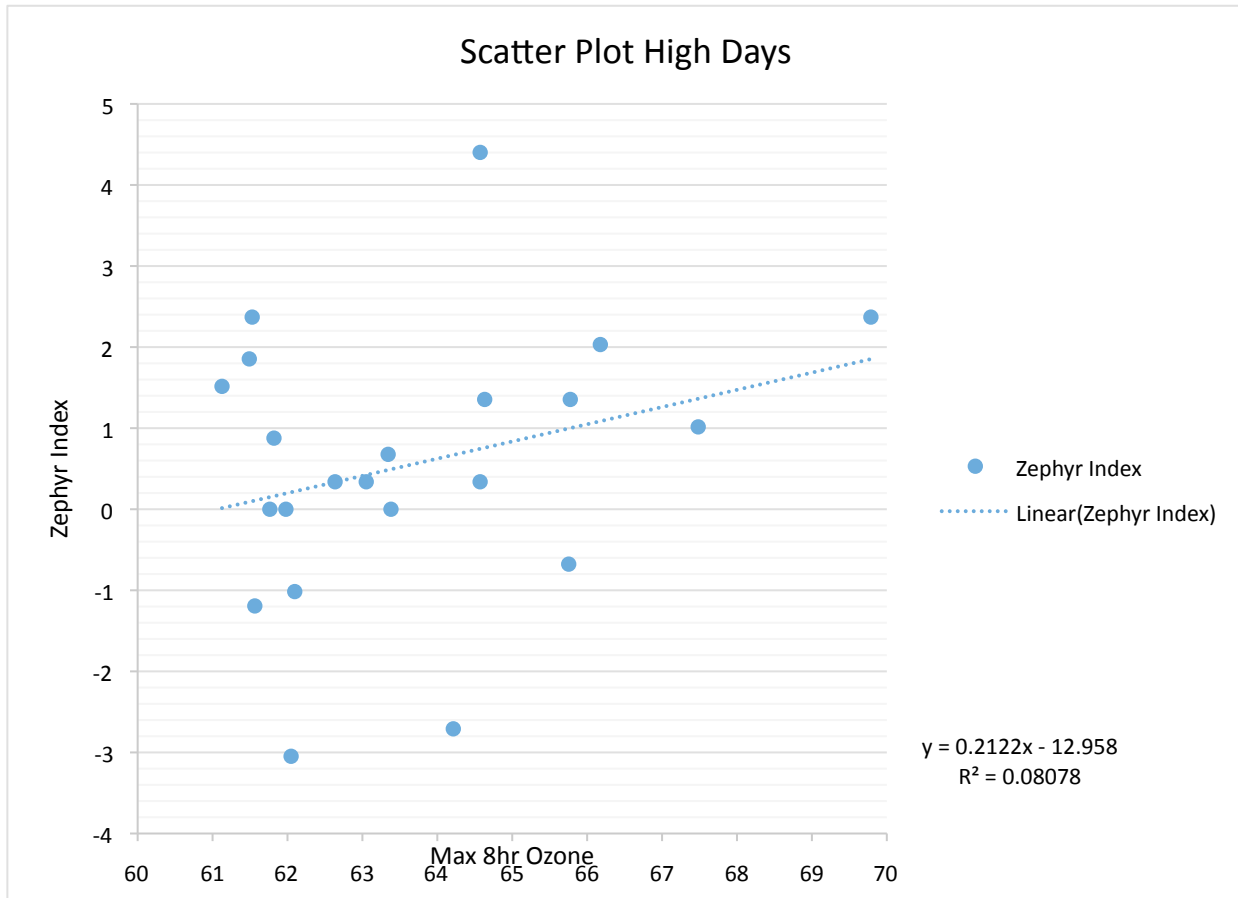


**Figure 3.7.** Scatter plot of Washoe Zephyr Index and Max 8 hr O<sub>3</sub> for the high O<sub>3</sub> days.

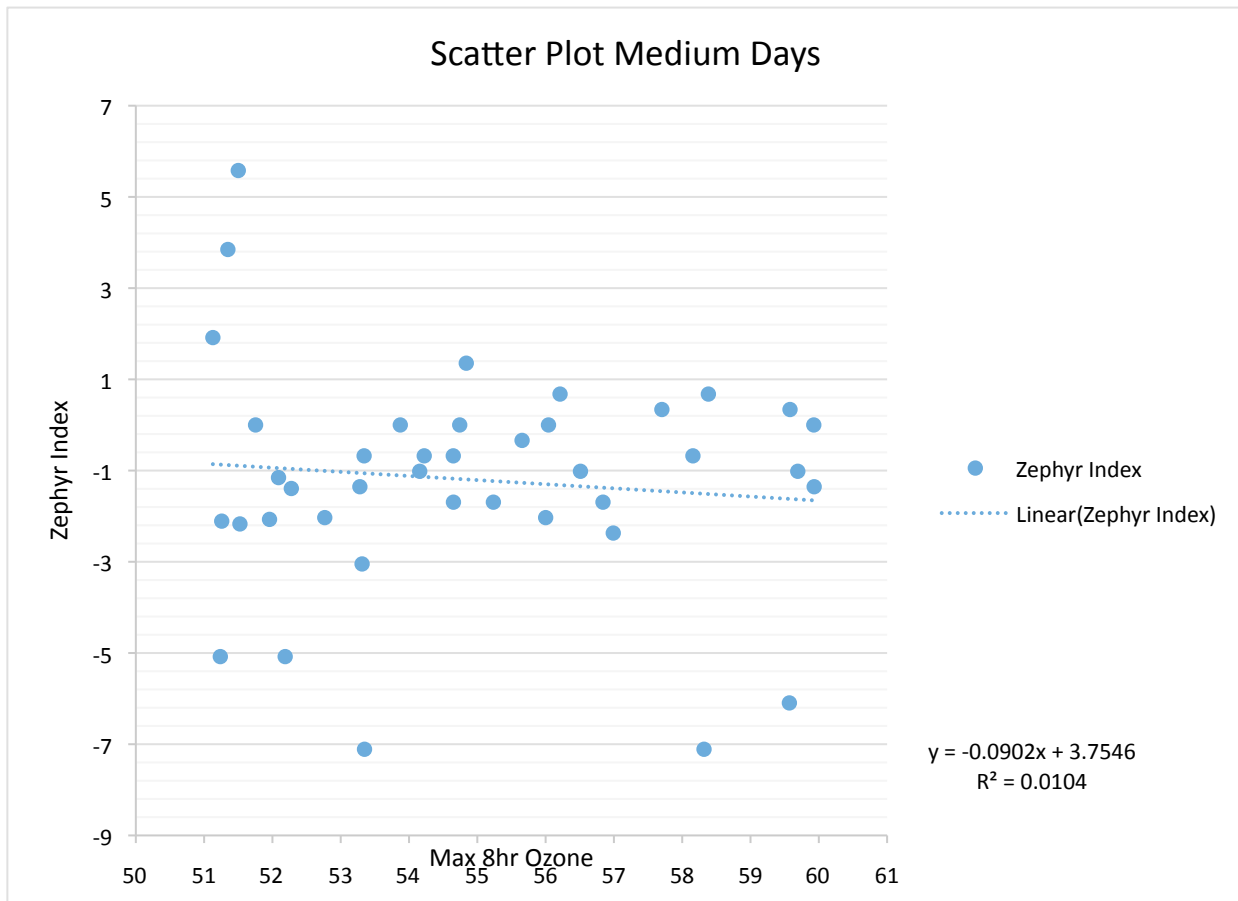


**Figure 3.8.** Scatter plot of Washoe Zephyr Index and Max 8 hr O<sub>3</sub> for the medium O<sub>3</sub> days.

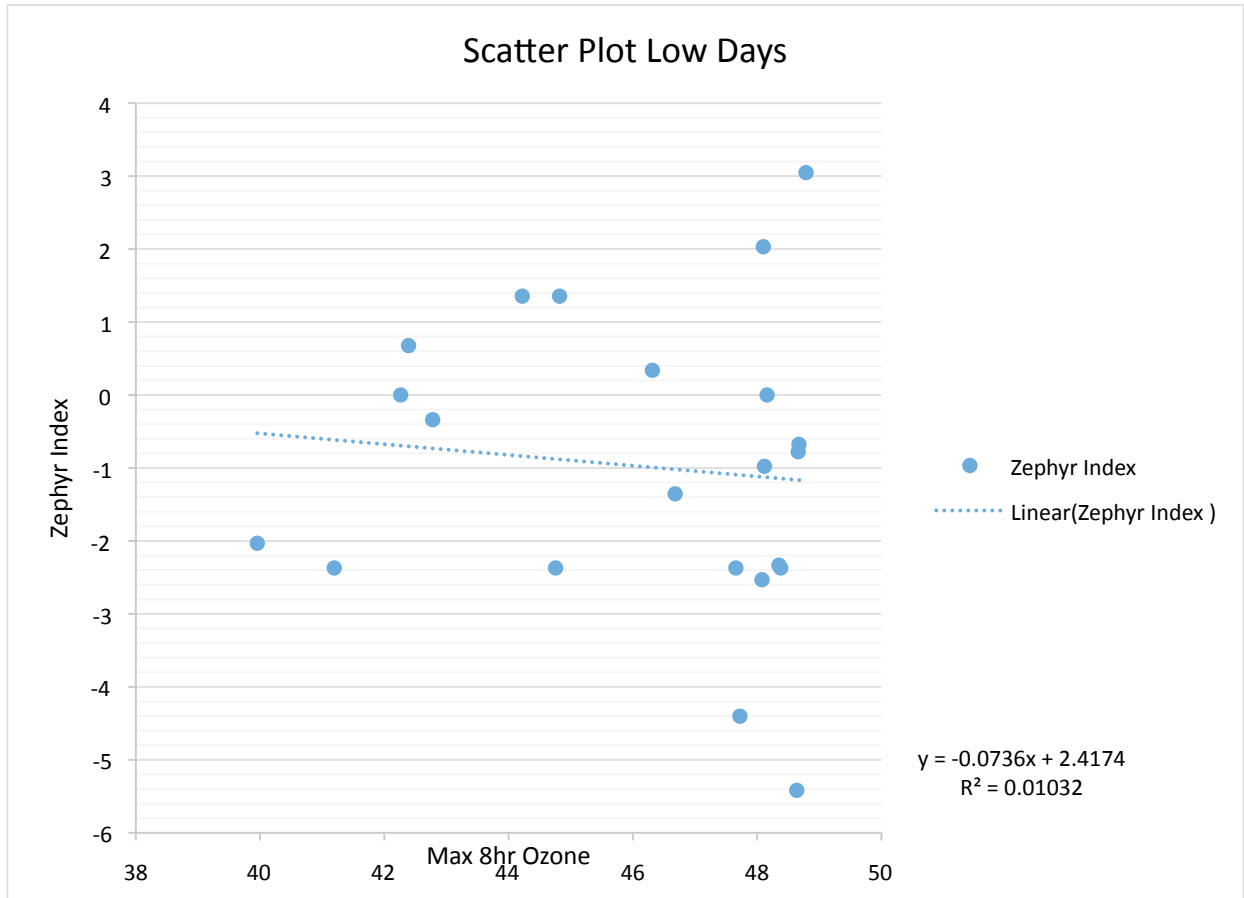


**Figure 3.9.** Scatter plot of Washoe Zephyr Index and Max 8 hr O<sub>3</sub> for the low O<sub>3</sub> days.

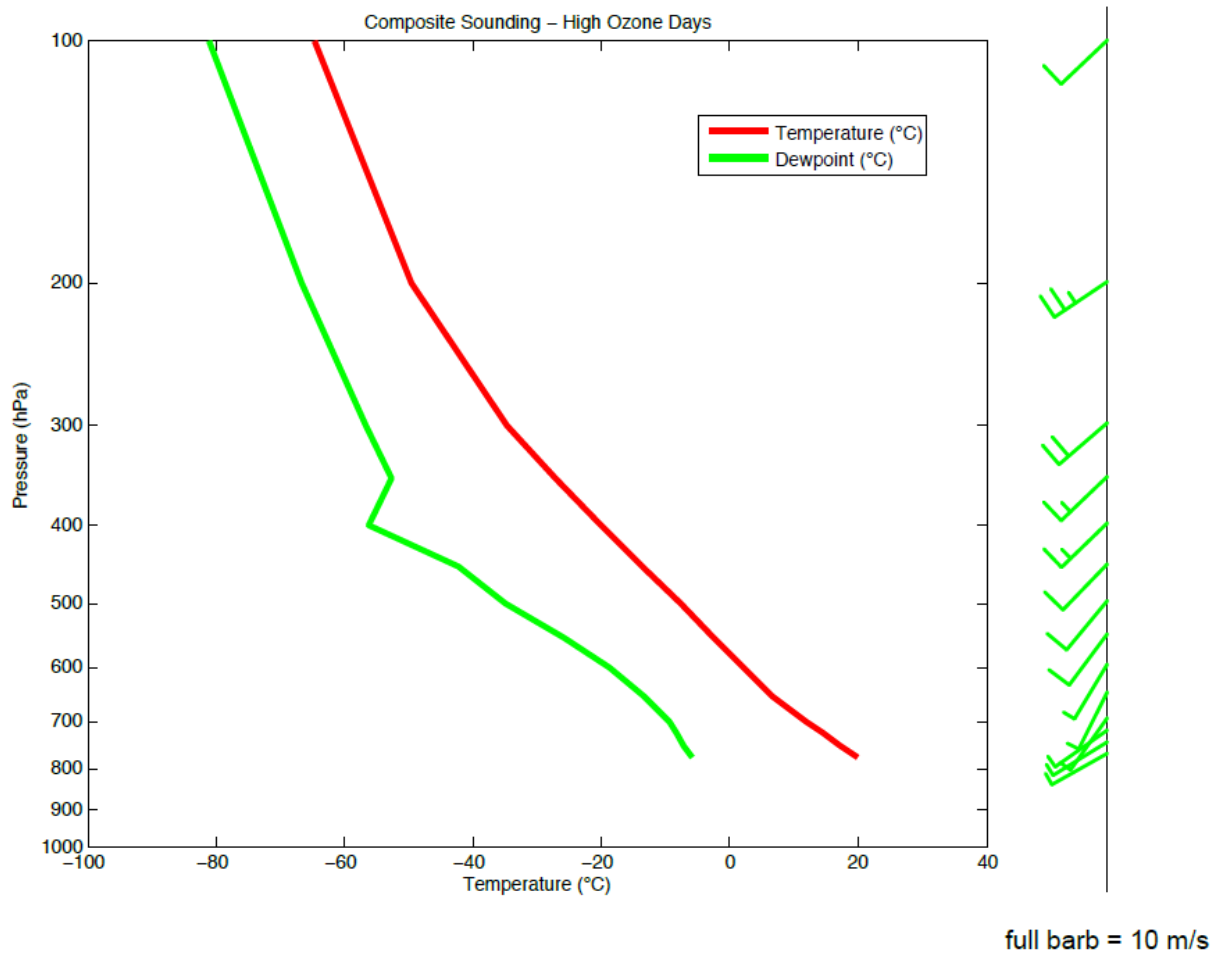


**Figure 3.10.** Sounding composite for the high O<sub>3</sub> days.

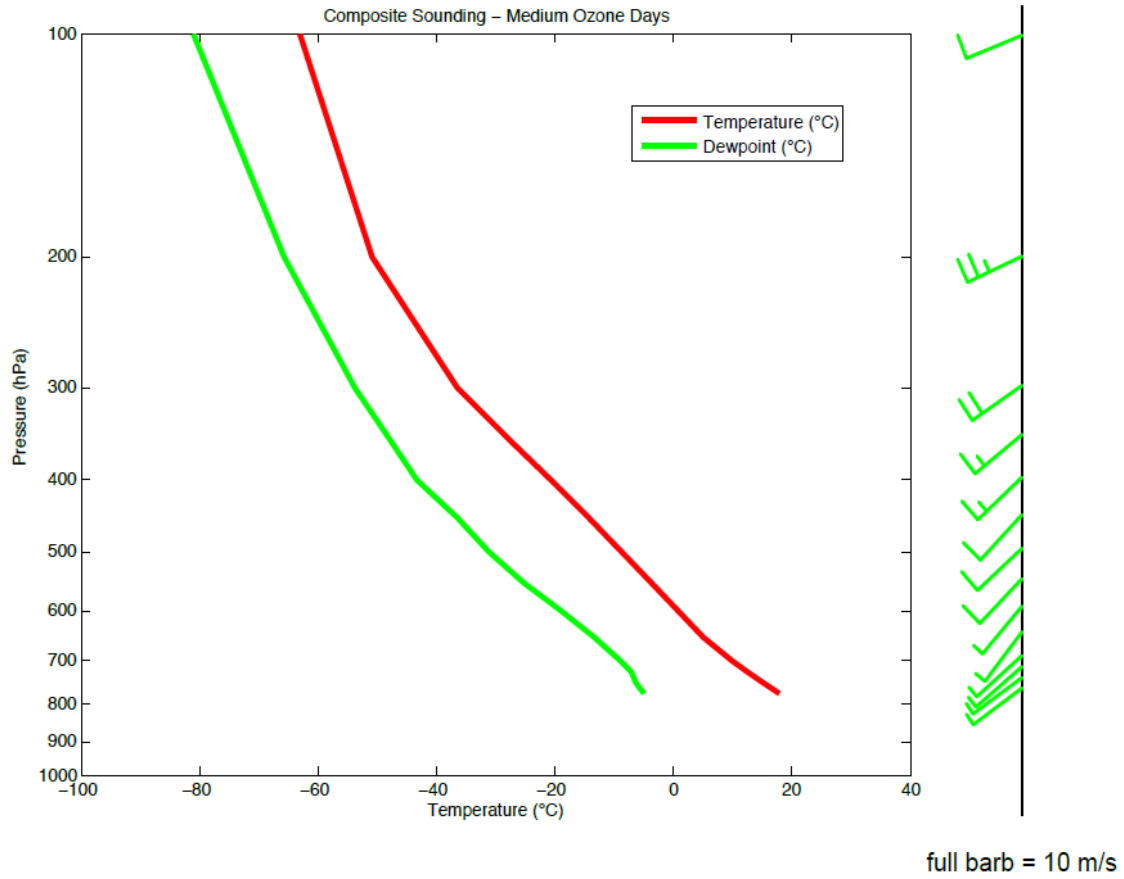


**Figure 3.11.** Sounding composite for the medium O<sub>3</sub> days.

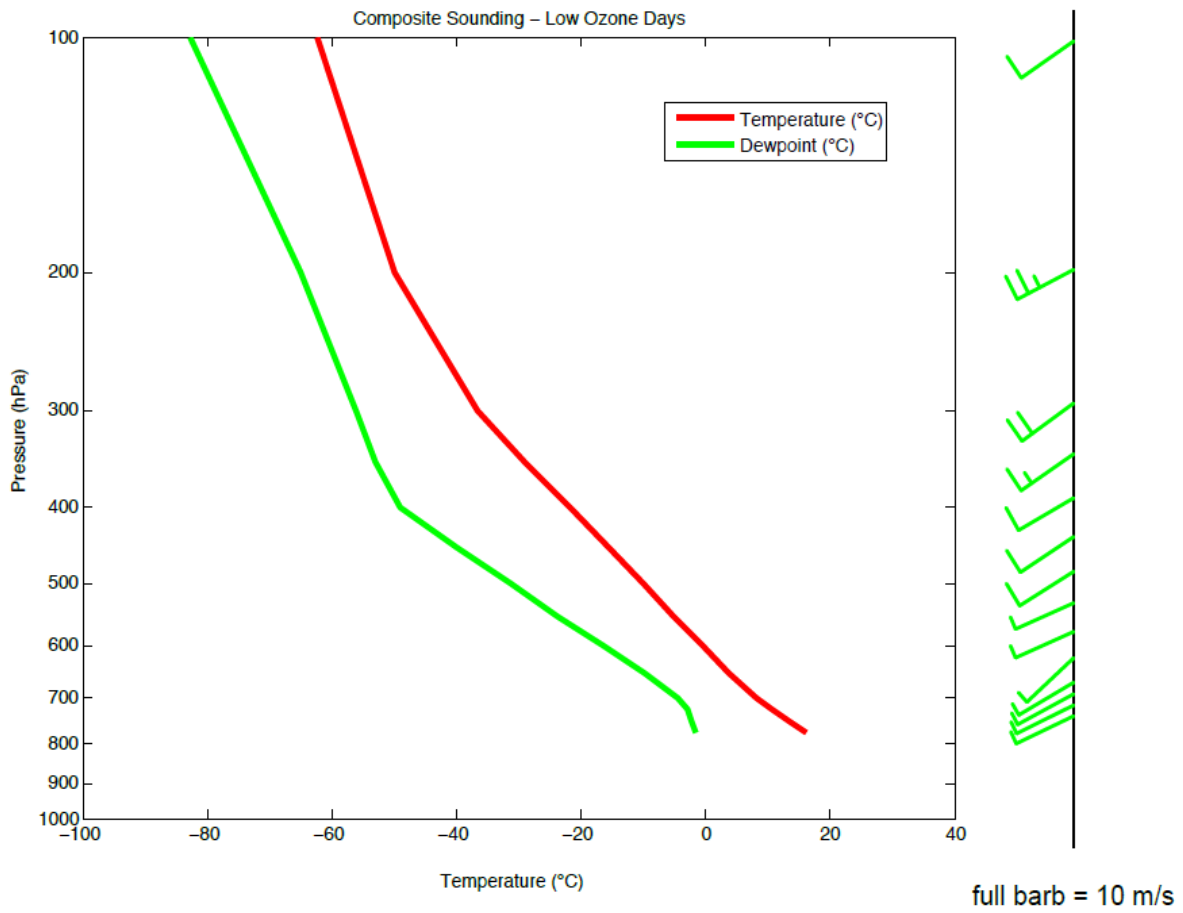


**Figure 3.12.** Sounding composite for the low O<sub>3</sub> days.

## **Chapter 4:**

### **Improving Air Quality Modeling for the Lake Tahoe Basin: Investigating Planetary Boundary Layer Schemes in the WRF Model**

Sandra Rayne <sup>a</sup>, Heather A. Holmes <sup>b</sup>, Barbara Zielinska <sup>a</sup>, and Alan Gertler <sup>a</sup>

<sup>a</sup> *Desert Research Institute, 2215 Raggio Parkway, Reno, NV 89512, USA*

<sup>b</sup> *Atmospheric Sciences Program, Department of Physics, University of Nevada Reno, 1664 N Virginia St., Reno, NV 89503, USA*

**Abstract**

The Lake Tahoe Basin, located on the border of California and Nevada, is facing problems related to air pollution. Since air quality modeling depends upon the accuracy of the meteorological inputs, there is a need to obtain better insight on the performance of meteorological models for this region. The purpose of this study is to evaluate different planetary boundary layer (PBL) schemes within the Weather Research and Forecast (WRF) model in order to determine the best meteorological modeling set-up to feed into air quality models. A model was run to replicate a one-week field study (July 2012) in the Lake Tahoe Basin, which was designed to characterize ozone formation in this region. An analysis was conducted in order to evaluate the performance of three WRF PBL schemes (Yonsei University Scheme, Mellor-Yamada Janjic Scheme and the Asymmetric Convective Model version 2 scheme) for this area. The ACM2 PBL scheme was found to most accurately capture wind directions and PBL height; and, consequently, results from this model scheme were then compared with ozone observations in order to investigate the thermally forced wind circulations in the region. Cross sections at two specific times show that transport from the east influences the ozone at the Upper Homewood (UH) site, while there is no indication of transport from the west. These findings suggest that the implementation of effective air quality modeling in the Lake Tahoe Basin should utilize the ACM2 PBL scheme, and more research is needed on transport potential from the east.

#### 4.1. Introduction

The Lake Tahoe Basin, located on the border of California and Nevada (Figure 1), is currently facing problems related to air pollution, including peak ozone concentrations that approach or slightly exceed various ambient air quality standards (Burley et al., 2015). During the period of 21 July to 26 July 2012, a field study was conducted in the Lake Tahoe Basin designed to characterize the precursors and pathways of secondary pollutant formation, including ozone and secondary organic aerosol (SOA) (Zielinska et al., 2015). However, in order to fully understand transport mechanisms of this pollution, the meteorology in the Lake Tahoe region should also be taken into consideration, especially since the area weather patterns are unusually complex due to influences from the Sierra Nevada Mountains and other topographical features. A summertime phenomenon unique to this geographical location is called the Washoe Zephyr. This is a thermally driven wind circulation that occurs due to the pressure difference between a daytime low pressure that sets up over the Great Basin and the high pressure over the Pacific Ocean. Thermally driven wind circulations and the structure of the boundary layer are critical for understanding the distribution and transport of atmospheric pollutants (Zhong et al., 2008) and precursors for the Lake Tahoe Basin.

Due to the lack of meteorological surface observations around Lake Tahoe, atmospheric modeling is necessary in order to analyze the weather patterns impacting ozone transport. These meteorological parameters are then fed into air quality models. The importance of meteorological inputs on regional air quality modeling has been clearly stated in previous research (Pielke and Uliasz, 1998; Seaman, 2000), thus, there is a need to have a better insight on

the sensitivity and performance of meteorological models implemented in this mountainous region. Vertical transport of heat, moisture, momentum and other physical properties are governed by the atmospheric physics associated with the turbulent layer of air in the lower atmosphere, known as the atmospheric or planetary boundary layer (PBL). The PBL scheme is an important meteorological parameterization used in these models, and each PBL scheme within the Weather Research and Forecast (WRF) model uses different assumptions to determine the transport of mass, moisture and energy within the model (Hue et al., 2010). Several studies have examined the sensitivity of WRF model predictions based on the PBL scheme used (Borge et al., 2008; Coniglio et al., 2013; Gilliam and Pleim, 2010; Hu et al., 2010, 2012; Xie et al., 2012, 2013; Yver et al., 2013), finding, overall, that the performance of each PBL scheme varies depending on the meteorological conditions, further emphasizing the importance of meteorological inputs when developing air quality control strategies. Given the previous findings, there is a need to determine the most appropriate model setup for air quality simulations in the Lake Tahoe Basin. The purpose of this study is to evaluate different PBL schemes within the WRF model in order to determine the best meteorological modeling set-up to feed into chemical models. Then using the results and compare with ozone observations, in order to investigate the thermally forced wind circulation (i.e. Washoe Zephyr) in the region

## **4.2. Methodology**

This analysis uses WRF, version 3.5.1, to examine and evaluate the regional performance of the following three frequently-used PBL schemes: the Yonsei University scheme (YSU), the Mellor-Yamada-Janjic (MYJ) scheme, and the asymmetric convective model, version 2 (ACM2) scheme [the default PBL scheme used by the Community Multiscale Air Quality (CMAQ) model (Hu et al., 2010)]. This sensitivity analysis compares both observed and modeled surface

meteorological variables as well as PBL height results for each PBL parameterization scheme using statistical evaluation methods. Based on the results of the PBL sensitivity analysis, the scheme that best represented the meteorology for ozone transport, was then selected to investigate the thermally-forced wind circulations in the region. Model cross-sections were made and then compared to ozone data collected during field experiments, in order to better understand the impact of meteorology on the transport of pollutants in this area.

#### *4.2 a Model Configuration*

WRF version 3.5.1 was run with three model domains using two-way nesting (Figure 2) and implementing 45 vertical levels, with the model top set at 100 hPa. The mother domain (d01) had a 36 km spatial resolution, which covers the entire continental United States. The first nested domain (d02 –white box, Figure 2) had a spatial resolution of 12 km and covered the western United States, including a portion of the Pacific Ocean. The innermost domain (d03 – red box, Figure 2) had a spatial resolution of 4 km and was centered on the Sierra Nevada Mountains, covering the Lake Tahoe Basin as well as the cities of Sacramento and San Francisco in California, and Carson City and Reno in Nevada. The physical parameterization schemes used in all model domains include the Morrison double-moment scheme microphysics (Morrison et al., 2009), rapid radiative transfer model (RRTM) longwave radiation (Mlawer et al., 1997), Dudhia shortwave radiation (Dudhia, 1989), and both observational and grid nudging. Nudging was done on domains 1 (d01) and 2 (d02) using the National Centers for Environmental Prediction (NCEP) Automated Data Processing (ADP) data for both surface and upper air. The Noah land surface scheme (Chen and Dudhia, 2001) was used for the YSU and MYJ PBL schemes. The Pleim-Xiu land surface scheme (Pleim and Xiu, 1995; Xiu and Pleim, 2001) was used for the ACM2 PBL scheme since that is the default land surface model for that scheme.

Although the Pleim-Xiu land surface model is typically run with soil moisture nudging, all runs used USGS geogrid data with no soil moisture nudging for consistency, in order to evaluate the PBL model. NCEP global forecast system (GFS) final (FNL) operational global analyses were used for initial conditions and boundary conditions. Three 7-day runs were used, one for each PBL scheme, initiated at 0000 UTC (1700 PDT) from 20 July to 27 July 2012. The first day (24 h) of each simulation were treated as spin-up, and the remaining days, 21 July to 27 July, were used for evaluation.

#### *4.2 b Description of PBL Schemes*

PBL schemes used in numerical weather prediction models face the challenge of parameterizing the turbulent low-level atmospheric layer. This is due to grid-point averaging plus turbulent perturbation terms in model equations, leading to a set of unresolved perturbation terms which require a closure scheme to obtain turbulent fluxes from the mean quantities (Holt and Raman 1988; Garcia-Diez et al. 2011). The PBL parameterizations analyzed in this study have either a local or non-local closure scheme (Stull, 1991). The local closure scheme estimates the turbulent fluxes at each point in model grids from the mean atmospheric variables and/or their gradients at that point (Hu et al., 2010), while non-local closure schemes use parameters that can depend on the whole vertical profile, or on relationships between separated levels (Garcia-Diez et al., 2011). Since these schemes are not able to directly represent transport between non-consecutive levels, local schemes are not expected to perform well in fully developed turbulent boundary layers (Stull, 1991), but can still compete with non-local schemes by adding higher order terms (Garcia-Diez et al., 2011). The YSU and ACM2 PBL schemes are classified as non-local closure schemes, since they do not require any additional prognostic equations to express the effects of turbulence on mean variables (Shin and Hong, 2011). The

MYJ PBL scheme is classified as a local closure scheme since it requires an additional prognostic equation (Shin and Hong, 2011).

The YSU PBL scheme (Hong et al., 2006; Hong, 2010) is a first-order nonlocal scheme, with a counter gradient term and an explicit entrainment term in the turbulence flux equation (Hu et al., 2013). The entrainment is made proportional to the surface buoyancy flux (Garcia-Diez et al., 2011). At the top of the PBL, the YSU scheme uses explicit treatment of the entrainment layer, which is proportional to the surface layer flux (Hong et al., 2006; Shin and Hong, 2011; Hu et al., 2010). The YSU scheme uses a critical bulk Richardson number, calculated starting from the surface, to define the PBL top (Hu et al., 2010). The critical bulk Richardson number has been increased since WRF version 3, from zero to 0.25 over land, enhancing the mixing in the stable boundary layer (Hong and Kim, 2008).

The ACM2 PBL scheme (Pleim 2007a, b) uses a first-order local closure eddy-diffusion component, as well as non-local upward transport from the surface (Pleim and Chang 1992) that transitions to local eddy diffusion in stable environments. For unstable conditions, local transport is used for downward fluxes, while upward fluxes are modeled by combining local eddy diffusion with a non-local approach that computes the transition probability between non-consecutive levels (Garcia-Diez et al., 2011). The ACM2 determines the top of the PBL as the height where the bulk Richardson number, calculated above the level of neutral buoyancy, first exceeds a critical bulk Richardson number (Pleim 2007a).

The MYJ PBL scheme is a local closure scheme that uses the 1.5 order and level 2.5 turbulence closure model of Mellor and Yamada (1982) to represent turbulence above the surface layer (Janjic 1990, 1994, 2001). The MYJ scheme determines eddy diffusion coefficients from prognostically-calculated turbulent kinetic energy (TKE) (Hu et al., 2013).

The equations for the heat and moisture fluxes include a term that allows these fluxes to go against the local gradient, so that counter-gradient fluxes caused by large eddies can be represented (Garcia-Diez et al., 2011). PBL height is determined using a TKE threshold (Garcia-Diez et al., 2011). Mellor and Yamada (1982) argued that the scheme is appropriate for all stable and slightly unstable flows, but that errors are more likely as the flow approaches the free-convection limit (Hu et al., 2013).

#### *4.2 c Meteorological Evaluation Data*

Data types implemented in the model evaluation included surface observations at multiple locations, as well as upper air data from the National Weather Service (NWS) Reno site. Daily and hourly statistics (including mean, root mean square errors and biases) were computed from these datasets and compared with the model output statistics using Techniques Development Laboratory (TDL) data. TDL data is part of the NCEP ADP global surface observational weather data network, which is composed of surface weather reports operationally collected by NCEP. These data include land and marine surface reports received via the Global Telecommunications System (GTS). Variables recorded in these reports include pressure, air temperature, dew point temperature, wind direction and speed. Report intervals range from hourly to 3 hourly. These data are the primary input to the NCEP Global Data assimilation System (GDAS) (Meteorological Development Laboratory/Office of Science and Technology/National Weather Service/NOAA/U.S. Department of Commerce, 1987). Also, mean sea level pressure was obtained from the Sacramento CA and Reno NV NWS sites in order to determine the existence of Washoe Zephyr days. Zhong et al. (2008) classified this pressure difference as a Washoe Zephyr Index (WZI) in which they took the sea level pressure difference

between Sacramento CA, and Reno, NV. When the difference is positive, a Washoe Zephyr occurs. Conversely, when the pressure difference was negative the Washoe Zephyr did not form.

#### *4.2 d Field Experiment and Ozone Data*

Ozone data was used from a field study conducted during the period of July 21 – 26 2012. Four sampling sites at varying elevations were established in the Lake Tahoe Basin (Figure 1) and include the following locations: Upper Homewood (UH) (2402 m), Lower Homewood (LH) (1897 m), Heavenly Ski Resort Sky Deck (HV) (2605 m), and Tahoe Regional Planning Agency (TRPA) (1954 m). Ozone was monitored continuously at all four sites. A portable UV absorption 2B Technologies Model 202 monitor was used at UH, LH and HV sites, and a Thermo Scientific Model 49 ozone analyzer was employed at the TRPA site. Prior to the commencement of the field study, a 24-hour inter-comparison of the continuous ozone instrumentation was conducted on the TRPA rooftop (July 19-20, 2012). Ozone samples were collected at the following three times per day: one in the morning, during the period of rapid ozone accumulation (0600 to 0930); one during the period when maximum ozone concentrations typically occur (1000 to 1730); and one overnight (1800 to 0530).

#### *4.2 e Cross Sections*

Cross sections, using the ACM2 PBL scheme, for every hour of model data were created along a line extending from the western-most point of Sacramento, CA; through the middle of Lake Tahoe; passing to the north of Carson City, NV; and ending at the eastern-most point of Fallon, NV (Figure 16). Three wind speed components were analyzed, including the u-component (east-west, top graph), the v-component (north-south, middle graph) and the w-component (vertical, bottom graph). The potential temperature was also overlaid on top of each

graph (black lines). Based on the ozone data, two time periods were then chosen to analyze with cross sections. The first time period was July 25<sup>th</sup> at 1200 PDT (1900 UTC), and the second was July 24<sup>th</sup> at 0300 PDT (1000 UTC).

### 4.3. Results

The hourly ozone (Figure 4) data reported by Zielinska et al. (2015) showed that during the first two days (July 21-22) of the field experiment, the ozone reached a maximum for all sites, with ozone levels between 50 and 60 ppb. During the afternoon hours of July 23<sup>rd</sup>, a cold front came through the region, bringing thunderstorms and rain. This changing weather pattern reduced the maximum daytime ozone at all sites to levels less than 50 ppb due to wet deposition. A wildfire was ignited by lightning, to the east of the Basin in the Minden-Gardnerville area, but was quickly extinguished on July 24<sup>th</sup>. However, at 21 PDT on July 23<sup>rd</sup> until 6 PDT on July 24<sup>th</sup>, the ozone at UH stayed very high, with levels between 50 and 60 ppb, while ozone at the other three sites dipped lower. The UH site typically had higher ozone values (above 50 ppb) during the nighttime hours, while the other three sites became low (below 50 ppb). The daytime period of July 25<sup>th</sup> was the highest daytime ozone peak for the sampling period, around 60 ppb for each site.

The averaged hourly ozone graph (Figure 5) from Zielinska et al. (2015) shows a similar trend to the 2010 study done by Burley et al. (2015), showing both a decrease in diurnal ozone variability as well as higher ozone values with an increase in elevation. A dip in ozone can be seen just before sunrise (0600 PDT) at HV, LH and TRPA sites, but this ozone dip lagged by half an hour at the UH site. Peak ozone at each site is seen throughout the daytime hours for HV, LH and TRPA sites, while the UH site had peak ozone levels during the early morning hours

(around 0400 PDT). Ozone levels at all sites dipped in the evening after sunset, except for at the UH site, where ozone levels remained high throughout the night (above 50 ppb).

Three WRF simulations of the study time period were run in order to investigate the atmospheric physics associated with the previously described ozone pollutant concentrations, as well as to compare three different boundary layer schemes. Atmospheric data from each WRF model run were compared to TDL surface data from 77 observational sites within the model domain 3 (d03), and comparative statistics were generated. Four atmospheric variables were compared, including wind speed ( $\text{ms}^{-1}$ ), wind direction (deg), temperature (K) and humidity ( $\text{gkg}^{-1}$ ). The comparison of daily data (Table 1) shows that the YSU PBL scheme and the ACM2 scheme both have a negative bias for wind speed (-0.27 and -0.52 respectively), while the MYJ scheme has a positive bias for wind speed (0.43), when compared to observations. For wind direction the MYJ scheme had the largest bias, followed by the YSU and ACM2 (3.15, 2.46 and 0.69 respectively). For humidity the ACM2 had the largest bias followed by the MYJ and YSU (0.95, 0.53, and 0.48 respectively). All schemes show a negative bias for temperature and ACM2 had the largest, followed by the YSU and MYJ (-1.12, -0.82 and -0.37 respectively).

In addition to this comparison analysis of daily data, a similar comparison analysis was conducted between modeled and observed hourly datasets, specifically for the period of 0000 UTC – 0001 UTC (Table 2). This time period was selected because it corresponded with the sounding data measurement timeframe, allowing for an additional comparison of these datasets with the 0000 UTC upper-air sounding dataset. The 0000 UTC hour comparison between modeled and observed data showed that the MYJ PBL scheme had a positive bias for wind speed (0.13), while the YSU and ACM2 scheme had a negative bias (-0.88 and -1.19 respectively). All PBL schemes showed a negative bias for temperature and the YSU had the largest followed by

the ACM2 and MYJ (-1.56, -1.38 and -0.94 respectively). The YSU had the largest positive bias for wind direction followed by the MYJ and ACM2 (8.76, 7.81 and 1.98 respectively). The ACM2 had the largest positive bias for humidity followed by the MYJ and YSU (1.08, 0.84 and 0.63 respectively).

A graphical comparison between observed and modeled data was performed using hourly temperature and dewpoint data, specifically for the Reno, NV and Elko, NV National Weather Service sites, as these were the two sites in d03 closest to Lake Tahoe geographically and also located in complex terrain. Correlation coefficients were calculated for each model and variable in order to determine which scheme most closely followed the observations.

The temperature comparison graph for Reno (Figure 5) shows that all PBL schemes have a negative daytime temperature bias when compared to the observations, but the MYJ and the YSU schemes have a positive nighttime bias. Out of all the model runs, the ACM2 scheme model most closely follows the temperature observations for the Reno site, having a correlation coefficient of 0.963, as followed by MYJ (0.945) and YSU (0.919).

The temperature comparison graph for Elko (Figure 6) also shows negative daytime temperature biases for all PBL schemes. During nighttime hours, however, all schemes have a positive temperature bias, except during the time period of July 22<sup>nd</sup> and July 23<sup>rd</sup>. On July 22<sup>nd</sup>, the ACM2 and YSU schemes have a negative temperature bias, while the MYJ scheme has a positive temperature bias. On July 23<sup>rd</sup>, all schemes have a negative temperature bias. Out of all model schemes, the MYJ scheme follows the temperature observations closest overall, having a correlation coefficient of 0.947, followed by the YSU (0.942) and the ACM2 (0.928).

The dewpoint temperature comparison graph for Reno (Figure 7) shows the ACM2 scheme having a negative bias on July 22<sup>nd</sup> and July 26<sup>th</sup>, while the MYJ and YSU schemes have

a positive bias. The MYJ and YSU schemes displayed similar temporal patterns overall, and also had similar observation correlation coefficients of 0.743 and 0.737 respectively, while the ACM2 had a correlation coefficient of 0.884. The dewpoint temperature comparison graph for Elko (Figure 8) shows that all three schemes generally have a negative bias from observed values, except during a period before noon, when, on most days, the ACM2 has a positive dewpoint temperature bias. Overall, the MYJ and YSU schemes both had similar temporal patterns with similar correlation coefficients of 0.892 and 0.895 respectively, while the ACM2 had a correlation coefficient of 0.864.

Different methods can be used to calculate the PBL height from sounding data (e.g. using a critical bulk Richardson number or using potential temperature). Additionally, the WRF model uses a variety of calculation methods to determine the simulated PBL height of model runs, as cited in the methods section, further complicating the PBL height comparative analysis process. PBL heights were thus calculated from sounding observations at both the Reno and Elko sites using the following two methods: a critical bulk Richardson number of 0.25; and a nonlocal static stability classification based on a potential temperature ( $\theta$ ) increase method, developed in Nielsen-Gammon et al. (2008). In the later method, the authors calculated the PBL height as the level at which the observed potential temperature first exceeds the minimum potential temperature within the boundary layer by a threshold potential temperature exceedance amount of +1.5 (Nielsen-Gammon et al., 2008). When comparing the WRF-generated PBL with the two calculated PBLs used as observational data, biases were characterized as either negative or lower than the observed PBL, and positive or higher than the observed PBL.

The PBL comparison graph for Reno (Figure 9) shows that each PBL scheme (WRF calculated PBL height) has a negative (lower) PBL bias when compared to PBLs generated from both

observational methods and for all study days. The ACM2 generated a PBL closest to the PBL observation as calculated by the bulk Richardson method, having a correlation coefficient of 0.942, followed by the YSU and MYJ (0.841, 0.652 respectively). For the theta increase method, the MYJ showed the closest correlation (0.871) to the calculated PBL observation, followed by the YSU and the ACM2 (0.832 and 0.819 respectively).

The PBL comparison graph for Elko (Figure 10) shows that all schemes had a negative PBL bias when compared to the theta method of PBL calculation, with the exception the ACM2 on July 23<sup>rd</sup>, which had no strong bias. Additionally, all model schemes showed a negative bias when compared to the bulk Richardson-calculated PBL for the entire study period, with the exception of July 22<sup>nd</sup> and 23<sup>rd</sup>. The YSU showed a negative PBL bias on July 22<sup>nd</sup>, while both the MYJ and ACM2 had positive (higher) PBL biases. Additionally, on July 23<sup>rd</sup>, both the ACM2 and the YSU had positive biases, while the MYJ had a slightly positive PBL bias. The correlation coefficients for the theta increase PBL method for MYJ, ACM2 and YSU were 0.497, 0.426, and 0.383 respectively. The correlation coefficients for the bulk Richardson method for MYJ, ACM2 and YSU were 0.628, 0.491 and 0.341 respectively.

Since a variety of techniques were used to calculate the PBL height for each WRF-based PBL scheme, the modeled PBL height was re-calculated in the same two ways that the PBL height was calculated from the observational sounding data in order to provide a common means of comparison. The PBL height calculated using the 1.5 theta increase method comparison graph for Reno (Figure 11) shows that the MYJ scheme closely followed the observations until July 23<sup>rd</sup>, when it transitioned to have a negative (lower) bias. The YSU scheme had a negative bias for the entire time period, while the ACM2 scheme had a positive bias until July 23<sup>rd</sup>, when the bias became negative. The correlation coefficients for the ACM2, YSU and MYJ were 0.841,

0.782 and 0.661 respectively. The PBL height calculated using the theta increase method comparison graph for Elko (Figure 12) shows all PBL schemes having a negative (lower) bias on July 20<sup>th</sup> and from July 24<sup>th</sup> through 26<sup>th</sup>. The PBL bias was positive (higher) on July 21<sup>st</sup> for ACM2 and YSU, but negative for MYJ. The bias was positive for all schemes on July 22<sup>nd</sup> and 23<sup>rd</sup>. The correlation coefficients for the ACM2, YSU and MYJ are 0.431, 0.732 and 0.091 respectively.

The PBL heights calculated using the critical bulk Richardson method comparison graph for Reno (Figure 13) showed the MYJ and YSU schemes having a negative bias during the study period. The ACM2 scheme had a slightly positive PBL bias until July 22<sup>nd</sup>, a negative bias until the middle of July 24<sup>th</sup>, and a positive bias until July 27<sup>th</sup>. The correlation coefficients for the YSU, MYJ and ACM2 are 0.845, 0.831, and 0.779 respectively. The PBL heights calculated using the critical bulk Richardson method comparison graph for Elko (Figure 14) showed all PBL model schemes having a negative bias, except on July 22<sup>nd</sup> and 23<sup>rd</sup>, when they had a positive bias. The correlation coefficients for the YSU, ACM2 and MYJ are 0.816, 0.807 and 0.771 and respectively.

Figure 15 shows a WZI comparison graph among all three schemes and the observational pressure difference taken at the NWS sites located in Sacramento, CA and Reno, NV. The MYJ and the YSU scheme did not have a positive pressure difference until July 27<sup>th</sup>. Out of all model schemes, the ACM2 scheme followed the observations most closely, with a correlation coefficient of 0.934. The MYJ had a correlation coefficient of 0.932, and the YSU had a correlation coefficient of 0.931.

Finally, to investigate thermally forced wind circulations in the Lake Tahoe Basin, cross sections were created across Lake Tahoe from the WRF model data. Because wind direction is a

crucial meteorological variable to consider when determining the direction of ozone transport, and because the WRF model run that used the ACM2 PBL scheme most accurately reproduced the observed wind direction, PBL height, and WZI, the ACM2 model run was selected to produce these lake cross sections. The first time period selected was July 25<sup>th</sup> at 1200 PDT (1900 UTC), as this period consisted of all sites showing the highest maximum ozone for the daytime during the study period. The second time period selected for analysis was July 24<sup>th</sup> at 0300 PDT (1000 UTC), as this period was a “wash-out” or wet deposition period after the thunderstorm event on July 23<sup>rd</sup>. During this time period, the WZI was negative, and while ozone levels at the UH site rose into the 55-60 ppb range, ozone levels at the other three sites (LH, HE and TRPA) dipped down to below 40 ppb.

#### **4.4. Discussion**

As previously discussed, the WRF model run implementing the ACM2 PBL scheme best captured wind direction, PBL height, and WZI, a finding that was anticipated due to the type of land-surface model used in this scheme (Gilliam and Pleim, 2010). During the first time period used in the cross-section analysis (July 25), the vertical winds displayed strong mixing over and around the lake, shown as strong vertical wind speed gradients in the bottom graph of Figure 17. Although the calculated planetary boundary layer height for Reno during this time period was only 4088 magl, a PBL height lower than the level required to provide access to the free troposphere, the vertical mixing over the lake was strong enough to bring polluted air down into the Basin. However, the u-component during this time period indicated the presences of easterly winds, except at levels close to the ground where the winds were slightly westerly, a wind pattern indicative of possible Washoe Zephyr development. Additionally, the WZI was positive at this time, further indicating the possible presence of the Washoe Zephyr. This wind pattern

allowed cities to the east of the lake, such as Reno and Carson City, to become a potential source for ozone transport, in addition to those cities west of the lake, such as Sacramento and San Francisco. The v-component during this time period indicated that slight northerly winds were occurring on the eastern side of the lake, with southerly winds occurring on the western side.

Analysis of the cross-section region 24 hours earlier (July 24, Figure 18) reveals that there was strong vertical upward motion east of the lake, but no vertical motion over the Sacramento area. The u-component showed easterly winds at mid-levels of the atmosphere, with a slight westerly component near the ground, again indicating Washoe Zephyr development during this time period, even with the WZI near neutral. The v-component showed neutral to slightly southerly winds. This analysis indicates that ozone transport from the west was not likely occurring during this period, as there was no vertical motion over Sacramento to lift pollutants and precursors up, nor westerly mid-level winds to transport these pollutants over the mountains. Even if the Washoe Zephyr did develop during this time period, any entrained pollutants or ozone-forming precursors would have been deposited along the forested western side of the mountains due to the shallow nature of the Zephyr, making transport unlikely.

The cross section associated with the wash-out period (Figure 19) shows a stable boundary layer over Sacramento and weak vertical mixing over the Lake Tahoe Basin. During this period, the overall wind pattern had both an easterly component and a slight northerly component, as the dew point temperature decreased by 18.8 C at the calculated planetary boundary height in Reno (3186 magl). Because the planetary boundary layer height was lower during this period, the higher UH site was more accessible to and more easily influenced by transport occurring within the free troposphere; however, due to overall weak vertical mixing during this time period, the lower sites probably did not tap into any polluted air being

transported within the free troposphere. Additionally, analysis of the cross-section region five hours earlier (Figure 20) shows that both strong vertical mixing and a strong easterly wind component was occurring to the east of the Lake Tahoe Basin during this period, indicating that transport from the wildfire to the east of Lake Tahoe in the Minden-Gardnerville area, was influencing higher ozone levels at the UH site.

#### **4.5. Summary and Conclusions**

In order to analyze the atmospheric physics and transport of ozone and ozone precursors, three WRF (v3.5.1) simulations were run using three different PBL schemes (YSU, MYJ and ACM2). Results of the model simulations were compared statistically to 77 surface observation sites in the finest resolution domain (domain three, d03). The model evaluation showed that each PBL scheme had a positive bias with wind direction and humidity, and a negative bias with regard to temperature. The YSU and ACM2 schemes had a negative bias with wind speed observations, while the MYJ scheme had a positive bias.

Additionally, a PBL analysis was performed, using consistent methods to calculate PBL height from both model results and observations. Results from the PBL analysis show that ACM2 performed best when used for calculating the PBL height for Reno. The results also show that the ACM2 and YSU model PBL height output both correlated better with the observational PBL calculated using the bulk Richardson method, for both Reno and Elko; however, the MYJ correlated better with the theta increase method for Reno, as well as the bulk Richardson method for Elko. The ACM2 scheme was also found to perform best when calculating the WZI.

The ACM2 PBL scheme was used to create cross sections in order to analyze the wind circulation patterns across the Lake Tahoe Basin. These cross sections indicated that transport from the west did not influence higher ozone values for this time period; however, transport from

cities to the east (e.g. Reno and Carson City) as well as a wildfire to the east did increase ozone levels at the higher elevation site (UH). Also, although the cross sections showed the potential development of a Washoe Zephyr, vertical and u-component winds during this period suggest that the Zephyr did not largely impact transport.

Based on these findings, the ACM2 performed best in the Tahoe region, and should be implemented in future modeling research, including in air quality simulations. Additionally, there is a need for further air quality modeling in order to better quantify the contributions from in-basin and out-of-basin sources as well as, how wildfires influence pollution levels within the Basin. This would enable the development of more effective ozone control strategies for the Lake Tahoe Basin.

### **Acknowledgements**

This study was supported by the grant from the U.S. Department of Agriculture Forest Service through the Tahoe Science Program funded by the Southern Nevada Public Lands Management Act (SNPLMA). The authors of the report would like to thank: Tiffany Van Huysen of the USDA Forest Service PSW Research Station for administrative support for the study; Heavenly and Homewood Ski Resorts for providing access to their areas; Joey Keely of the USDA Forest Service Lake Tahoe Basin Management Unit for logistical help; We would like to acknowledge high-performance computing support from Yellowstone ([ark:/85065/d7wd3xhc](https://doi.org/10.7554/ark:/85065/d7wd3xhc)) provided by NCAR's Computational and Information Systems Laboratory, sponsored by the National Science Foundation. Thanks to Nyssa Perryman for all of your support.

## References

- Borge, R., V. Alexandrov, J. J. del Vas, J. Lumbreras, and E. Rodriguez, **2008**. A comprehensive sensitivity analysis of the WRF model for air quality applications over the Iberian Peninsula. *Atmos. Environ.*, **42**, 8560–8574.
- Burley, J. D., Theiss, S., Bytnerowicz, A., Gertler, A., Schilling, S., & Zielinska, B. **2015**. Surface ozone in the Lake Tahoe Basin. *Atmospheric Environment*, **109**, 351-369.
- Chen, F., and J. Dudhia, **2001**. Coupling an Advanced Land Surface-Hydrology Model with the Penn State–NCARMM5 Modeling System. Part I: Model implementation and sensitivity. *Mon. Wea. Rev.*, **129**, 569–585.
- Computational and Information Systems Laboratory. **2012**. Yellowstone: IBM iDataPlex System (NCAR Community Computing). Boulder, CO: National Center for Atmospheric Research. <http://n2t.net/ark:/85065/d7wd3xhc>.
- Coniglio, M. C., J. Correia, P. T. Marsh, and F. Kong **2013**. Verification of convection-allowing WRF model forecasts of the planetary boundary layer using sounding observations. *Weather Forecast*, **28**(3), 842–862.
- Dudhia, J., **1989**. Numerical study of convection observed during the winter monsoon experiment using a mesoscale two dimensional model. *J. Atmos. Sci.*, **46**, 3077–3107.
- García-Díez, M., Fernández, J., Fita, L., & Yagüe, C. **2013**. Seasonal dependence of WRF model biases and sensitivity to PBL schemes over Europe. *Quarterly Journal of the Royal Meteorological Society*, **139**(671), 501-514.
- Gilliam, R. C., and J. E. Pleim **2010**. Performance assessment of new land surface and planetary boundary layer physics in the WRF-ARW. *J. Appl. Meteorol. Climatol.*, **49**(4), 760–774.

- Holt, T., and S. Raman **1988**. A review and comparative evaluation of multilevel boundary layer parameterizations for first-order and turbulent kinetic energy closure schemes. *Rev. Geophys.*, **26**, 761–780.
- Hong S-Y, Noh Y, Dudhia J **2006**. A new vertical diffusion package with an explicit treatment of entrainment processes. *Mon Weather Rev.*, **134**, 2318–2341.
- , and S.-W. Kim **2008**. Stable boundary layer mixing in a vertical diffusion scheme. Proc. Ninth Annual WRF User’s Workshop, Boulder, CO, National Center for Atmospheric Research, 3.3. [Available online at <http://www.mmm.ucar.edu/wrf/users/workshops/WS2008/abstracts/3-03.pdf>.]
- , **2010**. A new stable boundary-layer mixing scheme and its impact on the simulated East Asian summer monsoon. *Q J Roy Meteorol Soc.*, **136**, 1481–1496
- Hu, X.-M., J. W. Nielsen-Gammon, and F. Q. Zhang **2010**. Evaluation of three planetary boundary layer schemes in the WRF model. *J. Appl. Meteorol. Climatol.*, **49**(9), 1831–1844.
- , D. C. Doughty, K. J. Sanchez, E. Joseph, and J. D. Fuentes **2012**. Ozone variability in the atmospheric boundary layer in Maryland and its implications for vertical transport model. *Atmos. Environ.*, **46**, 354–364.
- , Klein, P. M., & Xue, M. **2013**. Evaluation of the updated YSU planetary boundary layer scheme within WRF for wind resource and air quality assessments. *Journal of Geophysical Research: Atmospheres*, **118**(18), 10-490.
- Janjic, Z. I., **1990**. The step-mountain coordinate: Physical package. *Mon. Wea. Rev.*, **118**, 1429–1443.
- , **1994**. The step-mountain Eta coordinate model: Further developments of the convection,

- viscous layer, and turbulence closure schemes. *Mon. Wea. Rev.*, **122**, 927–945.
- , **2001**. Nonsingular implementation of the Mellor-Yamada level 2.5 scheme in the NCEP Meso model. NOAA/NWS/NCEP Office Note 437, 61 pp.
- Mellor, G. L., and T. Yamada, **1982**. Development of a turbulence closure model for geophysical fluid problems. *Rev. Geophys.*, **20**, 851–875.
- Meteorological Development Laboratory/Office of Science and Technology/National Weather Service/NOAA/U.S. Department of Commerce, **1987**: TDL U.S. and Canada Surface Hourly Observations, daily from December 1976 to present. Research Data Archive at the National Center for Atmospheric Research, Computational and Information Systems Laboratory, Boulder, CO. [Available online at <http://rda.ucar.edu/datasets/ds472.0/>.] Accessed 15 Jun 2015.
- Mlawer, E. J., S. J. Taubman, P. D. Brown, M. J. Iacono, and S. A. Clough, **1997**. Radiative transfer for inhomogeneous atmospheres: RRTM, a validated correlated-k model for the longwave. *J. Geophys. Res.*, **102D**, 16 663–16 682.
- Morrison, H., Thompson, G., & Tatarskii, V. **2009**. Impact of cloud microphysics on the development of trailing stratiform precipitation in a simulated squall line: Comparison of one-and two-moment schemes. *Monthly Weather Review*, **137**(3), 991-1007.
- Nielsen-Gammon, J. W., and Coauthors, **2008**. Multisensor estimation of mixing heights over a coastal city. *J. Appl. Meteor. Climatol.*, **47**, 27–43.
- Pielke, R.A., Uliasz, M., **1998**. Use of meteorological models as input to regional and mesoscale air quality models - limitations and strengths. *Atmospheric Environment*, **32**, 1455-1466.
- Pleim JE. **2007a**. A combined local and nonlocal closure model for the atmospheric boundary

- layer. Part I: Model description and testing. *Journal of Applied Meteorology and Climatology*, **46**(9): 1383–1395.
- Pleim J.E. **2007b**. A combined local and nonlocal closure model for the atmospheric boundary layer. Part II: Application and evaluation in a mesoscale meteorological model. *Journal of Applied Meteorology and Climatology*, **46**(9): 1396–1409.
- Pleim, J. E., & Xiu, A. **1995**. Development and testing of a surface flux and planetary boundary layer model for application in mesoscale models. *Journal of Applied Meteorology*, **34**(1), 16-32.
- Seaman, N.L, **2000**. Meteorological modeling for air-quality assessments. *Atmospheric Environment*, **34**, 2231-2259
- Shin, H. H., & Hong, S. Y., **2011**. Intercomparison of planetary boundary-layer parametrizations in the WRF model for a single day from CASES-99. *Boundary-Layer Meteorology*, **139**(2), 261-281.
- Stull RB. **1991**. Static stability—an update. *Bulletin of the American Meteorological Society*, **72**(10): 1521–1529.
- Xie, B., J. C. H. Fung, A. Chan, and A. Lau **2012**. Evaluation of nonlocal and local planetary boundary layer schemes in the WRF model. *J. Geophys. Res.*, **117**.
- Xie, B., J. C. R. Hunt, D. J. Carruthers, J. C. H. Fung, and J. F. Barlow **2013**. Structure of the planetary boundary layer over Southeast England: Modeling and measurements. *J. Geophys. Res. Atmos.*, **118**, 7799–7818.
- Xiu, A., & Pleim, J. E. **2001**. Development of a land surface model. Part I: Application in a mesoscale meteorological model. *Journal of Applied Meteorology*, **40**(2), 192-209.
- Yver, C. E., H. D. Graven, D. D. Lucas, P. J. Cameron-Smith, R. F. Keeling, and R. F. Weiss

- 2013.** Evaluating transport in the WRF model along the California coast. *Atmos. Chem. Phys.*, **13**(4), 1837–1852.
- Zielinska, B., Bytnerowicz, A., Gertler, A., Goliff, W., Theiss, S., Burley, J., McDaniel, M., Campbell, D., 2015. Secondary Pollutant Formation in the Lake Tahoe Basin. Final Technical Report for SNPLMA Contract P075, U.S. Department of Agriculture Forest Service, 68 pp.
- Zhong, Shiyuan, Ju Li, Craig B. Clements, Stephan F. J. De Wekker, Xindi Bian, 2008: Forcing Mechanisms for Washoe Zephyr—A Daytime Downslope Wind System in the Lee of the Sierra Nevada. *Journal of Applied Meteorological Climatology*, **47**, 339–350.

## Tables

*Daily Statistics*

		ACM2	MYJ	YSU	
<i>Wind Spd (<math>ms^{-1}</math>)</i>	Mean OBS	3.4	3.4	3.4	
	Mean PRD	2.89	3.84	3.13	
	Bias	-0.52	0.43	-0.27	
	Gross Error	1.52	1.55	1.47	
	RMSE	1.96	2.01	1.9	
	Sys RMSE	1.56	1.2	1.31	
	Unsys RMSE	1.18	1.6	1.37	
	IOA	0.7	0.75	0.74	
	<i>Wind Dir (deg)</i>	Mean OBS	265.59	265.59	265.59
		Mean PRD	269.69	272.04	268.09
		Bias	0.69	3.15	2.46
		Gross Error	39.47	40.59	40.17
<i>Temp (K)</i>		Mean OBS	297.4	297.4	297.4
	Mean PRD	296.28	297.04	296.58	
	Bias	-1.12	-0.37	-0.82	
	Gross Error	2.32	2.05	2.05	
	RMSE	2.86	2.6	2.57	
	Sys RMSE	1.7	1.23	1.49	
	Unsys RMSE	2.27	2.28	2.09	
<i>Humidity (<math>gkg^{-1}</math>)</i>	IOA	0.96	0.97	0.97	
	Mean OBS	7.31	7.31	7.31	
	Mean PRD	8.27	7.85	7.79	
	Bias	0.95	0.53	0.48	
	Gross Error	1.37	1.24	1.16	
	RMSE	1.83	1.65	1.52	
	Sys RMSE	1.16	1.04	0.93	
	Unsys RMSE	1.41	1.28	1.2	
	IOA	0.78	0.78	0.82	

**Table 4.1.** Daily statistics of three PBL schemes with 77 observational sites in domain 3 (4-km resolution).

*0000 UTC Statistics*

		ACM2	MYJ	YSU
<i>Wind Spd (ms<sup>-1</sup>)</i>	Mean OBS	5.05	5.05	5.05
	Mean PRD	3.86	5.18	4.16
	Bias	-1.19	0.13	-0.88
	Gross Error	2.37	2.14	2.23
	RMSE	2.01	1.18	1.67
	Sys RMSE	1.26	1.77	1.46
	Unsys RMSE	0.61	0.71	0.67
	IOA	272.71	272.71	272.71
<i>Wind Dir (deg)</i>	Mean OBS	278.59	284.05	279.26
	Mean PRD	1.98	7.81	8.76
	Bias	303.69	303.69	303.69
<i>Temp (K)</i>	Mean OBS	302.3	302.74	302.12
	Mean PRD	-1.38	-0.94	-1.56
	Bias	2.85	2.49	2.64
	Gross Error	2.03	1.31	1.77
	RMSE	1.95	2.1	1.92
	Sys RMSE	0.93	0.95	0.95
	Unsys RMSE	6.96	6.96	6.96
	IOA	8.05	7.81	7.59
<i>Humidity (gkg<sup>-1</sup>)</i>	Mean OBS	1.08	0.84	0.63
	Mean PRD	1.93	1.87	1.63
	Bias	1.32	1.28	1.07
	Gross Error	1.41	1.35	1.22
	RMSE	0.76	0.74	0.79
	Sys RMSE	5.05	5.05	5.05
	Unsys RMSE	3.86	5.18	4.16
	IOA	-1.19	0.13	-0.88

**Table 4.2.** 0000 UTC Hour statistics of three PBL schemes with 77 observational sites in d03

## List of Figures

**Figure 1.** Location of Lake Tahoe and site locations of 2012 field study.

**Figure 2.** Model domains. The mother domain (d01) is the black box, first nested domain (d02) is the white box and second nested domain (d03) is the red box.

**Figure 3.** Hourly ozone values for the 2012 sites: LH is Lower Homewood, UH is Upper Homewood, HE is Heavenly Ski Resort, and HQ is Tahoe Regional Planning Agency.

**Figure 4.** Averaged hourly ozone values for the 2012 sites: UH is Upper Homewood, HV is Heavenly Ski Resort, LH is Lower Homewood and TRPA is Tahoe Regional Planning Agency.

**Figure 5.** Temperature comparison between observations and the three WRF PBL model schemes. Data is hourly, observations taken at NWS surface observational site Reno, NV.

**Figure 6.** Temperature comparison between observations and the three WRF PBL model schemes. Data is hourly, observations taken at NWS surface observational site Elko, NV.

**Figure 7.** Dew point temperature comparison between observations and the three WRF PBL model schemes. Data is hourly, observations taken at NWS surface observational site Reno, NV.

**Figure 8.** Dew point temperature comparison between observations and the three WRF PBL model schemes. Data is hourly, observations taken at NWS surface observational site Elko, NV.

**Figure 9.** PBL comparison between observations calculated two different ways and the three WRF PBL model schemes. Observations taken at NWS sounding site Reno, NV. Only 0000 UTC data was used.

**Figure 10.** PBL comparison between observations calculated two different ways and the three WRF PBL model schemes. Observations taken at NWS sounding site Elko, NV. Only 0000 UTC data was used.

**Figure 11.** PBL height calculated using the +1.5 theta method comparison between observations and the three WRF PBL model schemes. Observations taken at NWS sounding site Reno, NV. Only 0000 UTC data was used.

**Figure 12.** PBL height calculated using the +1.5 theta method comparison between observations and the three WRF PBL model schemes. Observations taken at NWS sounding site Elko, NV. Only 0000 UTC data was used.

**Figure 13.** PBL height calculated using the critical bulk Richardson number of 0.25 method comparison between observations and the three WRF PBL model schemes. Observations taken at NWS sounding site Reno, NV. Only 0000 UTC data was used.

**Figure 14.** PBL height calculated using the critical bulk Richardson number of 0.25 method comparison between observations and the three WRF PBL model schemes. Observations taken at NWS sounding site Elko, NV. Only 0000 UTC data was used.

**Figure 15.** Washoe Zephyr Index calculated using the pressure difference between Sacramento and Reno comparison between observations and the three WRF PBL model schemes. Hourly observations taken at NWS sounding sites Sacramento, CA and Reno, NV.

**Figure 16.** Region of cross sections. Black line indicates line of cross section.

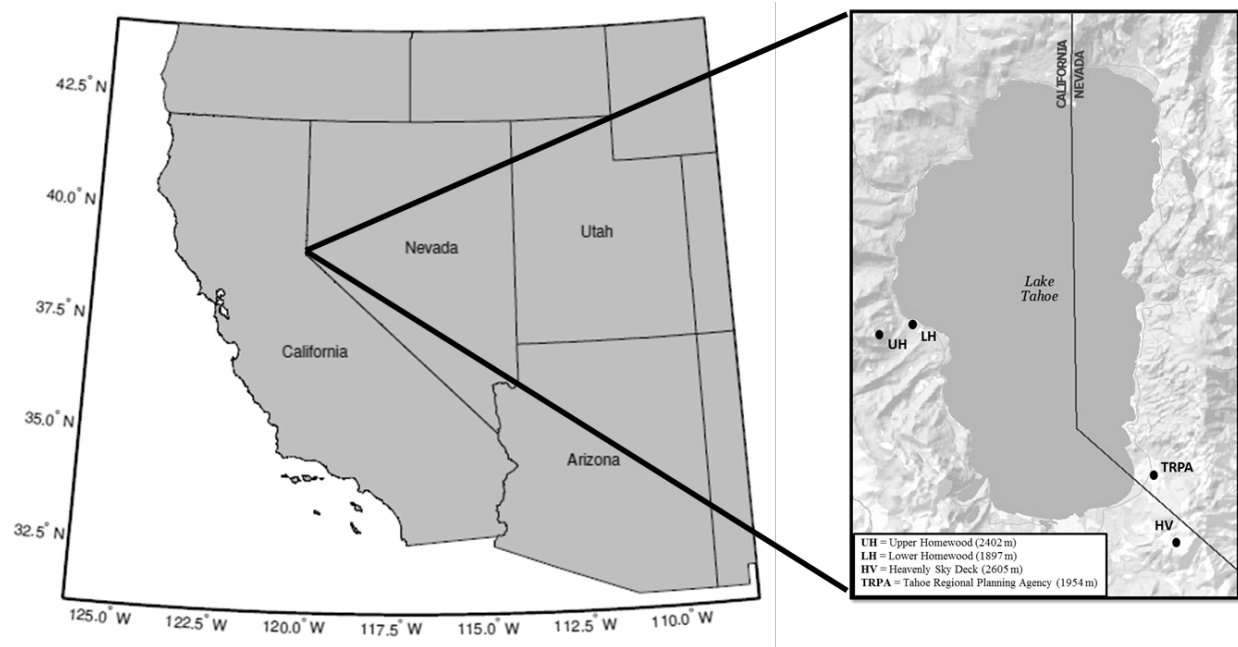
**Figure 17.** Cross section 25 July 1900 UTC. Top graph indicates u (east-west) component of winds, positive is red (coming from west). Middle graph indicates v (north-south) component of winds, positive is red (coming from south). Bottom graph indicates w (up-down) component of winds, positive is red (rising air). Black lines indicate potential temperature. Left point of graph is Sacramento, CA, right point is Fallon, NV.

**Figure 18.** Cross section 24 July 1900 UTC. Top graph indicates u (east-west) component of winds, positive is red (coming from west). Middle graph indicates v (north-south) component of

winds, positive is red (coming from south). Bottom graph indicates  $w$  (up-down) component of winds, positive is red (rising air). Black lines indicate potential temperature. Left point of graph is Sacramento, CA, right point is Fallon, NV.

**Figure 19.** Cross section 24 July 1000 UTC. Top graph indicates  $u$  (east-west) component of winds, positive is red (coming from west). Middle graph indicates  $v$  (north-south) component of winds, positive is red (coming from south). Bottom graph indicates  $w$  (up-down) component of winds, positive is red (rising air). Black lines indicate potential temperature. Left point of graph is Sacramento, CA, right point is Fallon, NV.

**Figure 20.** Cross section 25 July 1900 UTC. Top graph indicates  $u$  (east-west) component of winds, positive is red (coming from west). Middle graph indicates  $v$  (north-south) component of winds, positive is red (coming from south). Bottom graph indicates  $w$  (up-down) component of winds, positive is red (rising air). Black lines indicate potential temperature. Left point of graph is Sacramento, CA, right point is Fallon, NV.

**Figures**

**Figure 4.1.** Location of Lake Tahoe and site locations of 2012 field study.

## WPS Domain Configuration

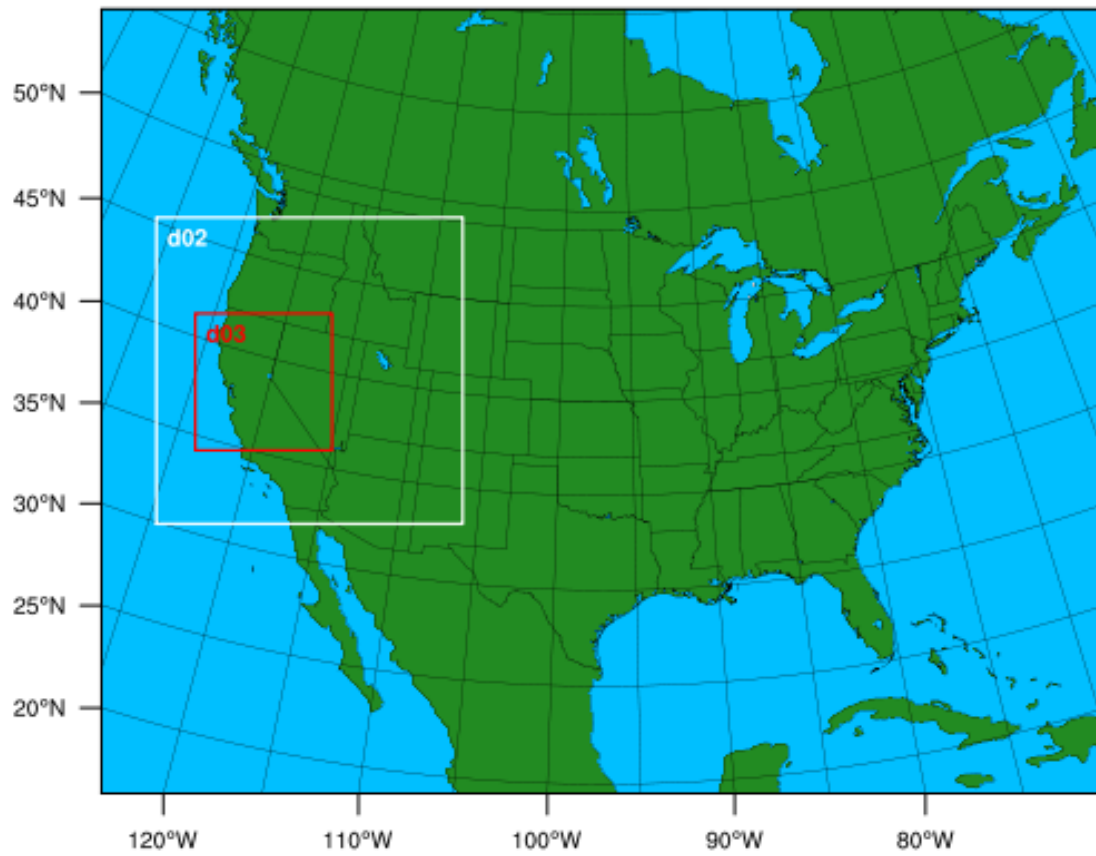


**Figure 4.2.** Model domains. The mother domain (d01) is the black box, first nested domain (d02) is the white box and second nested domain (d03) is the red box.

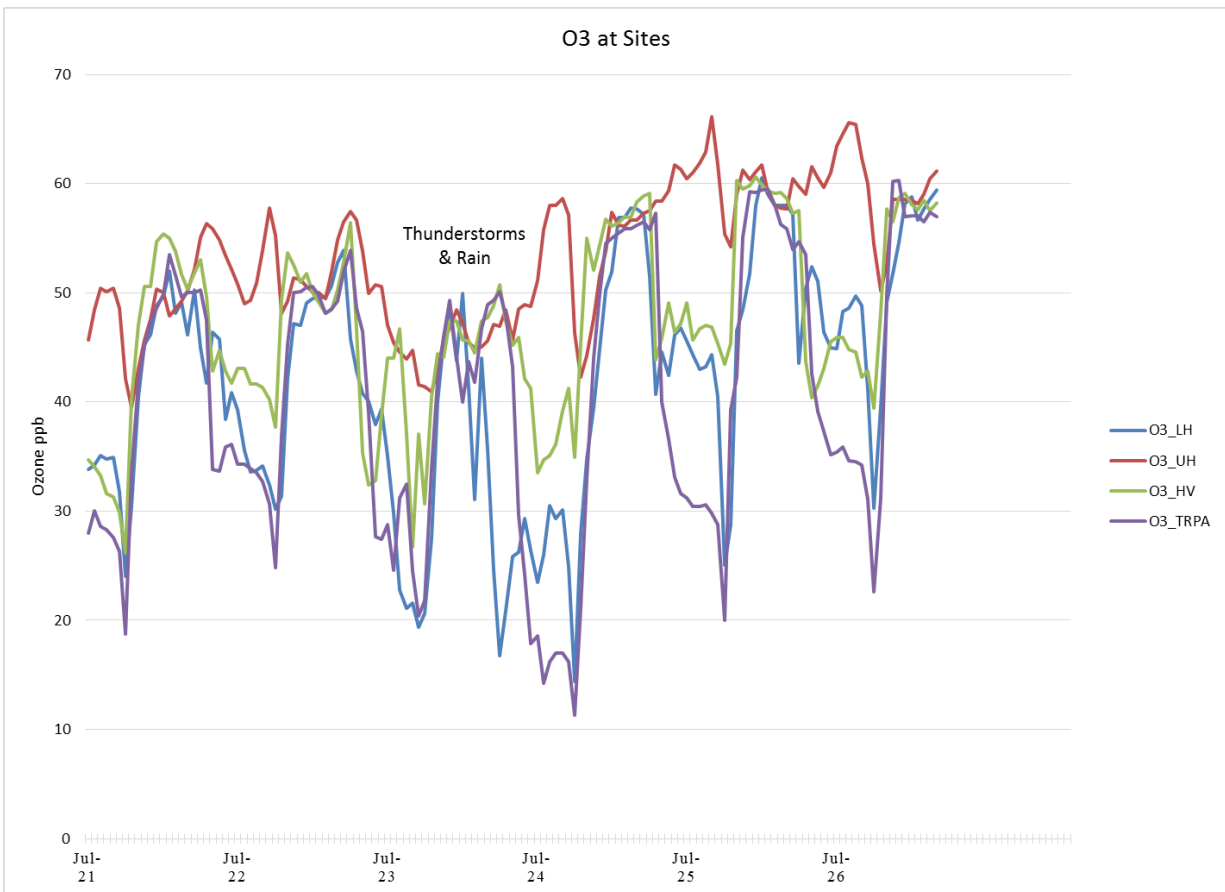


**Figure 4.3.** Hourly ozone values for the 2012 sites: LH is Lower Homewood, UH is Upper Homewood, HE is Heavenly Ski Resort, and HQ is Tahoe Regional Planning Agency.

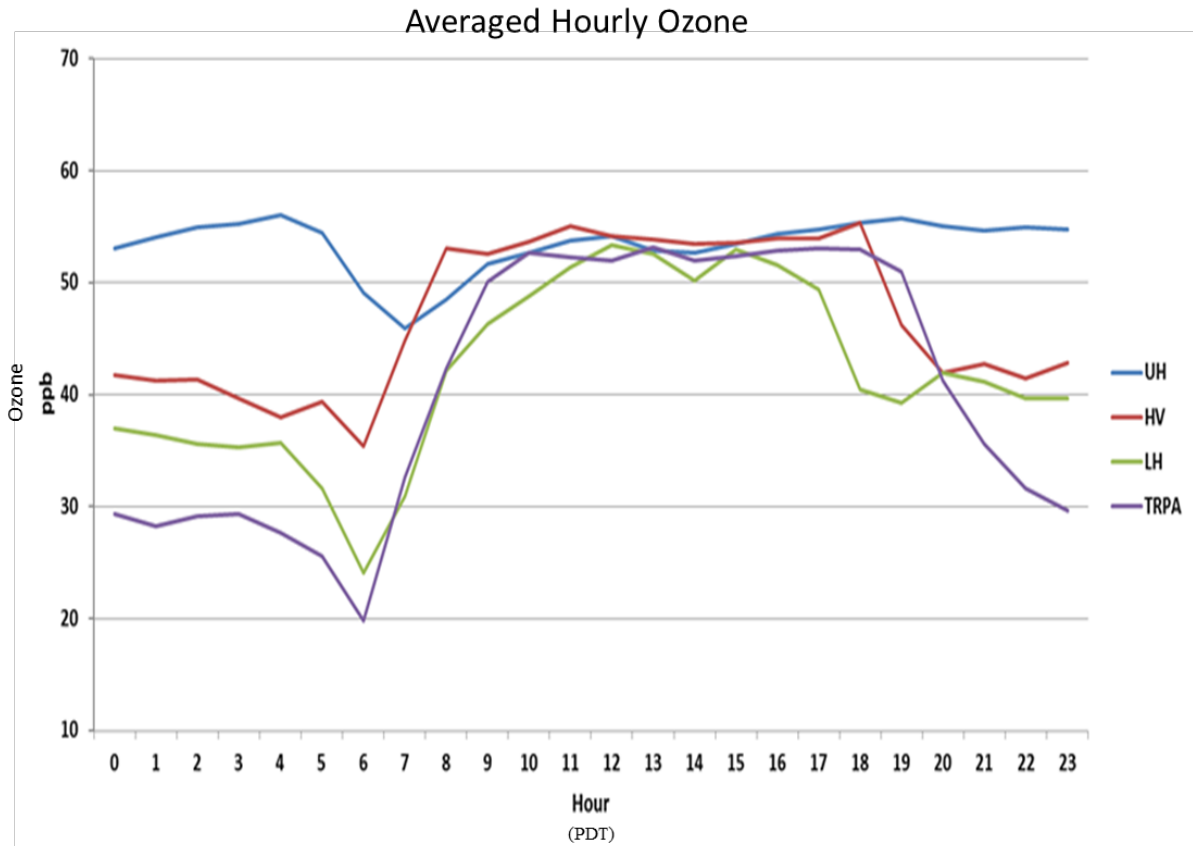


**Figure 4.4.** Averaged hourly ozone values for the 2012 sites: UH is Upper Homewood, HV is Heavenly Ski Resort, LH is Lower Homewood and TRPA is Tahoe Regional Planning Agency.

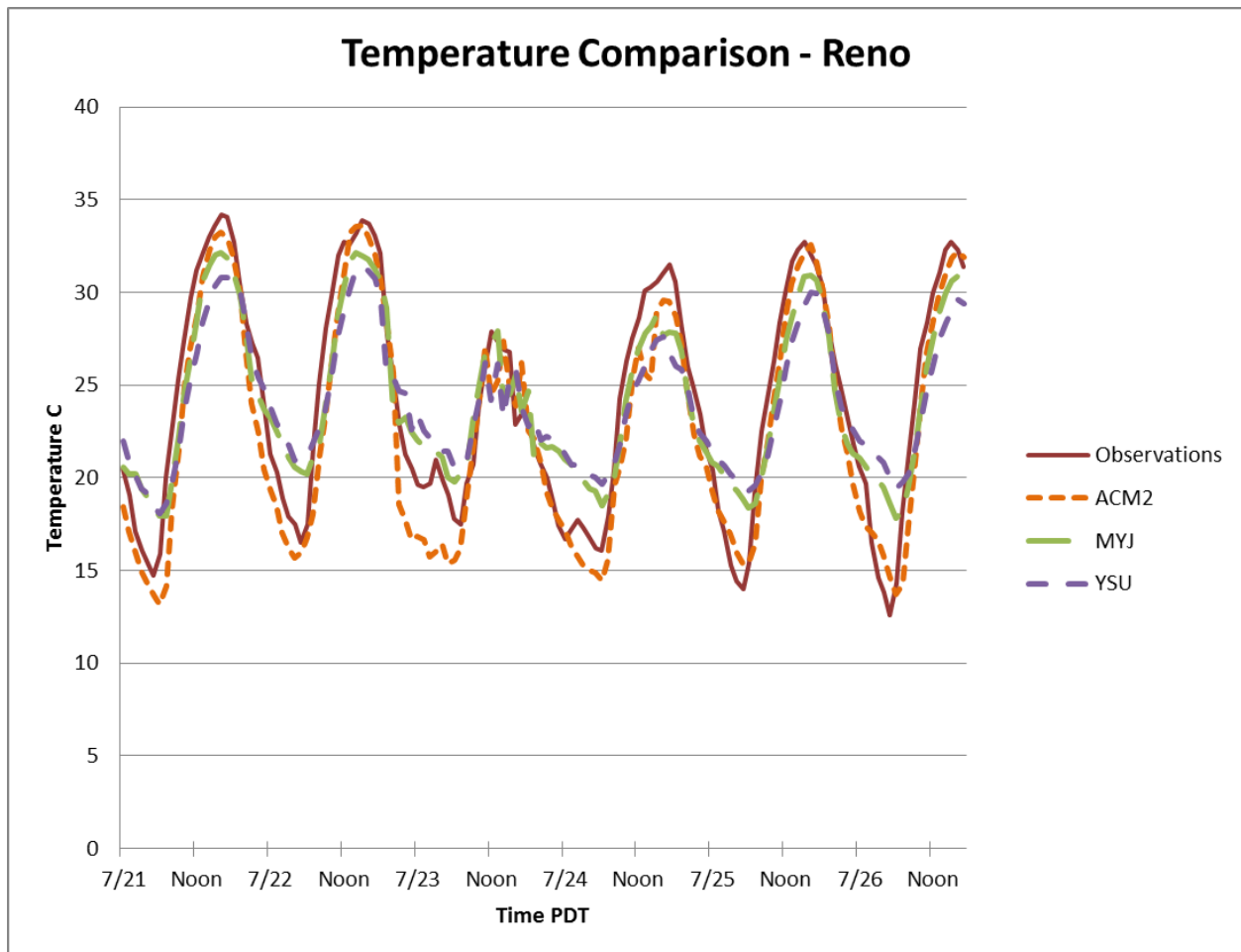


**Figure 4.5.** Temperature comparison between observations and the three WRF PBL model schemes. Data is hourly, observations taken at NWS surface observational site Reno, NV.

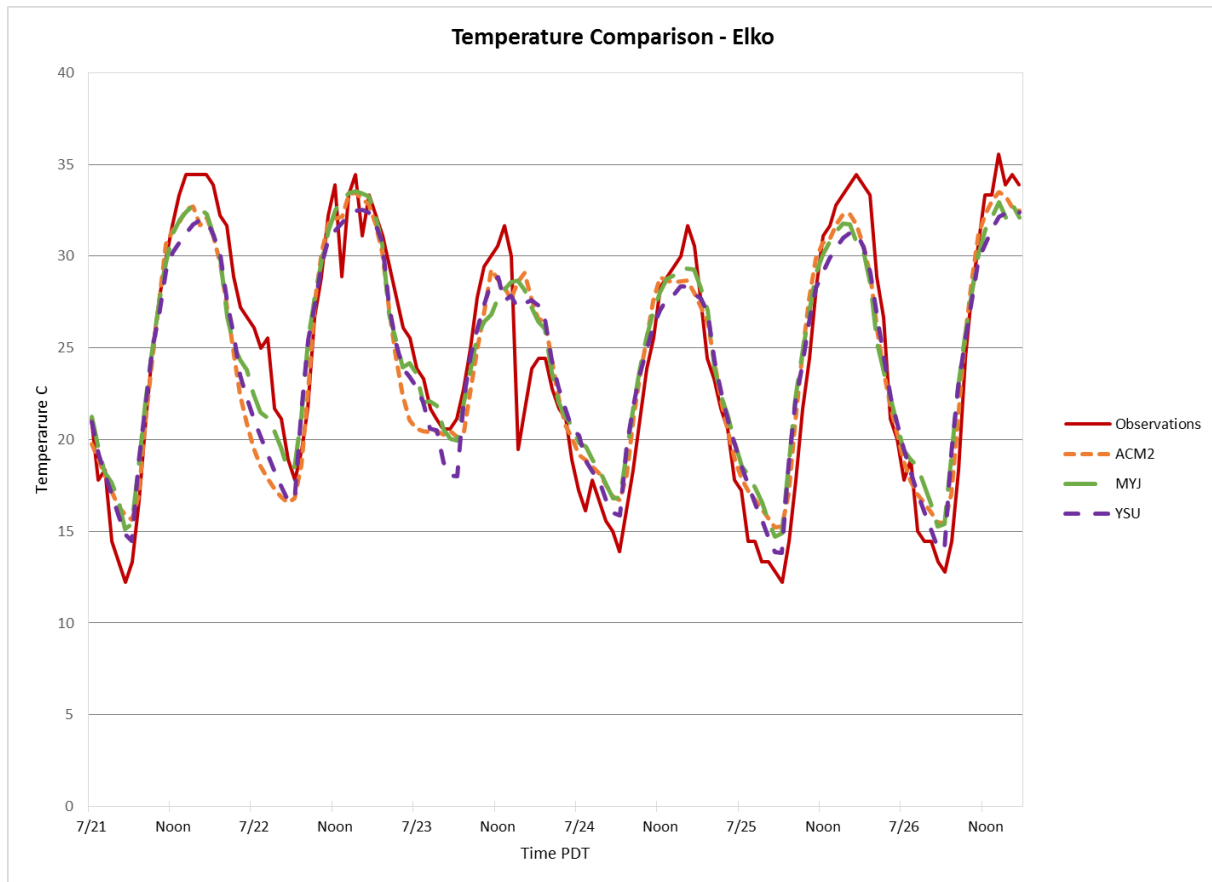


**Figure 4.6.** Temperature comparison between observations and the three WRF PBL model schemes. Data is hourly, observations taken at NWS surface observational site Elko, NV.

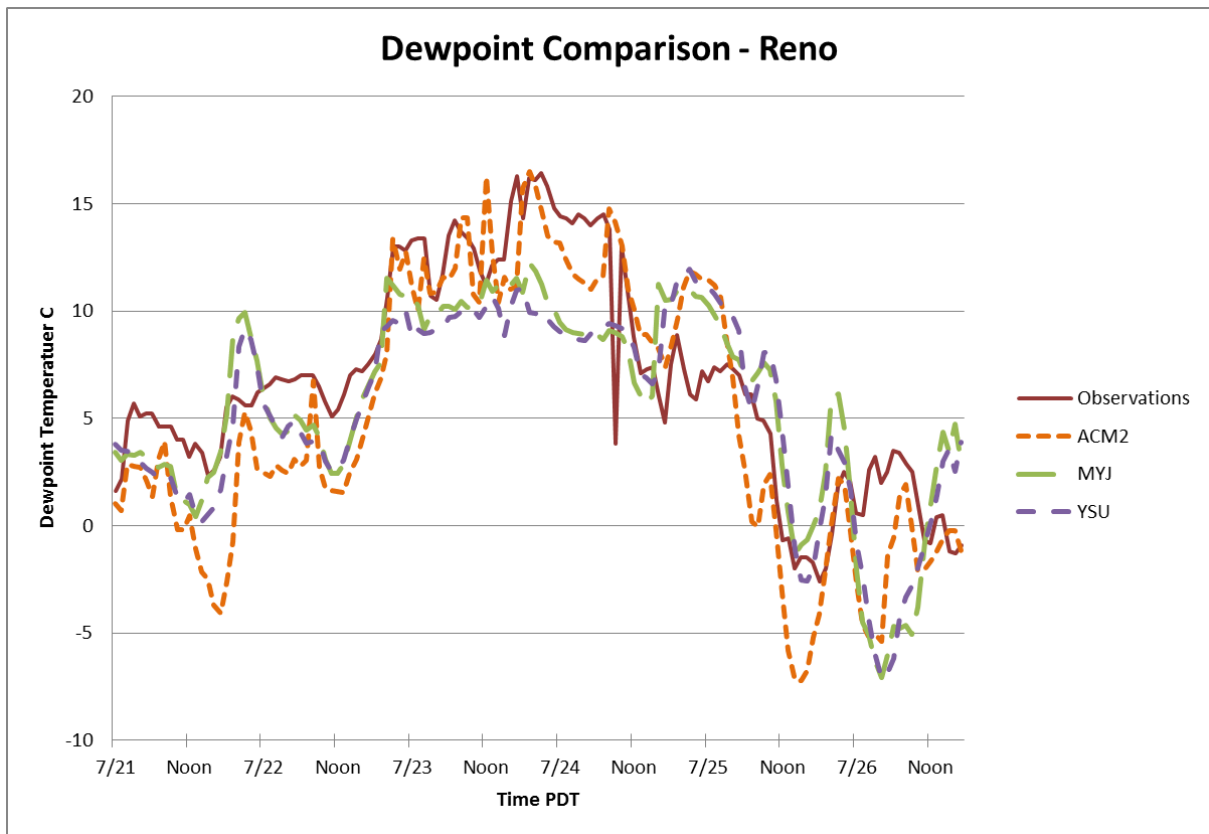


**Figure 4.7.** Dew point temperature comparison between observations and the three WRF PBL model schemes. Data is hourly, observations taken at NWS surface observational site Reno, NV.

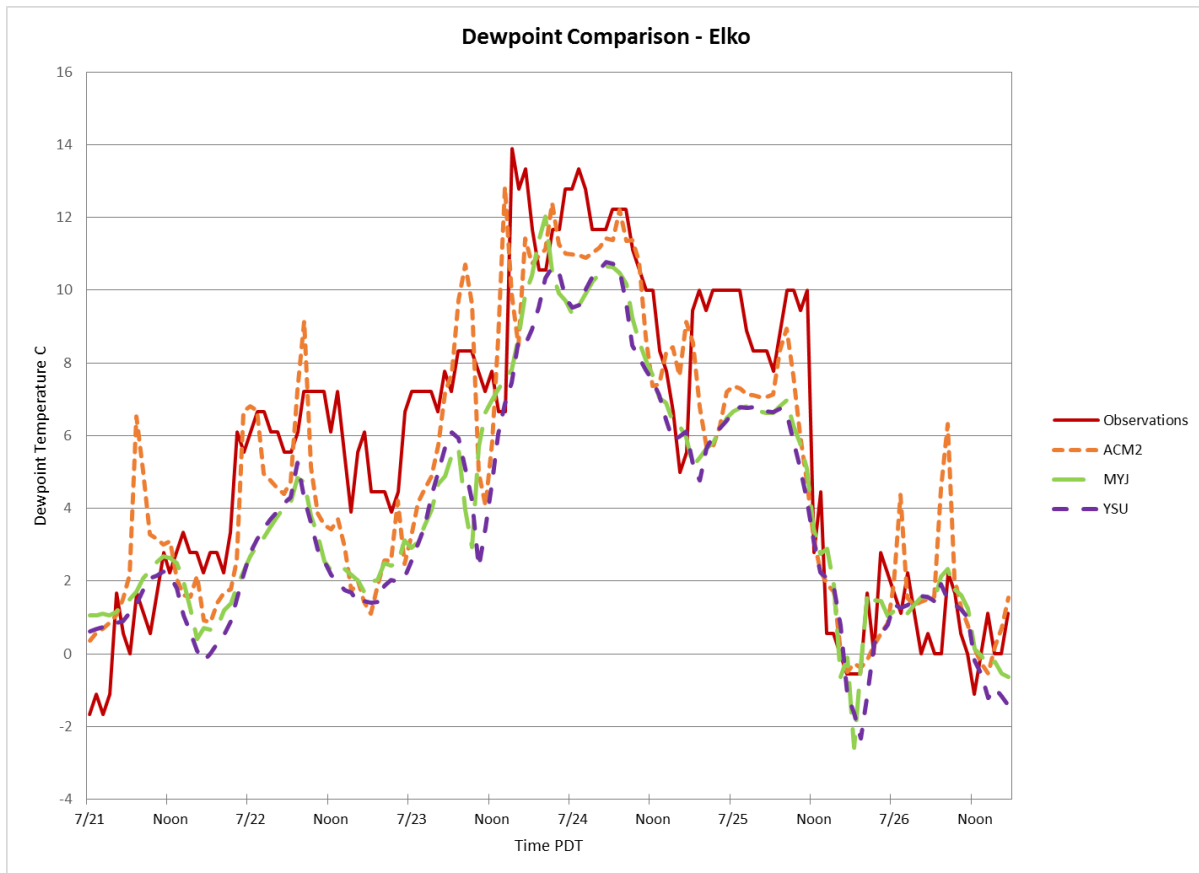


**Figure 4.8.** Dew point temperature comparison between observations and the three WRF PBL model schemes. Data is hourly, observations taken at NWS surface observational site Elko, NV.

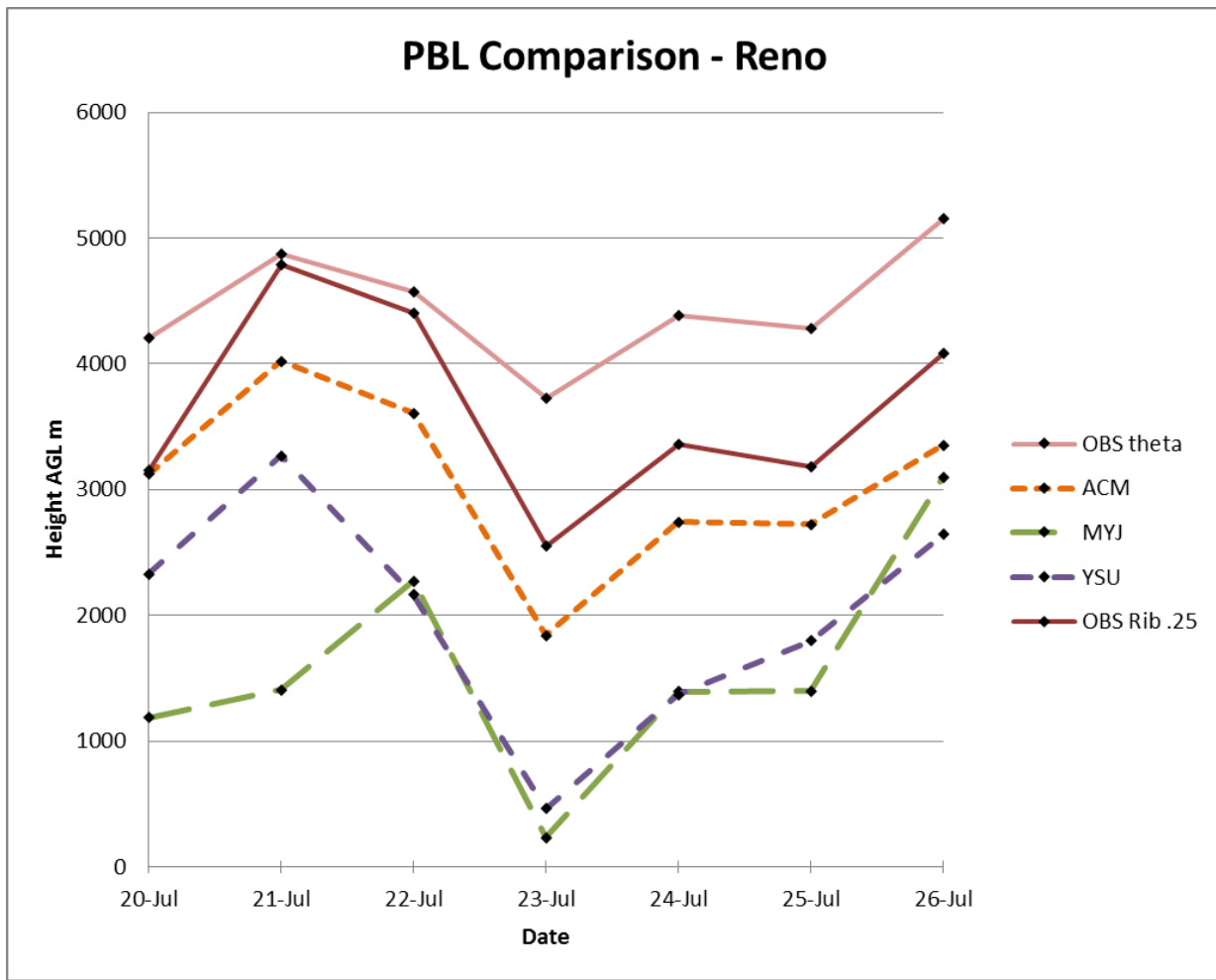


**Figure 4.9.** PBL comparison between observations calculated two different ways and the three WRF PBL model schemes. Observations taken at NWS sounding site Reno, NV. Only 0000 UTC data was used.

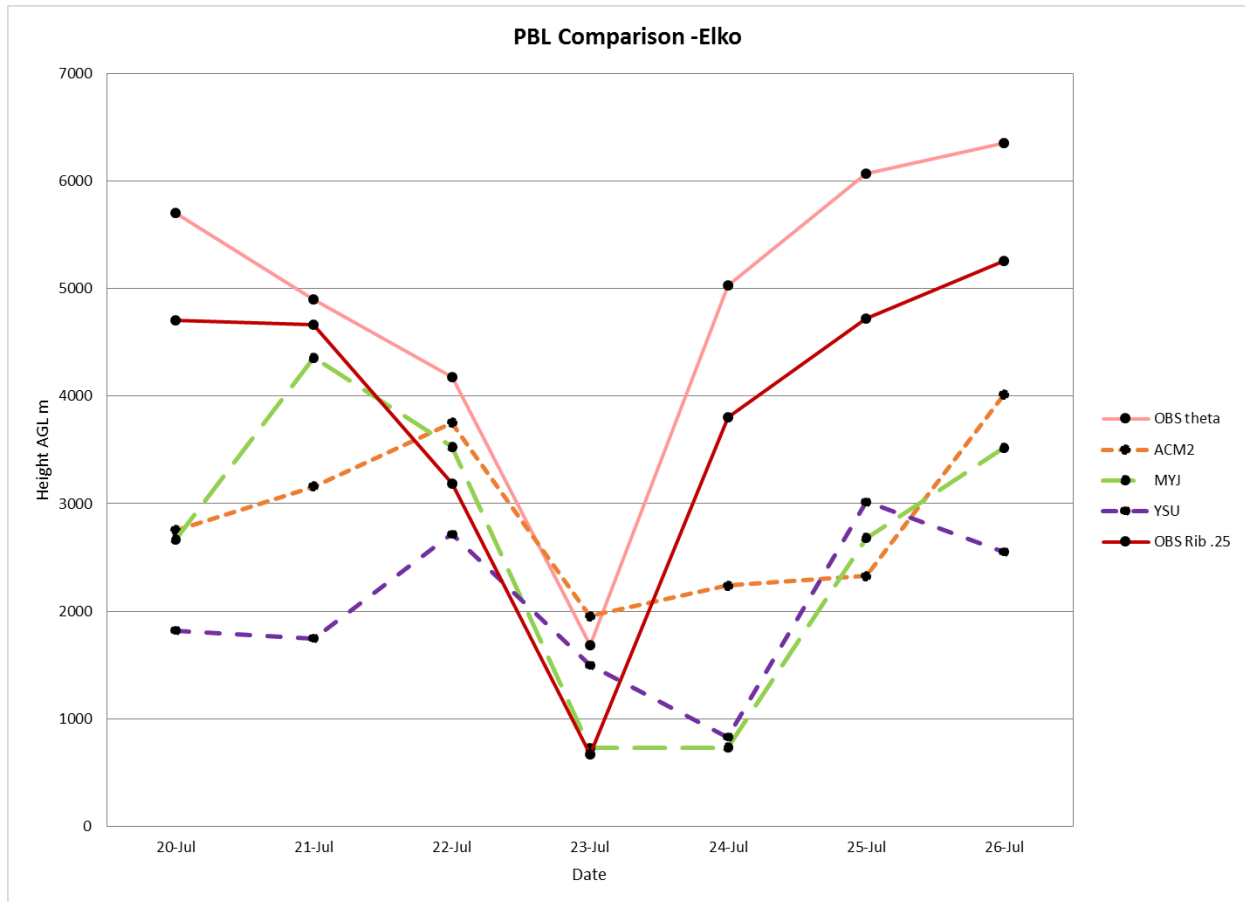


**Figure 4.10.** PBL comparison between observations calculated two different ways and the three WRF PBL model schemes. Observations taken at NWS sounding site Elko, NV. Only 0000 UTC data was used.

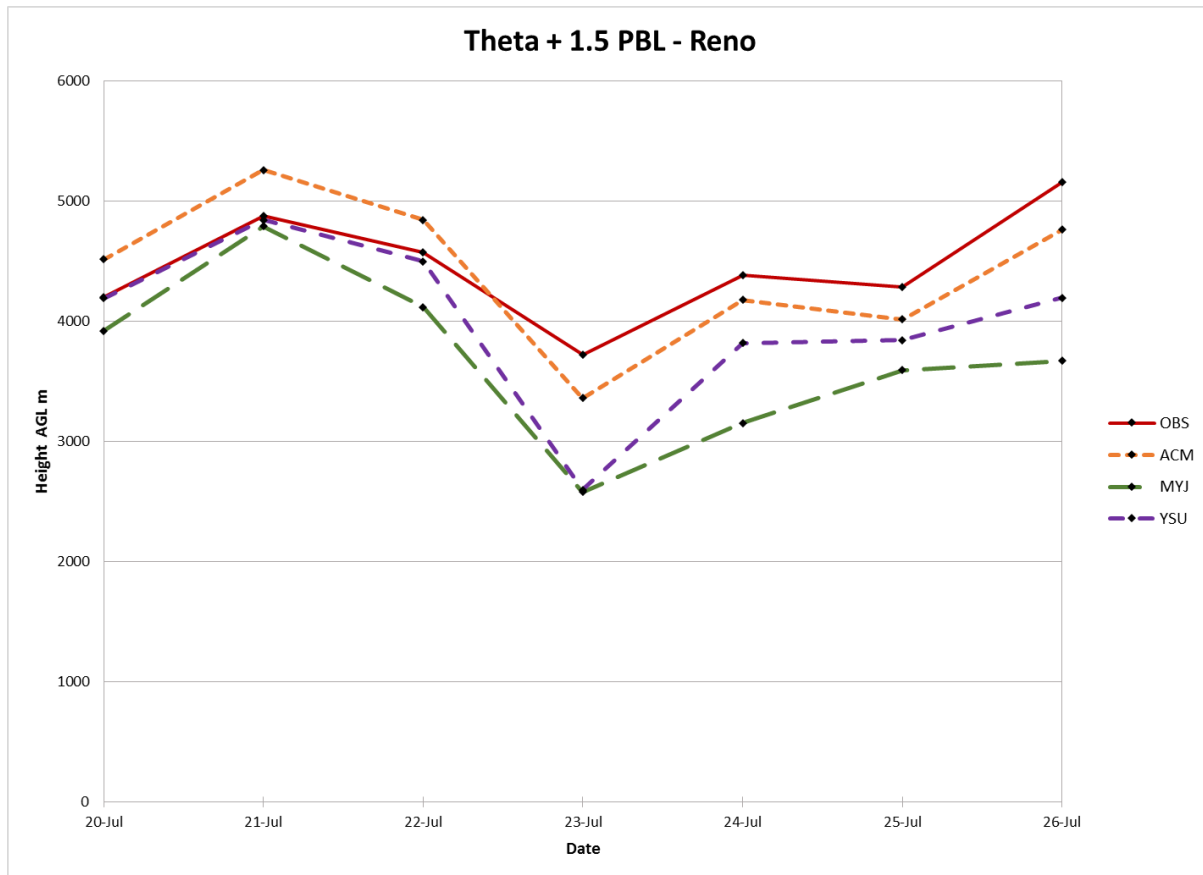


**Figure 4.11.** PBL height calculated using the +1.5 theta method comparison between observations and the three WRF PBL model schemes. Observations taken at NWS sounding site Reno, NV. Only 0000 UTC data was used.

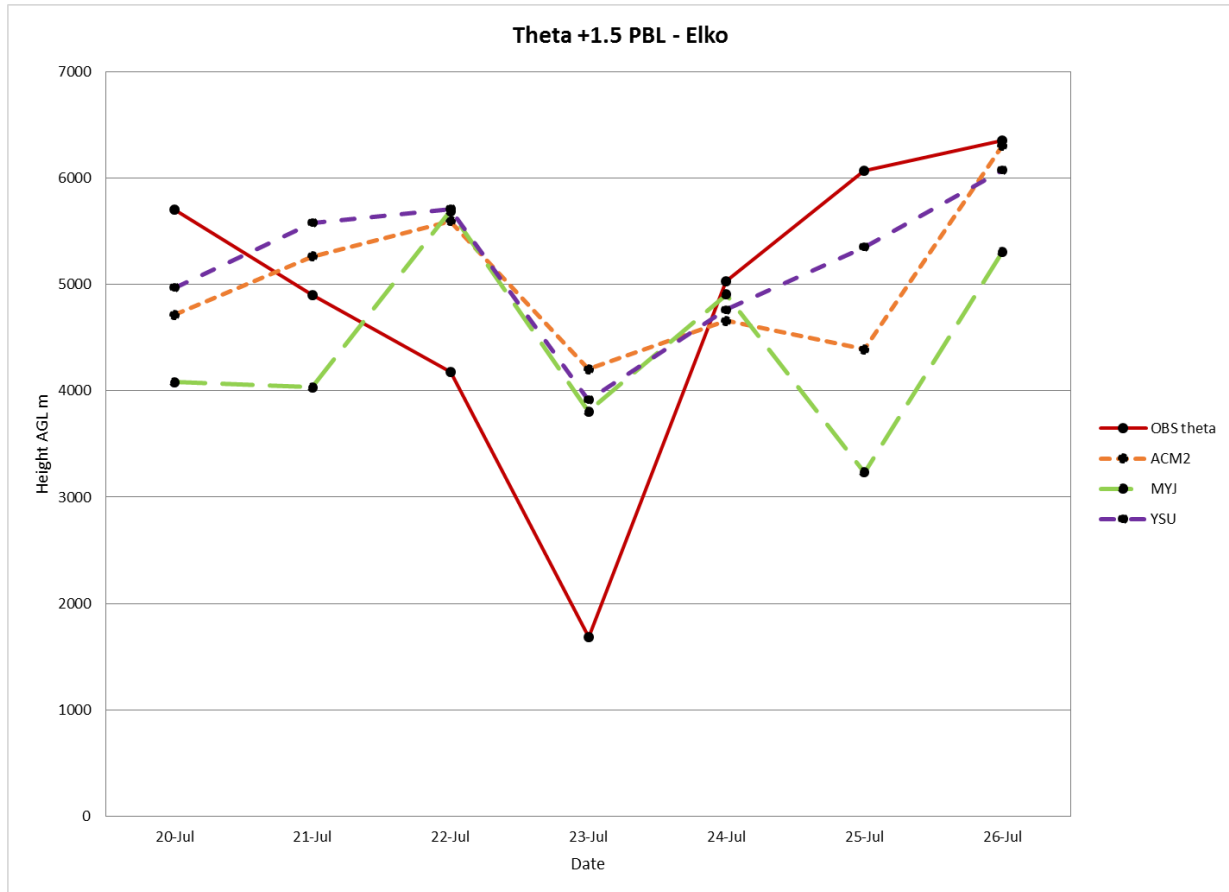


**Figure 4.12.** PBL height calculated using the +1.5 theta method comparison between observations and the three WRF PBL model schemes. Observations taken at NWS sounding site Elko, NV. Only 0000 UTC data was used.

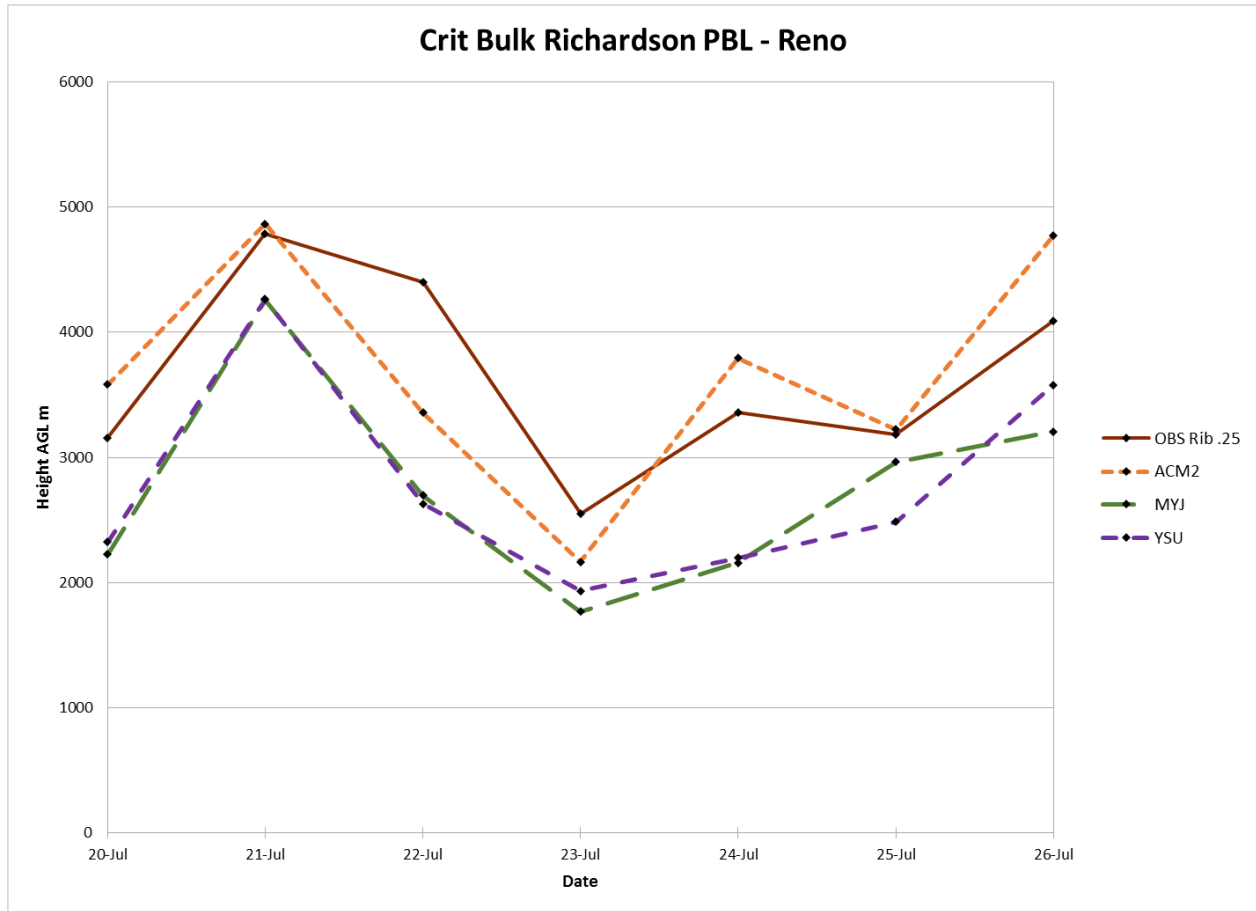


**Figure 4.13.** PBL height calculated using the critical bulk Richardson number of 0.25 method comparison between observations and the three WRF PBL model schemes. Observations taken at NWS sounding site Reno, NV. Only 0000 UTC data was used.

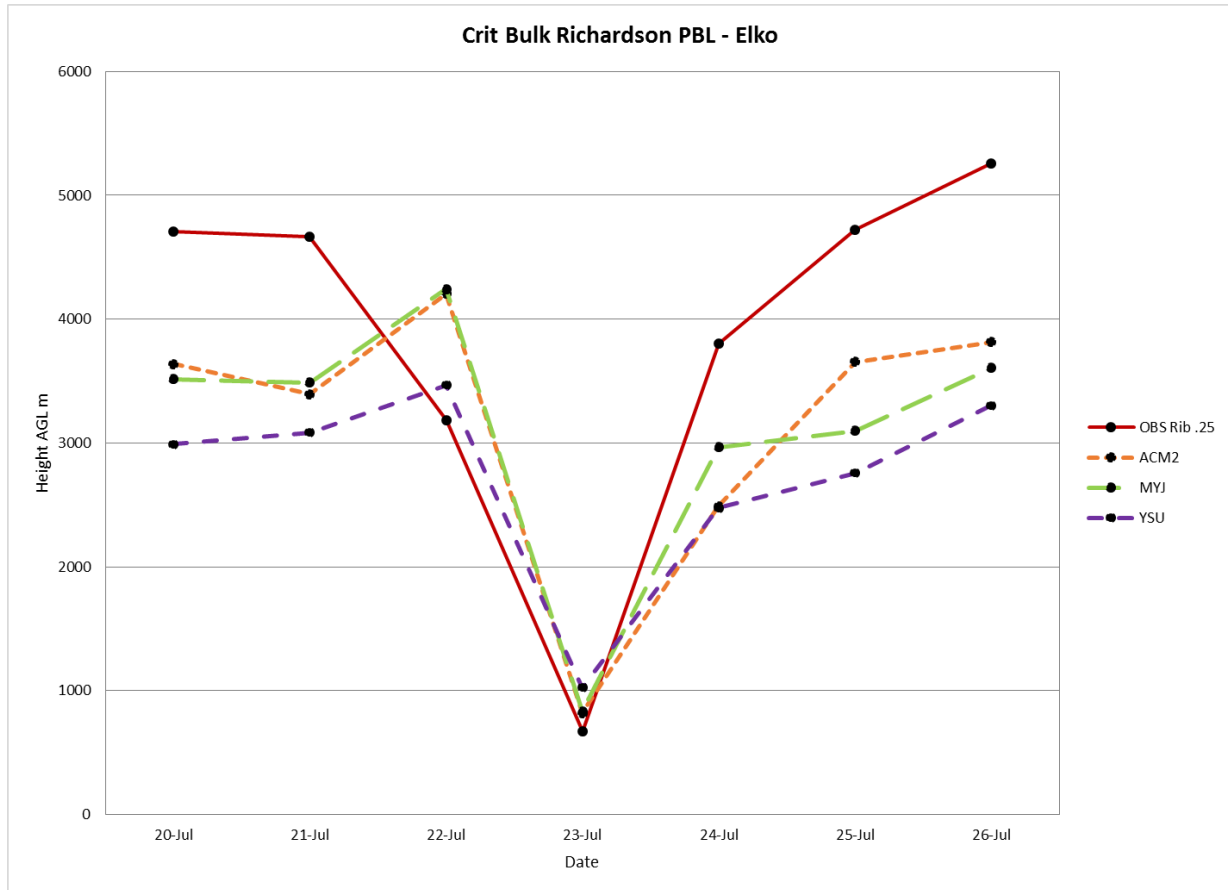


**Figure 4.14.** PBL height calculated using the critical bulk Richardson number of 0.25 method comparison between observations and the three WRF PBL model schemes. Observations taken at NWS sounding site Elko, NV. Only 0000 UTC data was used.

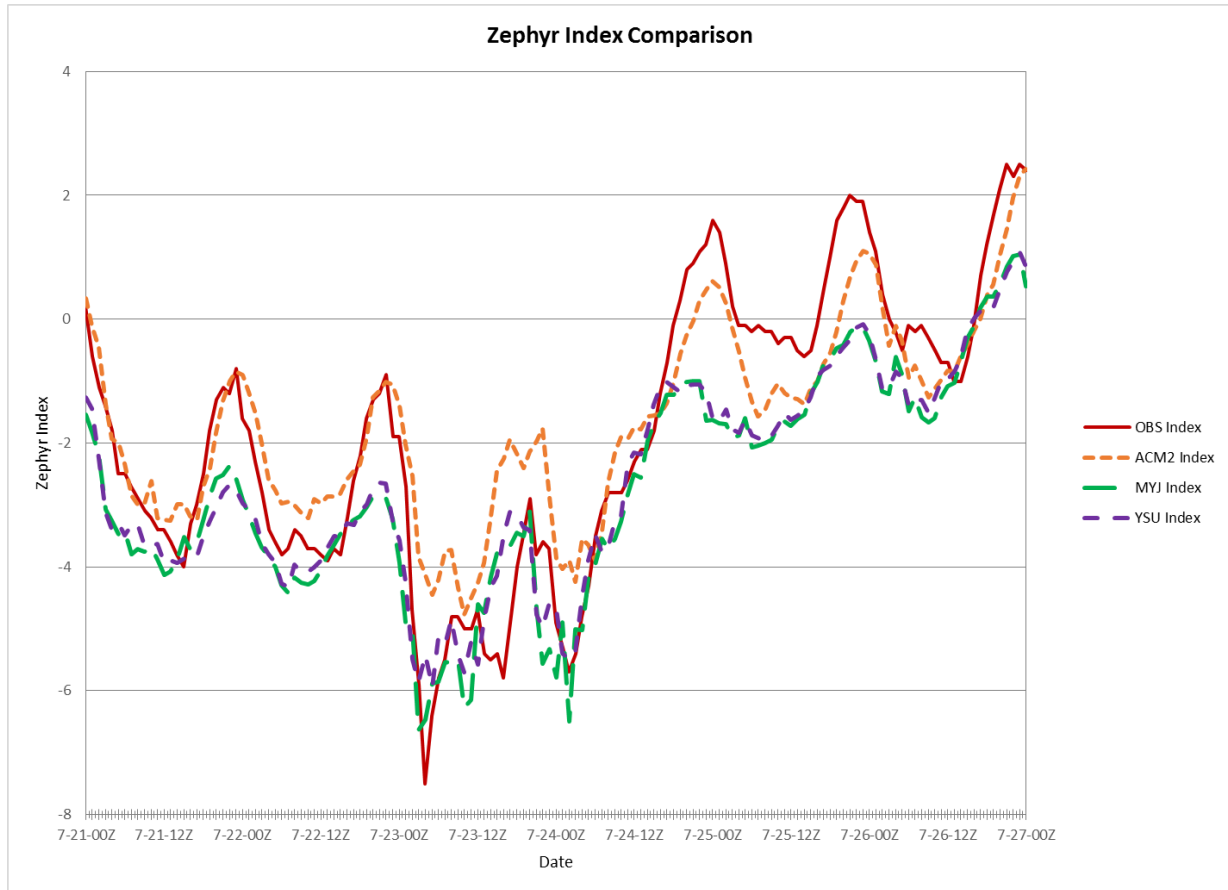


**Figure 4.15.** Washoe Zephyr Index calculated using the pressure difference between Sacramento and Reno comparison between observations and the three WRF PBL model schemes. Hourly observations taken at NWS sounding sites Sacramento, CA and Reno, NV.

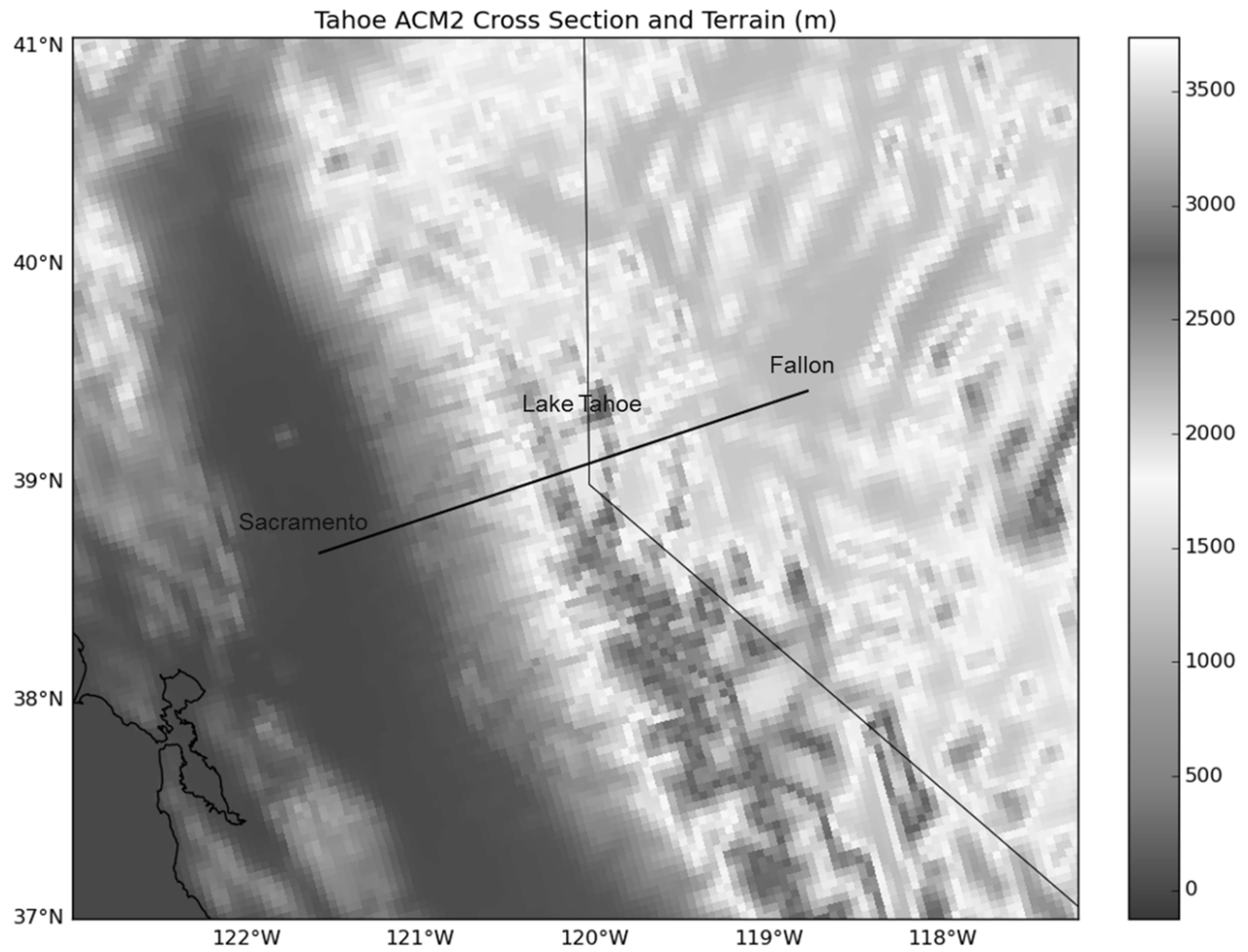


**Figure 4.16.** Region of cross sections. Black line indicates line of cross section.

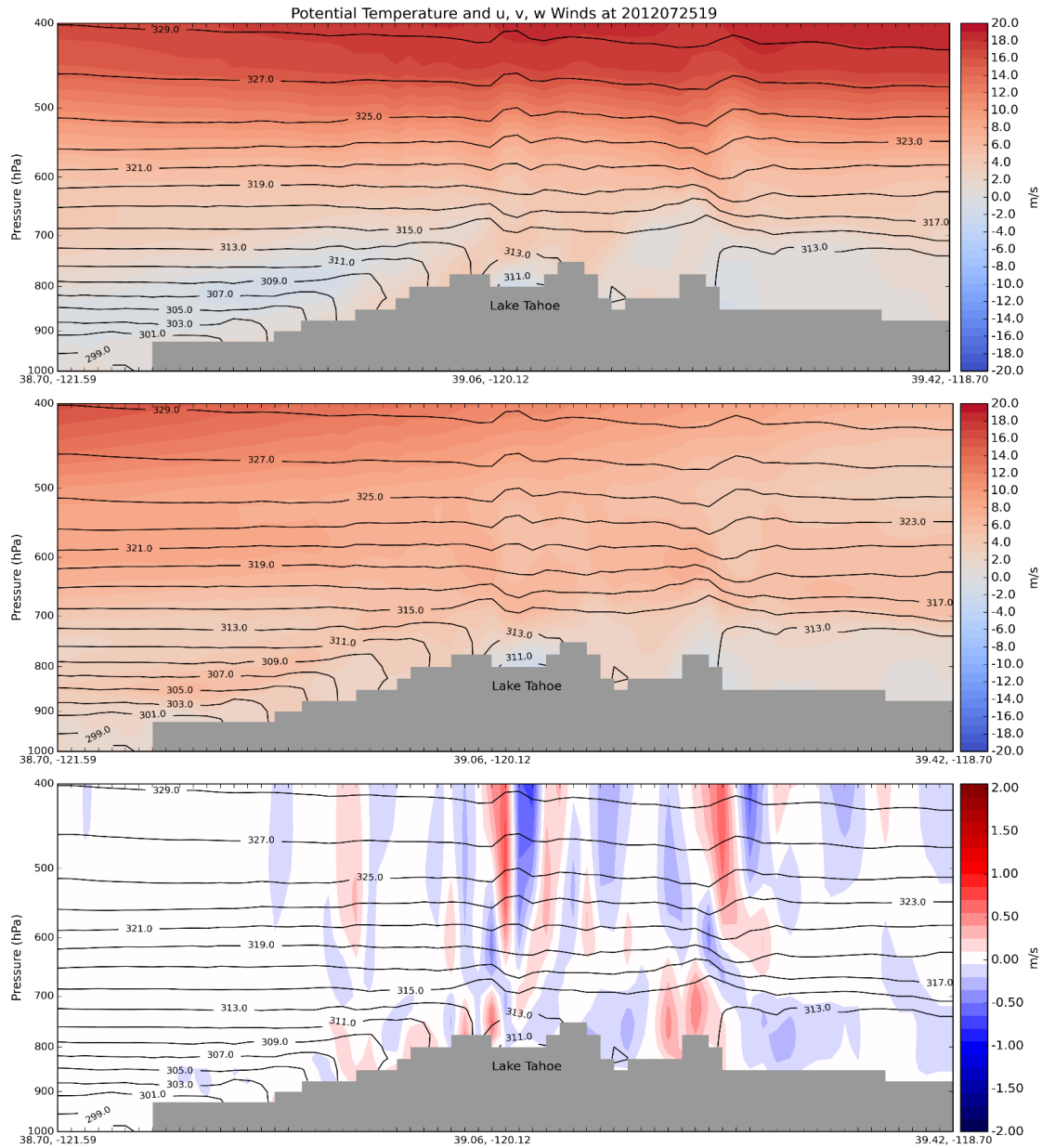


**Figure 4.17.** Cross section 25 July 1900 UTC. Top graph indicates u (east-west) component of winds, positive is red (coming from west). Middle graph indicates v (north-south) component of winds, positive is red (coming from south). Bottom graph indicates w (up-down) component of winds, positive is red (rising air). Black lines indicate potential temperature. Left point of graph is Sacramento, CA, right point is Fallon, NV.

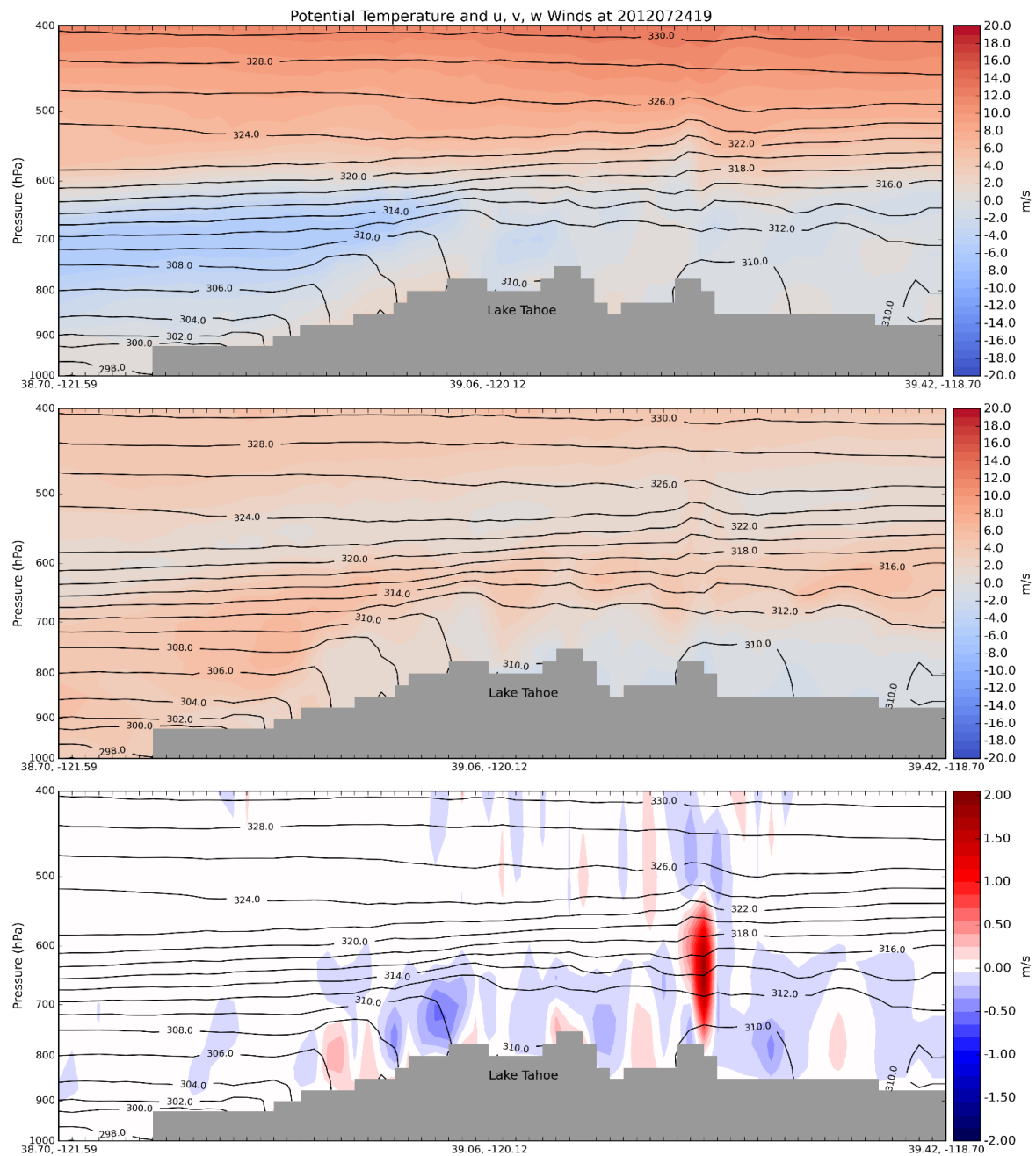


**Figure 4.18.** Cross section 24 July 1900 UTC. Top graph indicates u (east-west) component of winds, positive is red (coming from west). Middle graph indicates v (north-south) component of winds, positive is red (coming from south). Bottom graph indicates w (up-down) component of winds, positive is red (rising air). Black lines indicate potential temperature. Left point of graph is Sacramento, CA, right point is Fallon, NV.

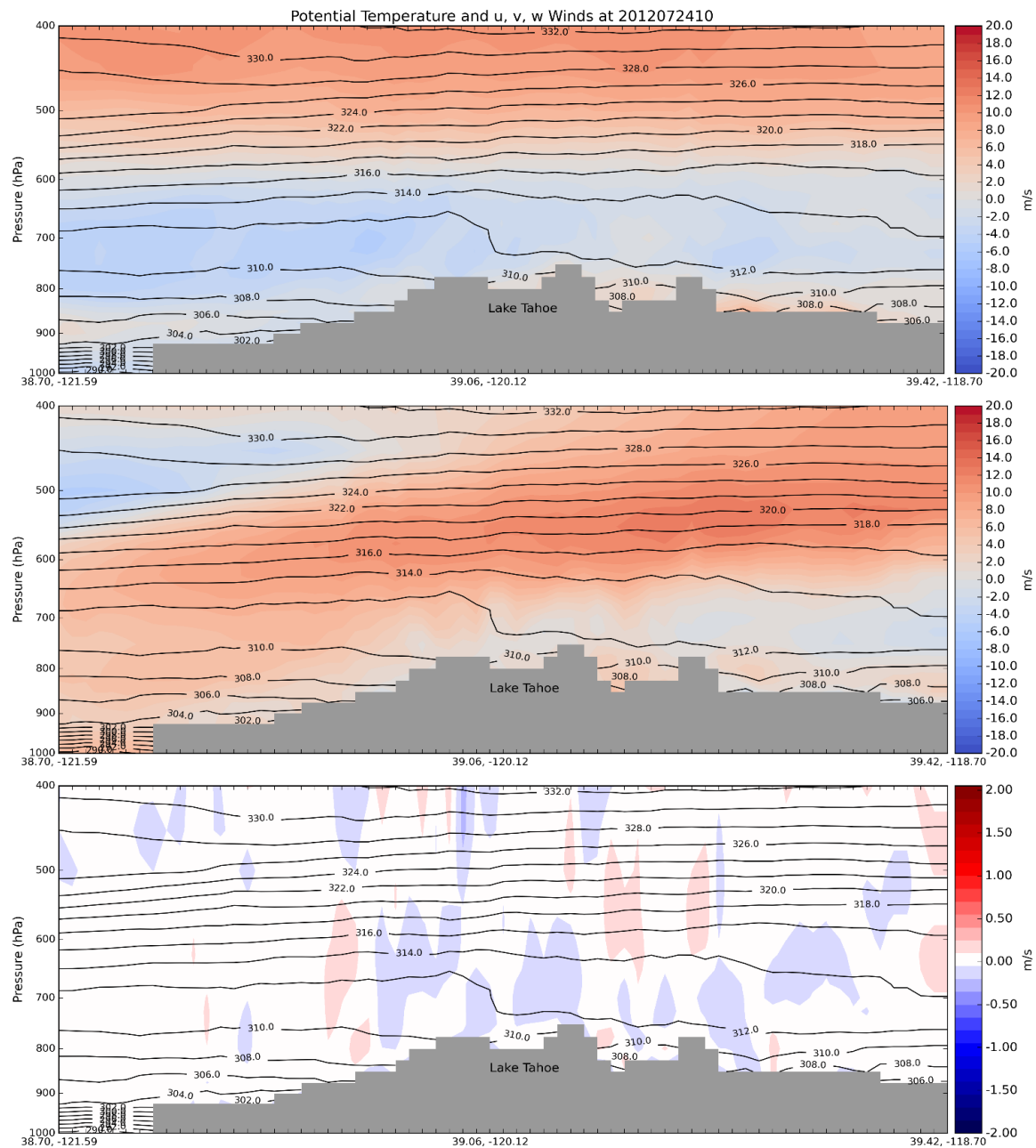


**Figure 4.19.** Cross section 24 July 1000 UTC. Top graph indicates u (east-west) component of winds, positive is red (coming from west). Middle graph indicates v (north-south) component of winds, positive is red (coming from south). Bottom graph indicates w (up-down) component of winds, positive is red (rising air). Black lines indicate potential temperature. Left point of graph is Sacramento, CA, right point is Fallon, NV.

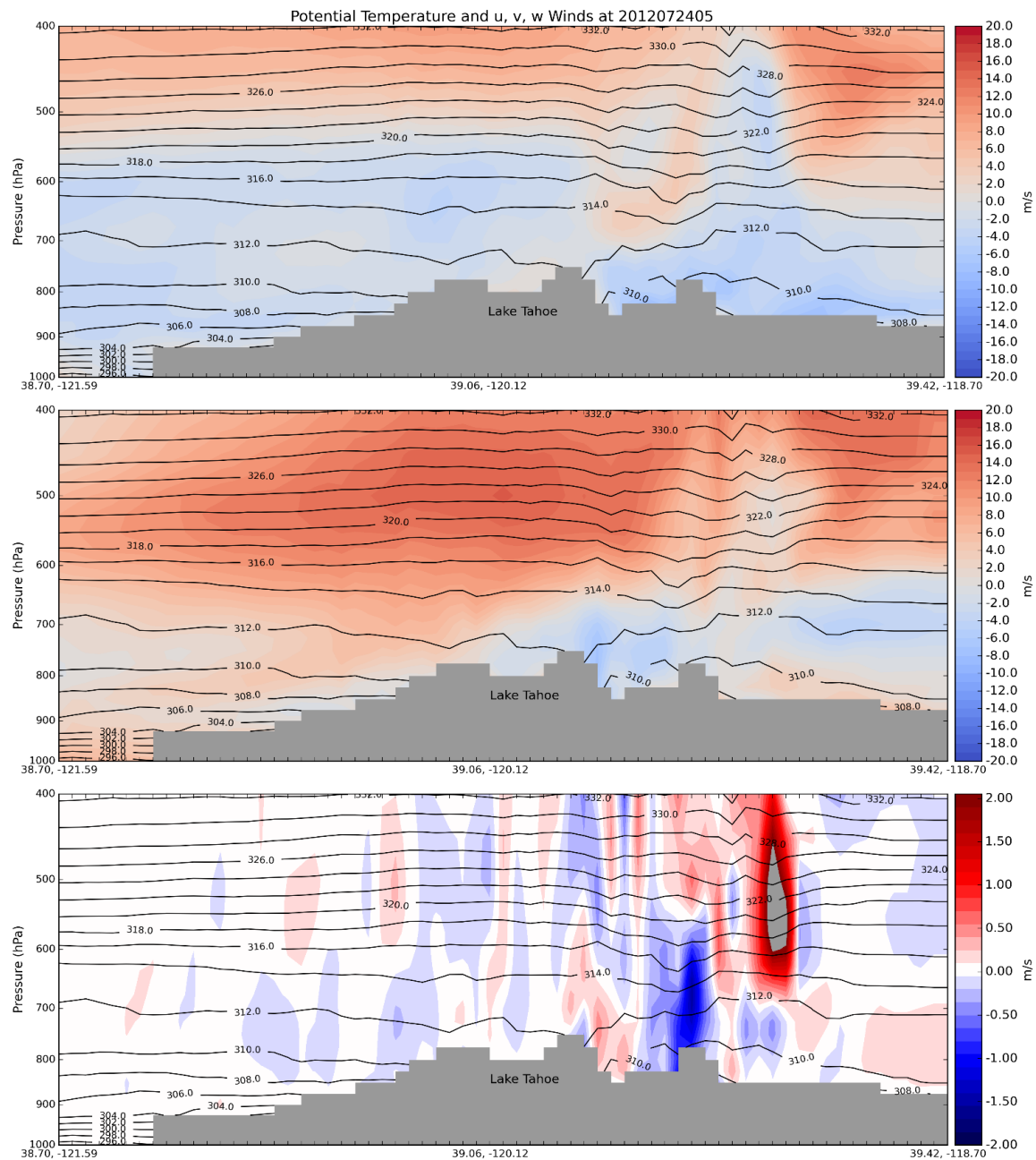


**Figure 4.20.** Cross section 25 July 1900 UTC. Top graph indicates u (east-west) component of winds, positive is red (coming from west). Middle graph indicates v (north-south) component of winds, positive is red (coming from south). Bottom graph indicates w (up-down) component of winds, positive is red (rising air). Black lines indicate potential temperature. Left point of graph is Sacramento, CA, right point is Fallon, NV.

## Chapter 5: Summary and Conclusions

The Lake Tahoe Basin had been in compliance with ambient air quality standards for ozone until 2005, when the Air Resources Board of the State of California (CARB) adopted a more stringent 8-hour ozone standard (not to exceed 70 ppb). Now some areas within the Basin violate this standard a few times each summer. This is detrimental to human health and the Lake Tahoe environment. Previous studies indicate that both the local generation of O<sub>3</sub> in the Basin and long-range transport from out-of-Basin sources are important in contributing to O<sub>3</sub> exceedances. However little is known about the impact of meteorology on the distribution of O<sub>3</sub> source regions. In order to develop a better understanding of the factors affecting O<sub>3</sub> levels and sources in the Lake Tahoe Basin, this study performed a comprehensive meteorological analysis addressing the issue of local generation versus long-range transport of O<sub>3</sub> and O<sub>3</sub> precursors.

As part of a study designed to investigate the spatial and temporal patterns of ozone around the Lake Tahoe Basin during the summer months of 2010, the regional impact of meteorology on ozone distribution was analyzed. The highest ozone values were observed during the month of August. There was a period of low ozone values (33 – 62 ppb) during the middle of July. The highest site, Genoa 9000 and the southernmost site, Angora, experienced the highest ozone values and violations of the new 8-hour CARB standard for ozone. While all sites had similar ozone concentrations during the day (55 -60 ppb), the low elevation sites had much lower ozone concentrations during the night (10 – 30 ppb). This is due to a combination of factors including lack of long-range transport of ozone and ozone precursors from downwind areas, topography and landscape surfaces, ozone titration of NO emitted from local traffic and local campground wood fires as well as local wind circulation patterns.

Based on the diurnal patterns of ozone showing high ozone values with little diurnal variability, the higher values of the maximum daily 1-hour ozone and the maximum averaged 8-hour ozone as well as the variability in the HYSPLIT trajectories, we find the transport of ozone precursors from Sacramento and the San Francisco Bay area can contribute to the increased background levels of ozone at Genoa 9000 and Angora. This study could not identify a mechanism for mixing free troposphere ozone down to the lower sites however, with the indication of the lake breeze by the wind roses the other sites are affected by local wind flow patterns and local emissions. Even at a low elevation, Thunderbird has high ozone values due to the dominant wind flow and lake breeze coming from the west. This is an indication that high values of ozone and source pollutants occur on the Lake as shown by Burley et al. (2014). Thus based on this work, we observed that ozone levels in the Basin are affected by transport from the west at higher elevations.

We then performed a meteorological analysis to ascertain potential synoptic-scale influences, such as the Washoe Zephyr, on observed O<sub>3</sub> concentrations. Our meteorological assessment of O<sub>3</sub> levels showed that the 700 hPa wind flow increased background concentrations of O<sub>3</sub> when coming from a more southerly direction. This indicated transport from out-of-Basin sources from the south (such as the San Joaquin Valley) rather than from the west (such as Sacramento and San Francisco). Our study also suggests factors other than the Washoe Zephyr (such as mixed-layer depth, sinking or rising air, and dew point temperature) had a more significant impact on development of high or low O<sub>3</sub> days for the Basin based upon the atmospheric sounding and HYSPLIT analysis.

Atmospheric sounding and HYSPLIT analysis of O<sub>3</sub> distribution data indicated that O<sub>3</sub> and O<sub>3</sub>-forming precursors may be transported into the Basin at higher levels in the atmosphere

but need a high mixed-layer depth and rising air parcels to be mixed downward into the Basin. Based on these findings, there is a need for further modeling and measurement studies to better quantify the contributions from in-Basin and out-of-Basin sources as well as to determine the downward mixing mechanisms into the Basin.

In order to continue the research in the Lake Tahoe Basin another field study was conducted in July 2012. The ozone analysis was similar to a similar field study performed in 2010 which showed higher elevation sites having higher ozone values and a decrease in diurnal variability. In order to analyze the transport of ozone and ozone precursors, three WRF version 3.5.1 simulations were run using three different PBL schemes (YSU, MYJ and ACM2). Results of the model simulations compared statistically to 77 surface observation sites within domain three (d03) showed that each PBL scheme had a positive bias with wind direction and humidity, and a negative bias with regard to temperature. The YSU and ACM2 scheme had a negative bias with wind speed while the MYJ scheme had a positive bias. Results of the observational PBL analysis compared with the model data showed that ACM2 performed best with calculating the PBL height, this includes the common means of comparisons. Using the ACM2 PBL scheme to create cross sections which analyze the wind circulation across the Lake Tahoe Basin indicated that transport from the west did not influence higher ozone values for this time period, however transport from cities to the east, i.e. Reno and Carson City do influence higher ozone values at the higher elevation site UH.

Overall, this study concludes that transport from the west is less significant than transport from the south and east, however transport only influences ozone values at higher elevations. Within the Basin itself (at lower elevations), local factors including mixing depth, strong vertical mixing and lake/land breeze circulations are more significant in influencing ozone values. Based on

these findings, the development and implementation of effective ozone control strategies in the Lake Tahoe Basin should be focused on in-basin sources as well as contributions from the Central Valley to the south and cities such as Reno and Carson City to the east; however, more research should be performed using a detailed chemical model to confirm this conclusion.

In conclusion, for future work a few things should be addressed:

1. In order to understand the over-all changing climate (including air quality) in the Lake Tahoe Basin a routine monitoring system should be set up. This includes routine chemical measurements of the atmosphere (i.e. ozone and ozone forming precursors, PM 2.5, PM 10 etc.) as well as the meteorology in and around the Basin. These meteorological and chemical observations will help to improve meteorological and chemical models which will also improve air quality forecasting for the region as well as help in understanding how the climate of the Lake Tahoe Basin is changing.
2. Research involving weather balloons (rawinsonde data) in conjunction with LIDAR data will help in understanding the observed boundary layer and how pollutants evolve within the boundary layer of the Lake Tahoe Basin.

## APPENDIX 1: Surface Ozone in the Lake Tahoe Basin

### Surface Ozone in the 1 Lake Tahoe Basin

Joel D. Burley <sup>a,\*</sup>, Sandra Theiss <sup>b</sup>, Andrzej Bytnerowicz <sup>c</sup>, Alan Gertler <sup>b</sup>,  
Susan Schilling <sup>c</sup>, and Barbara Zielinska <sup>b</sup>

*<sup>a</sup>Department of Chemistry, Saint Mary's College of California,  
Moraga, CA 94575-4527, USA; e-mail = jburley@stmarys-ca.edu;  
office telephone = 925-631-4839; fax = 925-376-4027*

*<sup>b</sup>Desert Research Institute, 2215 Raggio Parkway,  
Reno, NV 89512, USA*

*<sup>c</sup>USDA Forest Service, Pacific Southwest Research Station,  
4955 Canyon Crest Drive, Riverside, CA 92507, USA*

## **Abstract**

Surface ozone (O<sub>3</sub>) concentrations were measured in and around the Lake Tahoe Basin using both active monitors (2010) and passive samplers (2002, 2010). The 2010 data from active monitors indicate average summertime diurnal maxima of approximately 50-55 ppb. Some site-to-site variability is observed within the Basin during the well-mixed hours of 10:00 to 17:00 PST, but large differences between different sites are observed in the late evening and pre-dawn hours. The observed trends correlate most strongly with elevation, topography, and surface vegetation. High elevation sites with steeply sloped topography and drier ground cover experience elevated O<sub>3</sub> concentrations throughout the night because they maintain good access to downward mixing of O<sub>3</sub>-rich air from aloft with smaller losses due to dry deposition. Low elevation sites with flat topography and more dense surface vegetation experience low O<sub>3</sub> concentrations in the pre-dawn hours because of greatly reduced downward mixing coupled with enhanced O<sub>3</sub> removal via efficient dry deposition. Additionally, very high average O<sub>3</sub> concentrations were measured with passive samplers in the middle of the Lake in 2010. This latter result likely reflects diminished dry deposition to the surface of the Lake. High elevation Tahoe Basin sites with exposure to nocturnal O<sub>3</sub>-rich air from aloft experience daily maxima of 8-hour average O<sub>3</sub> concentrations that are frequently higher than concurrent maxima from the polluted upwind comparison sites of Sacramento, Folsom, and Placerville. Wind rose analyses of archived NAM 12 km meteorological data for the summer of 2010 suggest that some of the sampling sites situated near the shoreline may have experienced on-shore “lake breezes” during daytime hours and/or off-shore “land breezes” during the night. Back-trajectory analysis with the

HYSPLIT model suggests that much of the ozone measured at Lake Tahoe results from the transport of “polluted background” air into the Basin from upwind pollution source regions. Calculation of ozone exposure indices indicates that the two most polluted sites sampled by active monitors in 2010 – the highest Genoa Peak site, located on the eastern side of the Lake at an elevation of 2734 m above sea level, and Angora Lookout, located to the south-southwest (SSW) of the Lake at an elevation of 2218 m above sea level – likely experienced some phytotoxic impacts, while the other Tahoe Basin locations received lower ozone exposures.

*Keywords:* Lake Tahoe

portable ozone monitor

passive samplers

spatial interpolation

ozone exposure indices

HYSPLIT

## 1. Introduction

Lake Tahoe (elevation 1897 m above sea level) is a large alpine lake that straddles the border between California and Nevada. With a maximum depth of 501 m, it is the fourth deepest lake in North America, and it is renowned for the clarity of its water (United States Geological Survey, 2014). Because of its importance as both a unique natural resource and a year-round vacation destination, Lake Tahoe has been extensively studied in terms of issues relating to hydrology and water clarity (Tahoe Environmental Research Center, 2014). The air quality within the Lake Tahoe Basin – especially the deposition of atmospheric pollutants into the lake – has also been investigated (Gertler et al., 2006; Dolislager et al., 2012a, VanCuren et al., 2012). Less attention, however, has been focused upon Lake Tahoe in terms of surface ozone and other air quality issues that are not directly linked to water clarity (Dolislager et al., 2012b).

Historically, the Tahoe Basin had been in compliance with ambient air quality standards for ozone until 2005, when the Air Resources Board of the State of California (CARB) adopted a more stringent 8-hour ozone standard (not to exceed 70 ppb). Now some areas within the Basin violate this standard a few times each summer. Given that typically observed in-Basin ozone concentrations have remained low enough so that human health impacts are not a pressing concern (at least in comparison to heavily polluted regions like the western slope of the southern Sierra Nevada), many prior Tahoe Basin ozone studies have instead focused upon the impact of ozone on the health of the extensive pine forests that surround the Lake (Dolislager et al., 2012a and 2012b). Ambient ozone has pronounced adverse effects on forest health in California's mountain regions (Arbaugh et al., 1998). According to large-scale distribution maps of the Sierra

Nevada bioregion, the Lake Tahoe Basin's summer-season, 24-hour ozone levels are approximately 50 to 60 ppb (Fraczek et al., 2003). Such ozone levels may be toxic to vegetation (Krupa et al., 1998) and can adversely affect tree health (Arbaugh et al., 1998). Ozone has been observed to cause foliar injury to ponderosa (*Pinus ponderosa*) and Jeffrey (*Pinus jeffreyi*) pines in the central Sierra Nevada (Miller et al., 1996), including the Lake Tahoe Basin (Pedersen et al., 1989).

In addition to potential impacts on surrounding forests, prior Tahoe Basin ozone investigations have also examined the transport of ozone and ozone precursors from upwind source regions. Carroll and Dixon (2002) performed aircraft measurements of a Sacramento pollution plume and found that maximum ozone concentrations were frequently observed in the afternoon, 40-80 km downwind of the city, but subsequently decreased by about 50% at distances 120 km downwind. Zhang et al. (2002) used aircraft measurements to study nitrogen and phosphorus in and around the Lake Tahoe Basin. Bytnerowicz et al. (2004) studied spatial and temporal ozone distributions as two-week integrated averages measured by passive samplers during the 2002 summer season for the entire Lake Tahoe Basin and for upwind areas on the western slopes of the Sierra Nevada. They concluded that the Sierra Nevada crest west of the Lake Tahoe Basin acts as a barrier that restricts polluted air masses and high ozone concentrations from the Sacramento Valley and Sierra Nevada foothills from entering the Basin. Dolislager et al. (2012b) assessed the relative impacts of transport versus local photochemical production by making continuous measurements during the summer of 2003 along the axis of predominant airflow (i.e., roughly southwest to northeast). They utilized two transport assessment sites at Big Hill and Echo Summit, along with other monitoring sites at various locations on the western slope of the Sierra Nevada, plus four in-Basin monitoring sites. Also

incorporating aircraft data, they concluded that pollutants from upwind regions act to raise background concentrations entering the Tahoe Basin to the extent that local contributions do not need to be large to cause exceedances of air quality standards.

While the prior Tahoe Basin studies noted above are most relevant to the results presented in the present report, it should be noted that the more general topics of surface ozone (i) in alpine environments and (ii) near large bodies of water with persistent “lake breeze” (onshore flow) or “land breeze” (offshore flow) conditions have been thoroughly investigated in recent decades. Readers interested in a review of surface ozone measurements at high elevation sites should consult section 4.2 of Burley and Bytnerowicz (2011), which compares high-elevation results from the White Mountains along the California-Nevada border to similar sites across North America, Europe, and Asia. Other recent studies of interest might also include the paper from Ambrose et al. (2011) on results from the Mt. Bachelor Observatory (2763 m) in central Oregon, or the paper from Macdonald et al. (2011) on data collected at Whistler Mountain (2180 m) in British Columbia, Canada. Readers looking for more background on surface O<sub>3</sub> measurements where “lake/sea breeze” or “land breeze” conditions are prevalent are similarly encouraged to consult the recent papers from Goldberg et al. (2014), Stauffer et al. (2012), and Cleary et al. (2014).

This report presents ozone data measured in 2010 by portable ozone monitors deployed at ten different sites surrounding the lake, plus simultaneous data from long-term monitors at Incline Village and Echo Summit. It also presents two years (2002, 2010) of ozone data from passive samplers that were deployed across a more extensive network of sites that included both the Tahoe Basin and the area immediately to the west. (Three of the sites from this extended network of passive samplers also measured ozone in 2006.) Additional passive sampler data

from 2010 for ozone precursors such as NO<sub>x</sub> and volatile organic compounds (VOC) are also utilized to better understand the factors that influence ambient ozone levels within the Lake Tahoe Basin. In addition to mixing ratio data for O<sub>3</sub>, NO<sub>x</sub>, and VOC, an analysis of local winds is presented to help identify some of the meso-scale phenomena that can influence temporal and spatial variations in ozone. Back trajectories using the Hybrid Single-Particle Lagrangian Integrated Trajectory (HYSPLIT) model are also utilized to highlight the long-range transport patterns that can bring ozone into the Tahoe Basin.

## **2. Experimental methods and procedures**

### **2.1. Sampling locations**

Sampling locations where ozone concentrations were measured using both portable monitors and passive samplers are listed in Table 1, along with the long-term monitoring stations at Echo Summit (ECHO) and Incline Village (IVL). Three additional sites – Sacramento (SAC), Folsom (FOL), and Placerville (PLA) – that are used to provide simultaneous comparison data are also included. Table 2 presents analogous information for the sampling sites where ozone was measured only with passive samplers. A map of the sampling locations used in this study is presented in Figure 1.

The eleven sites equipped with both active monitors and passive samplers span the complete circumference of the lake, with lower elevation locations typically positioned within a few hundred meters of the shoreline and higher elevation sites usually located within a few kilometers of the shoreline. While most of these active sites were in relatively remote locations with minimal and/or infrequent exposure to vehicular emissions, some locations – Valhalla (VAL), Echo Summit (ECHO), Incline Village (IVL) – were adjacent to busy highways. At all of the measurement sites the sampling hardware was installed, whenever possible, so as to

minimize potential impacts from nearby vehicular emissions or other local sources of pollution. For those sites equipped with both portable monitors and passive samplers the two different measurements were typically positioned within approximately 10 m of one another, with similar sampling heights (~1.75 m above ground level for the portable monitors; ~2.0 m above ground level for the passive samplers).

The sites equipped only with passive samplers included approximately a dozen locations that were located within ~10 km of the shoreline plus another ten locations that extended data collection further to the west (~75 km), north (~20 km), and south (~30 km). These outermost sites lie outside the Tahoe Basin, and enable direct in-Basin vs. out-of-Basin comparisons.

## 2.2. Sampling timelines

Although data collection in 2010 commenced at some locations in mid-June, the hourly data used to calculate daily averages, daily maxima of 8-hour averages, and average diurnal cycles have been restricted to 12:00 PST on July 14 through 11:00 PST on September 22, which corresponds to exposure periods #3 through #7 for the passive samplers. Restricting the hourly data in this manner facilitates direct comparisons between the active ozone monitors and the passive samplers within a uniform 70-day window. Calculations of ozone exposure indices, however, utilized all available hourly data, with simple linear extrapolations to either a four month period of June through September (a 24-hour index calculated across an interval of 120 days, or 2880 hours in total), or a three-month period of July through September (a 12-hour index calculated across an interval of 90 days, or 1080 hours in total). Along these lines, a preliminary 24-hour exposure index based upon 2300 hours of continuous ozone data would be multiplied by a factor of  $2880/2300 = 1.252$  in order to obtain the appropriate value for the four

month exposure period. For the passive sampler data from 2002, data collection commenced on June 5 and continued until October 7. However, to enable more direct comparisons to the 2010 results, the 2002 data presented here have been restricted to July 16 – September 24.

In addition to the data from 2010 and 2002, passive sampler data for ozone were collected in 2006 (June 1 – October 5) at a limited network of six sites, all in close proximity to the Lake Tahoe shoreline. The 2006 sampling locations included three sites used in both 2002 and 2010 – 64 Acres (64A), Sugar Pine Point State Park (SPP), and Valhalla (VAL) – plus Cave Rock (CR), which was also sampled in 2002. The remaining two sites sampled in 2006 (Crystal Towers, Nevada Beach) were not utilized in either 2002 or 2010. The 2006 passive sampler data that are briefly discussed in section 3.4 have been limited to the three sites that were sampled in all three years and are restricted to an observation window of July 13 through September 21 to facilitate comparisons with results from 2002 and 2010.

## 2.3. Sampling protocols and calibrations

### 2.3.1. Data from portable ozone monitors

Ozone concentrations were measured using Model 202 Ozone Monitors from 2B Technologies, which employ UV absorption (Beer's Law) at a wavelength of 254 nm. Ambient air was sampled approximately 1.75 m above ground level via a 2.5 m length of 6.35 mm (0.25 inch) o.d. Teflon tubing. The sampling inlet consisted of a downward-facing 47 mm diameter Teflon filter holder equipped with a 1-2  $\mu$ m Teflon filter membrane, which was shielded from precipitation by a plastic rain shield. Power for the ozone monitors was provided by 12-volt solar power systems at all locations except for Thunderbird Lodge (THB), where local AC power was employed. To ensure protection from the elements, the ozone monitors and accompanying

electronics were enclosed in weatherproof plastic cases. Ozone concentrations were measured every 10 s, and were automatically recorded into internal monitor memory as 5-minute averages. These 5-minute averages were subsequently downloaded from the ozone monitors and converted into hourly averages.

Multi-point factory calibrations of the portable ozone monitors were conducted by 2B Technologies before deployment to the Lake Tahoe sites. While in the field, a mid-deployment calibration was performed at eight sites – all except Angora Lookout (AGL) and Thunderbird Lodge (THB) – using the model 306 Ozone Calibration Source from 2B Technologies. Extensive post-deployment calibrations were also carried out with the Model 306 after the conclusion of fieldwork. Based on these multiple comparisons, it is estimated that the hourly data from the portable ozone monitors have a precision of  $\pm 5$  ppb and an accuracy of  $\pm 5\%$ . Readers interested in prior field-based assessments of monitor performance should consult Burley and Ray (2007) or Burley and Bytnerowicz (2011).

### 2.3.2. Data from the CARB monitoring sites

Hourly data for the ozone monitors operated at Echo Summit along U.S. highway #50 (ECHO), 1309 T Street in Sacramento (SAC), Natoma Street in Folsom (FOL), and Gold Nugget Way in Placerville (PLA) by the California Air Resources Board were downloaded from the CARB website (California Air Resources Board, 2014a). Echo Summit, Sacramento, and Placerville lack hourly values for 04:00 PST because their daily calibrations occur at that time. The Folsom site is missing approximately half of the hourly values for 03:00 PST for a similar reason.

### 2.3.3. Data from the Incline Village monitoring site

Hourly data for the ozone monitor operated at Incline Village (IVL) by the Air Quality Management Division of the Washoe County Health District were downloaded from the Air Quality System (AQS) Data Mart website maintained by the United States Environmental Protection Agency (EPA, 2014a).

Both Incline Village and the CARB sites are subjected to rigorous quality assurance (QA) protocols that adhere to EPA-mandated criteria. Annual data quality reports indicate that the hourly ozone data from these sites typically have an accuracy of  $\pm 2\%$ , and an approximate precision of  $\pm 3\%$  (California Air Resources Board, 2014a). Readers who are interested the specific QA procedures that are employed at these sites should consult the EPA and CARB web pages for further information.

Diurnal plots prepared from data sets that have a recurring gap at a specific time have been interpolated to fill in the missing data. In these cases the ozone concentration for the missing hour is set equal to the average of the values on either side.

### 2.4. Data from passive samplers

Ogawa passive samplers for O<sub>3</sub> (Koutrakis et al., 1993) were deployed for 2-week intervals throughout the 70-day sampling period. Samplers were hung on wooden stands 2.0 m above ground level, suspended beneath PVC plastic caps that provided protection from direct sunlight and rain. Each sampler contained two cellulose filters coated with a nitrite solution, which is oxidized by ozone to nitrate (Ogawa, 2014). The nitrite-coated filters were extracted in a lab and the extracts were analyzed quantitatively for nitrate using ion chromatography. The rate of NO<sub>3</sub> – formation (amount of NO<sub>3</sub> – formed on a filter divided by time of exposure) served as

a measure of average O<sub>3</sub> concentration. Whenever possible, the raw results from the passive samplers were compared to the real-time O<sub>3</sub> concentrations determined by the co-located portable ozone monitors. These comparisons yielded empirically derived calibration coefficients that were then averaged across multiple exposure periods to produce a single calibration coefficient for the entire season. The average calibration coefficient for the entire season was then applied to the raw passive sampler data to yield the 2-week average O<sub>3</sub> concentrations for each site and exposure period. The average calibration coefficients from 2002 and 2010 indicated excellent reproducibility, with magnitudes of 677.8 and 675.8, respectively (a difference of less than 0.3%). The average difference between the 2-week averages measured in 2010 by the passive samplers and those recorded by the portable O<sub>3</sub> monitors was 6.7% (or 3.4 ppb for an ambient ozone concentration of 50 ppb). The overall precision / reproducibility of the O<sub>3</sub> passive samplers, measured as the coefficient of variation (CV) of replicate samples, was 3%.

Volatile organic compounds (VOC) were collected using passive VOC Radiello samplers. Radiello diffusive samplers consist of stainless steel mesh cylinders (3x8 µm mesh, 4.8 mm diameter x 60 mm length) packed with Carbograph 4 (adsorbing cartridge code R145, used for all VOC except isoprene and 1,3-butadiene) and Carbopack X (cartridge code R141, used for isoprene and 1,3-butadiene). The cartridges were deployed in the diffusive sampling bodies according to the manufacturer's instructions (Radiello, 2014). After sample collection cartridges were analyzed by the thermal desorption-cryogenic pre-concentration method, followed by high resolution gas chromatographic separation and mass spectrometric detection (GC/MS) of individual compounds (Mason et al., 2011). Thirteen anthropogenic (1,3-butadiene, n-hexane, cyclohexane, n-octane, n-nonane, n-decane, n-undecane, benzene, toluene, ethylbenzene,

styrene, m/p-xylene, 1,2,4-trimethylbenzene) and two biogenic (isoprene and  $\alpha$ -pinene) VOC were monitored.

## 2.5. Spatial interpolations of data from passive samplers

Interpolated contour plots of ozone concentrations (Figures 5a and 5b) were prepared using the Geostatistical Analyst, an extension of the ArcGIS software (Environmental Systems Research Institute, Redlands, California, USA). Point data were converted into continuous interpolated surface values by application of the inverse distance weighted (IDW) method with 0.5 smoothing (Johnston et al., 2001). Interpolation parameters were selected so that the number of points included in the interpolation was limited to the five nearest values, all of which had to be within a range of 200 km. No adjustments were made to compensate for the presence of topographic features that can impede (or promote) the transport of O<sub>3</sub> across the interpolated surface.

## 2.6. Ozone exposure indices

Selected ozone exposure indices were calculated with the Ozone Calculator Program (Jackson, 2014) at the ten sites equipped with portable ozone monitors. The SUM00 index is an exposure dose obtained by multiplying all hourly concentrations (ppm) by a uniform time interval of one hour (h). Indices SUM06 and SUM07 indicate the integrated doses of all O<sub>3</sub> concentrations at or above 0.06 ppm and 0.07 ppm, respectively. The W126 index is a sigmoidally-weighted value (Lefohn and Runeckles, 1987) in which higher concentrations receive greater weighing. These four O<sub>3</sub> exposure indices were calculated for 24-hour periods using all available hourly data and then extrapolated (as discussed in section 2.2) to the 4-month

(120-day) interval of June through September. Among the calculated indices, SUM00, SUM06 and W126 are most commonly used in the United States for the evaluation of potential phytotoxic effects (Musselman et al., 2006). The SUM00 index has been successfully used for predicting O<sub>3</sub> phytotoxic effects on ponderosa and Jeffrey pines throughout California (Arbaugh et al., 1998). In addition to the values calculated for 24-hour periods, the W126 index was also determined for a 12-hour window between 8:00 and 20:00 PST for the 3-month (90-day) period of July – September. The use of a 12-hour W126 calculation, applied to the highest 3-month period of ozone during a given year, has been proposed as a secondary federal ozone standard that would focus upon ecological effects (Environmental Protection Agency, 2014b).

## 2.7. Meteorological analyses

Meteorological data were obtained through the National Weather Service's National Centers for Environmental Prediction (NCEP). NOAA's Air Resources Laboratory (ARL) routinely uses NCEP model data for air quality transport and dispersion modeling calculations (Air Resources Laboratory, 2014). Site-specific wind roses for the present study were calculated using archived wind data from the North American Mesoscale (NAM) 12 km meteorological model. The NAM 12 km model was chosen because it provided the best possible resolution and could be verified against the National Climatic Data Center (NCDC) observational cooperative data site, Tahoe Valley. The NAM model outputs data at three-hour intervals starting at 00:00 UTC. For the present analysis, the data are restricted to July 1st through September 23rd, 2010, which is approximately coincident with the July 14 – September 22 timeframe for the collection of ozone data. The daily data intervals correspond to three-hour increments, starting at 01:00 PST, with eight intervals within every 24-hour period.

## 2.8. HYSPLIT calculations

Regional-scale transport patterns responsible for bringing elevated ozone concentrations into the Lake Tahoe Basin were investigated by conducting back-trajectory calculations with the online version of the HYSPLIT model (Draxler and Rolph, 2014; Rolph 2014). Calculations were performed using the 40 km EDAS (Eta Data Assimilation System) archived meteorological data, with a run time of 30 hours, and arrival heights of 100, 500, and 1500 m above ground level.

## 3. Results and Discussion

### 3.1. Daily average ozone concentrations, summer 2010

Daily average ozone concentrations calculated from hourly data are presented in Figure 2. Figure 2a shows results from the 12 active monitors that operated at Lake Tahoe, while Figure 2b shows results from comparison sites in Sacramento (SAC), Folsom (FOL), and Placerville (PLA). Average ozone concentrations measured at most of the Tahoe sites are roughly similar to those recorded at Folsom and Placerville – in the range of 40-60 ppb – and higher than those recorded in downtown Sacramento (20-40 ppb). However, two of the high elevation Tahoe sites – Genoa Peak 9000 (GP9) and Angora Lookout (AGL) – frequently have higher ozone than the upwind comparison sites, especially for days 200-240. As discussed in section 3.9, this result likely reflects the predominance of regional transport at these two locations, which are also expected to experience diminished dry deposition due to steep topography and sparse vegetation. Figure 2 also indicates that the timing of the minima and maxima at the Lake Tahoe sites deviates from the timing observed at the comparison sites. For example, the local maximum occurring on days 204-205 for Sacramento, Folsom, and Placerville is not present in the Tahoe

data. The sharply resolved maximum from day 237 for the three comparison sites (Figure 2b) does not occur concurrently at the Tahoe sites (Figure 2a), but is instead diminished and delayed (to day 239).

The observation of generally similar average ozone values combined with poorly correlated temporal patterns in the daily averages is consistent with the previous work of Dolislager et al. (2012b), who found that intact 1- or 2-day transport of pollutants from upwind air basins to Lake Tahoe occurs very infrequently. Instead of direct transport of intact air masses, they concluded that emissions from upwind regions were acting to raise background concentrations of pollutants that were subsequently transported into the Tahoe Basin.

While most of the O<sub>3</sub> that is transported into the Tahoe Basin originates from the Central Valley of California, it is very likely that there are also contributions from Asian sources, and possible episodes of down-mixing of ozone-rich air from the upper troposphere / lower stratosphere. The importance of long distance transport of Asian O<sub>3</sub> (and/or ozone precursors) to western North America has been addressed in many prior studies, including Jaffe et al. (2003), Jaffe and Ray (2007), Macdonald et al. (2011), and Ambrose et al. (2011). In the latter report, measurements at the Mt. Bachelor Observatory (2763 m) in central Oregon identified a total of 25 high-ozone events (defined as 8-hour average O<sub>3</sub> > 70.0 ppb) between 2004 and 2009, all of which occurred between early March and late September. Of those 25 high-ozone events, 18 could be explicitly analyzed in terms of ozone sources, and it was found that subsidence of ozone-rich air from the upper troposphere / lower stratosphere played a role in 78% (14/18) of the high-ozone episodes, while long-range transport from Asia played a role in 56% (10/18) of those events (Ambrose et al., 2011). Compared to the well-exposed Mt. Bachelor, the Lake Tahoe sites utilized in the present study should experience fewer episodes of subsidence from the

upper troposphere / lower stratosphere because of their lower elevations and more sheltered topography. The Tahoe sites should also be less impacted by direct long-range transport from Asia because the Sierra Nevada crest located to the west of the Tahoe Basin will act as a barrier that inhibits westerly transport. Another key difference between the two locations is the presence of upwind emission source regions (San Francisco Bay Area, Sacramento, Central Valley) for Lake Tahoe, while Mt. Bachelor is largely unaffected by local anthropogenic emissions.

### 3.2. Exceedances of the 8-hour NAAQS and CAAQS

Figure 3 presents the daily maximum values for the 8-hour averages calculated from hourly ozone data. Presentation of the results in this format allows for direct comparisons with both the National Ambient Air Quality Standard (NAAQS) for ozone, which is currently 75 ppb (EPA, 2014c), and the California Ambient Air Quality Standard (CAAQS), which is currently 70 ppb (CARB, 2014b). Of the 12 Tahoe sites, only three exceeded the NAAQS for ozone: Genoa Peak 9000 (GP9), which had 6 days with exceedances; Angora Lookout (AGL), which had 4 days with exceedances; and Upper Incline (ICN), which had 1 day with an exceedance. Two of the three upwind comparison sites also exceeded the NAAQS: Folsom (FOL), which had 15 days with exceedances; and Placerville (PLA), which had 6 days with exceedances. If the CAAQS is used as the threshold, then four of the Tahoe sites show exceedances: Genoa Peak 9000 (16 days with exceedances), Angora Lookout (11 days), Upper Incline (2 days), and Watson Creek (WC), which had 1 day with an exceedance. All of the upwind comparison sites exceeded the CAAQS at least once: Folsom (18 days with exceedances), Placerville (16 days), and Sacramento (1 day).

The observation that Genoa Peak 9000 (GP9, the highest elevation Tahoe site) experienced essentially the same number of CAAQS exceedances as the most polluted

comparison site (Folsom, FOL) but significantly fewer violations of the NAAQS further supports the hypothesis that Tahoe exceedances primarily reflect elevated levels of background ozone rather than transport of intact air masses from source regions. Folsom is well-positioned – approximately 30 km downwind of downtown Sacramento – to see frequent NAAQS exceedances because the travel time from the upwind emission sources is sufficient to allow the required photochemistry to convert primary pollutants into ozone, but not so lengthy as to allow for significant dilution of the “Sacramento plume.” Genoa 9000, in contrast, lies roughly 150 km downwind of downtown Sacramento, so there is much greater likelihood that the plume will be diluted / dispersed before arriving. Compared to Folsom there are thus fewer violations of the 75 ppb NAAQS, but a similar number of violations of the 70 ppb CAAQS.

### 3.3. Diurnal cycles

Average diurnal cycles calculated from hourly data are presented for the 12 Lake Tahoe sites in Figure 4a, while the cycles for the comparison sites of Sacramento (SAC), Folsom (FOL), and Placerville (PLA) are presented in Figure 4b. The Tahoe sites display great site-to-site variability during the evening and pre-dawn hours of 19:00 to 07:00 PST, but consistent maxima of 50 to 55 ppb from 10:00 to 17:00 PST. Genoa Peak 9000 (GP9) and Angora Lookout (AGL) differ from other Tahoe sites because of their very small diurnal cycle magnitudes and the observation of increasing ozone between the hours of 17:00 to 20:00 PST. This latter result – an increase in O<sub>3</sub> despite the shutdown of photochemical production pathways – is seen only at these two locations. The comparison sites of Sacramento, Folsom, and Placerville also show great variability in their evening and pre-dawn behavior, but their afternoon maxima differ significantly from what is seen at the Tahoe sites. Rather than flat-topped maxima of 50-55 ppb

that commence by 10:00 PST and last for approximately eight hours, the diurnal maxima for the comparison sites do not arrive until approximately 14:00-16:00 (Sacramento, Folsom) or 16:00-17:00 (Placerville), and they last for only 1-3 hours, at values ranging from ~67 ppb (Folsom) to ~50 ppb (Sacramento).

#### 3.4. Spatial distributions of ozone from passive sampler data

Ozone distribution maps for the 2002 and 2010 seasons (Figures 5a and 5b, respectively, which present the average ozone concentrations listed in Tables 2 and 3) show the highest O<sub>3</sub> concentrations in the western portion of the monitoring domain, outside the Lake Tahoe Basin. These high O<sub>3</sub> levels reflect the closer proximity of the westernmost passive sampler sites to anthropogenic emissions of O<sub>3</sub> precursors from the Central Valley (which includes the greater Sacramento metropolitan area), and biogenic emissions from the Sierra Nevada foothills (Dillon et al., 2002; Dreyfus et al., 2002). Figures 5a and 5b strongly suggest that high elevation mountain ranges west of the Basin (especially those in the Desolation Wilderness) act as an effective barrier in preventing movement of those polluted air masses eastward into the Basin. However, there is also evidence of elevated O<sub>3</sub> concentrations at high elevation sites adjacent to the Lake, especially Genoa Peak 9000 (GP9), which saw average values of 60.2 ppb in 2002 and 59.2 ppb in 2010. Within the Tahoe Basin in 2010, the highest mean O<sub>3</sub> concentration (63.5 ppb) was observed at the NASA buoy site in the middle of the Lake (TB2). This result, which was markedly higher than the closest onshore result of 47.2 ppb for Thunderbird Lodge (THB), likely reflects diminished dry deposition to the surface of the Lake, a phenomenon that has been observed in prior studies of surface O<sub>3</sub> above large bodies of water (Goldberg et al., 2014; Stauffer et al., 2014; Cleary et al., 2012).

While generally similar O<sub>3</sub> distribution patterns occurred in 2002 and 2010, the 2010 levels of O<sub>3</sub> were significantly lower ( $p < 0.01$ ) than those measured in 2002 (Figure 6). The differences between the two years were caused primarily by differences in August and September, while the July data were similar in both years. These differences in measured O<sub>3</sub> do not appear to result from differences in meteorology, as the average monthly temperatures measured in 2002 (July = 18.1°C, August = 16.1°C, September = 13.6°C) are very similar to the average monthly temperatures measured in 2010 (July = 17.6°C, August = 16.1°C, September = 18.1°C). A direct comparison of average O<sub>3</sub> concentrations in 2002, 2006 and 2010 for three representative lakeshore sites yields 44.1, 42.2 and 39.8 ppb for 64 Acres (64A), 44.3, 43.2 and 37.0 ppb for Sugar Pine Point State Park (SPP), and 46.7, 46.5 and 43.3 ppb for Valhalla (VAL), respectively. All of these inter-annual comparisons are consistent with the previously reported decrease of ambient O<sub>3</sub> concentrations in the western US (Lefohn et al., 2008).

### 3.5. Passive sampler results for volatile organic compounds (VOC)

Tables 4 (sites with active ozone monitors) and 5 (sites without active ozone monitors) show the average 2010 concentration sums of thirteen anthropogenic VOC (1,3-butadiene, n-hexane, cyclohexane, n-octane, n-nonane, n-decane, n-undecane, benzene, toluene, ethylbenzene, styrene, m/p-xylene, 1,2,4-trimethylbenzene), two biogenic VOC (isoprene and  $\alpha$ -pinene), and their ratios (anthropogenic/biogenic, A/B). It is important to note that the absolute A/B ratios are not meaningful, since only limited numbers of anthropogenic species were measured (primarily those representative of fossil fuel combustion). Instead, the site-to-site variability of this ratio is more important. In general, biogenic species are more abundant than anthropogenic species ( $A/B < 1$ ) at all sites with the exception of TB2 Buoy (TB2), which is situated in the middle of the

Lake ( $A/B = 1.6$ ). This site also shows the highest average ozone concentration measured at any site in either 2002 or 2010. The observation of a higher A/B ratio at the TB2 site may indicate the influence of local spark ignition and diesel engine emissions (for example from large boats), and/or emissions from developed areas that are located near the shoreline, and/or the absence of biogenic VOC emissions from the Lake itself. Overall, with the exception of the TB2 site, higher A/B ratios are frequently observed for sites with main roadways nearby: TB2 Buoy > Desolation Wilderness (DW) > Tahoe Regional Park (TRP)  $\approx$  Upper Incline (ICN) > Valhalla (VAL).

### 3.6 Wind rose data

The daytime (07:00 to 16:00 PST) wind roses (Figure 7) show a dominant southwesterly flow. Lower Blackwood Creek (LBC) and Sugar Pine Point State Park (SPP) on the western side of the Lake have a stronger easterly component than the other sites. Genoa Peak 9000 (GP9) on the eastern side of the Lake has more of a westerly component than southwesterly, and also shows a small northwesterly component that is also observed at Angora Lookout (AGL) and Valhalla (VAL). The nighttime (19:00 to 04:00 PST) wind roses (Figure 8) show a dominant westerly component except for the southern sites of Angora Lookout and Valhalla, which show a more southwesterly component. Angora Lookout and Valhalla also show a small southeasterly component. The nighttime wind rose for Genoa Peak 9000 is very similar to the one obtained during daytime hours.

The wind rose data presented in Figures 7 and 8 suggest the presence of a “lake breeze” during daytime hours, and/or a “land breeze” during nighttime hours, at some of the Tahoe sites situated close to the shoreline. During periods of insolation the land surface is heated and its temperature increases, whereas the water surface remains at a relatively constant temperature due

to its very high heat capacity. The surface temperature influences the overlying air and as a result there is warmer and less dense air over land, while the air over the water is cooler and denser. Near the shoreline a pressure gradient is established due to the buoyant effects created by the temperature differences. Thus, if the prevailing conditions are such that the synoptic-scale wind is light, the local buoyant force is the dominant force and an on-shore lake breeze is established (Biggs and Graves, 1962). Lyons and Olsson (1973) showed that the lake breeze may favor the occurrence of high air pollution in shoreline areas. This is due to three factors: (1) formation of low-level temperature inversions as cool lake air moves inland, (2) continuous fumigation of elevated plumes from shoreline pollution sources, and (3) recirculation of pollutants within the lake breeze circulation pattern. All of these factors are a consequence of the unique features of the lake breeze temperature and wind structure. At night, the solar insolation of the land surface is diminished, and the air over the land becomes cooler and more dense relative to the air over the water. If the prevailing conditions are again such that the synoptic-scale wind is light, an off shore land breeze is established. Figure 7 indicates an easterly component of wind coming off the lake during daytime hours at Lower Blackwood Creek (LBC) and Sugar Pine Point State Park (SPP). Since both of these sites are located on the western side of the Lake and have eastern-facing exposures, these components likely correspond to on-shore lake breezes. This feature is less apparent, however, for the western-facing Thunderbird Lodge site (THB), which is located near the shoreline on the eastern side of the Lake. In this case the lake breeze would come from the west and would be obscured by the dominant westerly winds. The nighttime wind rose data (Figure 8) show a southeasterly component at Valhalla (VAL) that could indicate a nighttime land breeze. Lower Blackwood Creek and Sugar Pine Point State Park might also be experiencing a nighttime land breeze, but once again the wind rose evidence is obscured by the

dominant westerly wind flow. Thunderbird Lodge does not show a nighttime land breeze; in this case the elevated nocturnal ozone concentrations (Figure 4a) may instead suggest onshore transport of ozone during evening hours – a possibility that is consistent with the elevated ozone concentrations measured by passive samplers at the TB2 buoy (section 3.4, Table 2, Figure 5b).

It should be emphasized that the wind rose results shown in Figures 7 and 8 – which are based upon calculations that have limited spatial and temporal resolution – are not intended to rigorously reproduce the meso-scale circulation patterns that are actually present within the Lake Tahoe Basin. Instead, these results are intended to serve as a stand-in for the lack of *in situ* wind data from the sampling sites and provide potential insight into the differences / distinctions that might exist between the different sampling locations. Because of the limited resolution of the input data, the wind rose patterns in Figures 7 and 8 tend to be dominated by the synoptic-scale winds coming from the west and southwest, with an underestimation of the meso-scale lake breeze and land breeze contributions. (This underestimation of local onshore and offshore flows will likely be a bigger problem for those sites that are close to the shoreline and less of an issue for the higher elevation sites that are further away from the Lake.) While this underestimation of meso-scale behavior diminishes the accuracy and usefulness of the wind rose results, the resolution of the calculation nonetheless appears to be good enough to identify the sites (LBC, SPP) that are more likely to experience sustained onshore or offshore flows. Readers who are interested in a rigorous review of the meso-scale wind patterns that have been measured within the Lake Tahoe Basin – at sites (mostly along the shoreline) that differ from those used in the current study – are encouraged to consult Pederson (2005) and VanCuren et al. (2012).

### 3.7 HYSPLIT back-trajectories

In order to assess the effects of synoptic-scale atmospheric transport, 30-hour air mass back trajectories were performed with the HYSPLIT model (Draxler and Rolph, 2014; Rolph 2014). August 21 (day-of-year = 233 in Figure 3a) was chosen as the representative high-ozone day (Figure 9), while August 29 (day-of-year = 241 in Figure 3a) was chosen as the representative low-ozone day (Figure 10). Angora Lookout (AGL) was selected as the arrival site because it had the highest ozone value for the high-ozone day. Trajectories were calculated for 100, 500, and 1500 m above ground level; the 100-meter height (red triangles) approximates the lower part of the boundary layer and should experience many interactions with the surface, while the 1500- meter height trajectory (green circles) approximates the top of the boundary layer. While Figures 9 and 10 indicate very similar trajectories at the 100-meter and 500-meter heights – originating over the Pacific Ocean to the west of Marin County, and then proceeding through the San Francisco Bay and Delta region and the Central Valley before ascending the western slope of the Sierra Nevada – they indicate very dissimilar trajectories at 1500 m above ground level. The high-ozone trajectory passes through the heavily polluted San Joaquin Valley (located to the southwest of the Tahoe Basin) whereas the low-ozone trajectory approaches from the north, passing through the less polluted Lassen National Forest.

### 3.8. Factors that influence surface level ozone concentrations

Table 3 and Figure 4a summarize the 2010 results from the 12 Tahoe sites equipped with active ozone monitors. These results indicate that the average ozone concentration measured at any given site depends primarily on the ozone mixing ratios observed during the evening and predawn hours, rather than the mixing ratios measured during the hours of 10:00 to 17:00 PST. The observation that all of the Tahoe sites tend to rapidly reach the same middle of day

maximum (of roughly 50 to 55 ppb) between the hours of 06:00 and 10:00 PST suggests that this initial rise in surface ozone is due primarily to the vigorous vertical mixing that occurs in the hours immediately after sunrise, when ozone-depleted air near the surface is warmed (via solar heating of the surface) while cooler, ozone-rich air from aloft is simultaneously mixed downwards. These well-mixed conditions persist throughout the Tahoe Basin until approximately 17:00 PST, when there is marked decrease in solar insolation. During the evening hours, those sites that have good exposure to ozone-rich air from aloft, which is being transported in via regional-scale and long-range transport, continue to exhibit high ozone concentrations. Sites that are more conducive to the formation of nocturnal temperature inversions see a decrease in surface level ozone, primarily via dry deposition.

The extent to which a given site experiences elevated or diminished ozone concentrations during the evening and pre-dawn hours appears to depend on a combination of factors that include elevation, topography, and ground cover. Local emissions of NO can also play a role, as NO is known to “titrate” ozone very efficiently at night (Sillman, 1999). However, NO data collected in July 2012 with active monitors (Burley, 2014) indicate that ambient NO concentrations within the Tahoe Basin are typically  $\leq 3$  ppb, even at sites that are located near major roadways. Since nocturnal titration of ozone by NO is a stoichiometric (as opposed to catalytic) process where 1 ppb of freshly emitted NO can destroy no more than an equivalent 1 ppb of O<sub>3</sub>, the observation of low NO mixing ratios would seem to limit the overall contribution of NO titration to the diurnal cycle differences seen in Figure 4a.

### 3.9. Site-by-site analysis of 2010 data from active ozone monitors

#### 3.9.1. Genoa Peak 9000, Angora Lookout

Genoa Peak 9000 (GP9, 2734 m) and Angora Lookout (AGL, 2218 m) see high levels of nocturnal ozone, typically around 60 ppb for 20:00 to 00:00 PST, followed by a gradual decrease in the early morning hours (Figure 4a). For these two sites, the well-mixed hours of 10:00 – 17:00 PST therefore represent a broad minimum (Genoa Peak 9000), or an intermediate plateau (Angora Lookout), rather than a mid-day maximum in O<sub>3</sub>. The efficient vertical mixing that takes place during this period decreases ozone at these two sites because of vigorous upward mixing of ozone-depleted air from lower elevations. At night, the effective mixing with lower elevations – which can be viewed in this context as an ozone “sink” – is shut off, while access to ozone-rich air from aloft continues.

Genoa Peak 9000 (GP9) and Angora Lookout (AGL) both possess features that will tend to promote mixing from aloft while simultaneously minimizing dry deposition of ozone during evening hours. These include high elevation, steeply sloped topography that will inhibit the formation of stable temperature inversions during evening hours, and dry / rocky ground cover that will be a relatively inefficient ozone sink (compared to wet, leafy green plant matter). While Angora Lookout is situated at a lower elevation than Genoa Peak 9000, it is also closer to the upwind pollution source regions of Sacramento and the Central Valley, and positioned along a main conduit – the south-southwest corner of the Basin, near Fallen Leaf Lake and the U.S. highway #50 corridor – for surface-level regional transport. It is possible that the positioning of the Angora Lookout site, coupled with observed shift in wind patterns – from a more westerly flow during the daytime (Figure 7) to a more southwesterly flow at night (Figure 8) – may contribute to the observed increase in nocturnal ozone at Angora Lookout. Shifting wind patterns do not, in contrast, appear to play a role at Genoa Peak 9000, as the daytime and nighttime wind roses are very similar to one another.

It should be emphasized that these two sites experience average ozone concentrations (57.3 ppb for GP9 and 55.1 ppb for AGL, Table 3) that are substantially higher than concurrent values measured at the polluted urban / suburban comparison sites of Sacramento (SAC, 27.5 ppb), Folsom (FOL, 41.4 ppb), and Placerville (PLA, 51.8 ppb). This result suggests nocturnal exposure to ozone-rich air from the “polluted background” of the free troposphere – rather than close proximity to emission or primary pollutants – is the most important factor in determining the average overall ozone exposure. This assessment agrees with the prior analysis from Van Ooy and Carroll (1994), who investigated the spatial variability of ozone climatology at six remote sites along the western slope of the Sierra Nevada. They concluded that local topographical characteristics and their effect on local three-dimensional transport of polluted air had a much greater impact on the diurnal ozone signature at a given site than the “remoteness” of the site from pollution source regions.

### 3.9.2. Upper Incline, Thunderbird Lodge, Echo Summit

Upper Incline (ICN), Thunderbird Lodge (THB), and Echo Summit (ECHO) all yield average ozone concentrations around 50 ppb, with small diurnal cycle magnitudes and elevated nighttime ozone concentrations in the range of 40-50 ppb (Table 3, Figure 4a). While this outcome is not surprising for Upper Incline (2536 m, on a steep hillside with excellent exposure) or Echo Summit (2250 m, positioned in closer proximity to the emission sources located to the southwest of the Tahoe Basin), it is somewhat unexpected for Thunderbird Lodge, which lies at a much lower elevation (1915 m) near the Lake Tahoe shoreline. The observation of elevated levels of nocturnal ozone at the Thunderbird location may reflect (i) the steep topography of the sampling site, which prevents the formation of a stable nocturnal boundary layer; and (ii) an

efficient on shore flow of ozone-rich air during evening hours (Figure 8, section 3.6). At Echo Summit, the relatively large difference between the average value measured in 2010 by the CARB monitoring station (47.4 ppb) and the concurrent value obtained by passive samplers (56.1 ppb) likely reflects the different locations of the two measurements. In this case the CARB monitor was located in a parking lot just off of U.S. highway #50, while the passive samplers were further removed from the highway by an additional 100 m or so, and positioned on top of a heavily forested hill. While both locations had good access to the open sky, the lower elevation and closer exposure to fresh NO emissions likely reduced the O<sub>3</sub> concentrations measured by the CARB monitor compared to those recorded by the passive samplers. Since in this instance the active monitor and the passive samplers were not co-located, the CARB data from Echo Summit were not used to calibrate the passive samplers.

### 3.9.3. Incline Village, Genoa Peak 8000, Genoa Peak 7000

Incline Village (IVL), Genoa Peak 8000 (GP8), and Genoa Peak 7000 (GP7) all display somewhat lower ozone concentrations compared to the sites discussed above, with average mixing ratios in the range of 40-45 ppb (Table 3) and larger diurnal cycle magnitudes (Figure 4a). All three of these sites possess gently sloping topography that is more amenable to the formation of nocturnal temperature inversions. The observation that Genoa Peak 8000 has higher average ozone and a smaller diurnal cycle magnitude than Genoa Peak 7000 reflects its higher elevation (2443 vs. 2232 m) and drier surface cover (ash and dirt vs. thick grass), which will reduce the likelihood of dry deposition during evening hours. The residential / commercial Incline Village site shows a pronounced diurnal minimum at 06:00 PST, which, is probably the

result of enhanced NO titration of ozone during the morning commute. This feature is not present at the Genoa Peak sites, consistent with their more remote locations.

#### 3.9.4. Valhalla, Watson Creek, Sugar Pine Point State Park, Lower Blackwood Creek

Valhalla (VAL), Watson Creek (WC), Sugar Pine Point State Park (SPP), and Lower Blackwood Creek (LBC) have average ozone concentrations below 40 ppb, and display very large diurnal cycle magnitudes – in the range of 25 to 40 ppb. The key factor for these locations is the flat terrain, which supports the formation of stable temperature inversions during the evening hours. While the flat topography is the dominant feature for these sites, other factors are also evident. Valhalla (VAL) is positioned along California state highway #89, which may provide slightly increased photochemical production of ozone during the afternoon hours and enhanced NO titration during the morning commute. Like Angora Lookout (AGL) and Echo Summit (ECHO), it is also closer to the main access point for regional transport of polluted air (generally from the southwest) into the Lake Tahoe Basin, which will increase observed ozone. Watson Creek (WC), in contrast, is a much more remote site, approximately 350 m higher in elevation, with very low average NO (Table 4). While the higher elevation and lack of NO will generally tend to favor higher ozone concentrations during evening hours, the flat terrain nonetheless predominates (with a likely assist from the leafy green ground cover), and the resulting diurnal cycle is very similar to what is observed at the lower, more heavily polluted Valhalla site.

The two remaining sites, Sugar Pine Point State Park (SPP) and Lower Blackwood Creek (LBC), yielded the largest diurnal cycle magnitudes and lowest average ozone values of the 12 Tahoe sampling locations. This outcome reflects their low elevation, flat terrain, and leafy green

ground cover that can enhance dry deposition of ozone during nighttime hours. The ground cover at the Lower Blackwood Creek site was grassy and very damp – characteristics that have been previously observed to correlate with large magnitude diurnal cycles and low average ozone at Tuolumne Meadows in Yosemite National Park (Burley and Ray, 2007) and the visitor center meadow at Devils Postpile National Monument (Bytnerowicz et al., 2013). These two sites may also experience mild enhancements in daytime ozone due to the presence of an on shore lake breeze, as discussed above in section 3.6.

### 3.10. Potential phytotoxic effects

Table 6 lists the exposure ozone indices that were calculated according to the methodology described in section 2.5. The SUM00 values range from 96.1 ppm h (Lower Blackwood Creek) to 161.9 ppm h (Genoa Peak 9000). The SUM06 values range from 6.8 ppm h (Genoa Peak 7000) to 69.3 ppm h (Genoa Peak 9000). The SUM07 values range from zero at Genoa Peak 7000 to 15.1 ppm h at Genoa Peak 9000. The 24-hour, 4-month W126 values range from 10.8 ppm h (Lower Blackwood Creek) to 46.6 ppm h (Genoa Peak 9000). The 12-hour, 3-month W126 values range from 6.8 ppm h (Genoa Peak 7000) to 14.5 ppm h (Genoa Peak 9000).

The magnitudes of the SUM00 values for the Lake Tahoe sites are lower than those determined for a San Joaquin River transect across the southern Sierra Nevada in 2002 (148 – 192 ppm h; Cisneros et al., 2010), but somewhat above the values determined in 2007 and 2008 (110 and 98 ppm h, respectively) at the Devils Postpile National Monument (Bytnerowicz et al., 2013). In general, the present results for SUM00 are roughly similar to the values of 90 – 160 ppm h recorded in the San Bernardino Mountains of southern California in 2006 (Bytnerowicz et al., 2008). From this perspective, Angora Lookout and Genoa Peak 9000 can be viewed as sites

that experience a high phytotoxic potential while the other Tahoe locations are more comparable to the low pollution sites in the San Bernardino Mountains or at the Devils Postpile National Monument. However, when the SUM00 calculation is replaced by SUM06 or W126, the results for Angora Lookout and Genoa Peak 9000 (SUM06 values of 50.1 and 69.3 ppm h; W126 values of 37.8 and 46.6 ppm h, respectively) indicate that even these two most polluted Tahoe Basin sites have much lower phytotoxic indices than the western slope of the southern Sierra Nevada Mountains (SUM06 values of 140 – 150 ppm h and W126 values of 110 – 125 ppm h, respectively; Cisneros et al., 2010) or the sites in the San Bernardino Mountains that are most severely impacted by Los Angeles smog (SUM06 values of 85 – 105 ppm h and W126 values of 65 – 85 ppm h, respectively; Bytnerowicz et al., 2008). If Angora Lookout and Genoa Peak 9000 are excluded, then the remaining sites in the Tahoe Basin have SUM06 and W126 indices that are similar to the low values determined for Devils Postpile National Monument (SUM06 values of 29 and 23 ppm h; W126 values of 21 and 19 ppm h, in 2007 and 2008, respectively; Bytnerowicz et al., 2013).

The hypothesis that Angora Lookout and Genoa Peak 9000 are more likely to experience phytotoxic impacts is also supported by the 12-hour (daytime) W126 results calculated over the 90-day interval of July through September, which show both Genoa Peak 9000 (14.5 ppm h) and Angora Lookout (13.3 ppm h) to be above the 13 ppm h threshold associated with phytotoxic damage. Since the present results for the 12-hour W126 calculation correspond to the months of July-August-September, with data unavailable for other possible intervals (e.g., May-June-July, June-July-August), the 12-hour W126 values reported here probably underestimate the values that would have been obtained if the calculation had been applied to the highest 3-month period for the entire year. The restriction of the 12-hour W126 calculation to daytime data is also likely

to produce an underestimation of the overall ozone exposure at these two particular sites because both Angora Lookout and Genoa Peak 9000 frequently see higher ozone values during at night, with lower values during daytime hours (Figure 4a).

#### **4. Conclusions**

Data from passive samplers and active monitors indicate that the Lake Tahoe Basin experiences elevated concentrations of surface-level ozone. Different locations within the Basin generally experience similar mid-day maxima of ~ 50 to 55 ppb, which suggests that the Basin is well mixed during daytime hours. During the night there are large site-to-site variations in observed ozone; higher elevation sites that possess steeply sloped topography and maintain good exposure to “polluted background” air from the free troposphere experience high ozone concentrations, while lower elevation sites with flat topography experience much lower nocturnal ozone concentrations. Because of their good exposure to nocturnal ozone, many of the higher elevation Tahoe locations experience average ozone concentrations that exceed those measured in heavily polluted upwind source regions (Sacramento, Folsom, Placerville). The observation of high average ozone on a NASA research buoy in the middle of the Lake likely reflects diminished dry deposition to the surface of the Lake, a phenomenon that has been observed in prior studies of surface O<sub>3</sub> above large bodies of water. Wind rose analyses of archived NAM 12 km meteorological data for the summer of 2010 suggest that some of the sampling sites situated near the shoreline may have experienced on-shore “lake breezes” during daytime hours and/or off shore “land breezes” during the night. Back-trajectory analysis with the HYSPLIT model suggests that much of the ozone measured at Lake Tahoe results from the transport of “polluted background” air into the Basin from upwind pollution source regions (e.g., Sacramento, San Joaquin Valley). Given the high elevation of the Tahoe Basin, it is likely that

this “polluted background” also included ozone transported from Asia. Ozone exposure indices indicate that the two most polluted sites (the highest Genoa Peak site, and Angora Lookout) sampled by portable ozone monitors during the summer of 2010 likely experienced some phytotoxic impacts, while the other Tahoe Basin locations experienced lower ozone exposures.

### Acknowledgements

This study was supported in part by a grant from the USDA Forest Service through the Tahoe Science Program funded by the Southern Nevada Public Lands Management Act (SNPLMA). The authors wish to thank: Katy Orr for overseeing the data downloads and in-field calibrations of the portable ozone monitors during the summer of 2010; Joey Keely, Chris Engelhardt, Paul McCulloch and Shana Gross of the USDA Forest Service Lake Tahoe Basin Management Unit for logistical help and data collection; Andrew Strain and Casey Blann of Heavenly Mountain Skiing Operations, Dennis Malone of Thunderbird Lodge, and Jack Coughlin of Diamond Peak Skiing Operations for assisting with the selection of the sampling sites; Brant C. Allen of the UC–Davis Environmental Research Center and Chris Ross of the USDA Forest Service PSW Research Station for help with the installations; and Jonathan Long and Tiffany Van Huysen of the USDA Forest Service PSW Research Station for administrative support. A special thanks is also extended to our scientific collaborators: Suraj Ahuja, Ricardo Cisneros, Glen Shaw, Don Schweizer, and Trent Procter of the US Forest Service Region 5; Leora Nanus of San Francisco State University; Mark McDaniel of Desert Research Institute; James Sickman and Michael Bell of University of California; and Miriam Rorig of USDA Forest Service PNW Research Station. Thanks also to Nyssa Perryman for her help and support. Finally, the authors gratefully acknowledge the NOAA Air Resources Laboratory (ARL) for the

provision of the HYSPLIT transport and dispersion model and/or READY website (<http://www.ready.noaa.gov>) used in this publication.

## References

- Air Resources Laboratory. 2014. Ready Archived Meteorology. <<http://www.arl.noaa.gov/>>
- Ambrose, J. L., Reidmiller, D. R., Jaffe, D. A., 2011. Causes of high O<sub>3</sub> in the lower free troposphere over the Pacific Northwest as observed at the Mt. Bachelor Observatory. *Atmospheric Environment* 45, 5302-5315.
- Arbaugh, M. J., Miller, P. R., Carroll, J. J., Takemoto, B. K., Procter, T. M., 1998. Relationship of ozone exposure to pine injury in the Sierra Nevada and San Bernardino Mountains of California. *Environmental Pollution* 101, 291-301.
- Biggs, W. G., Graves, M. E., 1962. A Lake Breeze Index. *Journal of Applied Meteorology* 1,474-480.
- Burley, J. D., Ray, J. D., 2007. Surface ozone in Yosemite National Park. *Atmospheric Environment* 41, 6048-6062.
- Burley, J. D., Bytnerowicz, A., 2011. Surface ozone in the White Mountains of California. *Atmospheric Environment* 45, 4591-4602.
- Burley, J. D., 2014. Unpublished results.
- Bytnerowicz, A., Arbaugh, M., and Padgett, P. 2004. Evaluation of ozone and HNO<sub>3</sub> vapor distribution and ozone effects on conifer forests in the Lake Tahoe Basin and eastern Sierra Nevada. Final Report to California Air Resources Board, Contract No. 01-334, USDA Forest Service, Pacific Southwest Research Station.
- Bytnerowicz, A., Arbaugh, M., Schilling, S., Fraczek, W., Alexander, D., 2008. Ozone

- distribution and phytotoxic potential in mixed conifer forests of the San Bernardino Mountains, southern California. *Environmental Pollution* 155, 398-408.
- Bytnerowicz, A., Burley, J. D., Cisneros, R., Preisler, H. K., Schilling, S., Schweizer, D., Ray, J., Dulen, D., Beck, C., Auble, B., 2013. Surface ozone at the Devils Postpile National Monument receptor site during low and high wildland fire years. *Atmospheric Environment* 65, 129-141.
- California Air Resources Board, 2014a. <<http://www.arb.ca.gov/html/ds.htm>>
- California Air Resources Board, 2014b. <<http://www.arb.ca.gov/research/aaqs/caaqs/ozone/ozone.htm>>
- Carroll, J. J., Dixon, A. J., 2002. Regional scale transport over complex terrain, a case study: Tracing the Sacramento plume in the Sierra Nevada of California. *Atmospheric Environment* 36, 23-58.
- Carslaw, D. C., 2012. The OPENAIR Project in R. <<http://www.openair-project.org>>
- Cisneros, R., Bytnerowicz, A., Schweizer, D., Zhong, S., Traina, S., Bennett, D. H., 2010. Ozone, nitric acid, and ammonia air pollution is unhealthy for people and ecosystems in southern Sierra Nevada, California. *Environmental Pollution* 158, 3261-3271.
- Cleary, P. A., Fuhrman, N., Schulz, L., Schafer, J., Fillingham, J., Bootsma, H., Langel, T., Williams, E. J., Brown, S. S., 2014. Ozone distributions over southern Lake Michigan: comparisons between ferry-based observations, shoreline-based DOAS observations and air quality forecast models. *Atmospheric Chemistry and Physics Discussions* 14, 23201-23236.
- Dillon, M.B., Lamanna, M.S., Schade, G.W., Goldstein, A.H., Cohen, R.C., 2002. Chemical evolution of the Sacramento urban plume: Transport and oxidation.

- Journal of Geophysical Research **107** (D5), 4045-4059.
- Dolislager, L. J., VanCuren, R., Pederson, J. R., Lashgari, A., McCauley, E., 2012a. A summary of the Lake Tahoe Atmospheric Deposition Study (LTADS). *Atmospheric Environment* **46**, 618-630.
- Dolislager, L. J., VanCuren, R., Pederson, J. R., Lashgari, A., McCauley, E., 2012b. An assessment of ozone concentrations within and near the Lake Tahoe Air Basin. *Atmospheric Environment* **46**, 645-654.
- Draxler, R.R., Rolph, G.D., 2014. HYSPLIT (HYbrid Single-Particle Lagrangian Integrated Trajectory) Model access via NOAA ARL READY Website. NOAA Air Resources Laboratory, College Park, Maryland, U.S.A.  
<<http://www.arl.noaa.gov/HYSPLIT.php>>
- Dreyfus, G.B., Schade, G.W., Goldstein, A.H., 2002. Observational constraints on the contribution of isoprene oxidation to ozone production on the western slope of the Sierra Nevada, California. *Journal of Geophysical Research* **107** (D19), 4365-4381.
- Environmental Protection Agency, 2014a. <<http://www.epa.gov/ttn/airs/aqsdatamart/>>
- Environmental Protection Agency, 2014b. <[http://www.epa.gov/ttnecas1/regdata/RIAs/s4-supplemental\\_analysis-secondary\\_standard11-5-09.pdf](http://www.epa.gov/ttnecas1/regdata/RIAs/s4-supplemental_analysis-secondary_standard11-5-09.pdf)>
- Environmental Protection Agency, 2014c. <<http://www.epa.gov/air/criteria.html>>
- Fraczek W, Bytnerowicz A, Arbaugh MJ. Bytnerowicz A, Arbaugh MJ, Alonso R, 2003. Use of geostatistics to estimate surface ozone patterns. *Ozone Air Pollution in the Sierra Nevada: Distribution and Effects on Forests, Developments in Environmental Science 2*. Amsterdam: Elsevier, pp. 215-247.
- Gertler, A. W., Bytnerowicz, A., Cahill, T. A., Arbaugh, M., Cliff, S., Kahyaoglu-Koracin, J.,

- Tarnay, L., Alonso, R., Fraczek, W., 2006. Local air pollutants threaten Lake Tahoe's clarity. *California Agriculture* 60 (2), 53-58.
- Goldberg, D. L., Loughner, C. P., Tzortziou, M., Stehr, J. W., Pickering, K. E., Marufu, L.T., Dickerson, R. R., 2014. Higher surface ozone concentrations over the Chesapeake Bay than over the adjacent land: Observations and models from the DISCOVER-AQ and CBODAQ campaigns. *Atmospheric Environment* 84, 9-19.
- Jackson, William, 2014. <<http://webcam.srs.fs.fed.us/>>
- Jaffe, D., Price, H., Parrish, D., Goldstein, A., Harris, J., 2003. Increasing background ozone during spring on the west coast of North America. *Geophysical Research Letters* 30 (12), Article Number 1613.
- Jaffe, D., Ray, J., 2007. Increase in surface ozone at rural sites in the western U.S. *Atmospheric Environment* 41, 5452-5463.
- Johnston, K., Ver Hoefk, J., Krivoruchko, K., Lucas, N. 2001. Using ArcGIS Geostatistical Analyst. Environmental Systems Research Institute, Redlands, California.
- Koutrakis, P., Wolsfson, J.M., Bunyaviroch, A., Froelich, S.E., Hirano, K., Mulik, J.D. 1993. Measurement of ambient ozone using a nitrite-saturated filter. *Analytical Chemistry* 65, 210-214.
- Krupa, S. V., Tonneijck, A. E. G., Manning, W. J., Flagler, R. B., 1998. Ozone. Recognition of air pollution injury to vegetation. *Air and Waste Management Assoc.* (2), 1-28.
- Lefohn, A. S., Runeckles, V. C., 1987. Establishing a standard to protect vegetation – ozone exposure / dose considerations. *Atmospheric Environment* 21, 561-568.
- Lefohn, A. S., Shadwick, D., Oltmans, S. J., 2008. Characterizing long-term changes in surface ozone levels in the United States (1980-2005). *Atmospheric Environment* 42, 8252-8262.

- Lyons, W. A., Olsson, L. E., 1973. Detailed mesometeorological studies of air pollution dispersion in the Chicago lake breeze. *Monthly Weather Review* 101, 387-403.
- Macdonald, A. M., Anlauf, K. G., Leitch, W. R., Chan, E., 2011. Interannual variability of ozone and carbon monoxide at the Whistler high elevation site: 2002-2006. *Atmospheric Chemistry and Physics Discussions* 11, 17621-17664.
- Mason, J. B., Fujita, E. M., Campbell, D. E., Zielinska, B., 2011. Evaluation of Passive Samplers for Assessment of Community Exposure to Toxic Air Contaminants and Related Pollutants. *Environmental Science and Technology* 45, 2243-2249.
- Miller, P. R., Guthrey, R., Schilling, S., Carroll, J., 1996. Ozone injury responses of ponderosa and Jeffrey pine in the Sierra Nevada and San Bernardino mountains in California. *Proceedings of the International Symposium on Air Pollution and Climate Change Effects on Forest Ecosystems*. USDA Forest Service, General Technical Report PSW-GTR-166, pp. 35-42.
- Musselman, R. C., Lefohn, A. S., Massman, W. J., Health, R. L., 2006. A critical review and analysis of the use of exposure- and flux-based ozone indices for predicting vegetation effects. *Atmospheric Environment* 40, 1869-1888.
- Ogawa, 2014. <<http://www.ogawausa.com/passive-sampler.php>>
- Pedersen, B. S., Olson, R. K., Lefohn, A. S., 1989. Ozone injury to Jeffrey and ponderosa pines surrounding Lake Tahoe, California and Nevada. *Effects of Air Pollution on Western Forests*. Air and Waste Management Association, Transactions Series Number 16, pp. 279-92.
- Pederson, J., 2005. *Meteorology of Lake Tahoe Basin*.  
<<http://www.arb.ca.gov/research/ltads/ltads-ws/2-tahoe-met.pdf>>

Radiello, 2014. <<http://www.radiello.com>>

Rolph, G.D., 2014. Real-time Environmental Applications and Display sYstem

(READY) Website. NOAA Air Resources Laboratory, College Park, Maryland, U.S.A.

<<http://www.ready.noaa.gov>>

Sillman, S., 1999. The relation between ozone, NO<sub>x</sub> and hydrocarbons in urban and polluted rural environments. *Atmospheric Environment* 33, 1821-1845.

Stauffer, R. M., Thompson, A. M., Martins, D. K., Clark, R. D., Goldberg, D. L., Loughner, C.

P., Delgado, R., Dickerson, R. R., Stehr, J. W., Tzortziou, M. A., 2012. Bay breeze influence on surface ozone at Edgewood, MD during July 2011. *Journal of Atmospheric Chemistry*. doi: 10.1007/s10874-012-9241-6.

Tahoe Environmental Research Center, 2014. <<http://tahoe.ucdavis.edu>>

United States Geological Survey, 2014. <<http://tahoe.usgs.gov/facts.html>>

VanCuren, R., Pederson, J., Lashgari, A., Dolislager, L., McCauley, E., 2012. Aerosol generation and circulation in the shore zone of a Large Alpine lake – 2 – Aerosol distributions over Lake Tahoe, CA. *Atmospheric Environment* 46, 631-644.

Van Ooy, D. J., Carroll, J. J., 1994. The spatial variation of ozone climatology on the western slope of the Sierra Nevada. *Atmospheric Environment* 29, 1319-1330.

Zhang, Q., Carroll, J. J., Dixon, A. J., Anastasio, C., 2002. Aircraft Measurements of Nitrogen and Phosphorus in and around the Lake Tahoe Basin: Implications for Possible Sources of Atmospheric Pollutants to Lake Tahoe, *Environmental Science & Technology* 36, 4981-4989.

### Figure Captions

Figure 1. Map of the sampling sites utilized in this study. Corresponding latitude / longitude / elevation data for each sampling site are presented in Tables 1 and 2.

Figure 2. Daily average ozone concentrations (ppb) measured by active monitors, 15 July to 21 September, 2010: (a) Tahoe sites; (b) Sacramento, Folsom, and Placerville.

Figure 3. Daily maxima of the 8-hour average ozone concentrations (ppb) measured by active monitors, 15 July to 21 September, 2010: (a) Tahoe sites; (b) Sacramento, Folsom, and Placerville.

Figure 4. Average diurnal cycles of observed ozone (ppb), based on data collected from 12:00 PST on July 14 through 11:00 PST on September 22, 2010: (a) Tahoe sites; (b) Sacramento, Folsom, and Placerville.

Figure 5. Spatial distributions of O<sub>3</sub> concentrations in and around the Lake Tahoe Basin, based on the passive sampler data presented in Tables 2 and 3: (a) 2002 summer seasonal averages for July 16 – September 24; (b) 2010 seasonal summer averages for July 14 – September 22. Individual site concentrations are specified using the colored circles shown in the upper part of the legend, while interpolated concentrations are expressed using a different color scheme shown by colored rectangles in the lower part of the legend.

Figure 6. Box-plots of the passive sampler ozone data for 2002 (July 16 – September 24) and 2010 (July 14 – September 22), combining data from all of the sampling sites. The overall summer seasonal median is represented by the thick horizontal bar, while the quartiles (25th & 75th percentiles) are denoted by the extremities of the box) and the ranges are denoted by the extremities of the whiskers. There is a significant difference in the mean O<sub>3</sub> values between 2002 and 2010. The 2010 values are, on average, 5.6 ppb less than the average in 2002 ( $P$ -value = 0.00016). At the 95% confidence level the difference between 2002 and 2010 varies between 3.6 and 7.6 ppb.

Figure 7. Daytime wind roses for six Tahoe Basin sites equipped with portable ozone monitors. Results are based upon data for 07:00, 10:00, 13:00 and 16:00 PST, calculated from 12 km NAM data for July 1 – September 23, 2010.

Figure 8. Nighttime wind roses for six Tahoe Basin sites equipped with portable ozone monitors. Results are based upon data for 19:00, 22:00, 01:00 and 04:00 PST, calculated from 12 km NAM data for July 1 – September 23, 2010.

Figure 9. Air mass back-trajectories at 100, 500, and 1500 meters above ground level for the high-ozone day of August 21, 2010. The arrival time at the Angora Lookout site (AGL) is 16:00 PST (00:00 next day UTC).

Figure 10. Air mass back-trajectories at 100, 500, and 1500 meters above ground level for the low-ozone day of August 29, 2010. The arrival time at the Angora Lookout site (AGL) is 16:00 PST (00:00 next day UTC).

**Table 1. Sampling locations equipped with both active monitors and passive samplers**

Location	Code	Latitude (degrees)	Longitude (degrees)	Elevation (masl)	Site Description
Angora Lookout	AGL	38.8817	-120.0548	2218	Steep hillside near top of ridge; extensive fire damage
Echo Summit (CARB site)	ECHO	38.8116	-120.0331	2250	Flat clearing / parking lot along U.S. Hwy. 50
Folsom* (CARB site)	FOL	38.6833	-121.1644	108	Suburban location near green open space
Genoa Peak 7000	GP7	39.0789	-119.9091	2232	Small clearing on mild slope; thick grass
Genoa Peak 8000	GP8	39.0504	-119.9072	2449	Open clearing on moderate slope; heavy fire damage
Genoa Peak 9000	GP9	39.0438	-119.8834	2734	Rocky outcropping near summit; excellent exposure
Incline Village* (SLAMS site)	IVL	39.2504	-119.9567	1957	Rooftop in residential/commercial neighborhood
Lower Blackwood Creek	LBC	39.1098	-120.1901	1948	Flat open meadow with wet grass
Placerville* (CARB site)	PLA	38.7253	-120.8219	612	Semi-rural location in Sierra foothills
Sacramento* (CARB site)	SAC	38.5684	-121.4931	15	Rooftop near downtown Sacramento
Sugar Pine Point State Park	SPP	39.0419	-120.1448	1951	Flat open meadow; a few nearby trees
Thunderbird Lodge	THB	39.1739	-119.9316	1915	On the roof of a shed at the base of a steep incline
Upper Incline	ICN	39.2856	-119.9241	2523	Wide, open, steep slope with lots of green plants
Valhalla	VAL	38.9360	-120.0448	1906	Flat sandy terrain with low scrub; near CA Hwy. 89
Watson Creek	WC	39.2294	-120.1251	2293	Flat open meadow with leafy green plants

*\*Note: the four long-term monitoring sites marked with an asterisk did not collect any passive sampler data.*

**Table 2. Sampling locations equipped only with passive samplers**

Location	Code	Latitude (degrees)	Longitude (degrees)	Elevation (masl)	Ave. O <sub>3</sub> in 2010 (ppb)	Ave. O <sub>3</sub> in 2002 (ppb)
64 Acres	64A	39.163	-120.143	1900	39.8	44.1
Barker Pass	BPS	39.071	-120.230	2344	52.8	60.7
Blodgett	BLOD	38.897	-120.664	1298	54.7	58.7
Cave Rock	CR	39.044	-119.948	1902	N/A	52.3
Clear Creek	CCK	39.126	-119.884	2099	49.5	52.4
Desolation Wilderness	DW	38.934	-120.122	2436	53.9	N/A
Diamond Peak	DIP	39.258	-119.901	2571	55.5	54.4
Forest Hill	FH	39.085	-120.741	1252	58.0	68.5
Heavenly Gun Barrel	HGB	38.929	-119.931	2509	56.0	57.1
Heavenly Ridge Bowl	HRB	38.918	-119.915	2782	55.2	57.5
Heavenly Sky Express	HSE	38.917	-119.903	3043	56.7	57.0
Hobart Mills	HM	39.409	-120.185	1806	35.9	44.8
Kelly Lake	KLAKE	39.313	-120.574	1816	51.9	58.0
Little Valley	LIL	39.253	-119.877	1956	47.0	44.2
Loon Lake	LLK	38.988	-120.334	1927	47.6	66.7
Riverton Ridge	RT	38.779	-120.428	1227	46.1	66.2
Serene Lakes	SLAKE	39.323	-120.360	2246	57.1	61.7
Sly Park	SPK	38.708	-120.593	1067	42.6	61.0
Tahoe Regional Park	TRP	39.252	-120.051	1962	40.8	49.9
TB2 Buoy	TB2	39.108	-120.006	1897	63.5	N/A
Upper Blackwood	UBW	39.079	-120.216	2179	51.1	56.2
Watson Mtn. Road	WMR	39.193	-120.166	2187	50.3	54.4
White Cloud	WHC	39.316	-120.847	1279	56.8	66.6
Woodford's	WF	38.772	-119.836	1811	54.8	60.2

**Table 3. Ozone data for Lake Tahoe sites equipped with active ozone monitors in 2010**

Location	Active O <sub>3</sub> (ppb) <sup>*</sup> 2010	Diurnal Magnitude (ppb) <sup>**</sup>	Passive O <sub>3</sub> (ppb)		Site Topography	Ground Cover
			2010	2002		
Angora Lookout	55.1	5.7	53.3	N/A	very steep hillside near the top of a ridge	heavy fire damage; low scrub / bushes
Echo Summit	47.4	12.6	56.1	50.2	flat site near the base of an incline	paved parking lot, gravel, sparse grass
Genoa Peak 7000	41.2	19.5	44.1	54.1	open meadow with gentle slope	thick grass
Genoa Peak 8000	44.2	14.4	45.4	54.1	gentle slope on western side of Genoa Peak	extensive fire damage; mostly ash and dirt
Genoa Peak 9000	57.3	~ 0	59.2	60.2	exposed outcropping just below Genoa Peak	mostly rocks interspersed with tufts of grass
Incline Village	43.8	22.2	N/A	N/A	gentle slope facing towards the southwest	rooftop inlet, with some tall conifers nearby
Lower Blackwood Creek	33.8	39.0	35.1	41.0	large, flat open meadow	grassy and very wet
Sugar Pine Point State Park	38.3	36.3	37.0	44.3	flat open meadow	mostly grass, a few mountain mules' ears
Thunderbird Lodge	49.9	9.7	47.2	N/A	at the base of a steep hillside near the Lake	rooftop inlet; building surrounded by thick brush
Upper Incline	50.3	6.7	52.2	52.2	broad, steep hillside with good exposure	dry soil with extensive mtn. mules' ears coverage
Valhalla	39.0	32.1	43.3	46.7	flat, near the shoreline of Lake Tahoe	dry, sandy soil with thick low scrub / bushes
Watson Creek	38.6	26.7	43.2	47.2	flat open meadow	gravel with nearby mountain mules' ears

*\*Average hourly ozone for 12:00 PST on July 14, 2010, through 11:00 PST on September 22, 2010.*

*\*\*Diurnal magnitude is defined as (the diurnal average concentration at 13:00 PST) – (the diurnal average minimum); see Figure 4.*

**Table 4. 2010 NO<sub>x</sub> and VOC passive sampler data for sites equipped with active ozone monitors in 2010**

<b>Location</b>	<b>Ave. NO (ppb)</b>	<b>Ave. NO<sub>2</sub> (ppb)</b>	<b>Ave. NO<sub>x</sub> (ppb)</b>	<b>Ave. Anthropogenic VOC (ppb)</b>	<b>Ave. Biogenic VOC (ppb)</b>	<b>(Anthropogenic/Biogenic) Ratio</b>
Angora Lookout	2.05	1.39	3.44	0.14	0.64	0.22
Echo Summit	2.55	0.88	3.43	0.12	0.64	0.19
Genoa Peak 7000	2.70	0.96	3.66	0.14	0.64	0.22
Genoa Peak 8000	2.16	0.95	3.11	0.12	0.43	0.29
Genoa Peak 9000	2.04	0.94	2.98	0.13	0.33	0.41
Incline Village	N/A	N/A	N/A	N/A	N/A	N/A
Lower Blackwood Creek	2.80	1.29	4.09	0.24	1.44	0.25
Sugar Pine Point State Park	2.83	0.88	3.71	0.17	0.81	0.21
Thunderbird Lodge	2.25	1.40	3.65	0.17	0.50	0.39
Upper Incline	2.29	0.82	3.11	0.23	0.36	0.65
Valhalla	3.15	2.57	5.72	0.36	0.72	0.49
Watson Creek	1.11	0.73	1.84	0.20	0.71	0.28

**Table 5. 2010 NO<sub>x</sub> and VOC passive sampler data for sites without active ozone monitors in 2010**

Location	Ave. NO (ppb)	Ave. NO <sub>2</sub> (ppb)	Ave. NO <sub>x</sub> (ppb)	Ave. Anthropogenic VOC (ppb)	Ave. Biogenic VOC (ppb)	(Anthropogenic/Biogenic) Ratio
64 Acres	3.88	4.22	8.10	0.32	0.87	0.37
Barker Pass	2.87	0.68	3.55	0.17	0.54	0.32
Blodgett	1.86	1.61	3.47	0.33	0.96	0.34
Clear Creek	1.78	0.77	2.55	0.11	0.48	0.24
Desolation Wilderness	2.21	1.05	3.26	0.44	0.51	0.85
Diamond Peak	1.84	0.92	2.76	0.12	0.31	0.40
Forest Hill	2.34	0.92	3.26	0.17	1.05	0.16
Heavenly Gun Barrel	2.51	0.77	3.28	0.13	0.31	0.40
Heavenly Ridge Bowl	2.18	0.69	2.87	0.12	0.31	0.39
Heavenly Sky Express	2.11	0.64	2.75	0.09	0.26	0.36
Hobart Mills	2.99	2.13	5.12	0.28	1.13	0.25
Kelly Lake	2.96	3.43	6.39	0.19	0.68	0.21
Little Valley	2.59	0.90	3.49	0.18	0.75	0.24
Loon Lake	2.10	1.25	3.35	0.18	0.89	0.20
Riverton Ridge	2.31	1.45	3.76	0.28	1.33	0.21
Serene Lakes	3.25	1.25	4.50	0.23	0.66	0.35
Sly Park	2.57	1.62	4.19	0.32	1.64	0.19
Tahoe Regional Park	2.02	1.57	3.59	0.64	1.03	0.61
TB2 Buoy	2.41	1.44	3.85	0.73	0.45	1.60
Upper Blackwood	2.59	0.79	3.38	0.10	0.42	0.25
Watson Mtn. Road	1.94	0.80	2.74	0.15	0.35	0.42
White Cloud	2.36	1.38	3.74	0.18	0.89	0.21
Woodford's	2.18	1.17	3.35	0.22	0.55	0.39

**Table 6. Ozone exposure indices**

	120 day (24-hour) ppm•h	120 day (24-hour) ppm•h	120 day (24-hour) ppm•h	120 day (24-hour) ppm•h	90 day (12-hour) ppm•h	120 day (24-hour)	120 day (24-hour)
Site	SUM00	SUM06	SUM07	W126	W126*	Percent Complete (6/1 – 9/30)	Actual Sampling Period
Angora Lookout	154.0	50.1	11.2	37.8	13.3	79.5	6/15 - 9/23 <sup>#</sup>
Genoa Peak 7000	116.5	6.8	0.0	11.2	6.8	80.0	6/16 - 9/22
Genoa Peak 8000	125.6	10.3	0.2	14.2	7.6	68.9	6/30 - 9/22
Genoa Peak 9000	161.9	69.3	15.1	46.6	14.5	68.8	6/30 - 9/22
Lower Blackwood Canyon	96.1	9.3	0.3	10.8	7.2	81.3	6/16 - 9/23
Sugar Pine Point State Park	107.6	19.3	0.6	15.7	10.4	68.9	7/1 - 9/23
Thunderbird Lodge	141.3	21.3	0.4	22.0	10.2	69.5	7/1 - 9/24
Upper Incline	142.4	27.5	1.8	24.6	10.1	68.8	6/30 - 9/22
Valhalla	109.6	14.5	0.3	14.4	8.7	81.8	6/15 - 9/23
Watson Creek	109.6	11.6	0.5	12.5	7.3	77.0	6/16 - 9/23

\*Percent complete values for the 12-hour W126 calculation are 89 – 90%.

<sup>#</sup>Angora Lookout is missing seven days of hourly data for 22:00 to 06:00 PST.

Figure 1

[Click here to download high resolution image](#)

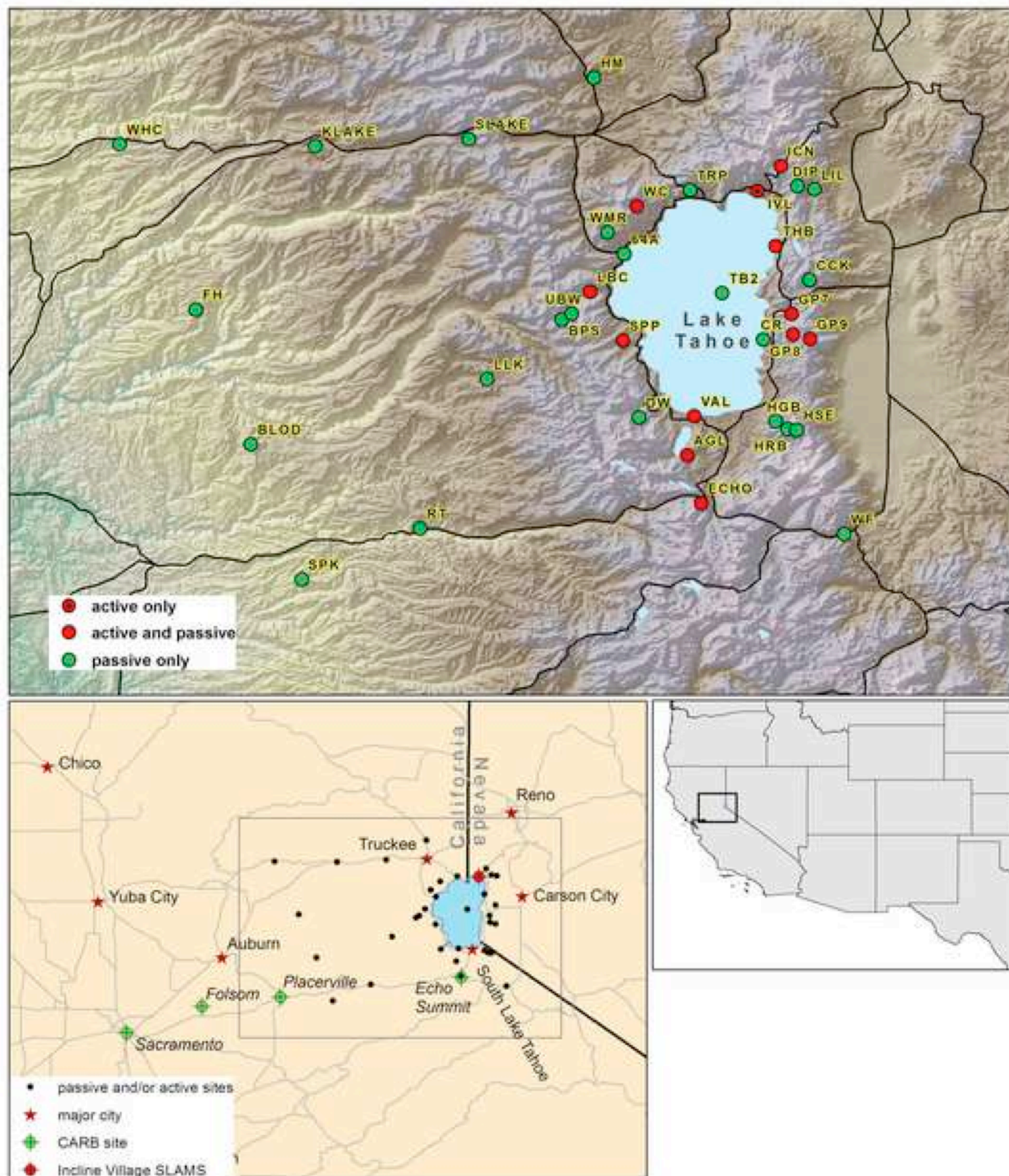


Figure 2a

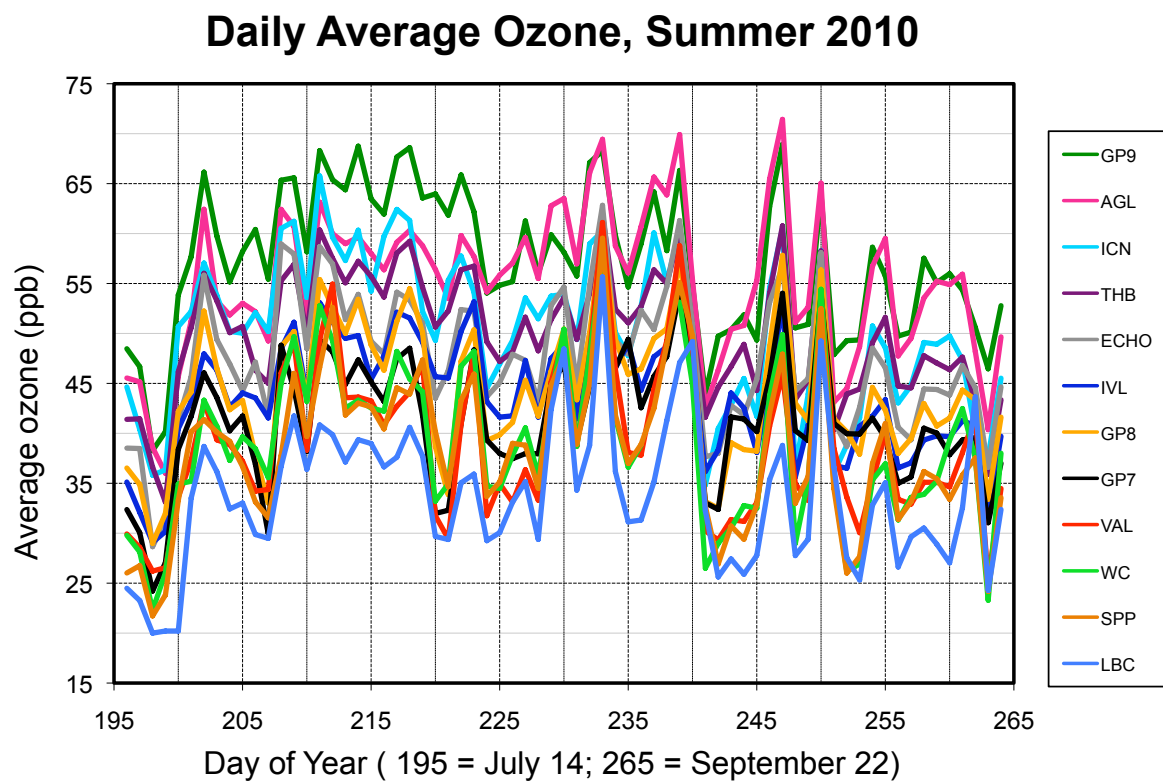


Figure 2a

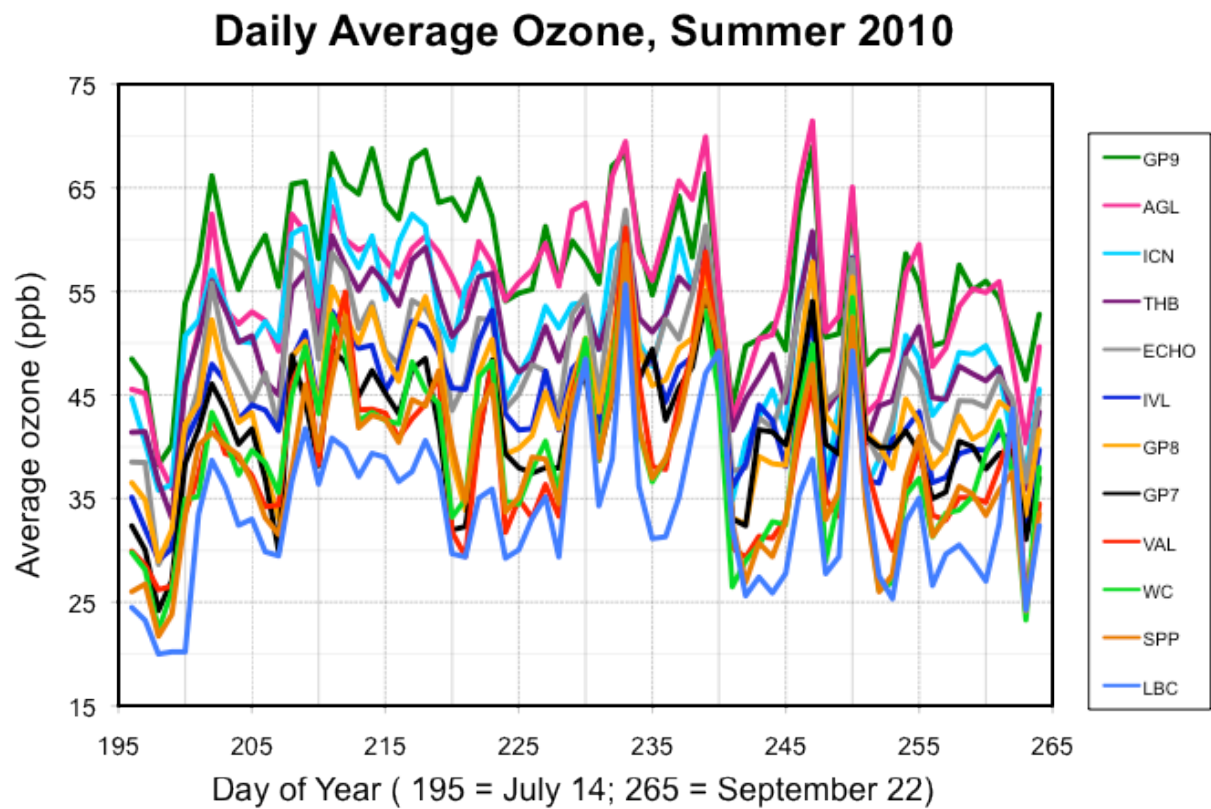




Figure 3b

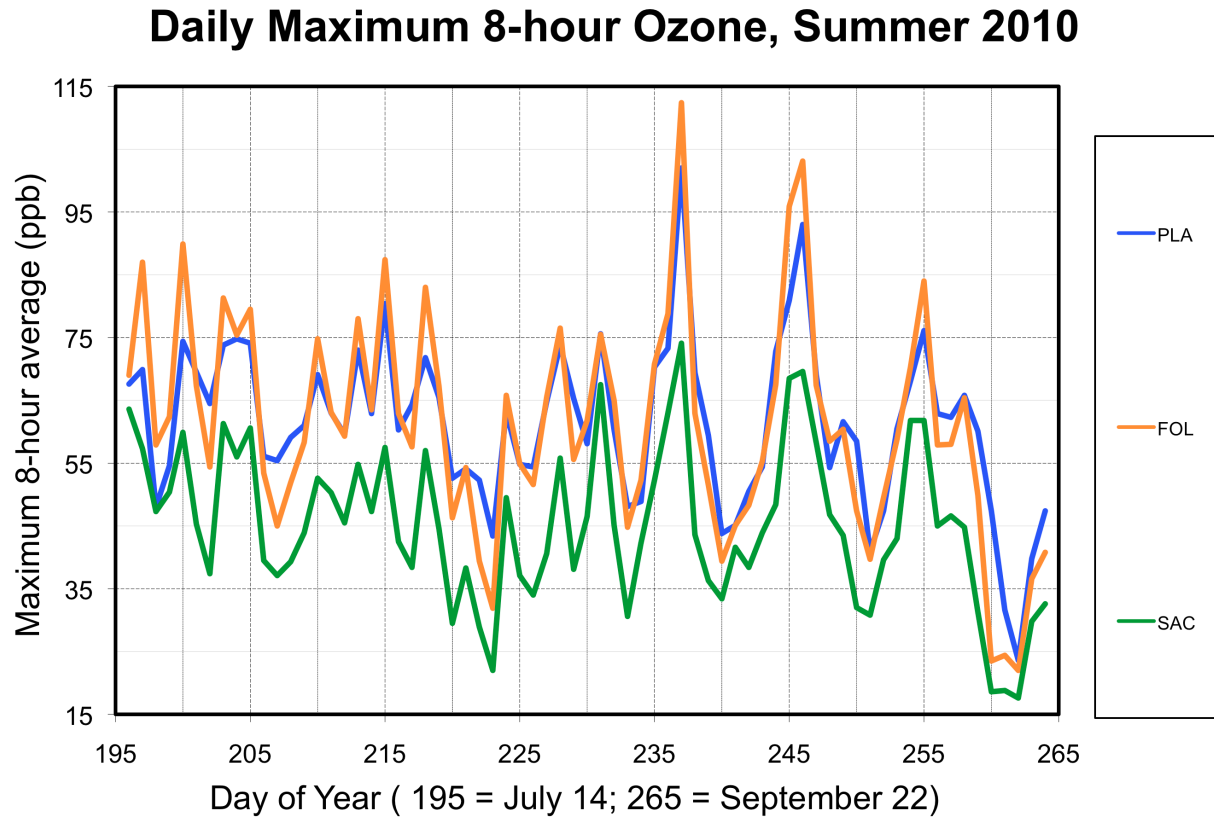


Figure 4a

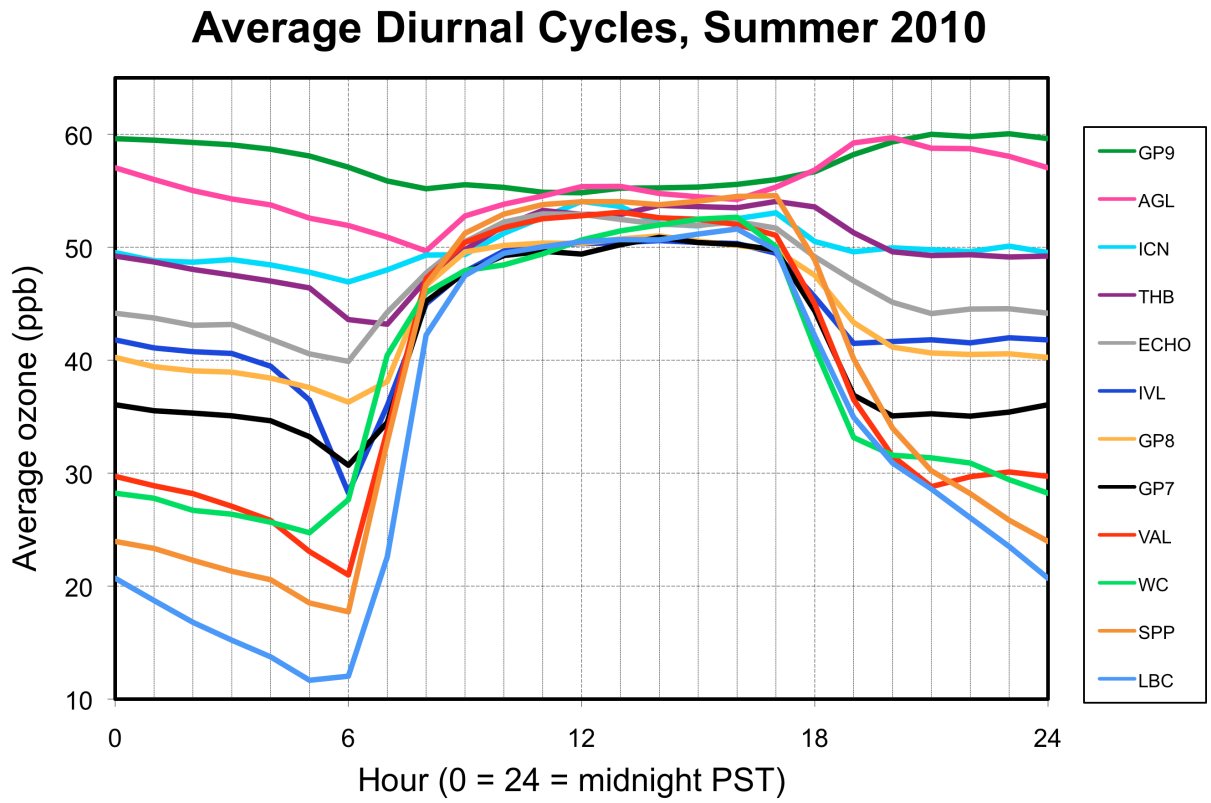


Figure 4b

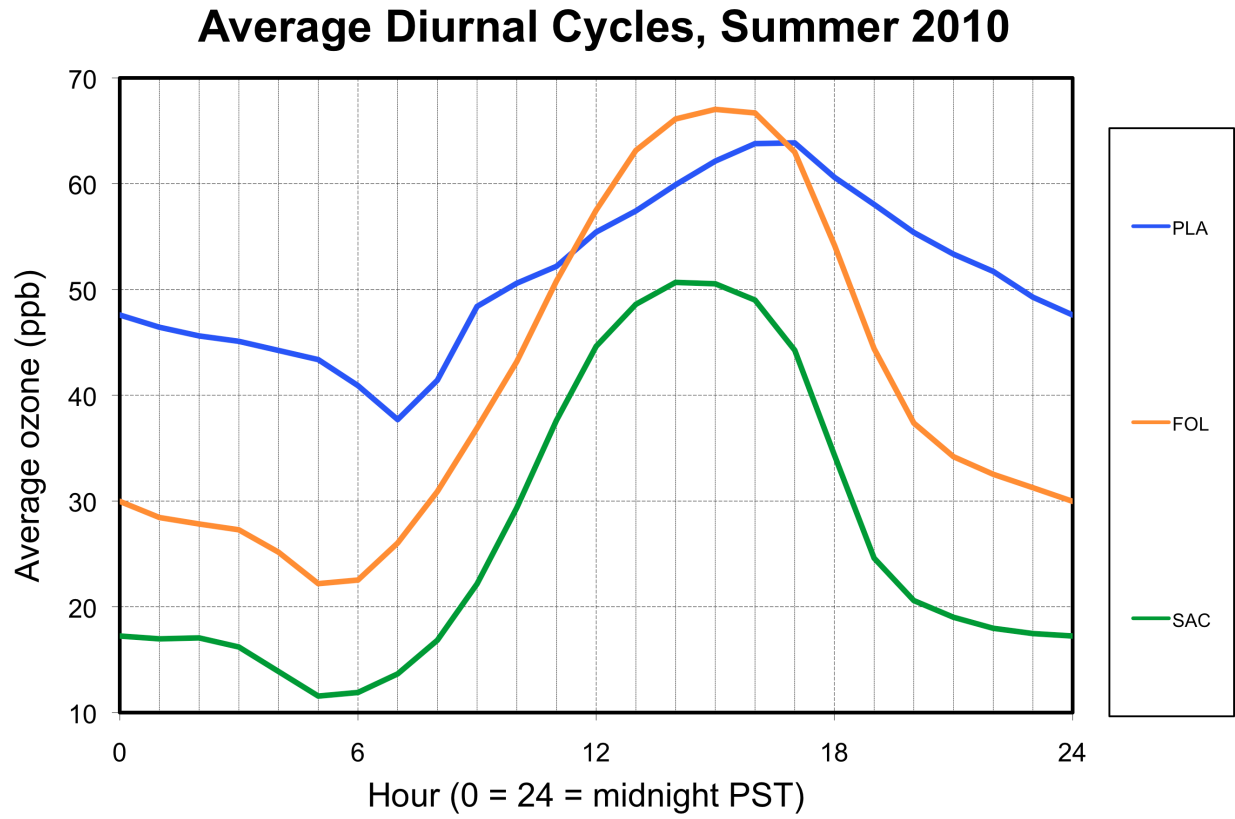


Figure 5a  
[Click here to download high resolution image](#)

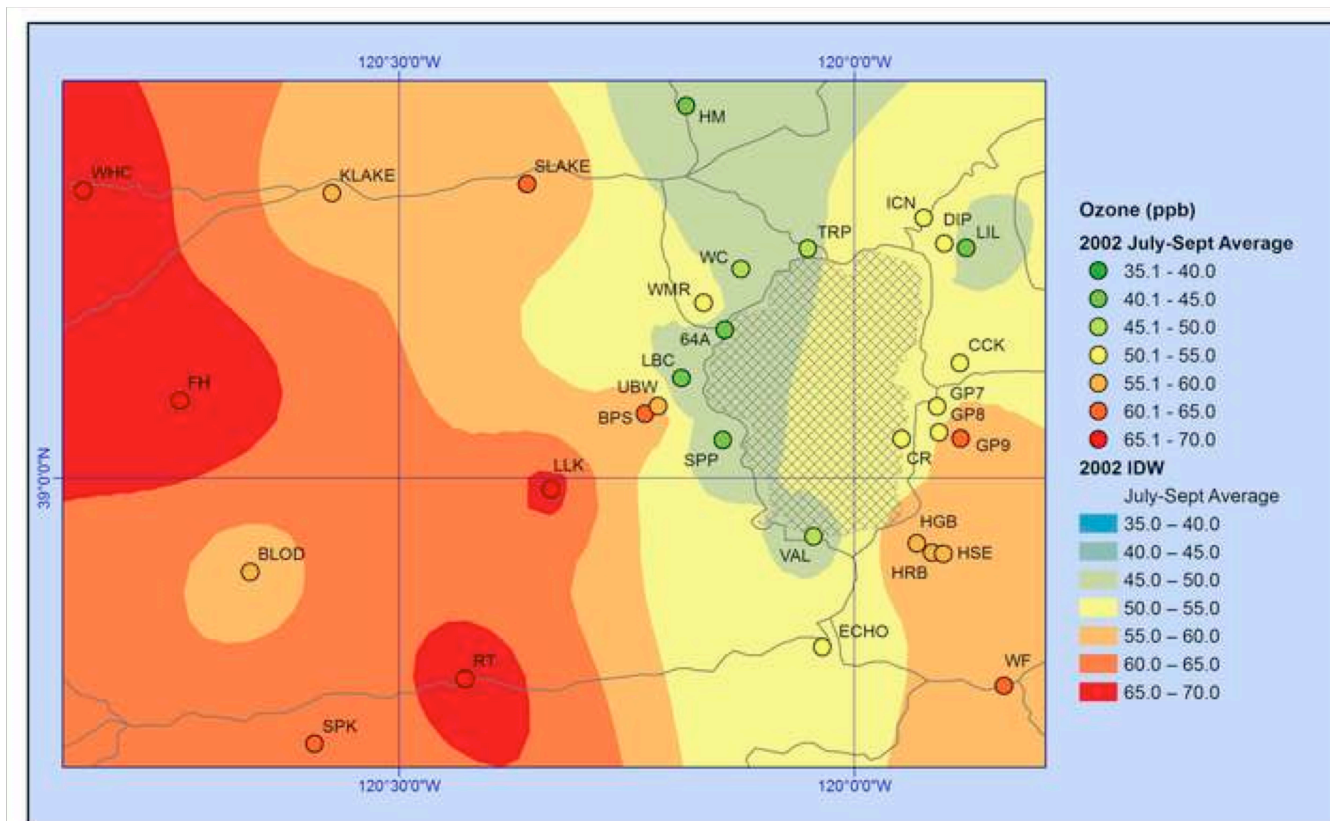


Figure 5b  
[Click here to download high resolution image](#)

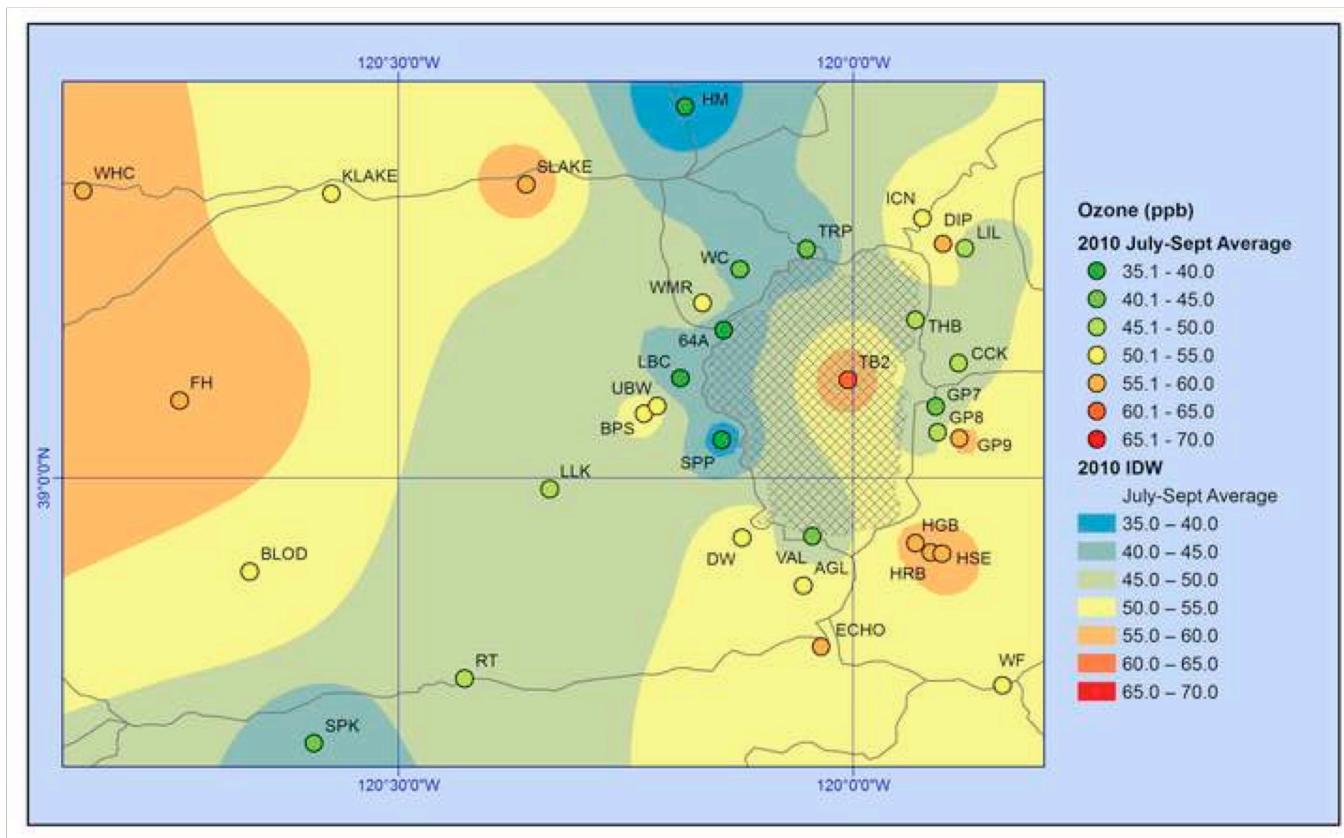


Figure 6

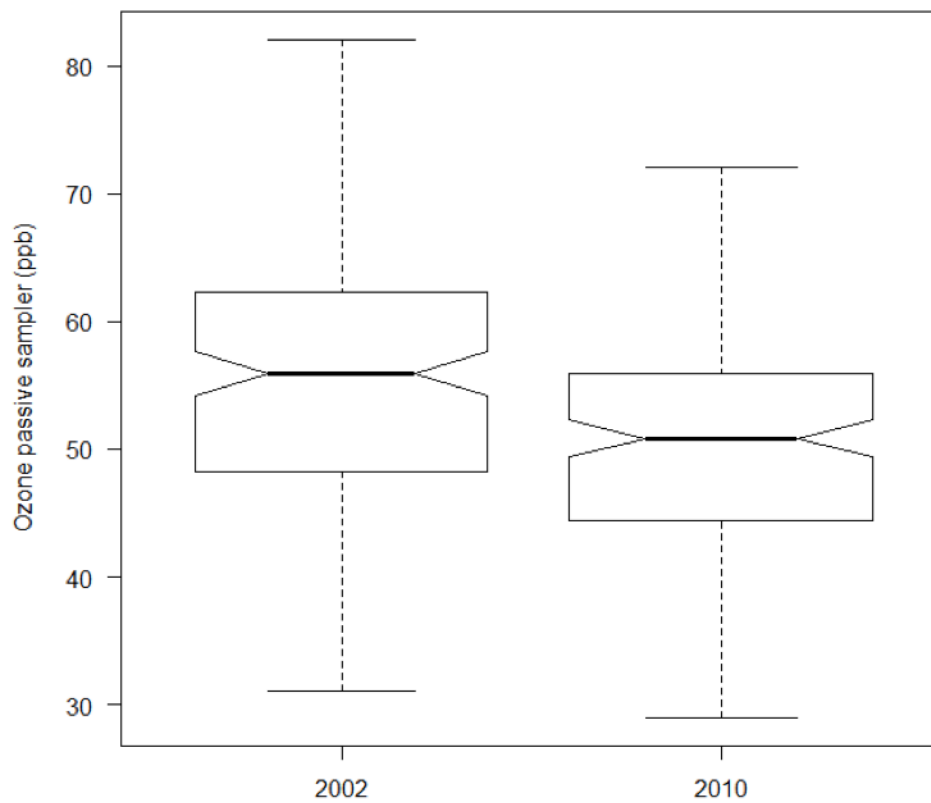


Figure 7

### Daytime Wind Roses by Site

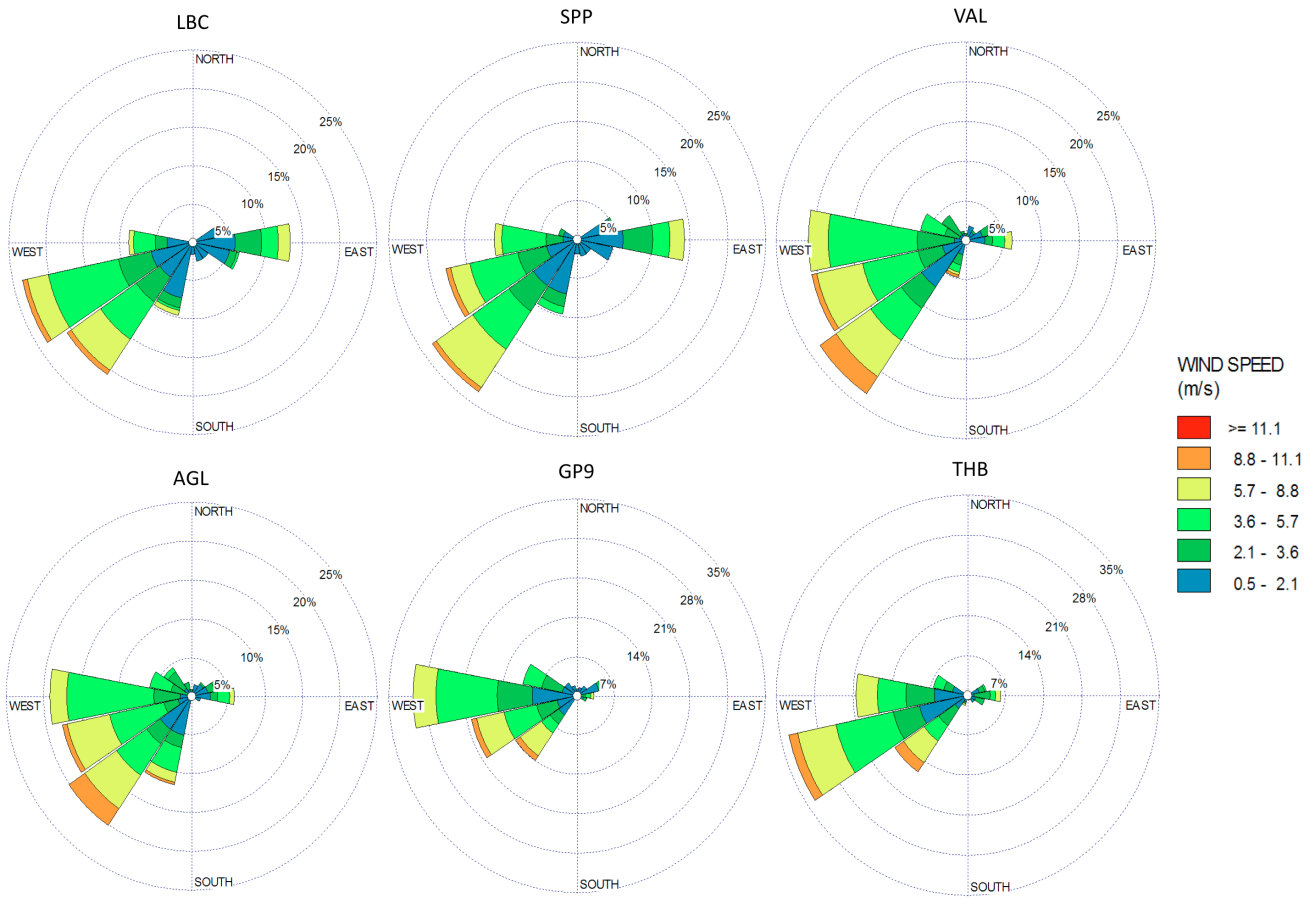


Figure 8

### Nighttime Wind Roses by Site

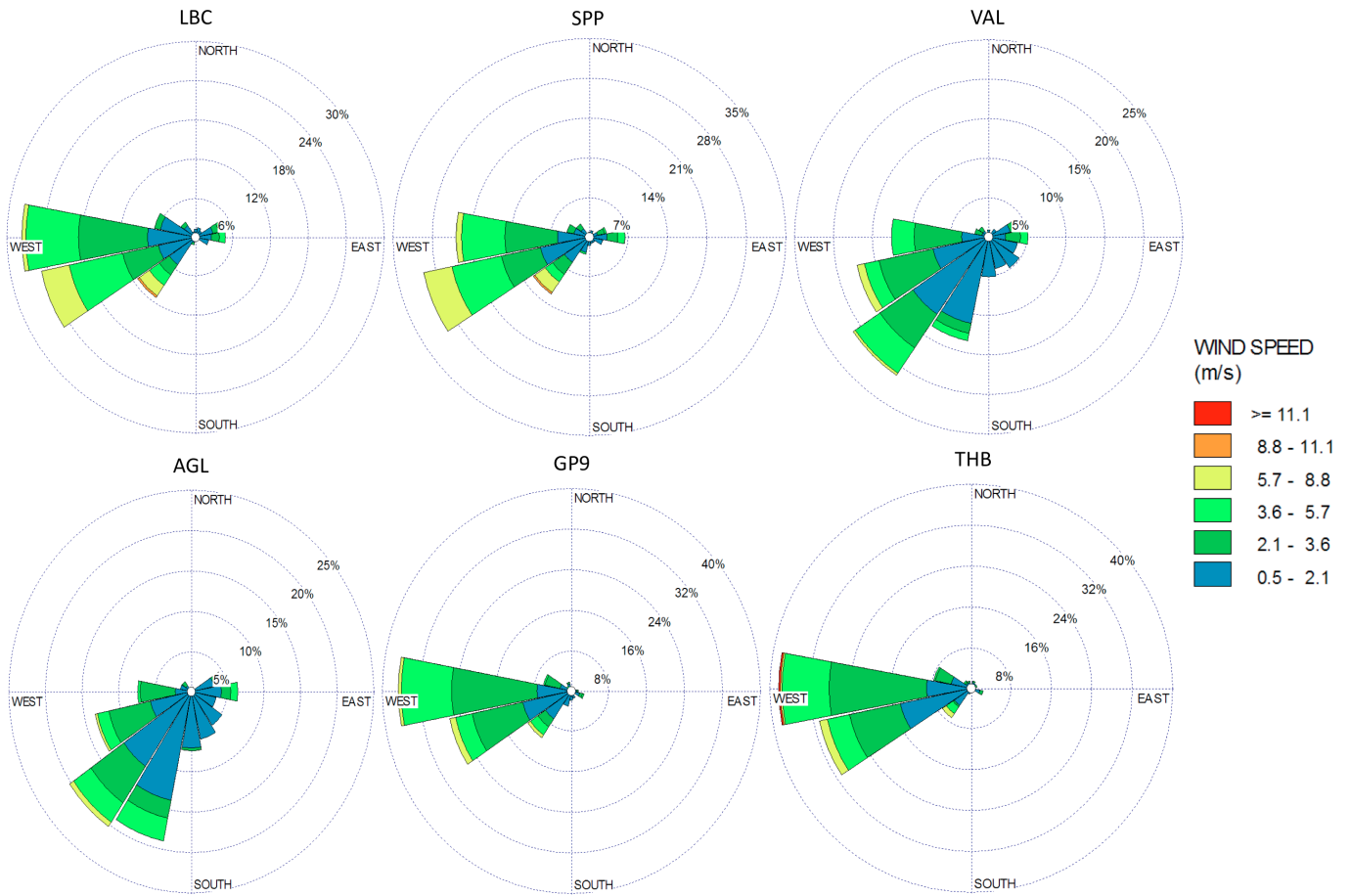


Figure 9

NOAA HYSPLIT MODEL  
 Backward trajectories ending at 0000 UTC 22 Aug 10  
 EDAS Meteorological Data

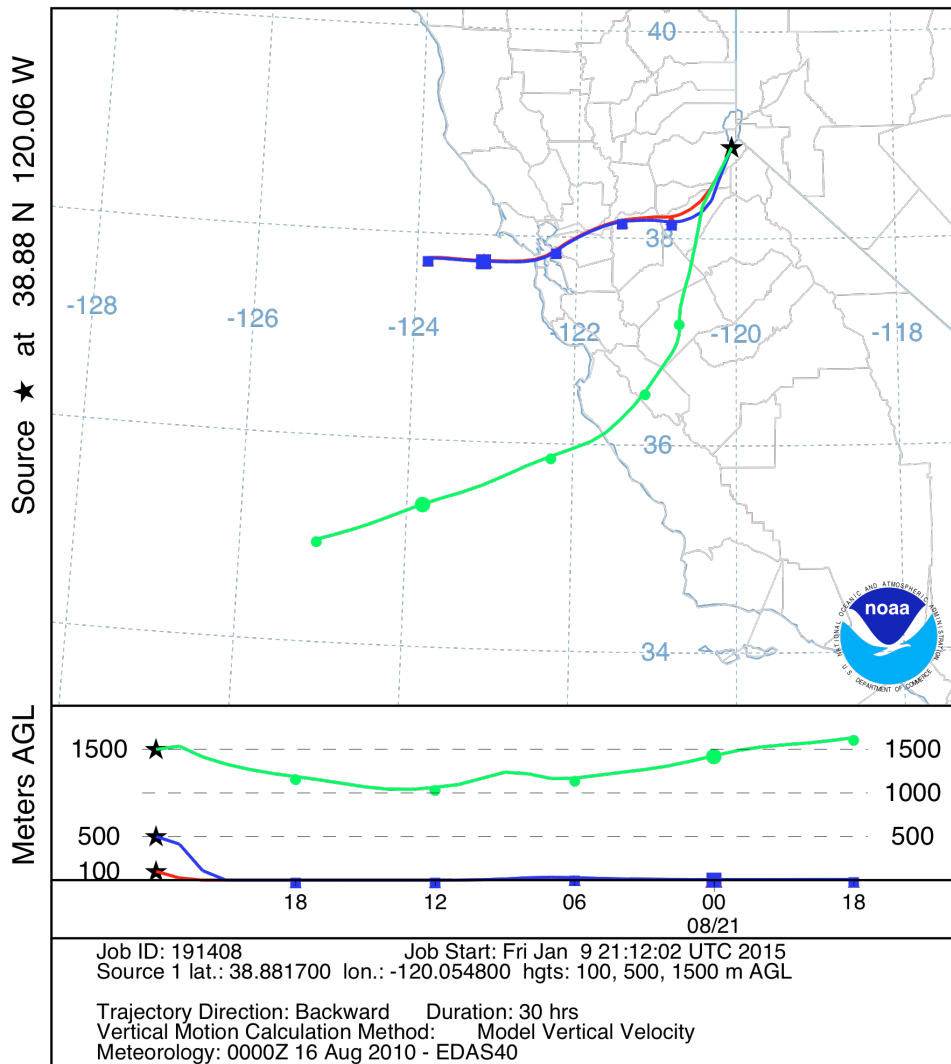


Figure 10

NOAA HYSPLIT MODEL  
 Backward trajectories ending at 0000 UTC 30 Aug 10  
 EDAS Meteorological Data

